2007

Transport properties, optical response and slow dynamics of ionic liquids

Zhonghan Hu
University of Iowa

TRANSPORT PROPERTIES, OPTICAL RESPONSE AND SLOW DYNAMICS OF IONIC LIQUIDS

by

Zhonghan Hu

An Abstract

Of a thesis submitted in partial fulfillment of the
requirements for the Doctor of Philosophy
degree in Chemistry
in the Graduate College of
The University of Iowa

July 2007

Thesis Supervisor: Assistant Professor Claudio J. Margulis

ABSTRACT

In this thesis, we report on our studies of the transport properties, optical response and slow dynamical nature of novel room temperature ionic liquids. Using computer simulations we have demonstrated that the diffusive dynamics of these systems is in many ways analogous to that of other glassy or supercooled liquids. These solvents show non-Gaussian rotational and translational diffusion which have a temporal extent on the order of nanoseconds at room temperature. Our study of their response upon application of an external mechanical perturbation shows that even for systems with a box length as large as 0.03 microns the viscosities computed from perturbation wavenumbers compatible with this box size have not yet reached the hydrodynamic limit. We found these systems to behave in a non-Newtonian fashion and we also observe a clear break down of linear response theory on the nano- or sub-micrometer scale.

Upon photoexcitation of an organic probe with lifetime shorter than the reorganization timescale in these ionic liquids, (which is quite long on the order of several nanoseconds at least), the emission spectrum is absorption wavelength dependent. Our computer simulations rationalized this observation in terms of local solvent environment around individual subensemble probe members. Excitation of different solute molecules in the liquid gives rise to site-specific optical responses. We revealed that the origin of this excitation wavelength dependence is the existence of persistent excited-state environments that do not get solvent averaged on a time scale relevant

to fluorescence. The computed time resolved fluorescence spectra show that the full loss of correlation between absorption and emission frequencies for probes in room temperature ionic liquids occur on a time scale of nanoseconds.

One of the most interesting features of ionic liquids is their uncommonly large range of dynamical time scales which in turn makes some of their properties to be quite different from that of most other conventional solvents. We hope that our understanding of these phenomena will be useful in the future in the development of tools to harness their potential to control the outcome of chemical and photo-chemical reactions.

Abstract Approved: _____
Thesis Supervisor

_____
Title and Department

_____
Date

TRANSPORT PROPERTIES, OPTICAL RESPONSE AND SLOW DYNAMICS OF IONIC LIQUIDS

by

Zhonghan Hu

A thesis submitted in partial fulfillment of the
requirements for the Doctor of Philosophy
degree in Chemistry
in the Graduate College of
The University of Iowa

July 2007

Thesis Supervisor: Assistant Professor Claudio J. Margulis

Graduate College
The University of Iowa
Iowa City, Iowa

CERTIFICATE OF APPROVAL

PH.D. THESIS

This is to certify that the Ph.D. thesis of

Zhonghan Hu

has been approved by the Examining Committee for the thesis requirement for the Doctor of Philosophy degree in Chemistry at the July 2007 graduation.

Thesis Committee: _____
Claudio Margulis, Thesis Supervisor

_____
Amnon Kohen

_____
Christopher M. Cheatum

_____
Lei Geng

_____
Adrian Elcock

ACKNOWLEDGEMENTS

I would like to thank the professors and students from physical chemistry seminar for their interesting questions and helpful suggestions. I am indebted to my advisor, Claudio J. Margulis, for his insights and enthusiasm.

ABSTRACT

In this thesis, we report on our studies of the transport properties, optical response and slow dynamical nature of novel room temperature ionic liquids. Using computer simulations we have demonstrated that the diffusive dynamics of these systems is in many ways analogous to that of other glassy or supercooled liquids. These solvents show non-Gaussian rotational and translational diffusion which have a temporal extent on the order of nanoseconds at room temperature. Our study of their response upon application of an external mechanical perturbation shows that even for systems with a box length as large as 0.03 microns the viscosities computed from perturbation wavenumbers compatible with this box size have not yet reached the hydrodynamic limit. We found these systems to behave in a non-Newtonian fashion and we also observe a clear break down of linear response theory on the nano- or sub-micrometer scale.

Upon photoexcitation of an organic probe with lifetime shorter than the reorganization timescale in these ionic liquids, (which is quite long on the order of several nanoseconds at least), the emission spectrum is absorption wavelength dependent. Our computer simulations rationalized this observation in terms of local solvent environment around individual subensemble probe members. Excitation of different solute molecules in the liquid gives rise to site-specific optical responses. We revealed that the origin of this excitation wavelength dependence is the existence of persistent excited-state environments that do not get solvent averaged on a time scale relevant

to fluorescence. The computed time resolved fluorescence spectra show that the full loss of correlation between absorption and emission frequencies for probes in room temperature ionic liquids occur on a time scale of nanoseconds.

One of the most interesting features of ionic liquids is their uncommonly large range of dynamical time scales which in turn makes some of their properties to be quite different from that of most other conventional solvents. We hope that our understanding of these phenomena will be useful in the future in the development of tools to harness their potential to control the outcome of chemical and photo-chemical reactions.

TABLE OF CONTENTS

LIST OF TABLES

Table

LIST OF FIGURES

Figure

CHAPTER 1
INTRODUCTION

Ionic Liquids (ILs) have recently attracted significant attention from academic and industrial sources. These novel solvents are important to chemists for three reasons. (1) They can dissolve a wide range of polar and nonpolar organic and inorganic molecules. (2) Although they are liquids at room temperature, their vapor pressures are negligible. (3) New chemical reactions and industrial processes are being discovered that can only be carried out in these solvents. As opposed to most other organic solvents, these liquids have the potential of being greener reaction media because they are non-volatile.

The number of different ionic liquids that can be made by choosing particular organic cations and non coordinating anions is enormous[17]. The reason why room-temperature ionic liquids (RTILs) are liquid at room temperature is still not fully understood. From recent X-ray crystal structure studies, we know that some tend to crystallize into disordered solids[46] and, depending upon the rate of cooling, crystal polymorphism[33] can be observed. On the basis of these observations, it has been speculated that the gain in energy upon formation of the crystal is not as large as in traditional inorganic salts and is not enough to compensate for the loss in entropy that accompanies the formation of the crystal at room temperature[46]. Experiments show that several of these systems have a tendency toward glassy behavior[58, 75] and, depending upon the length of alkyl substituents in the cations, their properties range from those of normal liquids to glassy or even liquid crystals[34]. As recently

discussed in an interesting review article by MacFarlane and co-workers[17], the possible number of compounds expected to form RTILs is extremely large. Only a very small fraction of these have been synthesized. Their selectivity as media for chemical and photochemical reactions remains *terra incognita* and invites for a thorough theoretical understanding of the trends to be anticipated as molecular modifications are applied.

In this thesis, we discuss our progress in understanding the dynamics, spectroscopy, and fluid dynamics of selected imidazolium- and pyridinium-based ionic liquids using computational and analytical tools we have developed during the last four years. All the mathematical tools required to understand our work are provided either in the corresponding chapters in which the theory and calculations are presented, or in appendices A and B. Our results and recent experiments indicate that some of these exciting systems appear to be dynamically heterogeneous at least at room temperature. Our studies also indicate the existence of locally heterogeneous environments on a time scale relevant to chemical and photo-chemical reactivity. When we study the fluid dynamics of these solvents on a nanometer length scale, we find that flow is non-Newtonian and we observe a clear break down of linear response theory. One of the main contributions to this field provided by our work is the understanding that widely different time scales dominate the dynamics of these systems[36]. We hope that in the future the tools and insight we have developed will help the ionic liquids community in the design of liquids and the control of chemical reactivity in these systems.

CHAPTER 2
DYNAMICAL VARIABLES AND TIME CORRELATION FUNCTIONS

The first two chapters provide the theoretical background for the analysis of the properties of room-temperature ionic liquids. The fundamentals of these statistical mechanics theories have been developed during the past forty years [30, 8, 27, 16]. In this work we reformulate and apply to the theory of transport properties and dynamics. The resulting formulation is quite general in the sense that it is always valid for any material state: gas, liquid or solid without limitation to a specific interaction. There will be closing remarks at the end of each section summarizing the importance and the applicability of the material presented. People who are not interested in fundamental theories of statistical mechanics can simply read the introduction and jump to the end of the sections of these two chapters.

The first chapter on dynamical variables and time correlation functions (TCFs) provides a general background on the theory used in our work. In this chapter we will show how to construct a framework to study dynamical properties of liquids. For our own purpose, transport properties such as diffusion and shear viscosity are used as examples to illustrate the use of the theories of TCFs. Excellent books and frequently cited papers can be found in references [8, 27, 77].

The starting point for our derivations in the first chapter is Hamilton's equations of motion in the frame work of classical mechanics. Informative results are derived by manipulating thermodynamical integrals instead of solving Hamiltonian

equations directly.

2.1 Time Evolution of Dynamical Variables

In the study of the dynamics of liquids, one usually focuses on experimentally measurable properties. From a theoretical point of view, one would like to understand what dynamical variables are associated with the experiment and how these variables evolve as a function of time. Without any loss of generality, we consider a system of interest containing N particles (atoms or molecules) with positions and momenta denoted by $(\mathbf{R}_j, j = 1, 2, \cdots, N)$ and $(\mathbf{p}_j, j = 1, 2, \cdots, N)$ respectively. The total volume of this system is V and the mass of each particle is m_j $(j = 1, 2, \cdots, N)$ The dynamics of the system is driven by Hamiltonian equations of motion:

$$\begin{cases} \dot{\mathbf{p}}_j &= -\dfrac{\partial H}{\partial \mathbf{R}_j} \\ \dot{\mathbf{R}}_j &= \dfrac{\partial H}{\partial \mathbf{p}_j} \end{cases} \qquad j = 1, 2, \cdots, N \tag{2.1}$$

The time evolution of an arbitrary dynamical quantity $A(\mathbf{R}^N, \mathbf{p}^N)$, not explicitly depending on time, can be written in terms of Liouville operator:

$$\frac{dA}{dt} = i\hat{L}A \tag{2.2}$$

where $\hat{L}$ is Liouville operator defined as:

$$\begin{aligned} i\hat{L}A &= \sum_j \left(-\frac{\partial H}{\partial \mathbf{R}_j}\frac{\partial A}{\partial \mathbf{p}_j} + \frac{\partial H}{\partial \mathbf{p}_j}\frac{\partial A}{\partial \mathbf{R}_j}\right) \\ &= \sum_{j=1}^{N} \frac{\mathbf{p}_j}{m_j} \cdot \nabla_{\mathbf{R}_j} A(\mathbf{R}^N, \mathbf{p}^N) + \sum_{j=1}^{N} \mathbf{F}_j \cdot \nabla_{\mathbf{p}_j} A(\mathbf{R}^N, \mathbf{p}^N) \end{aligned} \tag{2.3}$$

where F_j is the force on particle j. Throughout this thesis, we frequently use this kind of form $(\mathbf{R}^N)$ as the collective notation of $3N$ variables $(\mathbf{R}_1, \mathbf{R}_2, \cdots, \mathbf{R}_N)$. The

Liouville operator is Hermitian in the sense that:

$$Bi\hat{L}C = Ci\hat{L}B \tag{2.4}$$

where B,C are arbitrary dynamical variables. The proof of the Hermitian equality (2.4) can be found in standard books of statistical mechanics[52] and will not be repeated here. The solution to equation (2.2) can be formally written as

$$A(\mathbf{R}^N(t), \mathbf{p}^N(t)) = e^{i\hat{L}t} A(\mathbf{R}^N(0), \mathbf{p}^N(0)) \tag{2.5}$$

In general, operator $e^{it\hat{L}}$ displaces an arbitrary dynamical variable $A(\mathbf{p}^N, \mathbf{R}^N)$ by a distance t in time. This operator is called time displacement operator of the system. Though the displacement operator has a simple form, the solution itself is not useful because of the complicated structure of the Liouville operator (2.3). In principle, one has to solve the Hamiltonian equations (2.1) to explicitly write out the Liouville operator. However it is analytically unachievable to solve the set of $3N$ coupled equations (2.1) because any macroscopic system has a number of particles on the order of 10^{10} or even larger. Fortunately, experimentally observable quantities are usually ensemble averages of all possible value of A:

$$< A(t) > \equiv \int\int d\mathbf{R}^N d\mathbf{p}^N A(\mathbf{R}^N, \mathbf{p}^N) f(\mathbf{R}^N, \mathbf{p}^N, t) \tag{2.6}$$

where $f(\mathbf{R}^N, \mathbf{p}^N, t)$ is the distribution function or the phase density which determines the entire dynamical information of the ensemble. Equation (2.6) is an integral over all $3N$ degrees of freedom. Therefore, it is possible that we can extract useful information of the average by manipulating the integral rather than solving $3N$ coupled equations (2.1) directly.

In all of the cases we discussed in this thesis, the distribution function satisfies the so called Liouville equation[52]:

$$\frac{\partial f(\mathbf{R}^N, \mathbf{p}^N, t)}{\partial t} = -i\hat{L} f(\mathbf{R}^N, \mathbf{p}^N, t) \tag{2.7}$$

Similar to the solution of equation (2.2), we have

$$f(\mathbf{R}^N, \mathbf{p}^N, t) = e^{-i\hat{L}t} f(\mathbf{R}^N, \mathbf{p}^N, t = 0) \tag{2.8}$$

Note that the time factor t is explicitly included in the distribution function while it is only implicit in the dynamical variable A. A straightforward manipulation by using the Hermitian property of the Liouville operator along with Liouville equation (2.7) leads to another form of ensemble average:

$$\begin{aligned} < A(t) > &= \int\int d\mathbf{R}^N d\mathbf{p}^N A(\mathbf{R}^N, \mathbf{p}^N) f(\mathbf{R}^N, \mathbf{p}^N, t) \\ &= \int\int d\mathbf{R}^N d\mathbf{p}^N A(\mathbf{R}^N, \mathbf{p}^N) e^{-i\hat{L}t} f(\mathbf{R}^N, \mathbf{p}^N, t = 0) \\ &= \int\int d\mathbf{R}^N d\mathbf{p}^N (e^{i\hat{L}t} A(\mathbf{R}^N, \mathbf{p}^N)) f(\mathbf{R}^N, \mathbf{p}^N, t = 0) \\ &\equiv \int\int d\mathbf{R}^N d\mathbf{p}^N A(\mathbf{R}^N(t), \mathbf{p}^N(t)) f(\mathbf{R}^N, \mathbf{p}^N) \end{aligned} \tag{2.9}$$

where equations (2.6) and (2.9) are called Schrodinger and Heisenberg representations respectively. Before we pursue to reformat equation (2.2) in a more informative way, we introduce an important ensemble average and the definition of projection operator. It turns out that the most useful ensemble average is the equilibrium time correlation function (TCF) defined as:

$$C_{AB}(t) \equiv < A^*(0) B(t) > = \int\int A^*(0) B(t) f(0) d\mathbf{p}^N \, d\mathbf{R}^N$$

when $A = B$, the time correlation function is called auto correlation function (ACF). A^* denotes the complex conjugate of A. Clearly, we can project the component of an arbitrary variable B onto the dynamical variable A using the TCF C_{AB}:

$$\hat{P}B \equiv A < A^*A >^{-1} < A^*B >$$

Also, the complementary operator $\hat{Q}$ is defined as $\hat{Q} \equiv 1 - \hat{P}$. We have the following properties for the projection operator in general:

$$\hat{P}^2 = \hat{P} \qquad \hat{Q}^2 = \hat{Q} \qquad \hat{P}\hat{Q} = 0$$

for arbitrary dynamical variables B and C,

$$< C^*(\hat{P}B) > = < (\hat{P}C)^*B > \qquad \hat{P}(B + C) = \hat{P}B + \hat{P}C$$

With the definition of the time correlation functions and the projection operator, it is the right time to derive a more powerful and informative formula to describe the time evolution of a dynamical variable. The idea is to separate the entire driving force $i\hat{L}A$ in equation 2.2 into a friction force parallel to quantity A and a fluctuating force orthogonal to quantity A ($\hat{Q}A$). We start from equation (2.2):

$$\begin{aligned}
\frac{dA(t)}{dt} &= i\hat{L}A(t) = i\hat{L}e^{it\hat{L}}A(0) \\
&= e^{it\hat{L}}i\hat{L}A(0) = e^{it\hat{L}}(\hat{P} + 1 - \hat{P})i\hat{L}A(0) \\
&= e^{it\hat{L}}\hat{P}i\hat{L}A(0) + e^{it\hat{L}}\hat{Q}i\hat{L}A(0) \\
&= e^{it\hat{L}}A(0)\frac{< A^*(0)i\hat{L}A(0) >}{< A^*A >} + e^{it\hat{L}}\hat{Q}i\hat{L}A(0) \\
&= i\Omega A(t) + e^{it\hat{L}}\hat{Q}i\hat{L}A(0) \qquad (2.10)
\end{aligned}$$

we further write $e^{it\hat{L}}$ as:

$$e^{it\hat{L}} = e^{it\hat{L}}\theta(t) + e^{it\hat{Q}\hat{L}}$$

Differentiating both sides:

$$e^{it\hat{L}}(i\hat{L}) = i\hat{L}e^{it\hat{L}}\theta(t) + e^{it\hat{L}}\dot{\theta}(t) + i\hat{Q}\hat{L}e^{it\hat{Q}\hat{L}}$$

Insert the expression of $e^{it\hat{L}}$:

$$i\hat{L}(e^{it\hat{L}}\theta(t) + e^{it\hat{Q}\hat{L}}) = i\hat{L}e^{it\hat{L}}\theta(t) + e^{it\hat{L}}\dot{\theta}(t) + i\hat{Q}\hat{L}e^{it\hat{Q}\hat{L}}$$

$$e^{it\hat{L}}\dot{\theta}(t) = i\hat{P}\hat{L}e^{it\hat{Q}\hat{L}}$$

$$\theta(t) = \int_0^t d\tau e^{-i\tau\hat{L}} i\hat{P}\hat{L}e^{i\tau\hat{Q}\hat{L}}$$

with initial condition $\theta(t=0) = 0$. Therefore,

$$e^{it\hat{L}} = e^{it\hat{L}}\int_0^t d\tau e^{-i\tau\hat{L}} i\hat{P}\hat{L}e^{i\tau\hat{Q}\hat{L}} + e^{it\hat{Q}\hat{L}}$$

$$\begin{aligned} e^{it\hat{L}}\hat{Q}i\hat{L}A(0) &= e^{it\hat{L}}\int_0^t d\tau e^{-i\tau\hat{L}} i\hat{P}\hat{L}e^{i\tau\hat{Q}\hat{L}}\hat{Q}i\hat{L}A(0) + e^{it\hat{Q}\hat{L}}\hat{Q}i\hat{L}A(0) \\ &= \int_0^t d\tau e^{i(t-\tau)\hat{L}} i\hat{P}\hat{L}f(\tau) + f(t) \end{aligned}$$

where

$$f(t) = e^{it\hat{Q}\hat{L}}\hat{Q}i\hat{L}A(0)$$

Thus, we get a first order integral differential equation:

$$\frac{dA(t)}{dt} = i\Omega A(t) + \int_0^t d\tau e^{i(t-\tau)\hat{L}} i\hat{P}\hat{L}f(\tau) + f(t)$$

the integral kernel is further expressed as

$$\begin{aligned} i\hat{P}Lf(\tau) &= iA(0) < A^*(0)\hat{L}f(\tau) >< A^*A >^{-1} \\ &= iA(0) < (\hat{L}A(0))^* f(\tau) >< A^*A >^{-1} \end{aligned}$$

Here, using the properties of projection operator $\hat{Q}^2 = \hat{Q}$, we have

$$\begin{aligned}
< (\hat{L}A)^* f(\tau) > &= < \hat{L}A(0))^* e^{i\tau\hat{Q}\hat{L}} \hat{Q} i\hat{L}A(0) > \\
&= < \hat{L}A(0))^* i\hat{Q}\hat{L} e^{i\tau\hat{Q}\hat{L}} A(0) > \\
&= < \hat{L}A(0))^* i\hat{Q}^2\hat{L} e^{i\tau\hat{Q}\hat{L}} A(0) > \\
&= < \hat{L}A(0))^* i\hat{Q} f(\tau) \\
&= < (\hat{Q}\hat{L}A)^* f(\tau) > \\
&= i < (\hat{Q} i\hat{L}A)^* f(\tau) > \\
&= i < (f(0))^* f(\tau) >
\end{aligned}$$

then the integral kernel is reformatted as:

$$\begin{aligned}
i\hat{P}\hat{L}f(\tau) &= iA(0)i < f^*(0)f(\tau) >< A^*A >^{-1} \\
&= -A(0) < f^*(0)f(\tau) >< A^*A >^{-1}
\end{aligned}$$

Substitute the integral kernel into the first order integral differential equation, we eventually get the so called Generalized Langevin Equation (GLE):

$$\begin{aligned}
\frac{dA(t)}{dt} &= i\Omega A(t) + \int_0^t d\tau e^{i(t-\tau)\hat{L}} i\hat{P}\hat{L} f(\tau) + f(t) \\
&= i\Omega A(t) - \int_0^t d\tau e^{i(t-\tau)\hat{L}} A(0) < f^*(0)f(\tau) >< A^*A >^{-1} + f(t) \\
&= i\Omega A(t) - \int_0^t d\tau A(t-\tau) K(\tau) + f(t) \\
&= i\Omega A(t) - \int_0^t d\tau A(\tau) K(t-\tau) + f(t) \qquad (2.11)
\end{aligned}$$

where,

$$i\Omega =< A^*A >^{-1} < A^*(0) i\hat{L}A(0) >$$

$$f(t) = e^{it(1-\hat{P})\hat{L}}(1-\hat{P})i\hat{L}A(0)$$

$$K(\tau) =< f^*(0)f(\tau) >< A^*A >^{-1}$$

Note that

$$\begin{aligned} < A(0)f(t) > &= < \hat{P}A(0)(1-\hat{P})i\hat{L}e^{it(1-\hat{P})\hat{L}}A(0) > \\ &= < A(0)\hat{P}\hat{Q}B >= 0 \end{aligned} \tag{2.12}$$

The above method to derive the GLE (2.11) follows closely that in the reference[59]. We also present several other alternative methods to derive GLE for the time evolution of the dynamical variable or the TCF in Appendix A. Clearly, the GLE merely separates the total driving force into three components. Equation (2.12) ensures that the correlation between $f(t)$ and $A(0)$ vanishes thus making the variable $f(t)$ an orthogonal fluctuating force. The first term in the right hand side (rhs) of the GLE is still a driving force and the second term is a convolution between the dynamical variable at time τ and the memory kernel $K(t-\tau)$. In the Markoffian approximation we perform a substitution on the convolution integral

$$\int_0^t d\tau A(t-\tau)K(\tau) \simeq \left[\int_0^\infty d\tau K(\tau)\right] A(t) = \gamma A(t)$$

clearly γ plays the role of friction coefficient and the second term is essentially a frictional force.

Multiplying both sides of the GLE by $A^*(0)$ and taking the ensemble integral, we can get the GLE of the TCF $C(t) =< A^*(0)A(t) >$,

$$\frac{dC(t)}{dt} = i\Omega C(t) + \int_0^t d\tau C(\tau)K(t-\tau) \tag{2.13}$$

GLEs (2.11) and (2.13) are powerful starting points for analytical theories of TCFs (e.g. Mode Coupling Theory).

We shall close this section with the following general remarks. The time correlation functions play an essential role in the area of statistical mechanics. In this way, TCFs play a role of equal importance to that of partition functions in time independent statistical mechanics. This point will be more obvious when we extensively correlate a variety of nonequilibrium responses to the equilibrium TCFs in chapter 3. Nevertheless, our introductory discussion ending with the GLE provides a general background to study the dynamics of liquids. Case study of dynamical variables (e.g. number density, single particle velocity, transverse current density) relevant to transport properties are provided in the next sections of this chapter.

2.2 Transport Properties

For the purpose of studying transport properties of liquids, the fundamental dynamical variables of interest and their spatial Fourier transform are

the number density:

$$n(\mathbf{r},t)=\frac{1}{\sqrt{N}}\sum_{p=1}^{N}\delta(\mathbf{r}-\mathbf{R}_p(t)) \qquad n(\mathbf{k},t)=\frac{1}{\sqrt{N}}\sum_{p=1}^{N}e^{i\mathbf{k}\cdot\mathbf{R}_p(t)}$$

the current density:

$$\mathbf{j}(r,t)=\frac{1}{\sqrt{N}}\sum_{p=1}^{N}\mathbf{v}_p(t)\delta(\mathbf{r}-\mathbf{R}_p(t)) \qquad j_\alpha(\mathbf{k},t)=\frac{1}{\sqrt{N}}\sum_{p=1}^{N}v_{p\alpha}(t)e^{i\mathbf{k}\cdot\mathbf{R}_p(t)}$$

longitudinal and transverse part of the current density:

$$j_l(\mathbf{k},t)=\frac{1}{\sqrt{N}}\sum_{p=1}^{N}\hat{\mathbf{k}}\cdot\mathbf{v}_p(t)e^{i\mathbf{k}\cdot\mathbf{R}_p(t)} \qquad j_t(\mathbf{k},t)=\frac{1}{\sqrt{N}}\sum_{p=1}^{N}\hat{\mathbf{k}}_\perp\cdot\mathbf{v}_p(t)e^{i\mathbf{k}\cdot\mathbf{R}_p(t)} \quad (2.14)$$

the single particle density (particle 1):

$$n_s(\mathbf{r},t) = \delta(\mathbf{r} - \mathbf{R}_1(t)) \qquad n_s(\mathbf{k},t) = e^{i\mathbf{k}\cdot\mathbf{R}_1(t)}$$

the single particle velocity (particle 1):

$$\mathbf{v}_1(t)$$

and

$$\mathbf{j}_s(\mathbf{r},t) = \mathbf{v}_1(t)\delta(\mathbf{r} - \mathbf{R}_1(t)) \qquad \mathbf{j}_s(\mathbf{k},t) = \mathbf{v}_1(t)e^{i\mathbf{k}\cdot\mathbf{R}_1(t)}$$

where, N is the total number of particles, $\mathbf{R}_p(t)$ and $\mathbf{v}_p(t)$ are the position and velocity of particle p at time t.

By taking the equilibrium ensemble integral as in the equation (2.6), the average values of these variables are:

$$< n(\mathbf{r},t) >= \sqrt{N}/V \qquad < n(\mathbf{k},t) >= \sqrt{N}\delta_{\mathbf{k},0}$$

$$< n_s(\mathbf{r},t) >= 1/V \quad < n_s(\mathbf{k},t) >= \delta_{\mathbf{k},0} \quad < j_\alpha(\mathbf{k},t) >=< \mathbf{j}_s(\mathbf{k},t) >= 0$$

$$< \mathbf{v}_1(t) >=< \mathbf{j}(r,t) >=< \mathbf{j}_s(\mathbf{r},t) >= 0 \quad < \mathbf{j}(k,t) >=< \mathbf{j}(k=0,t) > \delta_{\mathbf{k},0}$$

Therefore the ACF of above fundamental variables and the temporal Fourier transformation (power spectra) are:

Density correlation function:

$$G(|\mathbf{r} - \mathbf{r}'|,t) = V < \delta n(\mathbf{r}',0)\delta n(\mathbf{r},t) >= \frac{1}{n} < \sum_{pq} \delta(\mathbf{r}' - \mathbf{R}_p(0))\delta(\mathbf{r} - \mathbf{R}_q(t)) > -n$$

$$
\begin{aligned}
G(\mathbf{r},t) &= \frac{1}{V}\int d\mathbf{r}' G(|(\mathbf{r}+\mathbf{r}')-\mathbf{r}'|,t) \\
&= \frac{1}{N} < \sum_{pq} \delta(\mathbf{r}'-\mathbf{R}_p(0))\delta(\mathbf{r}+\mathbf{r}'-\mathbf{R}_q(t)) > -n \\
&= \frac{1}{N} < \sum_{pq} \delta(\mathbf{r}+\mathbf{R}_p(0)-\mathbf{R}_q(t)) > -n = G_s(\mathbf{r},t)+G_d(\mathbf{r},t)-n \\
&= \frac{1}{N}\sum_{p} < \delta(\mathbf{r}+\mathbf{R}_p(0)-\mathbf{R}_p(t)) > + \frac{1}{N} < \sum_{p\neq q} \delta(\mathbf{r}+\mathbf{R}_p(0)-\mathbf{R}_q(t)) > -n
\end{aligned}
$$

van Hove self-correlation function:

$$
G_s(|\mathbf{r}-\mathbf{r}'|,t) = V < \delta n_s(\mathbf{r}',0)\delta n_s(\mathbf{r},t) >= V < \delta(\mathbf{r}'-\mathbf{R}_1(0))\delta(\mathbf{r}-\mathbf{R}_1(t)) > -\frac{1}{V}
$$

$$
\begin{aligned}
G_s(\mathbf{r},t) &= \frac{1}{V}\int d\mathbf{r}' G_s(|(\mathbf{r}+\mathbf{r}')-\mathbf{r}'|,t) + \frac{1}{V} =< \delta(\mathbf{r}+\mathbf{R}_1(0)-\mathbf{R}_1(t)) > \\
&= \frac{1}{N}\sum_{p} < \delta(\mathbf{r}+\mathbf{R}_p(0)-\mathbf{R}_p(t)) >
\end{aligned}
$$

normalized velocity autocorrelation function:

$$
\Psi(t) = \frac{< \mathbf{v}_1(0)\cdot\mathbf{v}_1(t) >}{< \mathbf{v}_1(0)\cdot\mathbf{v}_1(0) >} \qquad \Psi(\omega) = \int_{-\infty}^{\infty} e^{i\omega t}\Psi(t)
$$

intermediate scattering function:

$$
F(\mathbf{k},t) =< n^*(\mathbf{k},0)n(\mathbf{k},t) > -n(2\pi)^3\delta(\mathbf{k}) = \int_{-\infty}^{+\infty} e^{i\mathbf{k}\cdot\mathbf{r}}G(\mathbf{r},t)d\mathbf{r}
$$

$$
S(\mathbf{k},\omega) = \int_{-\infty}^{\infty} e^{i\omega t}F(\mathbf{k},t)
$$

incoherent intermediate scattering function:

$$
F_s(\mathbf{k},t) =< e^{i\mathbf{k}\cdot(\mathbf{R}_1(t)-\mathbf{R}_1(0))} >= \int_{-\infty}^{+\infty} e^{i\mathbf{k}\cdot\mathbf{r}}G_s(\mathbf{r},t)d\mathbf{r} \qquad S_s(\mathbf{k},\omega) = \int_{-\infty}^{\infty} e^{i\omega t}F_s(\mathbf{k},t)
$$

current correlation function:

$$
J_{\alpha\beta}(|\mathbf{r}-\mathbf{r}'|,t) = V < j^*_\alpha(\mathbf{r}',0)j_\beta(\mathbf{r},t) > \qquad J_{\alpha\beta}(\mathbf{k},t) =< j^*_\alpha(\mathbf{k},0)j_\beta(\mathbf{k},t) >
$$

longitudinal current correlation function:

$$J_l(\mathbf{k},t) = \frac{1}{N} < \sum_{pq} (\hat{\mathbf{k}} \cdot \mathbf{v}_p(0)) e^{-i\mathbf{k}\cdot\mathbf{R}_p(0)} (\hat{\mathbf{k}} \cdot \mathbf{v}_q(t)) e^{i\mathbf{k}\cdot\mathbf{R}_q(t)} >$$

$$J_l(\mathbf{k},\omega) = \int_{-\infty}^{\infty} e^{i\omega t} J_l(\mathbf{k},t)$$

transverse current correlation function:

$$J_t(\mathbf{k},t) = \frac{1}{N} < \sum_{pq} (\hat{\mathbf{k}}_\perp \cdot \mathbf{v}_p(0)) e^{-i\mathbf{k}\cdot\mathbf{R}_p(0)} (\hat{\mathbf{k}}_\perp \cdot \mathbf{v}_q(t)) e^{i\mathbf{k}\cdot\mathbf{R}_q(t)} >$$

$$J_t(\mathbf{k},\omega) = \int_{-\infty}^{\infty} e^{i\omega t} J_t(\mathbf{k},t)$$

where V and n are the volume and number density of the system respectively. the notation δA stands for $A - < A >$. The direction of $\mathbf{k}$ is the longitudinal direction. $\hat{\mathbf{k}}$ and $\hat{\mathbf{k}}_\perp$ denote unit vectors of longitudinal direction and transverse direction respectively. Recall that any dynamical variable of interest can be expressed as:

$$A(\mathbf{r},t) = e^{itL} A(\mathbf{r},0)$$

where the dependence of t is through $\mathbf{R}_q = \mathbf{R}_q(t)$ and $\mathbf{v}_q = \mathbf{v}_q(t)$. The Liouville operator L is a Hermitian first-order differential operator with the property of $iLf_{eq}(\mathbf{R}^N, \mathbf{v}^N) = 0$. Therefore, we have the identity for any TCF:

$$< A^*(k,0) \frac{\partial A(k,t)}{\partial t} > = - < \left. \frac{\partial A^*(k,t)}{\partial t} \right|_{t=0} A(k,t) >$$

Further, multiplying the Fourier transform $\int_{-\infty}^{\infty} dt e^{i\omega t} < A^*(k,0) A(k,t) >$ by ω^2 and

manipulating the integral by parts, we obtain

$$\begin{aligned}\omega^2\int_{-\infty}^{\infty}dte^{i\omega t}<A^*(k,0)A(k,t)> &= i^2\int_{-\infty}^{\infty}dt\left[\frac{\partial^2 e^{i\omega t}}{\partial t^2}\right]<A^*(k,0)A(k,t)> \\ &= -\int_{-\infty}^{\infty}dte^{i\omega t}<A^*(k,0)\frac{\partial^2 A(k,t)}{\partial t^2}> \\ &= \int_{-\infty}^{\infty}dte^{i\omega t}<\frac{\partial A(k,t)}{\partial t}\Big|_{t=0}\frac{\partial A(k,t)}{\partial t}>\end{aligned}$$

The following equalities can be easily obtained from the above equation:

$$J_l(\mathbf{k},\omega)=\frac{\omega^2}{k^2}S(\mathbf{k},\omega)\qquad \Psi(\omega)=\lim_{k\to 0}\left(\frac{\omega}{kv_0}\right)^2 S_s(\mathbf{k},\omega)$$

In general, we find the following quantities from static correlation functions:

$$G(\mathbf{r},t=0)=\delta(\mathbf{r})+ng(\mathbf{r})-n\quad G_s(\mathbf{r},t=0)=\delta(\mathbf{r})\quad G_d(\mathbf{r},t=0)=ng(\mathbf{r})$$

$$F(\mathbf{k},t=0)=1+n\int d^3re^{i\mathbf{k}\cdot r}(g(r)-1)=S(k) \tag{2.15}$$

$$F_s(\mathbf{k},t=0)=1 \tag{2.16}$$

$$J_{\alpha\beta}(\mathbf{k},0)=v_0^2\delta_{\alpha\beta} \tag{2.17}$$

$$<\mathbf{v}_1(0)\cdot\mathbf{v}_1(0)>=3<v_\alpha(0)v_\alpha(0)>=3v_0^2 \tag{2.18}$$

where the last line is valid for any arbitrary Cartesian component α. $v_0=(k_bT/m)^{1/2}$ is the thermal speed. $g(r)$ is the equilibrium pair distribution function or called radial distribution function (RDF). $S(k)$ is called the static structure factor which can be directly measured by X-ray and neutron diffraction. Equations (2.15) (2.16) and (2.18) are straight forward to derive, while equation (2.17) is a little bit more involved. Assuming that the equilibrium distribution function $f_{eq}(\mathbf{R}^N,\mathbf{v}^N)$ is an even

function of any $R_{p\alpha}$ and $v_{p\alpha}$. From the definition of current correlation function:

$$\begin{aligned}
J_{\alpha\beta}(\mathbf{k},0) &= \frac{1}{N} < \sum_{pq} v_{p\alpha} v_{q\beta} e^{i\mathbf{k}\cdot\mathbf{R}_p} e^{-i\mathbf{k}\cdot\mathbf{R}_q} > \\
&= \frac{1}{N} \sum_p \sum_q \int d\mathbf{R}^N e^{i\mathbf{k}\cdot\mathbf{R}_p} e^{-i\mathbf{k}\cdot\mathbf{R}_q} \int d\mathbf{v}^N v_{p\alpha} v_{q\beta} f_{eq} \\
&= \frac{1}{N} \sum_p \sum_q \int d\mathbf{R}^N e^{i\mathbf{k}\cdot\mathbf{R}_p} e^{-i\mathbf{k}\cdot\mathbf{R}_q} \int d\mathbf{v}^N v_{p\alpha} v_{q\beta} \delta_{pq} f_{eq} \\
&= \frac{1}{N} \sum_p \int d\mathbf{R}^N \int d\mathbf{v}^N v_{p\alpha} v_{p\beta} f_{eq} \\
&= \frac{1}{N} \sum_p \int d\mathbf{R}^N \int d\mathbf{v}^N v_{p\alpha} v_{p\beta} f_{eq} \\
&= \frac{\delta_{\alpha\beta}}{N} \sum_p \int d\mathbf{R}^N \int d\mathbf{v}^N v_{p\alpha} v_{p\alpha} f_{eq} \\
&= \frac{\delta_{\alpha\beta}}{N} \sum_p < v_\alpha v_\alpha > = \delta_{\alpha\beta} < v_\alpha v_\alpha > = \delta_{\alpha\beta} v_0^2 \qquad (2.19)
\end{aligned}$$

Thus we proved the equality in equation (2.17). Integration over $\mathbf{r}$ shows that:

$$\int G_s(\mathbf{r},t) d\mathbf{r} = 1 \qquad \int G_d(\mathbf{r},t) d\mathbf{r} = N - 1$$

Also, at large t, $G_s(\mathbf{r},t)$ and $G_d(\mathbf{r},t)$ become independent of $\mathbf{r}$ while the behavior at large r is clearly the same as that at large t. Therefore,

$$\lim_{r\to\infty} G_s(\mathbf{r},t) = \lim_{t\to\infty} G_s(\mathbf{r},t) = \frac{1}{V} \simeq 0$$

$$\lim_{r\to\infty} G_d(\mathbf{r},t) = \lim_{t\to\infty} G_d(\mathbf{r},t) = \frac{N}{V} \simeq n$$

The above discussion provides the background involved in order to study two important transport properties: shear viscosity and diffusion. The rest of this section aims at deriving a set of equations to link the time correlation functions to transport properties of liquids.

2.2.1 Shear Viscosity

We start from the fundamental equation of continuous mechanics, the Navier-Stokes equation[8]:

$$\rho\frac{\partial \mathbf{u}}{\partial t} + \rho(\mathbf{u}\cdot\nabla)\mathbf{u} = \rho\mathbf{a} + \eta\nabla^2\mathbf{u} + (\frac{\eta}{3} + \kappa)\nabla(\nabla\cdot\mathbf{u}) - \nabla p$$

where ρ is the mass density, $\mathbf{u}$ is the velocity of a liquid, $\mathbf{a}$ is the external force per unit mass, p is the pressure and η, κ are coefficients of shear and bulk viscosity respectively. $\mathbf{u}(r,t)$ is the macroscopic expression for the current density $\mathbf{j}(r,t)$. In order to calculate the shear viscosity, it is sufficient to consider only the transverse part of the current. We therefore divide $\mathbf{j}(r,t)$ into longitudinal and transverse parts $\mathbf{j}(r,t) = \mathbf{j}_l(\mathbf{r},t) + \mathbf{j}_t(r,t)$, where $\nabla\cdot\mathbf{j}_t(r,t) = 0, \nabla\times\mathbf{j}_l(\mathbf{r},t) = 0$. Thus, we have the transverse part of Navier-Stokes equation in the absence of external force ($a = 0$):

$$\frac{\partial}{\partial t}\mathbf{j}_t(\mathbf{r},t) = \frac{\eta}{\rho}\nabla^2\mathbf{j}_t(\mathbf{r},t) \tag{2.20}$$

and the corresponding equation in $\mathbf{k}$ space:

$$\frac{\partial}{\partial t}j_t(\mathbf{k},t) = -\frac{\eta}{\rho}k^2 j_t(\mathbf{k},t) \tag{2.21}$$

It is worth to denote that this equation has the same form as the diffusion equation:

$$\frac{\partial}{\partial t}n_s(\mathbf{k},t) = -Dk^2 n_s(\mathbf{k},t) \tag{2.22}$$

which can be derived from (1) Fick's law:

$$\mathbf{j}_s(\mathbf{k},t) = i\mathbf{k}Dn_s(\mathbf{k},t) \tag{2.23}$$

and (2) the number density conservation law:

$$i\mathbf{k}\cdot\mathbf{j}_s(\mathbf{k},t)=\frac{\partial}{\partial t}n_s(\mathbf{k},t) \tag{2.24}$$

where D is the diffusion constant. Equation(2.23) is just the Fourier transform of normal Fick's law $\mathbf{j}_s=-D\nabla n$. It should be kept in mind that equation (2.20) is only valid at long time and large length scale. The solution to this equation in $\mathbf{k}$ space is

$$j_t(\mathbf{k},t)=j_t(\mathbf{k},0)exp(-\frac{\eta}{\rho}k^2t)$$

Furthermore, the time correlation function of current density $\mathbf{j}(r,t)$ is given by

$$J_t(\mathbf{k},t)=v_0^2exp(-\frac{\eta}{\rho}k^2t) \tag{2.25}$$

Again, this is valid only at long times and small k. For simplicity, we take the longitudinal direction (direction of $\mathbf{k}$) along the z axis and a transverse direction along the $\mathbf{x}$ axis. Recalling the definition of transverse current correlation function:

$$J_t(\mathbf{k},t)=\frac{1}{N}<\sum_{pq}v_{px}(t)v_{qx}(0)e^{ik(z_p(t)-z_q(0))}> \tag{2.26}$$

and comparing to the expansion in powers of k of equations (2.25) and (2.26), we get the expression for the coefficient of shear viscosity:

$$\eta=\lim_{t\to+\infty}\frac{m^2}{2tk_bTV}<\sum_{pq}v_{px}(t)v_{qx}(0)(z_p(t)-z_q(t))^2> \tag{2.27}$$

Notice that from the conservation of total momentum, the property of stationarity and the evenness of the equilibrium distribution function in momentum, we have the

following equalities:

$$\begin{aligned} < \sum_p v_{px}(t) z_p^2(t) \sum_q v_{qx}(0) > &= < \sum_p v_{px}(t) z_p^2(t) \sum_q v_{qx}(t) > \\ &= < \sum_p v_{px}(0) z_p^2(0) \sum_q v_{qx}(0) > \\ &= < \sum_p v_{px}^2(0) z_p^2(0) > \end{aligned} \tag{2.28}$$

The above equation enables us to rewrite equation (2.27) as:

$$\eta = \lim_{t \to +\infty} \frac{1}{2tk_bTV} < \Delta G(t)^2 > \tag{2.29}$$

where

$$\Delta G(t) = \sum_q (z_q(t) m v_{qx}(t) - z_q(0) m v_{qx}(0)) \tag{2.30}$$

In order to find the relation between ΔG and transverse current density $j(\mathbf{k}, t)$, we take the first derivative of the definition of $j_\alpha(\mathbf{k}, t)$:

$$\frac{\partial j_\alpha(\mathbf{k}, t)}{\partial t} = \frac{1}{\sqrt{N}} \sum_{p=1}^{N} v_{p\alpha}(t) i\mathbf{k} \cdot \mathbf{v}_p(t) e^{i\mathbf{k}\cdot\mathbf{R}_p(t)} + \frac{1}{m\sqrt{N}} \sum_{p=1}^{N} F_{p\alpha}(t)^{i\mathbf{k}\cdot\mathbf{R}_p(t)}$$

where the second term

$$\begin{aligned} \sum_{p=1}^{N} F_{p\alpha}(t) e^{i\mathbf{k}\cdot\mathbf{R}_p(t)} &= -\sum_{p=1}^{N} \sum_{q \neq p}^{N} \frac{du(R_{pq})}{R_{pq}} \frac{R_{pq}^\alpha}{R_{pq}} e^{i\mathbf{k}\cdot\mathbf{R}_p(t)} \\ &= -\frac{1}{2} \sum_{p=1}^{N} \sum_{q \neq p}^{N} \frac{du(R_{pq})}{R_{pq}} \frac{R_{pq}^\alpha}{R_{pq}} \left[e^{i\mathbf{k}\cdot\mathbf{R}_p(t)} - e^{i\mathbf{k}\cdot\mathbf{R}_q(t)} \right] \\ &= -\frac{1}{2} ik_\beta \sum_{p=1}^{N} \sum_{q \neq p}^{N} \frac{du(R_{pq})}{R_{pq}} \frac{R_{pq}^\alpha R_{pq}^\beta}{ik_\beta R_{pq}^\beta R_{pq}} \left[e^{i\mathbf{k}\cdot\mathbf{R}_p(t)} - e^{i\mathbf{k}\cdot\mathbf{R}_q(t)} \right] \\ &= -\frac{1}{2} ik_\beta \sum_{p=1}^{N} \sum_{q \neq p}^{N} \frac{du(R_{pq})}{R_{pq}} \frac{R_{pq}^\alpha R_{pq}^\beta}{R_{pq}} \frac{\left[e^{i\mathbf{k}\cdot\mathbf{R}_{pq}(t)} - 1 \right]}{i\mathbf{k}\cdot\mathbf{R}_{pq}} e^{i\mathbf{k}\cdot\mathbf{R}_q(t)} \end{aligned}$$

Therefore, we can write the differential equation as

$$m \frac{\partial}{\partial t} j_\alpha(\mathbf{k}, t) = \sum_\beta ik_\beta \sigma_{\alpha\beta}(\mathbf{k}, t) \tag{2.31}$$

where the $\alpha\beta$ component of the stress tensor is written as[63]:

$$\sigma^{\mathbf{k}}_{\alpha\beta} = \frac{1}{\sqrt{N}} \sum_{q=1}^{N} \left\{ m v_{q\alpha} v_{q\beta} - \frac{1}{2} \sum_{p \neq q} \frac{R^{\alpha}_{pq} R^{\beta}_{pq}}{R_{pq}} \frac{du(R_{pq})}{dR_{pq}} \frac{e^{i\mathbf{k}\cdot\mathbf{R}_{pq}} - 1}{i\mathbf{k}\cdot\mathbf{R}_{pq}} \right\} e^{i\mathbf{k}\cdot\mathbf{R}_q} \tag{2.32}$$

and $R_{pq} = |\mathbf{R}_p - \mathbf{R}_q|$. Equation (2.31) is a momentum conservation law which is an analogue to the number conservation equation (2.24). The first derivative of $\Delta G(t)$ gives:

$$\frac{d}{dt}\Delta G(t) = \sum_{q} (v_{qz}(t) m v_{qx}(t) + z_q(t) F_{qx}(t) \tag{2.33}$$

where F_{qx} is the x component of the force acting on particle q. we can write this result into a more conventional form[63]

$$\begin{aligned} \sum_{q} z_q F_{qx} &= -\sum_{q} z_q \sum_{p \neq q} \frac{\partial u(R_{pq})}{\partial R_{pq}} \frac{r^x_{pq}}{R_{pq}} \\ &= \sum_{q} z_q \sum_{p \neq q} \frac{\partial u(R_{pq})}{\partial r_{qp}} \frac{r^x_{pq}}{R_{pq}} \\ &= -\frac{1}{2} \sum_{q} \sum_{p \neq q} \frac{r^x_{pq} r^z_{pq}}{R_{pq}} \frac{\partial u(R_{pq})}{\partial R_{pq}} \end{aligned} \tag{2.34}$$

where $r^z_{pq} = z_p - z_q$. Therefore, we relate ΔG to the xz component of the stress tensor and the transverse current density as:

$$\frac{d}{dt}\Delta G(t) = \sqrt{N} \lim_{k \to 0} \sigma^{\mathbf{k}}_{xz}(t) = \sqrt{N} \lim_{k \to 0} \left\{ \frac{m}{ik} \frac{\partial j_t(\mathbf{k}, t)}{\partial t} \right\} = \sigma_{xz}(t)$$

Equation (2.29) can be written as

$$\eta = \lim_{t \to +\infty} \frac{1}{2tk_bTV} \int_0^t d\tau \int_0^t d\tau' < \sigma_{xz}(\tau)\sigma_{xz}(\tau') > \tag{2.35}$$

Manipulating the integral[8] and considering only the long time behavior, we obtain the desired result

$$\begin{aligned}
\eta &= \frac{1}{k_bTV}\int_0^{+\infty} dt < \sigma_{xz}(0)\sigma_{xz}(t) > \\
&= \frac{N}{k_bTV}\int_0^{+\infty} dt \lim_{k\to 0}\left\{\frac{m^2}{k^2} < \frac{\partial j_t^*(\mathbf{k},t)}{\partial t}\Big|_{t=0} \frac{\partial j_t(\mathbf{k},t)}{\partial t} >\right\} \\
&= \frac{N}{2k_bTV}\lim_{\omega\to 0}\lim_{k\to 0}\left\{\frac{m^2}{k^2}\int_{-\infty}^{+\infty} dt e^{i\omega t} < \frac{\partial j_t^*(\mathbf{k},t)}{\partial t}\Big|_{t=0} \frac{\partial j_t(\mathbf{k},t)}{\partial t} >\right\} \\
&= \frac{m^2N}{2k_bTV}\lim_{\omega\to 0}\lim_{k\to 0}\frac{\omega^2}{k^2}\int_{-\infty}^{+\infty} dt e^{i\omega t} < j_t^*(\mathbf{k},0) j_t(\mathbf{k},t) > \\
&= \frac{m^2N}{2k_bTV}\lim_{\omega\to 0}\lim_{k\to 0}\frac{\omega^2}{k^2} J_t(\mathbf{k},\omega) \qquad (2.36)
\end{aligned}$$

Note that in equation (2.36), we take the limit of $k \to 0$ before we take the limit of $\omega \to 0$. The order of two limits can not be changed! An alternative way to derive the last line is to Fourier transform equation (2.25) and then take the limit of low frequency and low wavenumber[27]. Set $\nu = \eta/\rho$, where ρ is the mass density and take Fourier transform of equation (2.25):

$$\frac{J_t(k,w)}{J_t(k,t=0)} = \frac{2}{\nu k^2 - i\omega} = 2\frac{\nu k^2 + i\omega}{(\nu k^2)^2 + \omega^2}$$

If we only consider the real part of the Fourier transform (i.e. the cos series):

$$\lim_{k\to 0}\frac{1}{k^2}\frac{J_t(k,w)}{J_t(k,t=0)} = \lim_{k\to 0}\frac{2}{k^2}\frac{\nu k^2 + i\omega}{(\nu k^2)^2 + \omega^2} = 2\lim_{k\to 0}\frac{\nu}{(\nu k^2)^2 + \omega^2} = \frac{2\nu}{\omega^2}$$

$$\lim_{\omega\to 0}\omega^2\lim_{k\to 0}\frac{1}{k^2}\frac{J_t(k,w)}{J_t(k,t=0)} = \lim_{\omega\to 0}\frac{2\nu\omega^2}{\omega^2} = 2\nu$$

Because $J_t(k,t=0)$ is just the constant v_0^2 which is independent of the variable k, we have

$$\lim_{\omega\to 0}\omega^2\lim_{k\to 0}\frac{J_t(k,\omega)}{k^2} = v_0^2 2\nu = \frac{2k_bT}{m}\nu = \frac{2k_bT}{m\rho}\eta = \frac{2k_bTV}{m^2N}\eta$$

This equation is well consistent with equation (2.36). Thus this is another proof for equation (2.36). Actually, if we take the limit of $\omega \to 0$ first, we have

$$\lim_{\omega\to 0} \frac{\omega^2}{k^2} \frac{J_t(k,\omega)}{J_t(k,t=0)} = \lim_{\omega\to 0} \frac{2\omega^2}{k^2} \frac{\nu k^2}{(\nu k^2)^2 + \omega^2} = \lim_{\omega\to 0} \frac{2\omega^2 \nu}{(\nu k^2)^2} = 0$$

This is the reason why we can NOT take the limit of $\omega \to 0$ before the limit of $k \to 0$.

2.2.2 Diffusion

We have already provided a detailed description of shear viscosity in terms of time correlation functions. As we have already mentioned, the similarity between equation (2.21) and (2.22) should make the formulation of diffusion follow exactly the same path that we have followed in determining shear viscosity. The momentum conservation law requires the introduction of the stress tensor, while the density conservation law is a scalar form. Due to its similarity and simplicity, we are not going to repeat the derivation in detail for the case of diffusion. Instead, we describe the close relation between diffusion and shear viscosity in Table 2.1. Note that the diffusion constant D has the same unit as the kinematic viscosity ν . All of the variables in the table have been previous defined in this section.

This section demonstrated how one can manipulate integrals to get transport properties. Actual calculations are provided in chapter 5.

Table 2.1: Comparison between diffusion and shear viscosity

Diffusion	Shear viscosity
$D = \lim_{t\to\infty} \frac{<\|\mathbf{R}_1(t) - \mathbf{R}_1(0)\|^2>}{6t}$	$\nu = \lim_{t\to\infty} \frac{<\|\mathbf{G}(t) - \mathbf{G}(0)\|^2>}{6k_bTt}$
$D = \frac{1}{2}\lim_{\omega\to 0}\lim_{k\to 0} \frac{\omega^2 J_t(k,\omega)}{J_t(k,t=0)}$	$\nu = \frac{1}{2}\lim_{\omega\to 0}\lim_{k\to 0} \frac{\omega^2 S_s(k,\omega)}{F_s(k,t=0)}$
$D = \frac{1}{6}\int_{-\infty}^{+\infty} dt \ <\mathbf{v}_1 \cdot \mathbf{v}_1(t)>$	$\nu = \frac{1}{2}\lim_{\omega\to 0}\lim_{k\to 0} \frac{\omega^2 S_s(k,\omega)}{F_s(k,t=0)}$
$D = \frac{1}{6}\int_{-\infty}^{+\infty} dt \ <\mathbf{v}_1 \cdot \mathbf{v}_1(t)>$	$\nu = \frac{1}{2Nk_bT}\int_{-\infty}^{+\infty} dt \ <\sigma_{xz}\sigma_{xz}(t)>$
$\mathbf{v}_1(t) = \lim_{k\to 0} \frac{1}{ik}\frac{\partial n_s(k,t)}{\partial t}$	$\sigma_{xz}(t) = \lim_{k\to 0} \frac{m}{ik}\frac{\partial j_t(k,t)}{\partial t}$
$\mathbf{v}_1(t) = \lim_{k\to 0} \mathbf{j}_s(\mathbf{k},t)$	$\sigma_{xz}(t) = \lim_{k\to 0} \sigma_{xz}(\mathbf{k},t)$
$\frac{\partial n_s(\mathbf{k},t)}{\partial t} = i\mathbf{k}\cdot\mathbf{j}_s(\mathbf{k},t)$	$m\frac{\partial j_\alpha(\mathbf{k},t)}{\partial t}$
$\mathbf{j}_s(\mathbf{k},t) = i\mathbf{k}Dn_s(\mathbf{k},t)$	$\sigma_{\alpha\beta} = ik_\beta \nu j_t(\mathbf{k},t)$
$\mathbf{j}_s(\mathbf{r},t) = -D\nabla n_s(\mathbf{r},t)$	$\mathbf{F}(\mathbf{r},t) = -\eta\nabla u(\mathbf{r},t)$

CHAPTER 3
LINEAR AND NONLINEAR RESPONSE THEORY

In this chapter, we are going to derive a set of equations linking the response of liquids upon an external perturbation and equilibrium time correlation functions. In general, this chapter seeks to find a perturbative solution based on equilibrium dynamics. The fundamental ideas of linear and nonlinear response have been pointed out as early as in the 1960s in statistical mechanics and nonlinear optics[77, 30]. For our own purpose, we will rederive these theories in a general fashion and illustrate them in our own cases of interest.

The construction of response theory can be based on either classical mechanics or quantum mechanics. Though nature strictly follows quantum mechanics, without any loss of intuitive information, we start from linear response theory (LRT) based on the framework of classical mechanics.

3.1 Linear Response Theory (LRT)

Assume at time $t = 0$, the system is in an equilibrium state and the system Hamiltonian is H_0. At time $t = 0$, an external perturbation is introduced and the new Hamiltonian is,

$$H(t) = H_0 - A(\mathbf{p}^N, \mathbf{R}^N)h(t) \tag{3.1}$$

where $H_0 = H(t = 0)$. Recall Livoulle equation (2.7):

$$\frac{\partial f(\mathbf{p}^N, \mathbf{R}^N, t)}{\partial t} = -i\hat{L}f(\mathbf{p}^N, \mathbf{R}^N, t)$$

where $f(\mathbf{p}^N, \mathbf{R}^N, t)$ is the number density or distribution function used to get the averaged value of an arbitrary dynamical variable:

$$< B(t) >_t = \int \cdots \int B(\mathbf{p}^N, \mathbf{R}^N) f(\mathbf{p}^N, \mathbf{R}^N, t)\, d\mathbf{p}^N d\mathbf{R}^N$$

where the time information is only included in $f(\mathbf{p}^N, \mathbf{R}^N, t)$. We may clearly write $< B(t) >_t = < B >_t$. LRT deals with how $< B(t) >$ responds under the external perturbation $H'(t) = -A(\mathbf{p}^N, \mathbf{R}^N)h(t)$. Therefore solving for $f(\mathbf{p}^N, \mathbf{R}^N, t)$ is the fundamental task in order to study the response of a dynamical variable under the external perturbation. Note that the above Liouville equation can not be written as:

$$f(\mathbf{p}^N, \mathbf{R}^N, t) \neq e^{-it\hat{L}} f(\mathbf{p}^N, \mathbf{R}^N, t = 0)$$

because $H(t)$ has both explicit and implicit dependence on the time t. We start by first writing $f(\mathbf{p}^N, \mathbf{R}^N, t)$ as the sum of the original distribution and a perturbed distribution:

$$f(\mathbf{p}^N, \mathbf{R}^N, t) = f_0(\mathbf{p}^N, \mathbf{R}^N) + f_1(\mathbf{p}^N, \mathbf{R}^N, t) = f(\mathbf{p}^N, \mathbf{R}^N, t = 0) + f_1(\mathbf{p}^N, \mathbf{R}^N, t)$$

Recall the definition of the Liouville operator and express

$$\begin{aligned} i\hat{L}^t &= i\hat{L}_0 + i\hat{L}_1^t \\ &= \sum_{j=1}^{N} (-\frac{\partial H_0}{\partial \mathbf{R}_j}\frac{\partial}{\partial \mathbf{p}_j} + \frac{\partial H_0}{\partial \mathbf{p}_j}\frac{\partial}{\partial \mathbf{R}_j}) - \sum_{j=1}^{N} (-\frac{\partial A}{\partial \mathbf{R}_j}\frac{\partial}{\partial \mathbf{p}_j} + \frac{\partial A}{\partial \mathbf{p}_j}\frac{\partial}{\partial \mathbf{R}_j})h(t) \end{aligned}$$

Insert the expression of $i\hat{L}$ and $f(\mathbf{p}^N, \mathbf{R}^N, t)$ into the above Liouville equation,

$$\begin{aligned} \frac{\partial f_0(\mathbf{p}^N, \mathbf{R}^N)}{\partial t} + \frac{\partial f_1(\mathbf{p}^N, \mathbf{R}^N, t)}{\partial t} &= -i\hat{L}_0 f_0(\mathbf{p}^N, \mathbf{R}^N) - i\hat{L}_0 f_1(\mathbf{p}^N, \mathbf{R}^N, t) \\ &\quad -i\hat{L}_1^t f_0(\mathbf{p}^N, \mathbf{R}^N) - i\hat{L}_1^t f_1(\mathbf{p}^N, \mathbf{R}^N, t) \end{aligned}$$

Here,

$$\frac{\partial f_0(\mathbf{p}^N, \mathbf{R}^N)}{\partial t} = -i\hat{L}_0 f_0(\mathbf{p}^N, \mathbf{R}^N) = 0$$

therefore,

$$\frac{\partial f_1(\mathbf{p}^N, \mathbf{R}^N, t)}{\partial t} = -i\hat{L}_0 f_1(\mathbf{p}^N, \mathbf{R}^N, t) - i\hat{L}_1^t f_0(\mathbf{p}^N, \mathbf{R}^N) - i\hat{L}_1^t f_1(\mathbf{p}^N, \mathbf{R}^N, t) \quad (3.2)$$

The assumption of LRT is that under weak perturbation ($\hat{L}_1^t$ weak, f_1 small),

$$-i\hat{L}_1^t f_1(\mathbf{p}^N, \mathbf{R}^N, t) = 0$$

Thus,

$$\frac{\partial f_1(\mathbf{p}^N, \mathbf{R}^N, t)}{\partial t} = -i\hat{L}_0 f_1(\mathbf{p}^N, \mathbf{R}^N, t) - i\hat{L}_1^t f_0(\mathbf{p}^N, \mathbf{R}^N) \quad (3.3)$$

with initial condition $f_1(\mathbf{p}^N, \mathbf{R}^N, t = 0) = 0$, where the first term of rhs is an unknown function of $\mathbf{p}^N, \mathbf{R}^N, t$ and the second term of rhs is a known function of $\mathbf{p}^N$,$\mathbf{R}^N$,and t. This equation has the form of the general first order differential equation:

$$\frac{dy(x)}{dx} = P(x)y(x) + Q(x) \quad (3.4)$$

with solution

$$y(x) = e^{P(x)x}\left[C + \int_0^x d\tau\, e^{-P(\tau)\tau} Q(\tau)\right]$$

Therefore, the solution to equation (3.3) is:

$$f_1(\mathbf{p}^N, \mathbf{R}^N, t) = e^{-it\hat{L}_0} \int_0^t d\tau\, e^{i\tau\hat{L}_0}(-i\hat{L}_1^\tau) f_0(\mathbf{p}^N, \mathbf{R}^N)$$

Take the canonical ensemble distribution function as the initial distribution function:

$$f_0(\mathbf{p}^N, \mathbf{R}^N) = \frac{e^{-\beta H_0(\mathbf{p}^N, \mathbf{R}^N)}}{Q}$$

then we have

$$\begin{aligned}
-i\hat{L}_1^{\tau} f_0(\mathbf{p}^N, \mathbf{R}^N) &= h(\tau) \sum_j (-\frac{\partial A}{\partial \mathbf{R}_j}\frac{\partial}{\partial \mathbf{p}_j} + \frac{\partial A}{\partial \mathbf{p}_j}\frac{\partial}{\partial \mathbf{R}_j}) \\
&= h(\tau) \sum_j \frac{\partial A}{\partial \mathbf{p}_j}\frac{e^{-\beta H_0}}{Q}(-\beta)\frac{\partial H_0}{\partial \mathbf{R}_j} - \frac{\partial A}{\partial \mathbf{R}_j}\frac{e^{-\beta H_0}}{Q}(-\beta)\frac{\partial H_0}{\partial \mathbf{p}_j} \\
&= -\beta\frac{e^{-\beta H_0}}{Q} h(\tau) \sum_j (\frac{\partial A}{\partial \mathbf{p}_j}\frac{\partial H_0}{\partial \mathbf{R}_j} - \frac{\partial A}{\partial \mathbf{R}_j}\frac{\partial H_0}{\partial \mathbf{p}_j}) \\
&= -\beta\frac{e^{-\beta H_0}}{Q} h(\tau)(-i\hat{L}_0 A) = \frac{\beta e^{-\beta H_0}}{Q} i\hat{L}_0 A(\mathbf{p}^N, \mathbf{R}^N) h(\tau)
\end{aligned}$$

Note here the time implicitly contained in $A(\mathbf{p}^N, \mathbf{R}^N)$ directly comes from $f(\mathbf{p}^N, \mathbf{R}^N)$, no extra or explicit time information is included. Therefore, the solution to equation (3.3) becomes,

$$f_1(\mathbf{p}^N, \mathbf{R}^N, t) = \frac{\beta e^{-\beta H_0}}{Q} \int_0^t d\tau\, e^{-i(t-\tau)\hat{L}_0} i\hat{L}_0 A(\mathbf{p}^N, \mathbf{R}^N) h(\tau)$$

And the time evolution of a dynamical quantity B of interest becomes,

$$
\begin{aligned}
< B(t) >_t &= \int\int B(\mathbf{p}^N, \mathbf{R}^N) f(\mathbf{p}^N, \mathbf{R}^N, t)\; d\mathbf{p}^N d\mathbf{R}^N \\
&= \int\int B f_0(\mathbf{p}^N, \mathbf{R}^N)\, d\mathbf{p}^N d\mathbf{R}^N + \int\int B f_1(\mathbf{p}^N, \mathbf{R}^N, t)\, d\mathbf{p}^N d\mathbf{R}^N \\
&= < B(0) > + \int\int B(\mathbf{p}^N, \mathbf{R}^N) f_1(\mathbf{p}^N, \mathbf{R}^N, t)\, d\mathbf{p}^N d\mathbf{R}^N \\
&= B_0 + \int\int d\mathbf{p}^N d\mathbf{R}^N \frac{\beta e^{-\beta H_0}}{Q} B(\mathbf{p}^N, \mathbf{R}^N) \\
&\qquad \int_0^t d\tau\, e^{-i(t-\tau)\hat{L}_0} i\hat{L}_0 A(\mathbf{p}^N, \mathbf{R}^N) h(\tau) \\
&= B_0 + \int\int d\mathbf{p}^N d\mathbf{R}^N \frac{\beta e^{-\beta H_0}}{Q} \\
&\qquad \int_0^t d\tau\, B(\mathbf{p}^N, \mathbf{R}^N) e^{-i(t-\tau)\hat{L}_0} i\hat{L}_0 A(\mathbf{p}^N, \mathbf{R}^N) h(\tau) \\
&= B_0 + \int\int d\mathbf{p}^N d\mathbf{R}^N \beta f_0 \\
&\qquad \int_0^t d\tau\, \left[e^{i(t-\tau)\hat{L}_0} B(\mathbf{p}^N, \mathbf{R}^N) \right] i\hat{L}_0 A(\mathbf{p}^N, \mathbf{R}^N) h(\tau) \\
&= B_0 + \beta \int\int d\mathbf{p}^N d\mathbf{R}^N\, f_0 \int_0^t d\tau\, B(t-\tau) i\hat{L}_0 A(\mathbf{p}^N, \mathbf{R}^N) h(\tau) \\
&= B_0 + \beta \int\int d\mathbf{p}^N d\mathbf{R}^N\, f_0 \int_0^t d\tau\, (-)\dot{B}(t-\tau) A(\mathbf{p}^N, \mathbf{R}^N) h(\tau) \\
&= B_0 - \beta \int_0^t d\tau \int\int d\mathbf{p}^N d\mathbf{R}^N\, \dot{B}(t-\tau) A(\mathbf{p}^N, \mathbf{R}^N) f_0(\mathbf{p}^N, \mathbf{R}^N) h(\tau) \\
&= B_0 - \beta \int_0^t d\tau \int\int d\mathbf{p}^N d\mathbf{R}^N\, \dot{B}(t-\tau) A(0) f_0 h(\tau) \\
&= B_0 + \int_0^t d\tau\, (-\beta) < \dot{B}(t-\tau) A(0) > h(\tau) \\
&= B_0 + \int_0^t d\tau\, \phi_{BA}(t-\tau) h(\tau) \qquad (3.5)
\end{aligned}
$$

where the retarded response function is defined as

$$\phi_{BA}(t-\tau) = -\beta < \dot{B}(t-\tau) A(0) >$$

Thus, equation (3.5) gives us the retarded response function (after effect function) in terms of the equilibrium average (unperturbed system average) of two dynamical

quantities. The result in equation (3.5) is quite striking given that the left hand side (lhs) is a nonequilibrium quantity while the right hand side(rhs) is a pure thermal average over the unperturbed equilibrium state.

We limited our discussion to classical mechanics in this section, it turns out that the generalization to quantum mechanics is also remarkably simple. In the next section, we will show that under the frame work of quantum mechanics, linear response theory reads as

$$< B(t) >_t - < B(0) >= \frac{i}{\hbar} \int_0^t d\tau \ < \left[\tilde{B}_0(t), \tilde{A}_0(\tau) \right] > h(\tau)$$

where $< B >= \mathrm{Tr}\{\rho_0 B\}$. For a dynamical variable B which does not explicitly depend on time, $< B(t) >_t = \mathrm{Tr}\{\rho(t) B\}$. $[\,,\,]$ represents a commutator. Heisenberg operators are defined as $\tilde{B}_0(t) = e^{iH_0 t/\hbar} B e^{-iH_0 t/\hbar}$, and $\tilde{A}_0(\tau) = e^{iH_0 \tau/\hbar} A e^{-iH_0 \tau/\hbar}$. The relation between quantum and classical expressions will be discussed in the next section.

3.2 Quantum Mechanical LRT

In this section, We are going to derive linear response theory based on the framework of quantum mechanics.

Assume the total system Hamiltonian is

$$H(t) = H_0 + H'(t)$$

where H_0 is the unperturbed Hamiltonian and $H'(t)$ is the external perturbation. The steady-state solution to an unperturbed state is described by

$$H_0 \psi_n(x) = E_n \psi_n(x)$$

and the initial probability of observing the system in the state $\psi_n(x)$ is ρ_n. An expectation value of a measurable quantity B is given by

$$< B >= \sum_n \rho_n \int \psi_n^*(x) \hat{B}(x) \psi_n(x) dx$$

where $\hat{B}(x)$ is the operator corresponding to dynamical variable B. Without loss of generality, we multiply a coefficient λ (eventually goes to 1) to the perturbation Hamiltonian:

$$H(t) = H_0 + \lambda H'(t)$$

Therefore, the purpose here is to first solve the time dependent Schrodinger equation with initial condition $\Psi(x, t = 0) = \psi_n(x)$ and then take the average over the wave function followed by another average over the initial probability ρ_n:

$$\begin{cases} i\hbar \dfrac{\partial \Psi(x,t)}{\partial t} & = & H\Psi(x,t) \\ \Psi(x, t=0) & = & \psi_n(x) \quad \text{with} \quad \text{probability} \quad \text{of} \quad \rho_n \end{cases}$$

A perturbative solution can be written as

$$\Psi(x,t) = \Psi^{(0)}(x,t) + \lambda \Psi^{(1)}(x,t) + \lambda^2 \Psi^{(2)}(x,t) + \cdots + \cdots$$

Inserting this solution into the time dependent Schrodinger equation yields the solution for each order as follows:

λ^0 zeroth order:

$$i\hbar \frac{\partial \Psi^{(0)}(x,t)}{\partial t} = H_0 \Psi^{(0)}(x,t)$$

the solution to zeroth order equation with initial condition $\Psi^{(0)}(x, t = 0) = \psi_n(x)$ is straightforward:

$$\Psi^{(0)}(x,t) = \psi_n(x) e^{-iE_n t/\hbar}$$

λ^1 first order:

$$\begin{aligned} i\hbar\frac{\partial\Psi^{(1)}(x,t)}{\partial t} &= H_0\Psi^{(1)}(x,t) + H'(t)\Psi^{(0)}(x,t) \\ &= H_0\Psi^{(1)}(x,t) + H'(t)\psi_n(x)e^{-iE_nt/\hbar} \end{aligned}$$

From the unperturbed steady-state solutions we construct the set $\{\psi_m(x), m = 1, 2, 3, \cdots\}$ which spans the whole space. The wave function $\Psi^{(1)}(x,t)$ can be written as the combination of basis set functions:

$$\Psi^{(1)}(x,t) = \sum_m C_m(t)\psi_m(x)$$

where the coefficient $C_m(t) = \int \psi_m^*(x)\Psi^{(1)}(x,t)dx$. Multiplying by $\psi_p(x)$ and then integrating over the whole space, we have

$$i\hbar\frac{dC_p(t)}{dt} = E_pC_p(t) + [H'(t)]_{pn}e^{-iE_nt/\hbar}$$

where $[H'(t)]_{pn} = \int \psi_p^*(x)H'(x,t)\psi_n(x)dx$. Noticing that the initial condition $\Psi^{(1)}(x, t = 0) = 0$, the solution to λ^1 first order equation is:

$$C_p(t) = \frac{1}{i\hbar}\int_0^t d\tau\, e^{i(E_p-E_n)\tau/\hbar}[H'(\tau)]_{pn}\, e^{-iE_pt/\hbar}$$

$$\Psi^{(1)}(x,t) = \sum_m \psi_m(x)\frac{1}{i\hbar}\int_0^t d\tau\, e^{i(E_m-E_n)\tau/\hbar}[H'(\tau)]_{mn}\, e^{-iE_mt/\hbar}$$

up to first order, the time evolution of the observable variable B is

$$
\begin{aligned}
< B(t) > \;&\simeq\; \sum_n \rho_n \int dx\, \Psi^*(x,t)\hat{B}(x)\Psi(x,t) \\
&=\; \sum_n \rho_n \int dx\, \Psi^{(0)^*}(x,t)\hat{B}(x)\Psi^{(0)}(x,t) + \\
&\quad \sum_n \rho_n \int dx\, \Psi^{(0)^*}(x,t)\hat{B}(x)\Psi^{(1)}(x,t) + \\
&\quad \sum_n \rho_n \int dx\, \Psi^{(1)^*}(x,t)\hat{B}(x)\Psi^{(0)}(x,t) \\
&=\; \sum_n \rho_n \int dx\, \psi_n^*(x)\hat{B}(x)\psi_n(x)\, dx + \\
&\quad \sum_n \rho_n \int dx\, \psi_n^*(x) e^{iE_n t/\hbar}\hat{B}(x) \\
&\qquad \sum_m \psi_m(x)\frac{1}{i\hbar}\int_0^t d\tau\, e^{i(E_m-E_n)\tau/\hbar}[H'(\tau)]_{mn}e^{-iE_m t/\hbar} + \\
&\quad \sum_n \rho_n \int dx\, \psi_m^*(x)\frac{-1}{i\hbar}\int_0^t e^{-i(E_m-E_n)\tau/\hbar}[H'(\tau)]_{nm}d\tau \\
&\qquad e^{iE_m t/\hbar}\hat{B}(x)\psi_n(x)e^{-iE_n t/\hbar}
\end{aligned}
$$

$$
\begin{aligned}
< B(t) > \;&=\; \sum_n \rho_n B_{nn} + \sum_n\sum_m \rho_n B_{nm}\frac{1}{i\hbar}e^{i(E_n-E_m)t/\hbar}\int_0^t d\tau\, e^{i(E_m-E_n)\tau)/\hbar}[H'(\tau)]_{mn} \\
&\quad -\sum_n\sum_m \rho_n B_{mn}e^{i(E_m-E_n)t/\hbar}\int_0^t d\tau\, e^{i(E_n-E_m)\tau)/\hbar}[H'(\tau)]_{nm} \\
&=\; \sum_n \rho_n B_{nn} + \\
&\quad \sum_n\sum_m (\rho_n-\rho_m)B_{nm}e^{i(E_n-E_m)t/\hbar}\frac{1}{i\hbar}\int_0^t d\tau\, e^{i(E_m-E_n)\tau/\hbar}[H'(\tau)]_{mn} \\
&=\; \sum_n \rho_n B_{nn} + \sum_n\sum_m (\rho_n-\rho_m)\frac{1}{i\hbar}\int_0^t d\tau\, [\tilde{B}(t)]_{nm}[\tilde{H}'(\tau)]_{mn} \\
&=\; \sum_n \rho_n B_{nn} + \\
&\quad \sum_n\sum_m \frac{1}{i\hbar}\int_0^t d\tau\, \rho_n([\tilde{B}(t)]_{nm}[\tilde{H}'(\tau)]_{mn} - [\tilde{H}'(\tau)]_{nm}[\tilde{B}(t)]_{mn}) \\
&=\; \sum_n \rho_n B_{nn} + \frac{1}{i\hbar}\int_0^t d\tau\, < [\tilde{B}(t),\tilde{H}'(\tau)] >
\end{aligned}
$$

where we have used $[H'(\tau)]^*_{nm} = [H'(\tau)]_{nm}$ and the average is taken over the equilibrium wavefunction $\psi_n(x)$ with initial probability ρ_n. Variables $\tilde{H}$ and $\tilde{B}$ are the usual Heisenberg picture operators:

$$\tilde{H} = e^{iH_0 t/\hbar} H e^{-iH_0 t/\hbar}$$

$$\tilde{B} = e^{iH_0 t/\hbar} \hat{B} e^{-iH_0 t/\hbar}$$

and the matrix element

$$\begin{aligned}
[\tilde{B}(t)]_{mn} &= \int dx\, \psi^*_m(x) \tilde{B}(t) \psi_n(x) \\
&= \int dx\, \psi^*_m(x) e^{iH_0 t/\hbar} \hat{B} e^{-iH_0 t/\hbar} \psi_n(x) \\
&= \int dx\, e^{i(E_m - E_n)t/\hbar} \psi^*_m(x) \hat{B} \psi_n(x) \\
&= e^{i(E_m - E_n)t/\hbar} B_{mn} \qquad (3.6)
\end{aligned}$$

The retarded response function ϕ is defined as

$$\phi_{AB}(t-\tau) = \frac{1}{i\hbar} < [\tilde{B}(t), \tilde{H}'(\tau)] > \qquad (3.7)$$

Hence we have derived linear response theory based on quantum mechanics. One point we can not avoid now is the relation between the classical and quantum versions of LRT. The intrinsic similarity is clear if we introduce the Kubo transform[45].

$$\phi_{AB}(t) = \int_0^\beta d\lambda < \dot{B}(-i\hbar\lambda) A(t) >_0$$

In the classical limit of $\hbar \to 0$:

$$\begin{aligned}
\phi_{AB}(t) &= \int_0^\beta d\lambda < \dot{B}(-i\hbar\lambda)A(t) >_0 \\
&= < \int_0^\beta d\lambda(-i\hbar\lambda)A(t) >_0 \\
&= < \dot{B}(0) \int_0^\beta d\lambda A(t) >_0 \\
&= \beta < \dot{B}(0)A(t) >_0
\end{aligned}$$

which is precisely the classical version of linear response theory. In the case of quantum mechanics:

$$\begin{aligned}
\dot{B}(t) &= \frac{1}{i\hbar}[B(t), H_0] = \frac{1}{i\hbar}[e^{iH_0t/\hbar}B(0)e^{-iH_0t/\hbar}, H_0] \\
&= \frac{1}{i\hbar}(e^{iH_0t/\hbar}B(0)e^{-iH_0t/\hbar}H_0 - H_0e^{iH_0t/\hbar}B(0)e^{-iH_0t/\hbar}) \\
&= \frac{1}{i\hbar}\left(e^{iH_0t/\hbar}(B(0)H_0 - H_0B(0))e^{-iH_0t/\hbar}\right)
\end{aligned}$$

$$
\begin{aligned}
\phi_{AB}(t) &= \int_0^\beta d\lambda < \dot{B}(-i\hbar\lambda)A(t) >_0 \\
&= < \frac{1}{i\hbar}\int_0^\beta d\lambda \left(e^{iH_0(-i\hbar\lambda)/\hbar)}(B(0)H_0 - H_0B(0))e^{-iH_0(-i\hbar\lambda)/\hbar}A(t)\right) > \\
&= \frac{1}{i\hbar} < \int_0^\beta d\lambda e^{H_0\lambda}(B(0)H_0 - H_0B(0))e^{-H_0\lambda}A(t) > \\
&= \frac{1}{i\hbar}\frac{1}{Q}\int_0^\beta d\lambda \sum_n \int dx \psi_n^*(x)e^{-\beta H_0}e^{H_0\lambda}[B(0), H_0]e^{-H_0\lambda}A(t)\psi_n(x) \\
&= \frac{1}{i\hbar}\frac{1}{Q}\int_0^\beta d\lambda \sum_n \sum_m e^{-\beta E_n}e^{\lambda E_n}e^{-\lambda E_m}\int dx\, \psi_n^*(x)[B(0), H_0]\psi_m(x) \\
&\qquad \int dx\, \psi_m^*(x)A(t)\psi_n(x) \\
&= \frac{1}{iQ\hbar}\sum_{n,m}\frac{e^{\beta(E_n-E_m)}-1}{E_n - E_m}e^{-\beta E_n} \\
&\qquad \int dx\, \psi_n^*(x)[B(0), H_0]\psi_m(x)\int dx\, \psi_m^*(x)A(t)\psi_n(x) \\
&= \frac{1}{iQ\hbar}\sum_{n,m}\frac{e^{\beta(E_n-E_m)}-1}{E_n - E_m}e^{-\beta E_n}(E_m - E_n)B_{nm}[A(t)]_{mn} \\
&= \frac{i}{Q\hbar}\sum_{n,m}(e^{-\beta E_m} - e^{-\beta E_n})B_{nm}[A(t)]_{mn} \\
&= \frac{i}{Q\hbar}\sum_{n,m}(e^{-\beta E_m}[A(t)]_{mn}B_{nm} - e^{-\beta E_n}B_{nm}[A(t)]_{mn}) \\
&= \frac{i}{Q\hbar}(\sum_m e^{-\beta E_m}[A(t)B]_{mm} - \sum_n e^{-\beta E_n}[BA(t)]_{nn}) \\
&= \frac{i}{Q\hbar}\sum_n e^{-\beta E_n}\int dx\, \psi_n^*(x)[A(t)B(0) - B(0)A(t)]\psi_n(x) \\
&= \frac{i}{\hbar}\sum_n \int dx \frac{e^{-\beta E_n}}{Q}\psi_n^*(x)[A(t), B(0)]\psi_n(x) \\
&= \frac{i}{\hbar} < [A(t), B(0)] >_0
\end{aligned}
$$

which is equivalent to the previous definition (3.7) of the retarded response function given an external perturbation $H' = -Ah(t)$ in case of quantum mechanics. Therefore, using the Kubo transform we see that the classical version of linear response theory is just the $\hbar \to 0$ limit of quantum mechanical theory.

In order to write the formulation in a simpler form, we introduce the definition of density matrix. In general, consider a system having a probability ρ_n in state $\Psi(x,t;n)$, the density matrix is formed by

$$\rho_{pm} = \sum_n \rho_n \int dx\, \psi_p^*(x)\Psi(x,t;n) \int dx\, \Psi^*(x,t;n)\psi_m(x)$$

Furthermore, up to first order in λ, for the case of perturbation just mentioned, we

have

$$
\begin{aligned}
[\rho(t)]_{pm} &\simeq \sum_n \rho_n \int dx\, \psi_p^*(x)\Psi^{(0)}(x,t) \int dx\, \Psi^{(0)^*}(x,t)\psi_m(x) \\
&\quad + \sum_n \rho_n \int dx\, \psi_p^*(x)\Psi^{(1)}(x,t) \int dx\, \Psi^{(0)^*}(x,t)\psi_m(x) \\
&\quad + \sum_n \rho_n \int dx\, \psi_p^*(x)\Psi^{(0)}(x,t) \int dx\, \Psi^{(1)^*}(x,t)\psi_m(x) \\
&= \sum_n \rho_n \int dx\, \psi_p^*(x)\psi_n(x)e^{-iE_nt/\hbar} \int dx\, \psi_n^*(x)e^{iE_nt/\hbar}\psi_m(x) + \\
&\quad + \sum_n \rho_n \int dx\, \psi_p^*(x) \sum_q \psi_q(x)\frac{1}{i\hbar}\int_0^t d\tau\, e^{i(E_q-E_n)\tau/\hbar}[H'(\tau)]_{qn}e^{-iE_qt/\hbar}\cdot \\
&\quad \cdot \int dx\, \psi_n^*(x)e^{iE_nt/\hbar}\psi_m(x) \\
&\quad + \sum_n \rho_n \int dx\, \psi_p^*(x)\psi_n(x)e^{-iE_nt/\hbar} \int dx\, \sum_q \psi_q^*(x)\frac{-1}{i\hbar}\cdot \\
&\quad \cdot \int_0^t d\tau\, e^{-i(E_q-E_n)\tau/\hbar}[H'(\tau)]_{nq}e^{iE_qt/\hbar}\psi_m(x) \\
&= \sum_n \rho_n\delta_{pn}\delta_{nm} + \sum_n\sum_q \rho_n\delta_{pq}\delta_{nm}\frac{1}{i\hbar}\int_0^t d\tau\, e^{i(E_q-E_n)\tau/\hbar}[H'(\tau)]_{qn}e^{i(E_n-E_q)t/\hbar} \\
&\quad \sum_n\sum_q \rho_n\delta_{pn}\delta_{qm}\frac{-1}{i\hbar}\int_0^t e^{-i(E_q-E_n)\tau/\hbar}[H'(\tau)]_{nq}e^{i(E_q-E_n)t/\hbar} \\
&= \sum_n \rho_n\delta_{pn}\delta_{nm} + \sum_n\sum_q \rho_n\delta_{pq}\delta_{nm}\frac{1}{i\hbar}\int_0^t d\tau\, e^{i(E_q-E_n)\tau/\hbar}[H'(\tau)]_{qn}e^{i(E_n-E_q)t/\hbar} \\
&\quad + \sum_n\sum_q \rho_q\delta_{pq}\delta_{nm}\frac{-1}{i\hbar}\int_0^t d\tau\, e^{i(E_q-E_n)\tau/\hbar}[H'(\tau)]_{qn}e^{i(E_n-E_q)t/\hbar} \\
&= \rho_p\delta_{pm} + \rho_m\frac{1}{i\hbar}\int_0^t d\tau\, e^{i(E_p-E_m)\tau/\hbar}[H'(\tau)]_{pm}e^{i(E_m-E_p)t/\hbar} \\
&\quad -\rho_p\int_0^t d\tau\, e^{i(E_p-E_m)\tau/\hbar}[H'(\tau)]_{pm}e^{i(E_m-E_p)t/\hbar} \\
&= \rho_p\delta_{pm} + (\rho_m-\rho_p)\frac{1}{i\hbar}e^{i(E_m-E_p)t/\hbar}\int_0^t d\tau\, e^{i(E_p-E_m)\tau/\hbar}[H'(\tau)]_{pm} \qquad (3.8)
\end{aligned}
$$

Therefore, the time evolution of observable variable B is

$$\begin{aligned}
< B(t) > &= \mathrm{Tr}(\rho_o \hat{B}) + \sum_n \sum_m (\rho_n - \rho_m) B_{nm} e^{i(E_n - E_m)t/\hbar} \cdot \\
&\qquad \cdot \frac{1}{i\hbar} \int_0^t d\tau \, e^{i(E_m - E_n)\tau/\hbar} [H'(\tau)]_{mn} \\
&= \mathrm{Tr}(\rho_o \hat{B}) + \sum_n \sum_m (\rho_m - \rho_n) B_{mn} e^{i(E_m - E_n)t/\hbar} \cdot \\
&\qquad \cdot \frac{1}{i\hbar} \int_0^t d\tau \, e^{i(E_n - E_m)\tau/\hbar} [H'(\tau)]_{nm} \\
&= \sum_p \sum_m \rho_p \delta_{pm} B_{mp} + \sum_p \sum_m (\rho_m - \rho_p) e^{i(E_m - E_p)t/\hbar} \cdot \\
&\qquad \cdot \frac{1}{i\hbar} \int_0^t d\tau \, e^{i(E_p - E_m)\tau/\hbar} [H'(\tau)]_{pm} B_{mp} \\
&= \sum_p \sum_m [\rho(t)]_{pm} B_{mp} = \sum_p (\sum_m [\rho(t)]_{pm} B_{mp}) = \mathrm{Tr}[\hat{\rho}(t)\hat{B}]
\end{aligned}$$

It turns out that the time evolution of dynamical variable $B(t)$ can be completely derived from the formulation of density matrix instead of wave functions. Clearly, the derivation from the density matrix formulation is simpler because the average over wavefunction on the n-th order involves both $\Psi^{(n)}(x,t)$ and its complex conjugate $\Psi^{(n)^*}(x,t)$, while the density matrix formulation on the n-th order only has one term of $\rho^{(n)}$. Thus, construction of nonlinear response theory using the frame work of quantum mechanics will be purely based on the density matrix. We will also see that the linear response formulation is just the simplest case where $n = 1$.

In closing this section of linear response theory, we have derived the response of the system upon an external weak perturbation based on the framework of quantum mechanics and the resulting formulation agrees with the classical mechanics version explained in the previous section by introducing the Kubo transform.

3.3 Dynamical Susceptibility

We have studied the response of a material upon an external perturbation based on the time evolution of a time correlation function. Because the usual perturbation is commonly associated with a certain frequency, it is instructive to study the response in frequency domain. For completeness, we provide this theory and make the connection to the previously studied time correlation functions. We first denote the Poisson bracket as,

$$\{A, B\} = \sum_{q=1}^{N} \left(\frac{\partial A}{\partial \mathbf{R}_q} \cdot \frac{\partial B}{\partial \mathbf{p}_q} - \frac{\partial A}{\partial \mathbf{p}_q} \cdot \frac{\partial B}{\partial \mathbf{R}_q} \right) = \sum_{q=1}^{N} \left(\nabla_{\mathbf{R}_q} A \cdot \nabla_{\mathbf{p}_q} B - \nabla_{\mathbf{p}_q} A \cdot \nabla_{\mathbf{R}_q} B \right)$$

Through integration by parts, we can prove an important identity,

$$\int \int d\mathbf{R}^N d\mathbf{p}^N \; \{A, B\} \, C = \int \int d\mathbf{R}^N d\mathbf{p}^N \; \{C, A\} \, B \tag{3.9}$$

For simplicity, we only write down the two dimension case,

$$\begin{aligned}
\int\int dpdq\,\{A,B\}C &= \int\int dpdq\left(\frac{\partial A}{\partial q}\cdot\frac{\partial B}{\partial p}-\frac{\partial A}{\partial p}\cdot\frac{\partial B}{\partial q}\right)C \\
&= \int\int dpdq\,\frac{\partial A}{\partial q}\cdot\frac{\partial B}{\partial p}C-\int\int dpdq\,\frac{\partial A}{\partial p}\cdot\frac{\partial B}{\partial q}C \\
&= \int dq\int dp\,\frac{\partial A}{\partial q}\cdot\frac{\partial B}{\partial p}C-\int dp\int dq\,\frac{\partial A}{\partial p}\cdot\frac{\partial B}{\partial q}C \\
&= \int dq\int \partial B\frac{\partial A}{\partial q}C-\int dp\int \partial B\frac{\partial A}{\partial p}C \\
&= \int dq\left[B\frac{\partial A}{\partial q}C\Big|_{-\infty}^{+\infty}-\int dp\,B\frac{\partial A}{\partial q}\cdot\frac{\partial C}{\partial p}-\int dp\,B\frac{\partial^2 A}{\partial q\partial p}C\right]- \\
&\quad \int dp\left[B\frac{\partial A}{\partial p}C\Big|_{-\infty}^{+\infty}-\int dq\,B\frac{\partial A}{\partial p}\cdot\frac{\partial C}{\partial q}-\int dq\,B\frac{\partial^2 A}{\partial q\partial p}C\right] \\
&= \int dq\left[-\int dp\,B\frac{\partial A}{\partial q}\cdot\frac{\partial C}{\partial p}-\int dp\,B\frac{\partial^2 A}{\partial q\partial p}C\right]- \\
&\quad \int dp\left[-\int dq\,B\frac{\partial A}{\partial p}\cdot\frac{\partial C}{\partial q}-\int dq\,B\frac{\partial^2 A}{\partial q\partial p}C\right] \\
&= \int\int dqdp\,B\left(\frac{\partial C}{\partial q}\cdot\frac{\partial A}{\partial p}-\frac{\partial C}{\partial p}\cdot\frac{\partial A}{\partial q}\right) \\
&\quad -\int\int dqdp\left(BC\frac{\partial^2 A}{\partial q\partial p}-BC\frac{\partial^2 A}{\partial q\partial p}\right) \\
&= \int\int dqdp\left(\frac{\partial C}{\partial q}\cdot\frac{\partial A}{\partial p}-\frac{\partial C}{\partial p}\cdot\frac{\partial A}{\partial q}\right)B \\
&= \int\int dpdq\,\{C,A\}B
\end{aligned}$$

Therefore, from the last line of equation (3.5), we have the following expression:

$$\begin{aligned}
\phi_{BA}(t) &= -\beta<\dot{B}(t),A>=\beta<B(t)\dot{A}>=\beta\int\int \dot{A}f_0B(t)d\mathbf{R}^Nd\mathbf{p}^N \\
&= -\int\int\{A,f_0\}B(t)d\mathbf{R}^Nd\mathbf{p}^N=-\int\int\{B(t),A\}f_0d\mathbf{R}^Nd\mathbf{p}^N \\
&= -<\{B(t),A\}>
\end{aligned}$$

where $\{A, f_0\} = -\beta \dot{A} f_0$. By taking f_0 as the canonical ensemble distribution function $f_0 = e^{-\beta H_0}/Q$, the general equality

$$\beta < \dot{B}(t)A >=< \{B(t), A\} >$$

is the generalization of Yvon equation for an arbitrary dynamical variable A and the potential of the system $V(\mathbf{R}^N)$ [29]

$$< A(\mathbf{R}^N, \mathbf{v}^N) \frac{\partial V(\mathbf{R}^N)}{\partial x_q} >= \frac{1}{\beta} < \frac{\partial A(\mathbf{R}^N, \mathbf{v}^N)}{\partial x_q} >$$

Considering $h(t)$ as of the form $h(t) = h_0 e^{-i(\omega + i\epsilon)t}$, the response defined by equation (3.5) can be written as:

$$\begin{aligned}
< \delta B >_t &= \int_{-\infty}^{t} \phi_{BA}(t-\tau) h(\tau)\, d\tau = \int_{-\infty}^{t} \phi_{BA}(t-\tau) h_0 e^{-i(\omega+i\epsilon)\tau}\, d\tau \\
&= h_0 e^{-i(\omega+i\epsilon)t} \int_{-\infty}^{t} \phi_{BA}(t-\tau) e^{i(\omega+i\epsilon)(t-\tau)}\, d\tau \\
&= h_0 e^{-i(\omega+i\epsilon)t} \int_{0}^{\infty} \phi_{BA}(t) e^{i(\omega+i\epsilon)t}\, dt \\
&= h_0 e^{-i(\omega+i\epsilon)t} \int_{0}^{\infty} \phi_{BA}(t) e^{izt}\, dt = h_0 e^{-i(\omega+i\epsilon)t} \chi_{BA}(z)
\end{aligned}$$

where the last line gives the definition for the complex susceptibility as:

$$\chi_{BA}(z) = \int_0^\infty \phi_{BA}(t) e^{izt}\, dt \qquad z = \omega + i\epsilon \quad (\epsilon > 0).$$

We can take the limit of $\epsilon \to 0^+$ to get the frequency domain function as,

$$\chi_{BA}(\omega) = \lim_{\epsilon \to 0^+} \chi_{BA}(z) = \lim_{\epsilon \to 0^+} \int_0^\infty dt \phi_{BA}(t) e^{i(\omega+i\epsilon)t} \tag{3.10}$$

The integral over the function $e^{i\omega t}$ may diverge theoretically, that is why we have to introduce a complex susceptibility and use its analyticity on the upper complex plane

and real axis. We have already introduced the definition of Fourier transform and Laplace transform for the time correlation function $C_{BA}(t)$. In general:

$$C_{BA}(w) = \int_{-\infty}^{\infty} dt\, C_{BA}(t) e^{i\omega t} \qquad \tilde{C}_{BA}(z) = \int_{0}^{\infty} dt\, C_{BA}(t) e^{izt}$$

Here, we use $\chi_{BA}(z)$ instead of $\tilde{\chi}(z)$ for simplicity. In case of $A = B$, the spectrum of the auto correlation function $C_{AA}(t)$ is always a real, even function of ω,

$$C_{AA}(\omega) = 2 \lim_{\epsilon \to 0} Re \tilde{C}_{AA}(z) \tag{3.11}$$

In general, the relation between Fourier transform and Laplace transform is:

$$\begin{aligned}
\tilde{C}_{AB}(z) &= \int_0^\infty e^{izt} C_{AB}(t) dt = \int_0^\infty dt\, e^{izt} \frac{1}{2\pi} \int_{-\infty}^{\infty} e^{-i\omega' t} C_{AB}(\omega') d\omega' \\
&= \frac{1}{2\pi} \int_{-\infty}^{\infty} d\omega'\, C_{AB}(\omega') \int_0^\infty e^{i(z-\omega')t}\, dt \\
&= \frac{1}{2\pi} \int_{-\infty}^{\infty} d\omega'\, C_{AB}(\omega') \frac{-1}{i(z-\omega')} \\
&= \frac{i}{2\pi} \int_{-\infty}^{\infty} \frac{C_{AB}(\omega')}{z-\omega'} d\omega' = \frac{i}{2\pi} \int_{-\infty}^{\infty} \frac{C_{AB}(\omega')}{\omega + i\epsilon - \omega'}\, d\omega'
\end{aligned} \tag{3.12}$$

where $z = \omega + i\epsilon$ with $\epsilon \geqslant 0$.

Now we study the properties of the complex susceptibility. We start from the retarded response function or after effect function:

$$\phi(t) = -\beta < \dot{B}(t) A >= -\beta < A \dot{B}(t) >= -\beta \dot{C}_{AB}(t)$$

Taking the Laplace transform and using equation (3.12),

$$\begin{aligned}
\chi_{BA}(z) &= -\beta(-iz)\tilde{C}_{AB}(z) + \beta C_{AB}(t=0) \\
&= i\beta z \frac{i}{2\pi}\int_{-\infty}^{\infty}\frac{C_{AB}(\omega')}{z-\omega'}d\omega' + \beta C_{AB}(t=0) \\
&= \frac{-\beta}{2\pi}\int_{-\infty}^{\infty}\frac{zC_{AB}(\omega')}{z-\omega'} + \frac{\beta}{2\pi}\int_{-\infty}^{\infty}C_{AB}(\omega')d\omega' \\
&= \frac{-\beta}{2\pi}\int_{-\infty}^{\infty}\frac{(z+\omega'-z)C_{AB}(\omega')}{z-\omega'}d\omega' = \frac{-\beta}{2\pi}\int_{-\infty}^{\infty}\frac{\omega' C_{AB}(\omega')}{z-\omega'}d\omega' \\
&= \frac{-\beta}{2\pi}\int_{-\infty}^{\infty}\frac{\omega' C_{AB}(\omega')}{\omega-\omega'+i\epsilon}d\omega'
\end{aligned}$$

Taking the limit of $\epsilon \to 0^+$, using equation (3.10), and considering the standard relation:

$$\lim_{\sigma\to 0}\frac{1}{x-i\sigma} = \mathcal{P}\left(\frac{1}{x}\right) + i\pi\delta(x) \tag{3.13}$$

where $\mathcal{P}$ denotes the principal part, we have

$$\begin{aligned}
\chi_{AB}(\omega) &= \frac{-\beta}{2\pi}\mathcal{P}\int_{-\infty}^{\infty}\frac{\omega' C_{AB}(\omega')}{\omega-\omega'}d\omega' + \frac{-\beta}{2\pi}(-i\pi)\int_{-\infty}^{\infty}\omega' C_{AB}(\omega')\delta(\omega-\omega')d\omega' \\
&= \frac{\beta}{2\pi}\mathcal{P}\int_{-\infty}^{\infty}\frac{\omega' C_{AB}(\omega')}{\omega'-\omega}d\omega' + \frac{\beta\omega}{2}C_{AB}(\omega) = \chi'_{AB}(\omega) + i\chi''_{AB}(\omega)
\end{aligned}$$

where χ'_{BA} and χ''_{BA} are the real and imaginary parts of $\chi_{BA}(\omega)$ respectively. We usually call the imaginary part $\chi''_{BA}(\omega)$ the response function based on the following relations:

$$\chi''_{BA}(\omega) = \frac{\beta\omega}{2}C_{AB}(\omega) \qquad \chi'_{BA}(\omega) = \frac{\beta}{2\pi}\mathcal{P}\int_{-\infty}^{\infty}\frac{\omega' C_{AB}(\omega')}{\omega'-\omega}d\omega' = \frac{1}{\pi}\mathcal{P}\int_{-\infty}^{\infty}\frac{\chi''_{BA}(\omega')}{\omega'-\omega}d\omega'$$

Here, I have implicitly used that $C_{AB}(\omega)$ is a real function which is the case for sure when $A = B$.

From the definition of $\chi_{BA}(\omega)$ (equation (3.10) with $e^{i\omega t} = \cos(\omega t) + i\sin(\omega t)$, $\cos, \sin$ are even and odd function respectively), we know that the real part is an even

function and the imaginary part is an odd function,

$$\chi_{BA}(-\omega) = \chi'_{BA}(-\omega) + i\chi''_{BA}(-\omega) = \chi'_{BA}(\omega) - i\chi''_{BA}(\omega)$$

Considering that $\chi_{BA}(z)$ is analytical in the upper half of the complex plane and in the real axis, the integral

$$Int = \int_{-\infty}^{\infty} \frac{\chi_{BA}(z')}{z' - \omega}\, dz \equiv \lim_{\sigma \to 0^+} \left[\int_{-\infty}^{\omega - \sigma} \frac{\chi_{BA}(z')}{z' - \omega}\, dz + \int_{\omega + \sigma}^{\infty} \frac{\chi_{BA}(z')}{z' - \omega}\, dz \right]$$

This is the usual convention in which the integral $\int_{-\infty}^{\infty}$ is given by taking the Cauchy principal value of the integral. Following the same steps as in page 57 of reference [9], we have,

$$\chi_{BA}(w) = \frac{1}{i\pi} \int_{-\infty}^{\infty} \frac{\chi_{BA}(\omega')}{\omega' - \omega}\, d\omega' = \frac{1}{\pi} \int_{-\infty}^{\infty} \frac{\chi''_{BA}(\omega')}{\omega' - \omega}\, d\omega' - \frac{i}{\pi} \int_{-\infty}^{\infty} \frac{\chi'_{BA}(\omega')}{\omega' - \omega}\, d\omega'$$

therefore, we arrive at the Kramers-Kronig relations:

$$\chi'_{BA}(w) = \frac{1}{\pi} \int_{-\infty}^{\infty} \frac{\chi''_{BA}(\omega')}{\omega' - \omega}\, d\omega' \qquad \chi''_{BA}(\omega) = -\frac{1}{\pi} \int_{-\infty}^{\infty} \frac{\chi'_{BA}(\omega')}{\omega' - \omega}\, d\omega'$$

Here the integrals are all principal values resulting from taking a limit at the point with singularity. The above relation is perfectly consistent with the previous expression we derived for $\chi'_{BA}(w)$.

In closing this short section, we studied the dynamical susceptibility in the frequency domain of the retarded response function. Although, we did not explicitly use the property of dynamical susceptibility in our own research of the response of ionic liquids to external perturbations, this short section makes the elegant linear response theory complete and therefore provides a background for future research.

3.4 Nonlinear Response Theory

The previous sections explained the elegant linear response theory in a variety of ways. Now we extend the theory to the general nonlinear response case up to n-th order directly based on the density matrix formulation of quantum mechanics. For our own case of interest, we use the example of optical perturbation to illustrate the theory based on the Born-Oppenheimer (B.O.) approximation.

We assume that the system has its total wave function $\Psi(x,t;j)$ with probability of ρ_j. The basis set used is that generated by the unperturbed steady-state solution $\{\psi_m(x), m = 1, 2, \cdots, \}$. Therefore, we express the total wavefunction in terms of a combination of the basis set functions:

$$\Psi(x,t;j) = \sum_m C_{jm}(t)\psi_m(x)$$

where the coefficient $C_{jm}(t)$ is defined as

$$C_{jm}(t) = \int dx\, \psi_m^*(x)\Psi(x,t;j)$$

The elements of density matrix are defined as

$$\begin{aligned}[\hat{\rho}(t)]_{nm} &= \sum_j \rho_j \int dx\, \psi_n^*(x)\Psi(x,t;j) \int dx\, \Psi^*(x,t;j)\psi_m(x) \\ &= \sum_j \rho_j C_{jn}(t) C_{jm}^*(t)\end{aligned}$$

In general, the time evolution of a dynamical variable A can be written as:

$$\begin{aligned}
< A >_t &= \sum_j \rho_j \int dx \Psi^*(x,t;j)\hat{A}(x)\Psi(x,t;j) \\
&= \sum_j \rho_j \sum_m \sum_n \int dx\, C^*_{jm}(t)\psi^*_m(x)\hat{A}(x) \int dx\, C_{jn}(t)\psi_n(x) \\
&= \sum_j \rho_j \sum_m \sum_n C^*_{jm}(t)C_{jn}(t) \int dx\, \psi^*_m(x)\hat{A}(x)\psi_n(x) \\
&= \sum_m \sum_n \sum_j \rho_j C^*_{jm}(t)C_{jn}(t)A_{mn} \\
&= \sum_m \sum_n [\hat{\rho}(t)]_{nm}A_{mn} = \sum_n \left(\sum_m [\hat{\rho}]_{nm}A_{mn} \right) \\
&= \sum_n [\hat{\rho}(t)\hat{A}]_{nn} = \mathrm{Tr}[\hat{\rho}(t)\hat{A}]
\end{aligned}$$

Note that there is no approximation in deriving the above equation. Therefore, the time evolution of a dynamical variable can be studied by looking at the trace of the product of Schrodinger operator $\hat{A}$ and the representative density matrix of the system $\hat{\rho}(t)$. Using the wave function representation of linear response theory, we have already derived the first order equation

$$[\hat{\rho}(t)]_{pm} = \rho_p\delta_{pm} + (\rho_m - \rho_p)\frac{1}{i\hbar}\int_0^t d\tau e^{i(E_p-E_m)\tau/\hbar}[H'(\tau)]_{pm}e^{i(E_m-E_p)t/\hbar}$$

given an initial condition $[\hat{\rho}(t=0)]_{pm} = \rho_p\delta_{pm}$. Now we are going to derive the time evolution of the density matrix without using the wavefunction explicitly. We will see above result from section 3.2 is just a special case of a first order approximation. An explicit differentiation of the expansion coefficient gives

$$\begin{aligned}
\frac{dC_{jn}(t)}{dt} &= \int dx\, \psi^*_n(x)\frac{\partial\Psi(x,t;j)}{\partial t} \\
&= \frac{1}{i\hbar}\int dx\, \psi^*_n(x)H(x,t)\Psi(x,t;j)
\end{aligned}$$

Thus the first derivative of the density matrix element is:

$$\begin{aligned}
\frac{d}{dt}[\hat{\rho}(t)]_{nm} &= \sum_j \rho_j \frac{1}{i\hbar}\int dx\, \psi_n^*(x) H(x,t)\Psi(x,t;j)C_{jm}^*(t) \\
&\quad + \sum_j \rho_j \frac{-1}{i\hbar}\int dx\, \Psi^*(x,t;j) H(x,t)\psi_m(x)C_{jn}(t) \\
&= \sum_j \rho_j \frac{1}{i\hbar}\int dx\, \psi_n^*(x) H \sum_p C_{jp}(t)\psi_p(x)C_{jm}^*(t) \\
&\quad - \sum_j \rho_j \frac{1}{i\hbar}\int dx\, \sum_p C_{jp}^*(t)\psi_p^*(x) H(x,t)\psi_m(x)C_{jn}(t) \\
&= \sum_j \sum_p \frac{\rho_j}{i\hbar} C_{jp}(t)C_{jm}^*(t)\int dx\, \psi_n^*(x) H(x,t)\psi_p(x) \\
&\quad - \sum_j \sum_p \frac{\rho_j}{i\hbar} C_{jn}(t)C_{jp}^*(t)\int dx\, \psi_p^*(x) H(x,t)\psi_m(x) \\
&= \frac{1}{i\hbar}\sum_p \{[\hat{\rho}(t)]_{pm}[H(t)]_{np} - [\hat{\rho}(t)]_{np}[H(t)]_{pm}\} \\
&= \frac{-1}{i\hbar}\sum_p ([\hat{\rho}(t)]_{np}[H(t)]_{pm} - [H(t)]_{np}[\hat{\rho}(t)]_{pm}) \\
&= \frac{-1}{i\hbar}([\hat{\rho}(t)H(t)]_{nm} - [H(t)\hat{\rho}(t)]_{nm})
\end{aligned}$$

Therefore, the time evolution of the density matrix is:

$$\dot{\rho}_{nm}(t) = \frac{-1}{i\hbar}[\hat{\rho}(t), H(t)]_{nm}$$

where $[,]$ is the communicator operation. This is the general law governing the time evolution of the density operator for a system in a mixture of states $\Psi(x,t;j)$ with probability ρ_j. The role of this equation is equivalent to the Schrodinger equation for the wavefunction. It is clear that the entire dynamics of the system can be derived from this density matrix evolution equation instead of solving the Schrodinger equation. Now we are going to provide the perturbative solution to the density matrix.

Recall that the equation and the initial condition are

$$\begin{cases} H(x,t) &= H^0(x) + \lambda H'(x,t) \\ \dot{\rho}_{nm}(t) &= \frac{1}{-i\hbar}\sum_\nu (\rho_{n\nu}(t)H_{\nu m}(t) - H_{n\nu}(t)\rho_{\nu m}(t)) \\ \rho_{nm}(t=0) &= \rho_{nm}(0) \end{cases}$$

The perturbative solution gives

$$\rho_{nm}(t) = \rho^{(0)}_{nm}(t) + \lambda\rho^{(1)}_{nm}(t) + \lambda^2\rho^{(2)}_{nm}(t) + \lambda^3\rho^{(3)}_{nm}(t) + \cdots$$

Clearly, the zeroth order λ^0 gives

$$\begin{aligned} \dot{\rho}^{(0)}_{nm}(t) &= \frac{-1}{i\hbar}\sum_\nu (\rho^{(0)}_{n\nu}(t)H^0_{\nu m}(t) - H^0_{n\nu}(t)\rho^{(0)}_{\nu m}(t)) \\ &= \frac{-1}{i\hbar}\sum_\nu (\rho^{(0)}_{n\nu}(t)E_\nu\delta_{\nu m} - E_\nu\delta_{n\nu}\rho^{(0)}_{\nu m}(t)) \\ &= \frac{-1}{i\hbar}(\rho^{(0)}_{nm}(t)E_m - E_n\rho^{(0)}_{nm}(t)) \\ &= \frac{-1}{i\hbar}(E_m - E_n)\rho_{nm}(t) = \frac{i}{\hbar}(E_m - E_n)\rho_{nm}(t) \end{aligned}$$

with initial condition $\rho^{(0)}_{nm}(t=0) = \rho_{nm}(0)$, it is straightforward to obtain the zeroth order solution of density matrix:

$$\rho^{(0)}_{nm}(t) = \rho_{nm}(0)e^{i(E_m - E_n)t/\hbar}$$

Considering the first order of λ we have

$$\begin{aligned}
\dot{\rho}^{(1)}_{nm}(t) &= \frac{i}{\hbar}\sum_{\nu}[\rho^{(0)}_{n\nu}H'_{\nu m}(t) - H'_{n\nu}(t)\rho^{(0)}_{\nu m}(t)] \\
&\quad + \frac{i}{\hbar}\sum_{\nu}[\rho^{(1)}_{n\nu}(t)H^{0}_{\nu m} - H^{0}_{n\nu}\rho^{(1)}_{\nu m}(t)] \\
&= \frac{i}{\hbar}[\rho^{(0)}(t), H'(t)]_{nm} \\
&\quad + \frac{i}{\hbar}\sum_{\nu}[\rho^{(1)}_{n\nu}(t)E_{\nu}\delta_{\nu m} - E_{\nu}\delta_{n\nu}\rho^{(1)}_{\nu m}(t)] \\
&= \frac{i}{\hbar}[\rho^{(0)}(t), H'(t)]_{nm} + \frac{i(E_m - E_n)}{\hbar}\rho^{(1)}_{nm}(t)
\end{aligned}$$

with initial condition $\rho^{(1)}_{nm}(t=0) = 0$, the solution is given by (see the first order linear differential equation (3.4))

$$\begin{aligned}
\rho^{(1)}_{nm}(t) &= e^{i(E_m - E_n)t/\hbar}\int_0^t d\tau\, e^{-i(E_m - E_n)\tau/\hbar}\frac{i}{\hbar}[\rho^{(0)}(\tau), H'(\tau)]_{nm} \\
&= \frac{i}{\hbar}e^{i(E_m - E_n)t/\hbar}\int_0^t d\tau\, e^{-i(E_m - E_n)\tau/\hbar}[\rho^{(0)}(\tau), H'(\tau)]_{nm} \\
&= \frac{i}{\hbar}\int_0^t d\tau\, e^{i(E_m - E_n)(t-\tau)/\hbar}\sum_{\nu}[\rho^{(0)}_{n\nu}(\tau)H'_{\nu m}(\tau) - H'_{n\nu}(\tau)\rho^{(0)}_{\nu m}(\tau)]
\end{aligned}$$

For the case we deal with in linear response theory, the initial density matrix is diagonal $\rho_{nm}(0) = \rho_{nn}(0)\delta_{nm}$, therefore, the zero-th order density matrix at time t stays stationary,

$$\rho^{(0)}_{nm}(t) = \rho_{nm}(0)e^{i(E_m - E_n)t/\hbar} = \rho_{nn}(0)\delta_{nm}e^{i(E_m - E_n)t/\hbar} = \rho_{nn}(0)\delta_{nm}$$

and the first order solution goes to

$$\begin{aligned}
\rho^{(1)}_{nm}(t) &= \frac{i}{\hbar}\int_0^t d\tau\, e^{i(E_m-E_n)(t-\tau)/\hbar}\sum_\nu [\rho^{(0)}_{n\nu}(\tau)H'_{\nu m}(\tau) - H'_{n\nu}(\tau)\rho^{(0)}_{\nu m}(\tau)] \\
&= \frac{i}{\hbar}\int_0^t d\tau\, e^{i(E_m-E_n)(t-\tau)/\hbar}\sum_\nu [\rho_{nn}(0)\delta_{n\nu}H'_{\nu m}(\tau) - H'_{n\nu}(\tau)\rho_{\nu\nu}(0)\delta_{\nu m}] \\
&= \frac{i}{\hbar}\int_0^t d\tau\, e^{i(E_m-E_n)(t-\tau)/\hbar}(\rho_{nn}(0)-\rho_{mm}(0))H'_{nm}(\tau)
\end{aligned}$$

Combining this with the zeroth order solution, it is easy to obtain the result in equation(3.8). In general for the j-th ($j>1$) order λ^j, the initial condition is $\rho^{(j)}_{nm}(t=0)=0$, and the corresponding equation is

$$\begin{aligned}
\dot\rho^{(j)}_{nm}(t) &= \frac{i}{\hbar}\sum_\nu(\rho^{(j-1)}_{n\nu}(t)H'_{\nu m}(t) - H'_{n\nu}(t)\rho^{(j-1)}_{\nu m}(t)) \\
&\quad + \frac{i}{\hbar}\sum_\nu(\rho^{(j)}_{n\nu}(t)H^0_{\nu m} - H^0_{n\nu}\rho^{(j)}_{\nu m}(t)) \\
&= \frac{i}{\hbar}\sum_\nu(\rho^{(j-1)}_{n\nu}(t)H'_{\nu m}(t) - H'_{n\nu}(t)\rho^{(j-1)}_{\nu m}(t)) \\
&\quad + \frac{i}{\hbar}(E_m-E_n)\rho^{(j)}_{nm}(t) \\
&= \frac{i}{\hbar}[\rho^{(j-1)}(t), H'(t)]_{nm} + \frac{i}{\hbar}(E_m-E_n)\rho^{(j)}_{nm}(t)
\end{aligned}$$

The solution can be directly written as:

$$\rho^{(j)}_{nm}(t) = \frac{i}{\hbar}\int_0^t d\tau\, e^{i(E_m-E_n)(t-\tau)/\hbar}[\rho^{(j-1)}(\tau), H'(\tau)]_{nm}$$

Therefore the time evolution of a dynamical variable $A(t)$ is:

$$\begin{aligned}
< A >_t &= \mathrm{Tr}(\hat{\rho}(t)\hat{A}) = \mathrm{Tr}(\hat{\rho}^{(0)}(t)\hat{A}) + \sum_{j=1} \mathrm{Tr}(\hat{\rho}^{(j)}(t)\hat{A}) \\
&= \sum_n \sum_m \rho^{(0)}_{nm}(t) A_{mn} + \\
&\quad \sum_j \frac{i}{\hbar} \sum_{n,m} \int_0^t d\tau\, e^{-i(E_m - E_n)\tau/\hbar} [\rho^{(j-1)}(\tau), H'(\tau)]_{nm} e^{i(E_m - E_n)t/\hbar} A_{mn} \\
&= \sum_n \sum_m \rho_{nm}(0) e^{(E_m - E_n)t/\hbar} A_{mn} + \\
&\quad \sum_j \frac{i}{\hbar} \sum_{n,m} \int_0^t d\tau\, e^{-i(E_m - E_n)\tau/\hbar} [\rho^{(j-1)}(\tau), H'(\tau)]_{nm} e^{i(E_m - E_n)t/\hbar} A_{mn} \\
&= \sum_{n,m} \rho_{nm}(0) \tilde{A}_{mn}(t) \\
&\quad + \sum_j \frac{i}{\hbar} \sum_{n,m} \int_0^t d\tau\, e^{i(E_n - E_m)\tau/\hbar} [\rho^{(j-1)}(\tau), H'(\tau)]_{nm} \tilde{A}_{mn}(t) \\
&= \sum_{n,m} \rho_{nm}(0) \tilde{A}_{mn}(t) + \sum_{j=1} \frac{i}{\hbar} \sum_{n,m} \int_0^t d\tau\, K_j(\tau, t)
\end{aligned}$$

where we have defined the kernel

$$K_j(\tau, t) = e^{i(E_n - E_m)\tau/\hbar} [\rho^{(j-1)}(\tau), H'(\tau)]_{nm} \tilde{A}_{mn}(t) \tag{3.14}$$

The first order term of the kernel at $j = 1$

$$\begin{aligned}
K_1(\tau, t) &= e^{i(E_n - E_m)\tau/\hbar} [\rho^{(j-1)}(\tau), H'(\tau)]_{nm} \tilde{A}_{mn}(t) \\
&= \tilde{A}_{mn}(t) e^{i(E_n - E_m)\tau/\hbar}\, . \\
&\quad \cdot \sum_\nu [\rho_{n\nu}(0) e^{i(E_\nu - E_n)\tau/\hbar} H'_{\nu m}(\tau) - H'_{n\nu}(\tau) \rho_{\nu m}(0) e^{i(E_m - E_\nu)\tau/\hbar}] \\
&= \tilde{A}_{mn}(t) \sum_\nu [\rho_{n\nu}(0) e^{i(E_\nu - E_m)\tau/\hbar} H'_{\nu m}(\tau) - e^{i(E_n - E_\nu)\tau/\hbar} \rho_{\nu m}(0)] \\
&= \tilde{A}_{mn}(t) \sum_\nu [\rho_{n\nu}(0) \tilde{H}'_{\nu m}(\tau) - \tilde{H}'_{n\nu}(\tau) \rho_{\nu m}(0)]
\end{aligned}$$

Manipulating the summation we arrive at

$$\begin{aligned}
\sum_n \sum_m K_1(\tau,t) &= \sum_{n,m,\nu} [\rho_{n\nu}(0)\tilde{H}'_{\nu m}(\tau)\tilde{A}_{mn}(t) - \rho_{\nu m}(0)\tilde{A}_{mn}(t)\tilde{H}'_{n\nu}(\tau)] \\
&= \sum_{n,m,\nu} [\rho_{\nu m}(0)\tilde{H}'_{mn}(\tau)\tilde{A}_{n\nu}(t) - \rho_{\nu m}(0)\tilde{A}_{mn}(t)\tilde{H}'_{n\nu}(\tau)] \\
&= \sum_{n,m,\nu} \rho_{\nu m}(0)[\tilde{H}'_{mn}(\tau)\tilde{A}_{n\nu}(t) - \tilde{A}_{mn}(t)\tilde{H}'_{n\nu}(\tau)] \\
&= \sum_m \sum_\nu \rho_{\nu m}(0)[\tilde{H}'(\tau), \tilde{A}(t)]_{m\nu} \\
&= \mathrm{Tr}(\rho(0)[\tilde{H}'(\tau), \tilde{A}(t)]) \qquad (3.15)
\end{aligned}$$

where we have used the exchange of $n \to \nu \to m \to n$ in the first term. In general

the j-th order term of the kernel goes to

$$
\begin{aligned}
K_j(\tau_j,t) &= e^{i(E_n-E_m)\tau_j/\hbar}[\rho^{(j-1)}(\tau_j),H'(\tau_j)]_{nm}\tilde{A}_{mn}(t) \\
&= \tilde{A}_{mn}(t)e^{i(E_n-E_m)\tau_j/\hbar}\,. \\
&\quad \sum_\nu [\rho^{(j-1)}_{n\nu}(\tau_j)H'_{\nu m}(\tau_j)-H'_{n\nu}(\tau_j)\rho^{(j-1)}_{\nu m}(\tau_j)] \\
&= \tilde{A}_{mn}(t)e^{i(E_n-E_m)\tau_j/\hbar}\sum_\nu \left\{ \frac{i}{\hbar}\int_0^{\tau_j} d\tau_{j-1}e^{i(E_\nu-E_n)(\tau_j-\tau_{j-1})/\hbar}\,\cdot\right. \\
&\quad \cdot[\rho^{(j-1)}(\tau_{j-1}),H'(\tau_{j-1})]_{n\nu}H'_{\nu m}(\tau_j)-H'_{n\nu}(\tau_j)\cdot \\
&\quad \left.\cdot\frac{i}{\hbar}\int_0^{\tau_j} d\tau_{j-1}e^{i(E_m-E_\nu)(\tau_j-\tau_{j-1})/\hbar}[\rho^{(j-1)}(\tau_{j-1}),H'(\tau_{j-1})]_{\nu m}\right\} \\
&= \tilde{A}_{mn}(t)\sum_\nu \left\{ e^{i(E_\nu-E_m)\tau_j/\hbar}H'_{\nu m}(\tau_j)\frac{i}{\hbar}\int_0^{\tau_j} d\tau_{j-1}\,\cdot\right. \\
&\quad e^{i(E_n-E_\nu)\tau_{j-1}/\hbar}[\rho^{(j-1)}(\tau_{j-1}),H'(\tau_{j-1})]_{n\nu}-e^{i(E_n-E_\nu)\tau_j/\hbar}H'_{n\nu}(\tau_j)\cdot \\
&\quad \left.\cdot\,\frac{i}{\hbar}\int_0^{\tau_j} d\tau_{j-1}e^{i(E_\nu-E_m)\tau_{j-1}}[\rho^{(j-1)}(\tau_{j-1}),H'(\tau_{j-1})]_{\nu m}\right\} \\
&= \tilde{A}_{mn}(t)\sum_\nu \left\{ \tilde{H}'_{\nu m}(\tau_j)\frac{i}{\hbar}\int_0^{\tau_j} d\tau_{j-1}\,\cdot\right. \\
&\quad e^{i(E_n-E_\nu)\tau_{j-1}/\hbar}[\rho^{(j-1)}(\tau_{j-1}),H'(\tau_{j-1})]_{n\nu}-\tilde{H}'_{n\nu}(\tau_j)\cdot \\
&\quad \left.\cdot\,\frac{i}{\hbar}\int_0^{\tau_j} d\tau_{j-1}e^{i(E_\nu-E_m)\tau_{j-1}}[\rho^{(j-1)}(\tau_{j-1}),H'(\tau_{j-1})]_{\nu m}\right\}
\end{aligned}
$$

Similar to the case of first order, manipulating the summation, we have

$$\begin{aligned}
\sum_n \sum_m K_j(\tau_j, t) &= \sum_{n,m,\nu} \tilde{A}_{mn}(t) \left\{ \tilde{H}'_{\nu m}(\tau_j) \frac{i}{\hbar} \int_0^{\tau_j} d\tau_{j-1} \cdot \right. \\
&\quad e^{i(E_n - E_\nu)\tau_{j-1}/\hbar} [\rho^{(j-1)}(\tau_{j-1}), H'(\tau_{j-1})]_{n\nu} - \tilde{H}'_{n\nu}(\tau_j) \cdot \\
&\quad \left. \cdot \frac{i}{\hbar} \int_0^{\tau_j} d\tau_{j-1} e^{i(E_\nu - E_m)\tau_{j-1}} [\rho^{(j-1)}(\tau_{j-1}), H'(\tau_{j-1})]_{\nu m} \right\} \\
&= \sum_{n,m,\nu} [\tilde{H}'_{mn}(\tau_j) \tilde{A}_{n\nu}(t) - \tilde{A}_{mn}(t) \tilde{H}'_{n\nu}(\tau_j)] \cdot \\
&\quad \cdot \left\{ \frac{i}{\hbar} \int_0^{\tau_j} d\tau_{j-1}\, e^{i(E_\nu - E_m)\tau_{j-1}} [\rho^{(j-1)}(\tau_{j-1}), H'(\tau_{j-1})]_{\nu m} \right\} \\
&= \sum_{m,\nu} [\tilde{H}'(\tau_j), \tilde{A}(t)]_{m\nu} \cdot \\
&\quad \cdot \left\{ \frac{i}{\hbar} \int_0^{\tau_j} d\tau_{j-1}\, e^{i(E_\nu - E_m)\tau_{j-1}} [\rho^{(j-1)}(\tau_{j-1}), H'(\tau_{j-1})]_{\nu m} \right\} \\
&= \sum_n \sum_m [\tilde{H}'(\tau_j), \tilde{A}(t)]_{mn} \cdot \\
&\quad \cdot \left\{ \frac{i}{\hbar} \int_0^{\tau_j} d\tau_{j-1}\, e^{i(E_n - E_m)\tau_{j-1}} [\rho^{(j-1)}(\tau_{j-1}), H'(\tau_{j-1})]_{nm} \right\}
\end{aligned}$$

Comparing the last line of the above equation with equation (3.14) and replacing $\tilde{A}$ with $[\tilde{H}'(\tau_j), \tilde{A}(t)]$, we can write the kernel as

$$\begin{aligned}
K_j(\tau_j, t) &= [\tilde{H}'(\tau_j), \tilde{A}(t)]_{mn} \cdot \\
&\quad \cdot \left\{ \frac{i}{\hbar} \int_0^{\tau_j} d\tau_{j-1}\, e^{i(E_n - E_m)\tau_{j-1}} [\rho^{(j-1)}(\tau_{j-1}), H'(\tau_{j-1})]_{nm} \right\} \\
&= [\tilde{H}'(\tau_{j-1}), [\tilde{H}'(\tau_j), \tilde{A}(t)]]_{mn} \cdot \left(\frac{i}{\hbar} \right)^2 \\
&\quad \int_0^{\tau_j} d\tau_{j-1} \int_0^{\tau_{j-1}} d\tau_{j-2}\, e^{i(E_n - E_m)\tau_{j-2}} [\rho^{(j-2)}(\tau_{j-2}), H'(\tau_{j-2})]_{nm} \\
&= [\tilde{H}'(\tau_2), \tilde{H}'(\tau_3) \cdots, [\tilde{H}'(\tau_{j-1}), [\tilde{H}'(\tau_j), \tilde{A}(t)]] \cdots]]_{mn} \cdot \left(\frac{i}{\hbar} \right)^{j-1} \\
&\quad \int_0^{\tau_j} d\tau_{j-1} \int_0^{\tau_{j-1}} d\tau_{j-2} \cdots \int_0^{\tau_2} d\tau_1 \\
&\quad e^{i(E_n - E_m)\tau_1/\hbar} [\rho^{(1)}(\tau_1), H'(\tau_1)]_{nm}
\end{aligned}$$

Manipulating the summation as we did for equation (3.15), we have

$$\begin{aligned}\sum_n \sum_m K_j(\tau_j, t) &= \left(\frac{i}{\hbar}\right)^{j-1} \int_0^{\tau_j} d\tau_{j-1} \int_0^{\tau_{j-1}} d\tau_{j-2} \cdots \int_0^{\tau_2} d\tau_1 \mathrm{Tr}\{\rho(0) \\ & [\tilde{H}'(\tau_1), [\tilde{H}'(\tau_2), \tilde{H}'(\tau_3) \cdots, [\tilde{H}'(\tau_{j-1}), [\tilde{H}'(\tau_j), \tilde{A}(t)]] \cdots]]]\}\end{aligned}$$

The time evolution of the dynamical variable $A(t)$ corresponds to

$$\begin{aligned}< A >_t &= \sum_{n,m} \rho_{nm}(0)\tilde{A}_{mn}(t) + \sum_{j=1} \frac{i}{\hbar} \sum_{n,m} \int_0^t d\tau\, K_j(\tau, t) \\ &= \mathrm{Tr}\{\rho(0)\tilde{A}(t)\} + \sum_{j=1} \left(\frac{i}{\hbar}\right)^j \\ & \int_0^t d\tau_j \int_0^{\tau_j} d\tau_{j-1} \int_0^{\tau_{j-1}} d\tau_{j-2} \cdots \int_0^{\tau_2} d\tau_1 \mathrm{Tr}\{\rho(0) \\ & [\tilde{H}'(\tau_1), [\tilde{H}'(\tau_2), \cdots, [\tilde{H}'(\tau_{j-1}), [\tilde{H}'(\tau_j), \tilde{A}(t)]] \cdots]]\}\end{aligned}$$

Born-Oppenheimer Approximation The above equation of nonlinear response theory is powerful but it involves too many degrees of freedom of electrons and atoms. For dynamical variables calculated when the system is in its ground electronic state, it is always a good approximation to solve the equations of electronic degrees of freedom first based on a fixed nuclear configuration and then take average of all possible nuclear configurations. Therefore, it is necessary to simplify the above nonlinear response theory based on the so called B.O. Approximation.

In general, for a system of N nuclei and M electrons, the unperturbed total

Hamiltonian of all degrees of freedom is:

$$\begin{aligned}
\hat{H}^0 &= -\sum_{i=1}^{M}\frac{1}{2}\nabla_i^2 - \sum_{j=1}^{N}\frac{1}{2m_j}\nabla_j^2 - \sum_{i=1}^{M}\sum_{j=1}^{N}\frac{q_j}{r_{ij}} \\
&\quad + \sum_{i=1}^{M}\sum_{s>i}^{M}\frac{1}{x_{is}} + \sum_{j=1}^{N}\sum_{s>j}^{N}\frac{q_j q_s}{R_{js}} \\
&= \left[-\sum_{i=1}^{M}\frac{1}{2}\nabla_i^2 - \sum_{i=1}^{M}\sum_{j=1}^{N}\frac{q_j}{r_{ij}} + \sum_{i=1}^{M}\sum_{s>i}^{M}\frac{1}{x_{is}}\right] \\
&\quad + \left[-\sum_{j=1}^{N}\frac{1}{2m_j}\nabla_j^2 + \sum_{j=1}^{N}\sum_{s>j}^{N}\frac{q_i q_s}{R_{js}}\right] \\
&= \hat{H}_e^o + \left[-\sum_{j=1}^{N}\frac{1}{2m_j}\nabla_j^2 + \sum_{j=1}^{N}\sum_{s>j}^{N}\frac{q_i q_s}{R_{js}}\right]
\end{aligned}$$

where x_{is} is the distance between i-th and s-th electron, r_{ij} is the distance between i-th electron and j-th nucleus, and R_{js} is the distance between j-th and s-th nucleus. m_j is the mass of the j-th nucleus. q_j is the charge of j-th nucleus. Based on the B.O. approximation, the problem of solving the Schrodinger equation

$$\hat{H}^0\psi = E\psi$$

can be split into the electronic part

$$\hat{H}_e^o\psi_e = E_e^o\psi_e$$

and the nuclear part

$$\hat{H}_N^0\psi_N = E\psi_N$$

where

$$\hat{H}_N^0 = \left[-\sum_{j=1}^{N}\frac{1}{2m_j}\nabla_j^2 + \sum_{j=1}^{N}\sum_{s>j}^{N}\frac{q_i q_s}{R_{js}}\right] + E_e^o$$

Note that the electronic wavefunction ψ_e, nuclear wavefunction ψ_N, and the electronic energy E_e^o are

$$\psi_e = \psi_e(\mathbf{x}^M, \mathbf{R}^N)$$

$$\psi_N = \psi_N(\mathbf{R}^N)$$

$$E_e^o = E_e^o(\mathbf{R}^N)$$

where $\mathbf{x}^M$ and $\mathbf{R}^N$ are collective notations for the coordinates of M electrons and N nuclei:

$$\mathbf{x}^M = (\mathbf{x}_1, \mathbf{x}_2, \cdots, \mathbf{x}_M)$$

$$\mathbf{R}^N = (\mathbf{R}_1, \mathbf{R}_2, \cdots, \mathbf{R}_N)$$

The total wavefunction corresponding to $\hat{H}^0\psi = E\psi$ is

$$\psi(\mathbf{x}^M, \mathbf{R}^N) \simeq \psi_e(\mathbf{x}^M, \mathbf{R}^N)\psi_N(\mathbf{R}^N)$$

Validity of BO approximation Insert the approximated wavefunction into the

Schrodinger equation, then the left hand side is

$$\begin{aligned}
\hat{H}\psi(\mathbf{x}^M,\mathbf{R}^N) &= \hat{H}_e^o + \left[-\sum_{j=1}^{N}\frac{1}{2m_j}\nabla_j^2 + \sum_{j=1}^{N}\sum_{s>j}^{N}\frac{q_i q_s}{R_{js}}\right]\psi_e\psi_N \\
&= \psi_N E_e^o(\mathbf{R}^N)\psi_e + \sum_{j=1}^{N}\sum_{s>j}^{N}\frac{q_j q_s}{R_{js}}\psi_e\psi_N \\
&\quad -\sum_{j=1}^{N}\frac{1}{2m_j}\nabla_j\cdot[(\psi_e\nabla\psi_N + \psi_N\nabla\psi_e] \\
&= \left[E_e^o + \sum_{j=1}^{N}\sum_{s>j}^{N}\frac{q_j q_s}{R_{js}}\right]\psi_e\psi_N - \sum_{j=1}^{N}\frac{1}{2m_j}(\nabla_j^2\psi_N)\psi_e \\
&\quad -\sum_{j=1}^{N}\frac{1}{2m_j}(\nabla_j^2\psi_e)\psi_N - \sum_{j=1}^{N}\frac{1}{m_j}(\nabla_j\psi_e)(\nabla_j\psi_N) \\
&= \psi_e\left[-\sum_{j=1}^{N}\frac{1}{2m_j}(\nabla_j^2\psi_N) + E_e^o\psi_N + \sum_{j=1}^{N}\sum_{s>j}^{N}\frac{q_j q_s}{R_{js}}\psi_N\right] \\
&\quad -\psi_N\sum_{j=1}^{N}\frac{1}{2m_j}(\nabla_j^2\psi_e) - \sum_{j=1}^{N}\frac{1}{m_j}(\nabla_j\psi_e)\cdot(\nabla_j\psi_N) \\
&= \psi_e(\hat{H}_N^0\psi_N) - \sum_{j=1}^{N}\frac{1}{m_j}\left[\frac{1}{2}\psi_N(\nabla_j^2\psi_e) + (\nabla_j\psi_e)(\nabla_j\psi_N)\right] \\
&= E\psi_e\psi_N - \sum_{j=1}^{N}\frac{1}{2m_j}[\psi_N(\nabla_j^2\psi_e) + 2(\nabla_j\psi_e)(\nabla_j\psi_N)] \\
&= E\psi(\mathbf{x}^M,\mathbf{R}^N) - \sum_{j=1}^{N}\frac{1}{2m_j}[\psi_N(\nabla_j^2\psi_e) + 2(\nabla_j\psi_e)(\nabla_j\psi_N)] \\
&\simeq E\psi(\mathbf{x}^M,\mathbf{R}^N)
\end{aligned}$$

The validity of B.O Approximation is guaranteed if the term

$$-\sum_{j=1}^{N}\frac{1}{2m_j}[\psi_N(\nabla_j^2\psi_e) + 2(\nabla_j\psi_e)(\nabla_j\psi_N)]$$

is much smaller than $E\psi(\mathbf{x}^M,\mathbf{R}^N)$. The former is on the order of the electronic kinetic energy and it is usually much smaller than the nuclear kinetic energy part in $E\psi(\mathbf{x}^M,\mathbf{R}^N)$ which is $-\psi_e\sum_{j=1}^{N}\frac{1}{2m_j}(\nabla_j^2\psi_N)$.

Application of the B.O approximation to Nonlinear Response theory

By using the B.O. approximation where we assume that the motion of electrons always follows that of nuclei, we can eliminate the degrees of freedom of electrons for a certain nuclear configuration and then take average of all possible nuclear configurations of the ensemble. Therefore the calculation of dynamical properties becomes much simpler. Recall that the total Hamiltonian of the system considered is

$$H(t) = H_0(\mathbf{x}^N, \mathbf{R}^N) + H'(\mathbf{x}^N, \mathbf{R}^N, t)$$

In case of an electric perturbation, H' has both electronic part and nuclear part:

$$H'(\mathbf{x}^M, \mathbf{R}^N, t) = H'_e(\mathbf{x}^M, t) + H'_N(\mathbf{R}^N, t)$$

A typical example is that at time $t = 0$ we turn on a constant external electric field: $\mathbf{E} = \mathbf{e}_x E_x + \mathbf{e}_y E_y + \mathbf{e}_z E_z$:

$$H'(\mathbf{x}^M, \mathbf{R}^N, t) = -\boldsymbol{\mu} \cdot \mathbf{E}$$

$$H'_e(\mathbf{x}^M, t) = \sum_{i=1}^{M} e x_{i\alpha} E_\alpha h(t)$$

$$H'_N(\mathbf{R}^N, t) = -\sum_{i=1}^{N} q_i R_{i\alpha} E_\alpha h(t)$$

where $h(t)$ is a step function. The normal procedure in the B.O. treatment of dynamics requires solving the electronic part first.

$$H_e \Psi_{en} = (H_e^o + H'_e)\Psi_{en} = E_n \Psi_{en}$$

The unperturbed state ψ_{en} satisfies

$$H_e^o \psi_{en} = E_{en} \psi_{en}, \quad n = 0, 1, 2, \cdots,$$

We assume the response of electrons is very fast when the perturbation is a constant within this time interval ($H'_e(\mathbf{x}^M, t) = H'_e(\mathbf{x}^M)$). Therefore, the steady-state of electrons will be achieved during each nuclear configuration. For the nondegenerate ground electronic state, the time independent perturbation theory (Rayleigh-Schrodinger Perturbation Theory) gives the steady-state ground state energy and wavefunction[62]:

$$E_o = E_o^{(0)} + E_o^{(1)} + E_o^{(2)} + \cdots +$$

$$\Psi_{e0} = \Psi_{e0}^{(0)} + \Psi_{e0}^{(1)} + \Psi_{e0}^{(2)} + \cdots + \cdots$$

$$E_o^{(0)} = \int d\mathbf{x}^M \psi_{e0}^* H_e^o \psi_{e0} = E_{e0}$$

$$\Psi_{e0}^{(0)} = \psi_{e0}$$

$$E_o^{(1)} = \int d\mathbf{x}^M \psi_{e0}^* H'_e(\mathbf{x}^M) \psi_{e0} = -\mu_\alpha E_\alpha$$

$$\Psi_{e0}^{(1)} = \sum_{n\neq 0} \psi_{en} \frac{\int d\mathbf{x}^M \psi_{en}^* H'_e(\mathbf{x}^M) \psi_{e0}}{E_{e0} - E_{en}}$$

$$E_o^{(2)} = \sum_{n\neq 0} \frac{|\int d\mathbf{x}^M \psi_{e0}^* H'_e(\mathbf{x}^M) \psi_{en}|^2}{E_{e0} - E_{en}} = -\frac{1}{2}\chi_{\alpha\beta} E_\alpha E_\beta$$

$$\Psi_{e0}^{(2)} = \sum_{n\neq 0} \psi_{en} \frac{\int d\mathbf{x}^M \psi_{en}^* H'_e(\mathbf{x}^M) \psi_{e0}^{(1)} - E_o^{(1)} \int d\mathbf{x}^M \psi_{en} \psi_{e0}^{(1)}}{E_{e0} - E_{en}}$$

$$E_o^{(3)} = -\frac{1}{3}\xi_{\alpha\beta\gamma} E_\alpha E_\beta E_\gamma$$

where μ_α and $\chi_{\alpha\beta}$ are the α component of the dipole moment and $\alpha\beta$ component of the electronic polarizability created by electrons for the fixed nuclear configuration $\mathbf{R}^N$

$$\mu_\alpha = -\int d\mathbf{x}^M \psi_{e0}^* \sum_{i=1}^{M} e x_{i\alpha} \psi_{e0}$$

$$\chi_{\alpha\beta} = 2\sum_{n\neq 0} \frac{\int d\mathbf{x}^M \psi^*_{e0} \sum_{i=1}^M ex_{i\alpha}\psi_{en} \int d\mathbf{x}^M \psi^*_{en} \sum_{j=1}^M ex_{j\beta}\psi_{e0}}{E_{en} - E_{e0}}$$

The expression for $\xi_{\alpha\beta\gamma}$ can also be calculated by following perturbative approach. This is very tedious and won't be done explicitly here. The nuclear Hamiltonian including the external perturbation part is

$$\begin{aligned}
H_N(t) &= E_{e0} - \sum_{j=1}^N \frac{1}{2m_j}\nabla_j^2 + \sum_{j=1}^N \sum_{s>j}^N \frac{q_i q_s}{R_{js}} - \sum_{i=1}^N q_i R_{i\alpha} E_\alpha h(t) \\
&\quad -\mu_\alpha E_\alpha h(t) - \frac{1}{2}\chi_{\alpha\beta}E_\alpha E_\beta h(t) - \frac{1}{3}\xi_{\alpha\beta\gamma}E_\alpha E_\beta E_\gamma h(t) + \cdots + \\
&= E_{e0} - \sum_{j=1}^N \frac{1}{2m_j}\nabla_j^2 + \sum_{j=1}^N \sum_{s>j}^N \frac{q_i q_s}{R_{js}} - \left(\mu_\alpha + \sum_{i=1}^N q_i R_{i\alpha}\right) E_\alpha h(t) \\
&\quad -\frac{1}{2}\chi_{\alpha\beta}E_\alpha E_\beta h(t) - \frac{1}{3}\xi_{\alpha\beta\gamma}E_\alpha E_\beta E_\gamma h(t) + \cdots + \\
&= E_{e0} - \sum_{j=1}^N \frac{1}{2m_j}\nabla_j^2 + \sum_{j=1}^N \sum_{s>j}^N \frac{q_i q_s}{R_{js}} \\
&\quad - \left(M_\alpha E_\alpha + \frac{1}{2}\chi_{\alpha\beta}E_\alpha E_\beta + \frac{1}{3}\xi_{\alpha\beta\gamma}E_\alpha E_\beta E_\gamma\right) h(t) + \cdots + \cdots \\
&= H_N^0(\mathbf{R}^N) + H'_N(\mathbf{R}^N, E_\alpha, t)
\end{aligned}$$

where M_α is the total dipole moment in the α direction and we have added the electronic energy modification to the nuclear perturbation Hamiltonian under the B.O. approximation. The new perturbation Hamiltonian is

$$H'_N(\mathbf{R}^N, E_\alpha, t) = -\left(M_\alpha E_\alpha + \frac{1}{2}\chi_{\alpha\beta}E_\alpha E_\beta + \frac{1}{3}\xi_{\alpha\beta\gamma}E_\alpha E_\beta E_\gamma\right) h(t) + \cdots + \cdots$$

The dynamical variable of interest in the case of external electronic perturbation is the usual polarization operator:

$$\mathbf{P} = \sum_{i=1}^N q_i \mathbf{R}_i - \sum_{j=1}^M e\mathbf{x}_j$$

under the B.O. approximation, the α component of the polarization vector is

$$\begin{aligned}
P_\alpha &= \sum_{j=1}^{N} q_j \mathbf{R}_{j\alpha} - \int d\mathbf{x}^N \Psi_{e0}^* \sum_{i=1}^{M} ex_{i\alpha} \Psi_{e0} \\
&= \sum_{j=1}^{N} q_j \mathbf{R}_{j\alpha} - \int d\mathbf{x}^M \psi_{e0}^* \sum_{i=1}^{M} ex_{i\alpha} \psi_{e0} - \int d\mathbf{x}^M \Psi_{e0}^{(1)^*} \sum_{i=1}^{M} ex_{i\alpha} \psi_{e0} - \\
&\quad \int d\mathbf{x}^M \Psi_{e0}^* \sum_{i=1}^{M} ex_{i\alpha} \Psi_{e0}^{(1)} - \int d\mathbf{x}^M \Psi_{e0}^{(1)^*} \sum_{i=1}^{M} ex_{i\alpha} \Psi_{e0}^{(1)} \\
&\quad - \int d\mathbf{x}^M \Psi_{e0}^{(2)^*} \sum_{i=1}^{M} ex_{i\alpha} \psi_{e0} - \int d\mathbf{x}^M \psi_{e0} \sum_{i=1}^{M} ex_{i\alpha} \Psi_{e0}^{(2)} + \cdots + \\
&= P_\alpha^{(0)} + P_\alpha^{(1)} + P_\alpha^{(2)} + \cdots + \cdots
\end{aligned}$$

where the 0-th order value is

$$P_\alpha^{(0)} = \sum_{j=1}^{N} q_j R_{j\alpha} - \int d\mathbf{x}^M \psi_{e0}^* \sum_{i=1}^{M} ex_{i\alpha} \psi_{e0} = M_\alpha$$

and the 1-st order value is

$$\begin{aligned}
P_\alpha^{(1)} &= - \int d\mathbf{x}^M \Psi_{e0}^* \sum_{i=1}^{M} ex_{i\alpha} \Psi_{e0}^{(1)} + \text{c.c.} \\
&= - \sum_{n \neq 0} \frac{\int d\mathbf{x}^M \psi_{e0}^* \sum_{i=1}^{M} ex_{i\alpha} \psi_{en} \int d\mathbf{x}^M \psi_{en}^* \sum_{i=1}^{M} ex_{i\beta} E_\beta \psi_{e0}}{E_{e0} - E_{en}} + \text{c.c.} \\
&= \frac{1}{2} \chi_{\alpha\beta} E_\beta + \text{c.c.} \\
&= \chi_{\alpha\beta} E_\beta
\end{aligned}$$

Following the same procedure, we can also see that

$$\begin{aligned}
P_\alpha^{(2)} &= - \int d\mathbf{x}^M \Psi_{e0}^{(1)^*} \sum_{i=1}^{M} ex_{i\alpha} \Psi_{e0}^{(1)} - \int d\mathbf{x}^M \Psi_{e0}^{(2)^*} \sum_{i=1}^{M} ex_{i\alpha} \psi_{e0} \\
&\quad - \int d\mathbf{x}^M \psi_{e0} \sum_{i=1}^{M} ex_{i\alpha} \Psi_{e0}^{(2)} \\
&= \xi_{\alpha\beta\gamma} E_\beta E_\gamma
\end{aligned}$$

Actually, we can directly derive the above equation by using the relation between energy and polarization:

$$\begin{aligned}
P_\alpha &= P_\alpha^{(0)} + P_\alpha^{(1)} + P_\alpha^{(2)} + \cdots + \cdots \\
&= \sum_{j=1}^{N} q_j R_{j\alpha} - \int d\mathbf{x}^N \Psi_{e0}^* \sum_{i=1}^{M} ex_{i\alpha} \Psi_{e0} \\
&= \sum_{j=1}^{N} q_j R_{j\alpha} - \int d\mathbf{x}^N \Psi_{e0}^* \frac{\partial H_e'}{\partial E_\alpha} \Psi_{e0} \\
&= \sum_{j=1}^{N} q_j R_{j\alpha} - \frac{\partial}{\partial E_\alpha}(E_o - E_{e0}) \\
&= \sum_{j=1}^{N} q_j R_{j\alpha} - \frac{\partial}{\partial E_\alpha}\left(-\mu_\alpha E_\alpha - \frac{1}{2}\chi_{\alpha\beta} E_\alpha E_\beta - \frac{1}{3}\xi_{\alpha\beta\gamma} E_\alpha E_\beta E_\gamma\right) + \cdots \\
&= \sum_{j=1}^{N} q_j R_{j\alpha} + \mu_\alpha + \chi_{\alpha\beta} E_\beta + \xi_{\alpha\beta\gamma} E_\beta E_\gamma + \cdots \\
&= M_\alpha + \chi_{\alpha\beta} E_\beta + \xi_{\alpha\beta\gamma} E_\beta E_\gamma + \zeta_{\alpha\beta\gamma\delta} E_\beta E_\gamma E_\delta \cdots
\end{aligned}$$

According to nonlinear response theory, the time evolution of an arbitrary dynamical variable A under the perturbation H' is

$$\begin{aligned}
< A >_t &= \mathrm{Tr}\{\rho(0)\tilde{A}(t)\} + \sum_{j=1}\left(\frac{i}{\hbar}\right)^j \\
&\quad \int_0^t d\tau_j \int_0^{\tau_j} d\tau_{j-1} \int_0^{\tau_{j-1}} d\tau_{j-2} \cdots \int_0^{\tau_2} d\tau_1 \mathrm{Tr}\{\rho(0) \\
&\quad [\tilde{H}'(\tau_1), [\tilde{H}'(\tau_2), \cdots, [\tilde{H}'(\tau_{j-1}), [\tilde{H}'(\tau_j), \tilde{A}(t)]] \cdots]]\}
\end{aligned}$$

Replacing A for P_α and H' for H_N' and considering the response to 1st order, 2nd order, and 3rd order on the external field E_α, we have

$$\begin{aligned}
< P_\alpha >_t^{(1)} &= \mathrm{Tr}[\hat{\rho}(0)\tilde{\chi}_{\alpha\beta}(t) E_\beta(t)] + \frac{i}{\hbar}\int_0^t d\tau_1 \mathrm{Tr}\{\hat{\rho}(0)[-\tilde{M}_\beta(\tau_1) E_\beta(\tau_1), \tilde{M}_\alpha(t)]\} \\
&= \mathrm{Tr}[\hat{\rho}(0)\tilde{\chi}_{\alpha\beta}(t)] E_\beta(t) + \frac{i}{\hbar}\int_0^t d\tau \mathrm{Tr}\{\hat{\rho}(0)[\tilde{M}_\alpha(t), \tilde{M}_\beta(\tau)]\} E_\beta(\tau) \quad (3.16)
\end{aligned}$$

where the Heisenberg operator in this B.O. treatment is defined as

$$\tilde{M}_\alpha(t) = e^{iH_N^0 t/\hbar} M_\alpha e^{-iH_N^0 t/\hbar}$$

$$H_N^0 = -\sum_{j=1}^{N} \frac{1}{2m_j}\nabla_j^2 + \sum_{j=1}^{N}\sum_{s>j}^{N} \frac{q_j q_s}{R_{js}} + E_{e0}(\mathbf{R}^N)$$

$$M_\alpha = \mu_\alpha + \sum_{j=1}^{N} q_j R_{j\alpha}$$

Similarly, we can get the 2nd order polarization:

$$\begin{aligned} < P_\alpha >_t^{(2)} \;=\; & \mathrm{Tr}[\hat{\rho}(0)\tilde{\xi}_{\alpha\beta\gamma}(t)E_\beta(t)E_\gamma(t)] \\ & + \frac{i}{\hbar}\int_0^t d\tau_1 \mathrm{Tr}\left\{\hat{\rho}(0)\left[-\frac{1}{2}\tilde{\chi}_{\beta\gamma}(\tau_1)E_\beta(\tau_1)E_\gamma(\tau_1), \tilde{M}_\alpha(t)\right]\right\} \\ & + \frac{i}{\hbar}\int_0^t d\tau_1 \mathrm{Tr}\left\{\hat{\rho}(0)\left[-\tilde{M}_\gamma(\tau_1)E_\gamma(\tau_1), \tilde{\chi}_{\alpha\beta}(t)E_\beta(t)\right]\right\} \\ & + \left(\frac{i}{\hbar}\right)^2 \int_0^t d\tau_2 \int_0^{\tau_2} d\tau_1 \\ & \mathrm{Tr}\left\{\hat{\rho}(0)[-\tilde{M}_\beta(\tau_1)E_\beta(\tau_1), [-\tilde{M}_\gamma(\tau_2)E_\gamma(\tau_2), \tilde{M}_\alpha(t)]]\right\} \end{aligned}$$

Because liquids are isotropic systems, 2nd nonlinear optical effects are not detected. It is common to study the 3rd order nonlinear spectra. The required expression for

3rd order polarization is:

$$
\begin{aligned}
< P_\alpha >_t^{(3)} &= \mathrm{Tr}[\hat{\rho}(0)\tilde{\zeta}_{\alpha\beta\gamma\delta}(t)E_\beta(t)E_\gamma(t)E_\delta(t)] && (3.17)\\
&+\frac{i}{\hbar}\int_0^t d\tau_1 \mathrm{Tr}\left\{\hat{\rho}(0)\left[-\frac{1}{3}\tilde{\xi}_{\beta\gamma\delta}(\tau_1)E_\beta(\tau_1)E_\gamma(\tau_1)E_\delta(\tau_1),\tilde{M}_\alpha(t)\right]\right\} && (3.18)\\
&+\frac{i}{\hbar}\int_0^t d\tau_1 \mathrm{Tr}\left\{\hat{\rho}(0)\left[-\frac{1}{2}\tilde{\chi}_{\beta\gamma}(\tau_1)E_\beta(\tau_1)E_\gamma(\tau_1),\tilde{\chi}_{\alpha\delta}(t)E_\delta(t)\right]\right\} && (3.19)\\
&+\frac{i}{\hbar}\int_0^t d\tau_1 \mathrm{Tr}\left\{\hat{\rho}(0)\left[-\tilde{M}_\beta(\tau_1)E_\beta(\tau_1),\tilde{\xi}_{\alpha\gamma\delta}(t)E_\gamma(t)E_\delta(t)\right]\right\} && (3.20)\\
&+\left(\frac{i}{\hbar}\right)^2\int_0^t d\tau_2\int_0^{\tau_2} d\tau_1 \mathrm{Tr}\\
&\left\{\hat{\rho}(0)\left[-\tilde{M}_\beta(\tau_1)E_\beta(\tau_1),\left[-\tilde{M}_\gamma(\tau_2)E_\gamma(\tau_2),\chi_{\alpha\delta}(t)E_\delta(t)\right]\right]\right\} && (3.21)\\
&+\left(\frac{i}{\hbar}\right)^2\int_0^t d\tau_2\int_0^{\tau_2} d\tau_1 \mathrm{Tr}\\
&\left\{\hat{\rho}(0)\left[-\tilde{M}_\beta(\tau_1)E_\beta(\tau_1),\left[-\frac{1}{2}\chi_{\gamma\delta}(\tau_2)E_\gamma(\tau_2)E_\delta(\tau_2),\tilde{M}_\alpha(t)\right]\right]\right\} && (3.22)\\
&+\left(\frac{i}{\hbar}\right)^2\int_0^t d\tau_2\int_0^{\tau_2} d\tau_1 \mathrm{Tr}\\
&\left\{\hat{\rho}(0)\left[-\frac{1}{2}\tilde{\chi}_{\beta\gamma}(\tau_1)E_\beta(\tau_1)E_\gamma(\tau_1),\left[-\tilde{M}_\delta(\tau_2)E_\delta(\tau_2),\tilde{M}_\alpha(t)\right]\right]\right\} && (3.23)\\
&+\left(\frac{i}{\hbar}\right)^3\int_0^t d\tau_3\int_0^{\tau_3} d\tau_2\int_0^{\tau_1} d\tau_1 \mathrm{Tr}\left\{\hat{\rho}(0)\left[-\tilde{M}_\beta(\tau_1)E_\beta(\tau_1),\right.\right.\\
&\left.\left.\left[-\tilde{M}_\gamma(\tau_2)E_\gamma(\tau_2),\left[-\tilde{M}_\delta(\tau_3)E_\delta(\tau_3),\tilde{M}_\alpha(t)\right]\right]\right]\right\} && (3.24)
\end{aligned}
$$

In most studied optical experiments, all of the frequencies in polarization and the external electrical field are "optical". For those frequencies, it turns out that only two terms (3.17) and (3.19) are important and the rest six terms are negligible.

Therefore,

$$\begin{aligned} < P_\alpha >_t^{(3)} &= \mathrm{Tr}[\hat{\rho}(0)\tilde{\zeta}_{\alpha\beta\gamma\delta}(t)E_\beta(t)E_\gamma(t)E_\delta(t)] \\ &\quad + \frac{i}{\hbar}\int_0^t d\tau_1 \mathrm{Tr}\left\{\hat{\rho}(0)\left[-\frac{1}{2}\tilde{\chi}_{\beta\gamma}(\tau_1)E_\beta(\tau_1)E_\gamma(\tau_1), \tilde{\chi}_{\alpha\delta}(t)E_\delta(t)\right]\right\} \\ &= \mathrm{Tr}\left[\hat{\rho}(0)\tilde{\zeta}_{\alpha\beta\gamma\delta}(t)\right]E_\beta(t)E_\gamma(t)E_\delta(t) + \frac{i}{2\hbar}\int_0^t d\tau_1 \\ &\quad \mathrm{Tr}\left\{\hat{\rho}(0)\left[\tilde{\chi}_{\alpha\delta}(t), \tilde{\chi}_{\beta\gamma}(\tau_1)\right]E_\beta(\tau_1)E_\gamma(\tau_1)E_\delta(t)\right\} \end{aligned} \tag{3.25}$$

We assume that initially the system is in its thermal equilibrium state at a given temperature T, therefore

$$\hat{\rho}(0) = \frac{e^{-\beta H_N^0}}{\mathrm{Tr}\left[e^{-\beta H_N^0}\right]}$$

$$\rho_{nn}(0) = \rho_{nn}(0)\delta_{nm}$$

The first term in the first order response of $< P_\alpha >$ (equation (3.16)) is

$$\begin{aligned} \mathrm{Tr}\left[\hat{\rho}(0)\tilde{\chi}_{\alpha\beta}(t)\right] &= \sum_n\sum_m \hat{\rho}(0)_{nm}(\tilde{\chi}_{\alpha\beta})_{mn} \\ &= \sum_n\sum_m \delta_{nm}\rho_{nn}(0)(\tilde{\chi}_{\alpha\beta})_{mn} \\ &= \sum_n\sum_m \delta_{nm}\rho_{nn}(0)\int d\mathbf{R}^N \phi_m^* e^{iH_N^0 t/\hbar}\chi_{\alpha\beta}e^{-iH_N^0 t/\hbar}\phi_n \\ &= \sum_n\sum_m \delta_{nm}\rho_{nn}(0)e^{i(E_m-E_n)t/\hbar}\int d\mathbf{R}^N \phi_m^*\chi_{\alpha\beta}\phi_n \\ &= \sum_n \rho_{nn}(0)\int d\mathbf{R}^N \phi_n^*\chi_{\alpha\beta}\phi_n \\ &= < \chi_{\alpha\beta} >_0 \end{aligned}$$

which is the equilibrium expectation value of $\chi_{\alpha\beta}$. Similarly, the first term in the third order response of $< P_\alpha >$ (equation (3.25)) is the equilibrium expectation value of $\zeta_{\alpha\beta\gamma\delta}$. The second term of equation (3.25) and (3.16), are equilibrium time correlation

functions. Equations (3.25) and (3.16) relate the response of the material to an external optical perturbation in terms of equilibrium quantities and time correlation functions of the dipole moment or the first order susceptibility. In chapter 7, we will use third order response theory (equation (3.25)) to study the optical Kerr effect (OKE) of ionic liquids.

In closing this section, we have derived a complete nonlinear response theory and explained the use of the B.O. approximation which simplifies the results for the computation of third order optical processes. The use of B.O. theory makes the final expression for optical response theory simpler and it is necessary because the calculation of time correlation functions through classical simulation only tracks the motion of nuclei and involves no degrees of freedom of electrons.

3.5 Non-Hamiltonian Systems

So far in this thesis linear response theory deals with the fluctuation under small external perturbations to the system Hamiltonian. However, the perturbation does not have to be written in a Hamiltonian form. A form of response theory of non-Hamiltonian case has been studied in the book [16]. This formulation provides the background to study the shear viscosity of ionic liquids.

In general, for a system subject to an external field $F_e(t)$, the dynamics of the system obeys the following equation[16]:

$$\dot{\mathbf{R}}_q = \mathbf{v}_q + \mathbf{C}_q F_e(t) \qquad m_q \dot{\mathbf{v}}_q = \mathbf{F}_q + \mathbf{D}_q F_e(t) \tag{3.26}$$

Where $\mathbf{R}_q$, $\mathbf{v}_q$ and m_q are the position, velocity and mass of particle q respectively.

$\mathbf{F}_q$ is the internal force on particle q. The dynamical variables $\mathbf{C}_q$ and $\mathbf{D}_q$ describe the coupling of the field to particle q. Note that the definition of Liouville operator (2.3) in chapter 2 is still valid. Having studied the linear response theory comprehensively in the previous sections, the derivation of LRT in this non-Hamiltonian case should be straightforward. This derivation can also be found in the literature[16] and thus won't be repeated here. We simply write the result analogous to equation (3.5). The time evolution of a dynamical variable B, is given by:

$$< B(t) >=< B(t=0) > -\beta \int_0^t d\tau \ < B(t-\tau)J(t=0) > F_e(\tau) \tag{3.27}$$

where the dissipative flux $J(t)$ is defined as:

$$J(t) \equiv \sum_q (-\mathbf{D}_q \cdot \mathbf{v}_q + \mathbf{C}_q \cdot \mathbf{F}_q) \tag{3.28}$$

In order to understand this non-Hamiltonian approach clearly in the case of shear viscosity, we give the following example. Assume an external force of $\mathbf{F} = \mathbf{e}_x F_x = \mathbf{e}_x m_q \cos(kz_q)a_0$ is imposed on the system, the equations of motion are

$$\begin{cases} \dot{x}_i &= \frac{p_{xi}}{m_i} \\ \dot{y}_i &= \frac{p_{yi}}{m_i} \\ \dot{z}_i &= \frac{p_{zi}}{m_i} \end{cases} \tag{3.29}$$

and

$$\begin{cases} \dot{p}_{qx} &= F_{qx} + m_q \cos(kz_q)a_0 \\ \dot{p}_{qy} &= F_{qy} \\ \dot{p}_{qz} &= F_{qz} \end{cases} \tag{3.30}$$

where k is the spatial frequency of the force and a_0 is the amplitude of the force. p_j is the momentum of particle j. It turns out that no Hamiltonian can be written

that corresponds to this perturbation! Clearly, the coupled dynamical variable $\mathbf{C}_q$ in equation (3.26) is always zero here. The dynamical variable $\mathbf{D}_q$ and the external field can be taken to be:

$$\mathbf{D}_q(k,t) = \mathbf{e}_x m_q \cos(kz_q) \qquad F_e(t) = a_0 h(t) \tag{3.31}$$

where the function $h(t)$ is a step function

$$h(t) = \begin{cases} 1 & t > 0 \\ \\ 0 & t < 0 \end{cases}$$

The dissipative flux is:

$$J(k,t) = -\sum_q m_q a_0 v_{qx} \cos(kz_q) \tag{3.32}$$

The dynamical variable B we are interested in is:

$$B(z,t) \equiv \sum_q m_q v_{qx}(t) \delta(z - z_q(t)) \tag{3.33}$$

We first manipulate the integral in equation (3.27) as follows:

$$\begin{aligned} < B(z,t) > &= < B(z,t=0) > - \int_0^t d\tau\, \beta < B(z,t-\tau) J(k,t=0) > a_0 h(\tau) \\ &= -\int_0^t d\tau\, \beta < B(\tau) J(k,t=0) > a_0 h(t-\tau) \\ &= -\int_0^t d\tau\, \beta a_0 < B(z,\tau) J(k,t=0) > \\ &= \int_0^t d\tau\, \beta a_0 < \sum_j m_j v_{jx}(\tau) \delta(z - z_j(\tau)) \sum_q m_q v_{qx} \cos(kz_q) > \\ &= \beta a_0 \int_0^t d\tau\, D(z,\tau) \end{aligned} \tag{3.34}$$

where the equilibrium average $< B(z,t=0) >$ vanishes due to the evenness of the equilibrium distribution function in momentum space. We have defined,

$$D(z,\tau) \equiv < \sum_j m_j v_{jx}(\tau) \delta(z - z_j(\tau)) \sum_q m_q v_{qx} \cos(kz_q) > \tag{3.35}$$

We also expand $\delta(z-z_j)$ in terms of a $\cos(kz)$ series in the interval $[-l_z/2, l_z/2]$,

$$\delta(z-z_j) = \frac{2}{l_z}\sum_{n=0}^{+\infty}\cos(\frac{2n\pi z}{l_z})\cos(\frac{2n\pi z_j}{l_z}) = \frac{2}{l_z}\sum_{k'}\cos(k'z)\cos(k'z_j) \tag{3.36}$$

where $k' = 2n\pi/l_z$. Inserting the above equation into equation (3.34), we obtain,

$$\begin{aligned}
D(z,\tau) &= \frac{2}{l_z}\sum_{k'} < \sum_j m_j v_{jx}(\tau)\cos(k'z)\cos(k'z_j(\tau))\sum_q m_q v_{qx} a_0\cos(kz_q) > \\
&= \frac{2}{l_z}\sum_{k'}\delta_{kk'} < \sum_j m_j v_{jx}(\tau)\cos(kz)\cos(kz_j(\tau))\sum_q m_q v_{qx} a_0\cos(kz_q) > \\
&= \frac{2}{l_z}\cos(kz) < \sum_j m_j v_{jx}(\tau)\cos(kz_j(\tau))\sum_q m_q v_{qx}\cos(kz_q) > \\
&= \frac{2}{l_z}\cos(kz) < \sum_j m_j v_{jx}(\tau)\sin(kz_j(\tau))\sum_q m_q v_{qx}\sin(kz_q) > \\
&= \frac{\cos(kz)}{l_z} < \sum_j m_j v_{jx}(\tau) e^{-ikz_j(\tau)}\sum_q m_q v_{qx} e^{ikz_q} > \\
&= \frac{M}{\beta l_z}\cos(kz)\frac{C(k,\tau)}{C(k,t=0)}
\end{aligned} \tag{3.37}$$

Here, the time correlation function of cross wavenumbers ($k \neq k'$) vanishes due to translational invariance. Inserting equation (3.36) into equation (3.34), we obtain the time evolution of $< B(z,t) >$ as follows:

$$< B(z,t) >= \frac{M}{l_z} a_0\cos(kz)\int_0^t d\tau\,\frac{C(k,\tau)}{C(k,t=0)} \tag{3.38}$$

The above equation is precisely the time evolution of dynamical variable $< B(z,t) >$ upon external shear perturbation. Recalling the definition of $B(z,t)$

$$B(z,t) = \sum_q m_q v_{qx}(t)\delta(z-z_p(t)) = \sum_q \frac{2m_q v_{qx}}{lz}\sum_{k'}\cos(k'z)\cos(k'z_q(t))$$

and noticing that only the wavenumber $k' = k$ contributes to the time evolution of $< B(z,t) >$ while the rest of the terms with $k' \neq k$ vanish, we define a new function

only including this $k' = k$ branch of $B(z,t) * l_z/(M\cos(kz))$ as follows:

$$V(t) = \sum_q 2m_q v_{qx}(t) cos(kz_q(t))/M \tag{3.39}$$

It is straightforward to show that,

$$< V(t) >= \frac{< B(z,t) > l_z}{M\cos(kz)} = a_0 \int_0^t d\tau \, \frac{C(k,\tau)}{C(k,t=0)} \tag{3.40}$$

We have derived the time evolution of two dynamical variable $B(t)$ in equation (3.33) and $V(t)$ in equation (3.39) which will be used in chapter 5 to study the shear viscosity of ionic liquids.

Nonlinear Response It turns out that it is necessary to study nonlinear response theory to obtain the complete response of our ionic liquids under external shear perturbations. We therefore derive the general n-th order nonlinear response for the dynamical variable $V(t)$ in equation (3.39) under the same perturbation as we just proposed. We will see that linear response version of equation (3.40) is just the simplest case in which $n = 1$. First we note that the internal energy is

$$H_0 = \sum_j \frac{p_j^2}{2m_j} + \Phi(\mathbf{R}^N) = \sum_j \frac{p_j^2}{2m_j} + \sum_{i<j} \phi(R_{ij})$$

where $\mathbf{R}^N$ is a collective notation of $(\mathbf{R}_1, \mathbf{R}_2, \cdots, \mathbf{R}_N)$. The notation x_i and R_{ix} are the same for the $\mathbf{e}_x$ direction coordinate, and so for $\mathbf{e}_y$ and $\mathbf{e}_z$ directions. The rate of

the change of the total energy after imposing the external force is

$$\begin{aligned}
\frac{dH_0}{dt} &= i\hat{L}H_0 = 2\sum_j \frac{\mathbf{p}_j}{2m_j}\cdot\dot{\mathbf{p}}_j + \frac{d\Phi(\mathbf{R}^N)}{dt} \\
&= \sum_j \frac{p_{jx}}{m_j}(F_{jx} + m_j\cos(kz_j)a_0) + \sum_j(\frac{p_{jy}}{m_j}F_{jy} + \frac{p_{jz}}{m_j}F_{jz}) + \sum_j \frac{\partial\Phi(\mathbf{R}^N)}{\partial\mathbf{R}_j}\cdot\dot{\mathbf{R}}_j \\
&= \sum_j \frac{\mathbf{p}_j}{m_j}\cdot\mathbf{F}_j + a_0\sum_j p_{jx}\cos(kz_j) - \sum_j \mathbf{F}_j\cdot\mathbf{p}_j \\
&= a_0\sum_j p_{jx}\cos(kz_j)
\end{aligned}$$

In general, the action of the Liouville operator on an arbitrary dynamical variable B is

$$\begin{aligned}
i\hat{L}B(\mathbf{p}^N,\mathbf{R}^N) &= i\hat{L}_0B(\mathbf{p}^N,\mathbf{R}^N) + (i\hat{L} - i\hat{L}_0)B(\mathbf{p}^N,\mathbf{R}^N) \\
&= i\hat{L}_0B(\mathbf{p}^N,\mathbf{R}^N) + a_0\sum_j m_j\cos(kz_j)\frac{\partial B}{\partial p_{jx}}
\end{aligned}$$

where the Liouville operator $i\hat{L}_0$ corresponds to that of equilibrium unperturbed system (i.e. in the absence of external field $\mathbf{e}_x a_0 m_q\cos(kz_q)$). For a constant perturbation, the phase space density (phase space distribution function) can be formally written as

$$\begin{aligned}
f(\mathbf{p}_0^N,\mathbf{R}_0^N,t) &= e^{-i\hat{L}t}f_0(\mathbf{p}_0^N,\mathbf{R}_0^N) \\
&= e^{-i\hat{L}t}\frac{e^{-\beta H_0}}{\int d\Gamma e^{-\beta H_0}} = \frac{e^{-\beta\tilde{H}_0(-t)}}{\int d\Gamma d^{-\beta H_0}}
\end{aligned}$$

where Γ is the collective notation for phase space variable $(\mathbf{p}^N,\mathbf{R}^N)$ and ˜ means the dynamics is driven by both the internal and the external field. $f_0(\mathbf{p}_0^N,\mathbf{R}_0^N)$ is the equilibrium phase density without external perturbations. The partial derivative of

phase density gives the phase density equation:

$$\begin{aligned}
\frac{\partial f(\mathbf{p}_0^N, \mathbf{R}_0^N, t)}{\partial t} &= -\beta \frac{e^{-\beta \tilde{H}_0(\mathbf{p}_0^N, \mathbf{R}_0^N; -t)}}{\int d\Gamma e^{-\beta H_0}} \frac{\partial \tilde{H}_0(\mathbf{p}_0^N, \mathbf{R}_0^N; -t)}{\partial t} \\
&= -\beta f(\mathbf{p}_0^N, \mathbf{R}_0^N, t) \frac{d\tilde{H}_0(-t)}{dt} \\
&= \beta f(\mathbf{p}_0^N, \mathbf{R}_0^N, t) \left. \frac{d\tilde{H}_0(\tau)}{d\tau} \right|_{\tau=-t} \\
&= \beta f(\mathbf{p}_0^N, \mathbf{R}_0^N, t) \left[a_0 \sum_j \tilde{p}_{jx}(-t) \cos(k\tilde{z}_j(-t)) \right]
\end{aligned}$$

Here it is important to understand the relation between phase space variables. $(\mathbf{p}_0^N, \mathbf{R}_0^N)$ denotes a fixed phase space point. Variables $(\mathbf{p}_0^N, \mathbf{R}_0^N; -t)$ of $\tilde{H}_0$ corresponds to the phase space point evolved from a initial value $(\mathbf{p}_0^N, \mathbf{R}_0^N)$ for a time $-t$ with the dynamics driven by the equations (3.29) and (3.30). The solution to the above phase density equation can be formally written as

$$\begin{aligned}
f(\mathbf{p}_0^N, \mathbf{R}_0^N, t) &= exp\left\{ \beta a_0 \int_0^t ds \sum_j \tilde{p}_{jx}(-s) \cos(k\tilde{z}_j(-s)) \right\} f(\mathbf{p}_0^N, \mathbf{R}_0^N, t=0) \\
&= exp\left\{ \beta a_0 \int_0^t ds \sum_j \tilde{p}_{jx}(-s) \cos(k\tilde{z}_j(-s)) \right\} f_0(\mathbf{p}_0^N, \mathbf{R}_0^N)
\end{aligned}$$

It is useful to define dynamical variables $u(t)$ to study the response of material under external shear perturbation in the form of $\mathbf{e}_x a_0 m_q \cos(kz_q)$.

$$u(t) = \sum_j p_{jx}(t) \cos(kz_j(t))$$

and then the dynamical variable $V(t)$ can be written as

$$V(t) = \sum_q 2p_{qx}(t) \cos(kz_q(t))/M = \frac{2}{M} u(t)$$

where $M = \sum_j m_j$ is the total mass of the system. The dynamical variable $u(t)$

driven by the presence of the external field is given by

$$\tilde{u}(t) = \sum_j \tilde{p}_{jx}(t)\cos(k\tilde{z}_j(t))$$

Therefore the non-equilibrium average of $V(t)$ becomes

$$\begin{aligned} < V(t) > &= \int d\Gamma_0 V(\mathbf{p}_0^N, \mathbf{R}_0^N) f(\mathbf{p}_0^N, \mathbf{R}_0^N, t) \\ &= \frac{2}{M}\int d\Gamma_0 u(0) e^{\beta a_0 \int_0^t ds \tilde{u}(-s)} f_0(\mathbf{p}_0^N, \mathbf{R}_0^N) \\ &= \frac{2}{M}\sum_{n=1}^{\infty}(a_0\beta)^n \int_0^t ds_1 \cdots \int_0^t ds_n < u(0)\tilde{u}(-s_1)\cdots\tilde{u}(-s_n) >_0 \end{aligned}$$

where $< u(0) >_0 = 0$ is the average over the equilibrium distribution function $f_0(\mathbf{p}_0^N, \mathbf{R}_0^N)$.

Up to the order a_0^3, we have

$$\begin{aligned} < V(t) > &\simeq \frac{2}{M}\sum_{n=1}^{2}(a_0\beta)^n \int_0^t ds_1 \cdots \int_0^t ds_n < u(0)\tilde{u}(-s_1)\tilde{u}(-s_2) >_0 \\ &= \frac{2}{M}a_0\beta \int_0^t ds_1 < u(0)\tilde{u}(-s_1) >_0 \\ &\quad \frac{2}{M}(a_0\beta)^2 \int_0^t ds_1 \int_0^t ds_2 < u(0)\tilde{u}(-s_1)\tilde{u}(-s_2) >_0 \\ &= \frac{2}{M}(a_0\beta) \int_0^t ds_1 < u(0)u(-s_1) >_0 + \\ &\quad \frac{2}{M}(a_0\beta) \int_0^t ds_1 < u(0)(\tilde{u}(-s_1) - u(-s_1)) >_0 + \\ &\quad + \frac{2}{M}(a_0\beta)^2 \int_0^t ds_1 \int_0^t ds_2 < u(0)\tilde{u}(-s_1)\tilde{u}(-s_2) >_0 \end{aligned} \tag{3.41}$$

Define the time correlation function

$$C(k,t) = < \sum_q p_{qx} e^{-ikz_q} \sum_j p_{jx}(t) e^{-ikz_q(t)} >$$

The initial value of $C(k,t)$ is

$$C(k, t=0) = < \sum_q m_q^2 v_{qx}^2 > = \frac{M}{\beta}$$

Therefore the first term in $< V(t) >$ (equation (3.41)) becomes

$$\begin{aligned} < V(t) >^{(1)} &= \frac{2}{M}(a_0\beta)\int_0^t ds_1 < u(0)u(-s_1) >_0 \\ &= \frac{2}{M}(a_0\beta)\int_0^t ds < u(0)u(s) >_0 \\ &= a_0\int_0^t d\tau \frac{C(k,\tau)}{C(k,t=0)} \end{aligned}$$

which is precisely the linear response part (equation (3.40)). In order to figure out the nonlinear response part, we have to decompose the dynamical variable $\tilde{u}(-s)$ into a combination of equilibrium variables. For this we introduce the Dyson decomposition to rewrite $\tilde{u}(-s)$ as a function of $u(-s)$ which evolves without the presence of external field.

In general, the Dyson decomposition is written as[16]:

$$\begin{aligned} e^{i\hat{L}t} &= e^{i\hat{L}_0 t} + \int_0^t ds e^{i\hat{L}s}(i\hat{L} - i\hat{L}_0)e^{i\hat{L}_0(t-s)} \\ &= e^{i\hat{L}_0 t} + \sum_{n=1}^{\infty}\int_0^t ds_1 \int_0^{s_1} ds_2 \cdots \int_0^{s_{n-1}} ds_n e^{i\hat{L}_0 s_n}(i\hat{L} - i\hat{L}_0)e^{i\hat{L}_0(s_{n-1}-s_n)} \\ &\quad \cdots (i\hat{L} - i\hat{L}_0)e^{i\hat{L}_0(s_1-s_2)}(i\hat{L} - i\hat{L}_0)e^{i\hat{L}_0(t-s_1)} \end{aligned} \tag{3.42}$$

A straightforward proof of Dyson decomposition is given in the Appendix B. Because the integration up n-th order corresponds to the order of magnitude a_0^n, we need to consider $n = 1$ for the second term in equation (3.41) and consider $n = 0$ for the

third term in equation (3.41).

$$\begin{aligned}
\tilde{u}(-t) - u(-t) &\simeq (e^{-i\hat{L}t} - e^{-i\hat{L}_0 t})u(0) \\
&= -\int_0^t ds_1 e^{-i\hat{L}_0 s_1}(i\hat{L} - i\hat{L}_0)e^{-i\hat{L}_0(t-s_1)}u(0) \\
&= -\int_0^t ds e^{-i\hat{L}_0(t-s)}(i\hat{L} - i\hat{L}_0)e^{-i\hat{L}_0 s}u(0) \\
&= -e^{-i\hat{L}_0 t}\int_0^t ds e^{i\hat{L}_0 s}(i\hat{L} - i\hat{L}_0)e^{-i\hat{L}_0 s}u(0) \\
&= -e^{-i\hat{L}_0 t}\int_0^t ds e^{i\hat{L}_0 s}(i\hat{L} - i\hat{L}_0)u(-s) \\
&= -a_0 e^{-i\hat{L}t}\int_0^t ds e^{i\hat{L}_0 s}\left[\sum_j m_j \cos(kz_j)\frac{\partial u(0)}{\partial p_{jx}}\right] \\
&= -a_0 e^{-i\hat{L}_0 t} t \sum_j m_j \cos(kz_j)\frac{\partial u(0)}{\partial p_{jx}}
\end{aligned}$$

Therefore up to order of magnitude a_0^2, we have:

$$\begin{aligned}
< V(t) > &= a_0\int_0^t d\tau \frac{C(k,\tau)}{C(k,t=0)} \\
&\quad + \frac{2}{M}a_0\beta\int_0^t ds < u(0)(-a_0)e^{-i\hat{L}_0 s}s\sum_j m_j\cos(kz_j)\frac{\partial u(0)}{\partial p_{jx}} > \\
&\quad \frac{2}{M}(a_0\beta)^2\int_0^t ds_1\int_0^t ds_2 < u(0)u(-s_1)u(-s_2) >_0 \\
&= a_0\int_0^t d\tau \frac{C(k,\tau)}{C(k,t=0)} \\
&\quad + a_0^2\frac{2}{C(k,t=0)}\int_0^t ds s < u(s)\sum_j m_j\cos(kz_j)\frac{\partial u(0)}{\partial p_{jx}} > \\
&\quad + \frac{2}{M}(a_0\beta)^2\int_0^t ds_1\int_0^t ds_2 < u(0)u(s_1)u(s_2) >_0
\end{aligned} \tag{3.43}$$

Equation (3.43) can be used to predict the nonlinear response behavior upon an external shear perturbation. We thus have completed the derivation of nonlinear response theory for our specific case of shear perturbation.

Initial Pulse Perturbation We have considered the case of a constant perturbation

starting at $t = 0$ ($h(t)$ is the step function). It is also interesting to study how the system will relax if initially a non-equilibrium state is created by a pulse perturbation.

We assume an initial velocity profile of the form:

$$u_x(z,t) = w_0 \cos(kz) \tag{3.44}$$

is created by a pulse interaction and the external force is zero ($a_0 = 0$). The initial distribution function can be written as,

$$f(\mathbf{R}^N, \mathbf{v}^N) = f_0(\mathbf{R}^N, \mathbf{v}_1 - \mathbf{e}_x w_0 \cos(kz_1), \mathbf{v}_2 - \mathbf{e}_x w_0 \cos(kz_2), \cdots, \mathbf{v}_N - \mathbf{e}_x w_0 \cos(kz_N))$$

where $\mathbf{R}^N, \mathbf{v}^N$ are collective notations for positions and velocities of $1, 2, \cdots, N$ particles and $f_0(\mathbf{R}^N, \mathbf{v}^N)$ is the equilibrium distribution function. Recalling again the definition of $B(z,t)$,

$$B(z,t) = \sum_q m_q v_{qx}(t) \delta(z - z_q(t)),$$

we have

$$\begin{aligned}
< B(z, t=0) > &= \int\int d\mathbf{v}^N d\mathbf{R}^N \sum_{p=1}^{N} m_p v_{px} \delta(z - z_p) f(\mathbf{R}^N, \mathbf{v}^N, t=0) \\
&= \sum_{p=1}^{N} \int\int d\mathbf{v}^N d\mathbf{R}^N \, m_p (v_{px} + w_0 \cos(kz_p)) \delta(z - z_p) f_0(\mathbf{R}^N, \mathbf{v}^N) \\
&= \sum_{p=1}^{N} \int\int d\mathbf{v}^N d\mathbf{R}^N \, m_p w_0 \cos(kz_p) \delta(z - z_p) f_0(\mathbf{R}^N, \mathbf{v}^N) \\
&= w_0 \cos(kz) \frac{M}{l_z}
\end{aligned} \tag{3.45}$$

where M/l_z is the length density of the system.

The evolution of the distribution function $f(\mathbf{R}^N, \mathbf{v}^N, t)$ is determined by Liouville's equation (2.8):

$$f(\mathbf{R}^N, \mathbf{v}^N, t) = e^{-it\hat{L}} f(\mathbf{R}^N, \mathbf{v}^N, 0) = e^{-it\hat{L}} f_0(\mathbf{R}^N, \{\mathbf{v}_p - \mathbf{e}_x w_0 \cos(kz_p)\}^{\{p=1,\cdots,N\}})$$

Assume that the perturbation $-\mathbf{e}_x w_0 \cos(kz_p)$ is small enough such that we only need to consider the first two terms in the Taylor expansion of $f(\mathbf{R}^N, \mathbf{v}^N, 0)$,

$$\begin{aligned}
f(\mathbf{R}^N, \mathbf{v}^N, 0) &= f_0(\mathbf{R}^N, \{\mathbf{v}_p - \mathbf{e}_x w_0 \cos(kz_p)\}^{\{p=1,\cdots,N\}}) \\
&= f_0(\mathbf{R}^N, \mathbf{v}^N) + \sum_{p=1}^{N} \frac{\partial f_0(\mathbf{R}^N, \mathbf{v}^N)}{\partial v_{px}}(-w_0)\cos(kz_p) + \cdots \\
&\simeq f_0(\mathbf{R}^N, \mathbf{v}^N) - w_0 \sum_{p=1}^{N} \frac{\partial f_0(\mathbf{R}^N, \mathbf{v}^N)}{\partial v_{px}} \cos(kz_p) \\
&= f_0(\mathbf{R}^N, \mathbf{v}^N) - w_0 \sum_{p=1}^{N} \frac{\partial (e^{-\beta H}/Q)}{\partial v_{px}} \cos(kz_p) \\
&= f_0(\mathbf{R}^N, \mathbf{v}^N) - w_0 \sum_{p=1}^{N} (-\beta)\frac{e^{-\beta H}}{Q}\frac{\partial H(\mathbf{R}^N, \mathbf{v}^N)}{\partial v_{px}} \cos(kz_p) \\
&= f_0(\mathbf{R}^N, \mathbf{v}^N) + \beta w_0 \sum_{p=1}^{N} f_0(\mathbf{R}^N, \mathbf{v}^N)\frac{\partial H(\mathbf{R}^N, \mathbf{v}^N)}{\partial v_{px}} \cos(kz_p) \\
&= f_0(\mathbf{R}^N, \mathbf{v}^N) + \beta w_0 \sum_{p=1}^{N} f_0(\mathbf{R}^N, \mathbf{v}^N) m_p v_{px} \cos(kz_p) \\
&= f_0(\mathbf{R}^N, \mathbf{v}^N) + \beta w_0 f_0(\mathbf{R}^N, \mathbf{v}^N) \sum_{p=1}^{N} m_p v_{px} \cos(kz_p)
\end{aligned}$$

Therefore,

$$\begin{aligned}
e^{-it\hat{L}} f(\mathbf{R}^N, \mathbf{v}^N, 0) &= e^{-it\hat{L}} f_0(\mathbf{R}^N, \mathbf{v}^N) + \beta w_0 e^{-it\hat{L}} \left[f_0(\mathbf{R}^N, \mathbf{v}^N) \sum_{p=1}^{N} m_p v_{px} \cos(kz_p) \right] \\
&= f_0(\mathbf{R}^N, \mathbf{v}^N) + \beta w_0 f_0(\mathbf{R}^N, \mathbf{v}^N) e^{-it\hat{L}} \sum_{p=1}^{N} m_p v_{px} \cos(kz_p) \qquad (3.46)
\end{aligned}$$

The average of $B(z,t)$ becomes,

$$\begin{aligned}
< B(z,t) > &= \int\int d\mathbf{v}^N d\mathbf{R}^N \, B(z,t=0) f(\mathbf{R},v,t) \\
&= \int\int d\mathbf{v}^N d\mathbf{R}^N \, B(z,t=0) e^{-it\hat{L}} f(\mathbf{R},v,0) \\
&\simeq \int\int d\mathbf{v}^N d\mathbf{R}^N \, B(z,t=0) \\
&\qquad \left\{ f_0 + \beta w_0 f_0(\mathbf{R}^N,\mathbf{v}^N) e^{-it\hat{L}} \left[\sum_{p=1}^{N} m_p v_{px} \cos(kz_p) \right] \right\} \\
&= \beta w_0 \int\int d\mathbf{v}^N d\mathbf{R}^N \, B(z,t=0) f_0(\mathbf{R}^N,\mathbf{v}^N) e^{-it\hat{L}} \left[\sum_{p=1}^{N} m_p v_{px} \cos(kz_p) \right] \\
&= \beta w_0 \int\int d\mathbf{v}^N d\mathbf{R}^N \, B(z,t) f_0(\mathbf{R}^N,\mathbf{v}^N) \left[\sum_{p=1}^{N} m_p v_{px} \cos(kz_p) \right] \\
&= \beta w_0 < B(z,t) \sum_{p=1}^{N} m_p v_{px} \cos(kz_p) > \\
&= \beta w_0 D(z,t) \qquad (3.47)
\end{aligned}$$

Recalling the expression for $D(z,t)$ from equation (3.37), we have,

$$< B(z,t) >= \beta w_0 \frac{M}{\beta l_z} \cos(kz) \frac{C(k,t)}{C(k,t=0)} =< B(z,0) > \frac{C(k,t)}{C(k,t=0)} \qquad (3.48)$$

where we have used equation (3.45). Thus, we complete the theory for the time evolution of the variable $B(t)$ under an initial pulse perturbation of the form (3.44).

In closing this section, we have derived the linear response and nonlinear theories in detail for the case of shear perturbations. The results in equations (3.38), (3.40), and (3.48) will be used in chapter 5 to study the response of room temperature ionic liquids upon shear perturbation. The formulation of nonlinear response theory (3.43) will be useful in future research involving nonlinear response of the ionic liquids.

CHAPTER 4
NUMERICAL SIMULATION OF IONIC LIQUIDS

In previous chapters we have derived general formulations for transport properties and linear and nonlinear response theories for a statical mechanical system upon external perturbations in terms of time correlation functions. Though the theoretical analysis in previous chapters is very informative, it is in general very hard to compute the required time correlation functions analytically. As we have mentioned in Chapter 2, people have developed analytical tools such as mode coupling theory [59] to uncouple GLE (2.13). Most of the applications of such theory are still limited to simple liquids like hard sphere fluids or atomic liquids with simple interaction[26]. Without any analytical solution available, a direct way to study the dynamics of complex liquids is to do numerical simulations. The main contribution of the author of this thesis is his exploration of transport and dynamical properties of ionic liquids through molecular dynamics (MD) simulations [35, 37, 38, 36]. This chapter will give a brief introduction to MD simulations and provide the potential energy function used for all the systems studied. Excellent references on molecular dynamics simulation are available [1, 19, 72].

4.1 Molecular Dynamics Simulation

Molecular dynamics has extensively enriched the understanding of the behavior of liquids since the middle of last century[1]. Simply speaking, the procedure of classical simulation is to solve Newton's equations numerically. For our NVE (

constant number of particle, constant volume and constant total energy) production runs, Newton's equations of motion are:

$$\dot{\mathbf{R}}_j = \mathbf{v}_j$$

$$m_j \dot{\mathbf{v}}_j = \mathbf{a}_j$$

One of the most popular algorithms to numerically solving this Newtonian equations of motion is the Verlet algorithm[74, 1].

Verlet Algorithm At time t, the system has a configuration $(\mathbf{R}^N(t), \mathbf{v}^N(t))$, the force is determined by the derivative of the potential:

$$\mathbf{a}_j(t) = -\frac{1}{m_j}\nabla_j(U\mathbf{R}^N(t)) \tag{4.1}$$

Taylor expansions at $t = t + \Delta t$ and $t = t - \Delta t$ gives the coordinates of next frame and previous frame respectively:

$$\mathbf{R}_j(t+\Delta t) = \mathbf{R}_j(t) + \mathbf{v}_j(t)\Delta t + \frac{1}{2}\mathbf{a}_j(t)\Delta t^2 + \frac{1}{6}\mathbf{b}(t)\Delta t^3 + \mathcal{O}(\Delta t^4)$$

$$\mathbf{R}_j(t-\Delta t) = \mathbf{R}_j(t) - \mathbf{v}_j(t)\Delta t + \frac{1}{2}\mathbf{a}_j(t)\Delta t^2 - \frac{1}{6}\mathbf{b}(t)\Delta t^3 + \mathcal{O}(\Delta t^4)$$

The Verlet algorithm calculates the configuration at the next frame $t = t+\Delta t$ through:

$$\mathbf{R}_j(t+\Delta t) = 2\mathbf{R}_j(t) - \mathbf{R}_j(t-\Delta t) + \mathbf{a}_j(t)\Delta t^2 + \mathcal{O}(\Delta t^4)$$

$$\mathbf{v}_j(t) = \frac{\mathbf{R}_j(t+\Delta t) - \mathbf{R}_j(t-\Delta t)}{2\Delta t} + \mathcal{O}(\Delta t^2)$$

Modifications to the above basic scheme have been proposed in the last thirty years[32, 56, 72]. The algorithm used in our simulation is the leap-frog scheme implemented in Gromacs software[47, 7, 72].

$$\mathbf{R}_j(t+\Delta t) = \mathbf{R}_j(t) + \Delta t\mathbf{v}(t+\frac{1}{2}\Delta t)$$

$$\mathbf{v}(t+\frac{1}{2}\Delta t) = \mathbf{v}(t-\frac{1}{2}\Delta t) + \Delta t\mathbf{a}(t)$$

Periodic Boundary Condition (PBC) We apply periodic boundary conditions to minimize edge effects in a finite system. There are no walls at the boundary of the center box. The properties calculated from the use of periodic boundary condition for a small system may be different from those of a real macroscopic system. In general, as people have already demonstrated in other liquids, properties not depending on long-wavelength fluctuations can be well reproduced by using a small box with the implementation of periodic boundary condition[1]. In our simulations, transport properties corresponding to diffusion and optical response will be independent of typical simulation boxes, while the shear viscosity computed from different simulation box sizes are wavelength dependent.

Calculating the force The most time-consuming part of molecular dynamics simulation is to calculate the force through equation (4.1) In our simulation of ionic liquids, we use a potential energy function of the form[50]

$$U = U_{stretch} + U_{bend} + U_{torsion} + U_{LJ} + U_{Coulomb} \tag{4.2}$$

where

$$U_{stretch} = \sum_{bonds} K_r(r - r_{eq})^2 \tag{4.3}$$

$$U_{bend} = \sum_{angles} K_\theta(\theta - \theta_{eq})^2 \tag{4.4}$$

$$U_{torsion} = \sum_{dihedrals} \sum_{n=0}^{5} C_n(\cos(\phi))^n) \tag{4.5}$$

$$U_{LJ} = \sum_{i<j} 4\epsilon_{ij} \left[(\frac{\sigma_{ij}}{r_{ij}})^{12} - (\frac{\sigma_{ij}}{r_{ij}})^6 \right] \tag{4.6}$$

$$U_{Coulomb} = \sum_{i<j} \frac{q_i q_j}{r_{ij}} \tag{4.7}$$

All of the parameters for the stretch, bend, torsion and, Lennard-Jones terms were taken from the OPLS/AA force field[39], while partial charges q_i were taken from fits to the electrostatic potential (ESP) by performing *ab initio* quantum calculations[67]. In the next section, we will provide those parameters in detail for all the molecules we studied.

4.2 Effective Potential of molecules

The ionic systems we studied are 1-butyl-3-methylimidazolium hexafluophosphate ([BMIM+][PF6-]), 1-hexyl-3-methylimidazolium chloride ([HMIM+][CL-]), 1-methoxy-ethylpyridinium dicyanoamide ([MOEPY+][DCA-]). Representations of these molecules are drawn in Figure 4.1.

The fluorescence probe used in studying the reorganization time scales of ionic liquids is 2-amino-7-nitrofluorene (ANF). All of potential parameters required for equations (4.2) through (4.7) and molecular geometries are listed in the Appendix D. The geometry of the ANF molecule was provided as an input for *ab initio* quantum calculation. The relative connectivity of each atom determines the atom type in the OPLSAA force field[39]. The ground state charges are obtained from ESP fitting of the electronic potential by performing an *ab initio* calculation at the (HF/6-31G*) theory level using the GAUSSIAN program[67, 20]. The excited-state charge distribution was estimated by computing the ground (S_0) and first singlet excited (S_1) charge difference using the ZINDO Hamiltonian with configuration interaction[61]. These

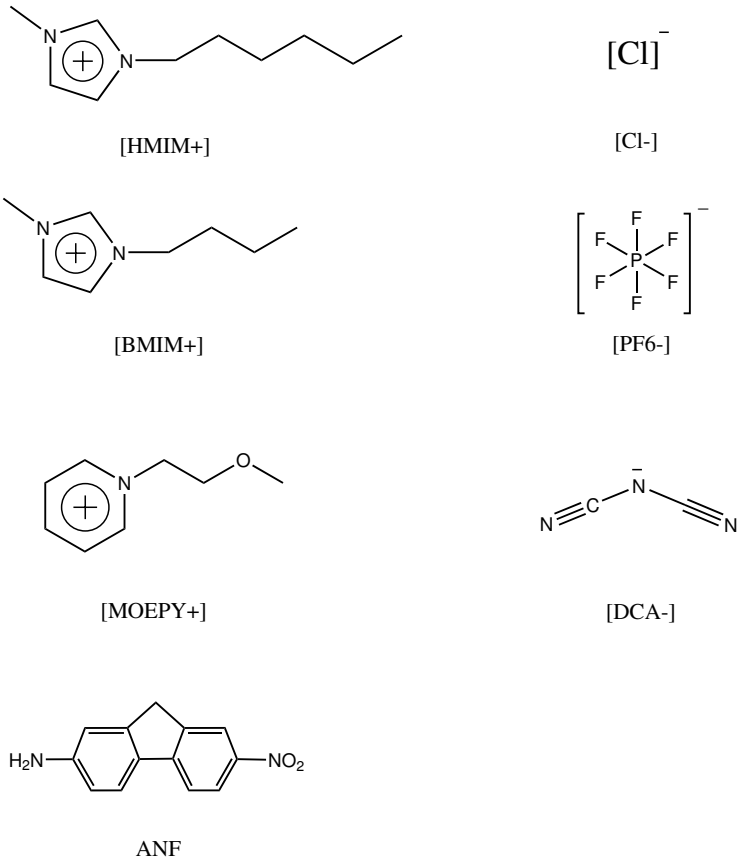

Figure 4.1: Molecular systems

calculations were performed with the software Hyperchem 7(Hypercube, Gainesville, FL). The charge distribution in the excited state used for our MD calculations was obtained by adding the charge difference obtained from the ZINDO calculation to the ground-state charges obtained by the Hartree-Fock method.

Stretching, bending and torsion parameters are all taken from OPLSAA force field.

CHAPTER 5
TRANSPORT PROPERTIES OF IONIC LIQUIDS

We have already provided the general theory of transport properties in terms of time correlation functions. In this chapter, we performed molecular dynamics of ionic liquid systems [BMIM+][PF6-] and [HMIM+][CL-] to compute the quantities previously defined in chapter 2 and to investigate the slow dynamical nature of ionic liquids[35, 38].

5.1 Diffusion and Dynamical Heterogeneity

Simulation Details We performed molecular dynamics simulation for the neat liquid system [BMIM+][PF_6-]. Simulations were carried out using the software GROMACS [47, 7]. Potential energy parameters are those previously explained in Chapter 4. Periodic boundary conditions were employed using the particle mesh Ewald (PME) method to treat long-range electrostatic interactions[15, 50, 49]. All systems were initially equilibrated for several hundred picoseconds in the NPT ensemble using the Berendsen method until trending in the volume was no longer observed[7]. This equilibration time was sufficient since initial liquid configurations were obtained from previously equilibrated long trajectories from reference[49]. Simulations were performed at 300K, 400K, 500K. Production runs were carried out in the NVE ensemble using 256 pairs of ions. These NVE runs were 3 ns in duration for the runs at 400K and 500K and 9 ns in the case of the run at 300K. The time step used is 0.001ps. We used a cutoff at 1.5nm and the total energy drift is less than 0.1%.

Results and Discussion We have studied the mean square displacement (MSD) of cations and anions as a function of time for 3 different temperatures. Fig. 5.1A shows a logarithmic plot of MSD as a function of time in the case of the center of mass of the cationic ring. Very similar functions are obtained in the case of the anions indicating that cationic and anionic diffusive rates are highly correlated. At all temperatures investigated the MSD displays three typical regions: an initial subpicosecond ballistic region, an intermediate cage region and a long time diffusive region. The subpicosecond ballistic region (slope=2) is separated from the diffusive region (slope=1) by a plateau with slope close to zero in which ions are trapped in local cages. The duration of this cage regime varies with temperature. At 500K this plateau is nearly absent as in a normal liquid, but close to room temperature the plateau region is of the order of nanoseconds as can be appreciated in Fig. 5.1A. The fact that the intermediate cage regime is so long compared to most other liquids at room temperature has significant consequences in terms of spectroscopy. This point will be discussed in detail in the following subsection. In order to better understand the translational behavior of the ionic liquid, we computed the self part of the time dependent van Hove correlation function [73]:

$$G_s(\mathbf{r},t) = \frac{1}{N}\langle\sum_{j=1}^{N}\delta(\mathbf{r}+\mathbf{r}_j(0)-\mathbf{r}_j(t))\rangle \tag{5.1}$$

Here, $4\pi r^2 G_s(r,t)dr$ is the probability of finding at time t an ion in the vicinity dr of points at the distance r given that initially the particle was located at the origin. For typical liquids $G_s(\mathbf{r},t)$ has a Gaussian form given by:

$$G_s^d(\mathbf{r},t) = [3/2\pi\langle r^2(t)\rangle]^{3/2} exp[-3r^2/2\langle r^2(t)\rangle] \tag{5.2}$$

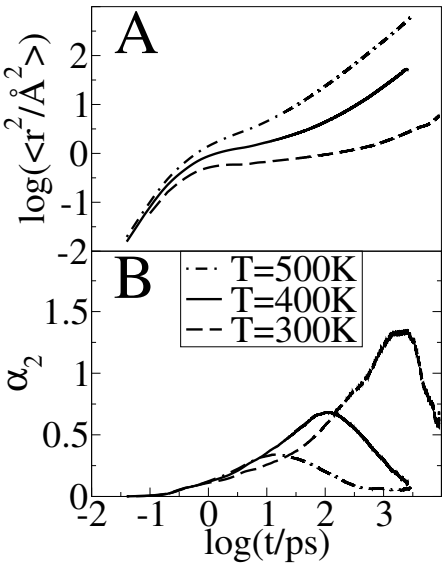

(A) Mean square displacement versus time for the center of mass of the cationic ring at 300,400 and 500K. (B) Comparison of the non-Gaussian parameter α_2 versus time for the cations at 300, 400 and 500K. At 400K the maximum is at at $t^* = 109$ps, while at 300k it shifts to 2.48ns.

Figure 5.1: MSD and non-Gaussian parameter

where $\langle r^2(t)\rangle$ is the mean square displacement of the particles. Deviations from Gaussian behavior can be characterized by the non-Gaussian parameter defined as: $\alpha_2(t) = 3\langle r^4(t)\rangle/5\langle r^2(t)\rangle^2 - 1$ [57, 42, 41, 43, 22]. Fig. 5.1B shows α_2 as a function of time in the case of the cations at 300 and 400K. At 300K the non-Gaussian parameter reaches its maximum at time $t^* = 2.48$ns where the self van Hove correlation function has its maximum deviation from Gaussian behavior. Consistent with the findings of Del Popolo and Voth[12] in a similar ionic liquid, we observe that at 400K the maximum deviation from Gaussian behavior occurs at 109 ps. Using the data at 300K we computed the self van Hove correlation function $G_s(\mathbf{r}, t^*)$ and the standard Gaussian function $G_s^d(\mathbf{r}, t^*)$. Fig. 5.2 clearly shows that $G_s(r, t^*)$ and $G_s^d(r, t^*)$ inter-

sect at a distance of about 2.9Å . As we can appreciate, most ions appear to diffuse slower than expected from Gaussian diffusion but a group of ions exist that diffuse much faster. This point can be seen from the fact that $G_s(r, t^*)$ has a much longer tail than the corresponding Gaussian function $G_s^d(\mathbf{r}, t^*)$. We use the approach previ-

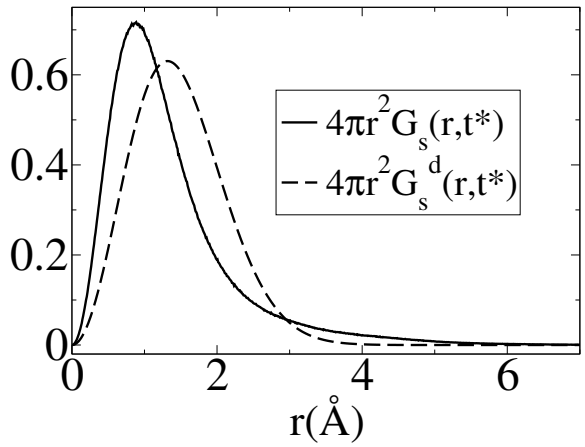

The self part of the van Hove correlation function for the cations and its standard Gaussian form at the time $t = t^*$ for the system at 300K. Because this system is isotropic we only consider the radial part: $4\pi r^2 G_s(r, t^*)$.

Figure 5.2: Self van Hove correlation funct.

ously introduced by Kob and coworkers in order to define two cationic and anionic subensembles[43]. We computed the displacement of all ions during time windows $[t_0, t_0 + t^*]$ and defined in each case the set of anions and cations with top 10 percent maximum mobility as cationic and anionic mobile subensembles. Cations and anions in the bottom 10 percent mobility range are defined as those belonging to the immobile subensembles. By analyzing $G_s(r, t)$ plotted in Fig. 5.2 A, B, C and D we find that anions in the mobile subensemble have in average moved further in 200 ps than those

in the immobile subensemble in 3000ps. The same phenomenon can be appreciated in the case of the cations where for the mobile subensemble the van Hove correlation function shows longer tails at 200ps than in the case of the immobile subensemble at 2000ps. Particularly interesting is the appearance of multiple peaks in the van Hove distribution at longer times. This is indicative of hopping processes[60]. These hopping processes imply that within the mobile subensemble, some particles move much faster than others. Interestingly these subensembles of "slow" and "fast" diffusing ions appear to be correlated in space. Proof that mobile ions are clustered in space and are far removed from the subset of immobile ions is given by corresponding radial distribution functions (RDFs) displayed in Fig. 5.4IA and IB. We can see from these plots that the diagonal terms $g_{mobile-mobile}$ and $g_{immobile-immobile}$ have large first peaks while the cross terms $g_{mobile-immobile}$ show a depletion of density at short distances. This means that the correlation between either the mobile or the immobile particles is much higher than the mobile-immobile cross correlation. Similar correlation was recently observed in the MD simulations of supercooled water and supercooled Lennard-Jones liquids[43, 22, 60, 14]. Rotational diffusion of solute and solvent is important in ILs because in a slow viscous solvent it provides a local mechanism for energy transfer and "fast" relaxation once a probe molecule has been photo-excited and its charge distribution distorted. In order to investigate solvent reorientational dynamics we use an approach previously introduced by Ribeiro in the study of a high temperature molten salt[60]. We define an orientation analog of the self van Hove correlation function, $G(\theta, t)$: $G(\theta, t) = \langle \delta[\theta - \theta_i(t)] \rangle$ where $\theta_i(t) = \cos^{-1}[\mathbf{u}_i(t) \cdot \mathbf{u}_i(0)]$.

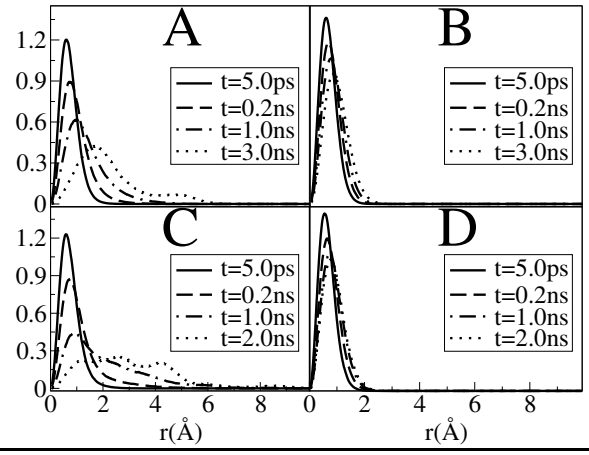

The self part of the van Hove correlation function $G_s(r,t)$ for anions ((A) and (B)) and cations ((C) and (D)) in the mobile ensemble ((A) and (C)) and the immobile ensemble ((B) and (D)) at three different times. Mobile and immobile subensembles are defined in the text.

Figure 5.3: Self van Hove correlation funct. of subensembles

In order to gauge whether translational mobility is decoupled from rotational mobility we display in Fig. 5.5II $G(\theta,t)$ for those anions and cations belonging to the translationally mobile and translationally immobile subensembles. Fig. 5.5A and Fig. 5.5B clearly prove that translational mobility is totally decoupled from rotational mobility in the case of the [PF6-] anions. In both cases, at 5.0ps, $G(\theta,t)$ has a primary peak and a secondary peak. The secondary peak corresponds to an angle of approximately 90 degrees. This peak becomes more prominent at larger times. This behavior is characteristic of rotational hopping processes that, due to the high degree of symmetry of the anion, leave the ion in an orientational configuration indistinguishable from the original one. As opposed to the anionic case, in the case of the cations we see that rotational and translational mobility are strongly coupled. $G(\theta,t)$ at 100ps in the case of the translationally mobile subensemble of cations is similar to $G(\theta,t)$ at 2000ps

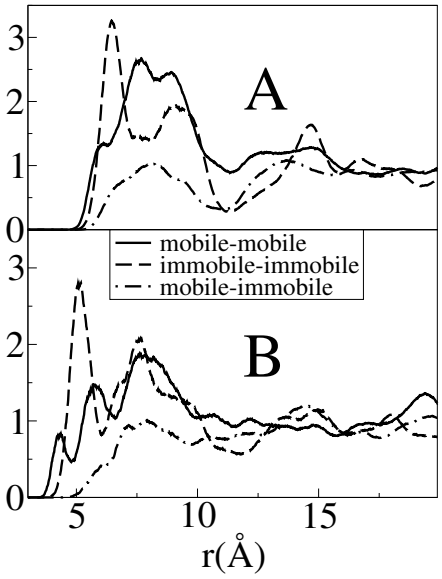

Diagonal (mobile-mobile) (immobile-immobile) and off-diagonal (mobile-immobile) radial distribution functions in the case of the anions (A) and the cations (B). First peaks in the case of the diagonal terms are large indicating strong spatial correlation and clustering. Off-diagonal terms show density depletion at short distances, consistent with the idea that groups of mobile and immobile particles are separated in space.

Figure 5.4: RDFs of mobile and immobile subensembles and their cross

in the case of the corresponding translationally immobile subensemble. For those cations in the mobile subensemble we find multiple peaks at large distance indicating the existence of reorientational hopping processes consistent with those observed for the same subgroup in our study of translational mobility.

5.2 Shear Viscosity

In this section attention is directed to three related problems; (1) the response of the Ionic liquid (IL) 1-hexyl-3 methylimidazolium chloride ([HMIM+][CL-]) to different external perturbations, (2) the calculation of its shear viscosity and (3)

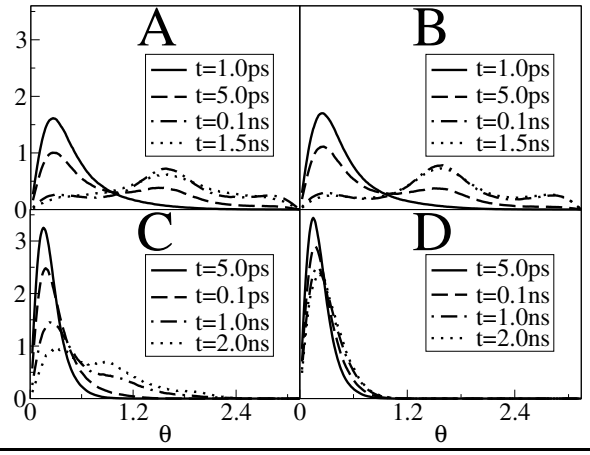

$G(\theta, t)$ in the case of the anions ((A) and (B)) and the cations ((C) and (D)) in the mobile subensemble ((A) and (C)) and in the immobile subensemble ((B) and (D)) at different times. The units of θ are in radians.

Figure 5.5: Angular distribution in subensembles

the investigation of the range of validity of linear response theory for these types of systems. Our study shows that even for systems with box length as large as $0.03\mu m$ the viscosity computed from perturbation frequencies compatible with this box size have not yet reached the bulk hydrodynamic limit. This is in sharp contrast with the case of other solvents such as water in which the hydrodynamic limit can be achieved by using perturbations on a length scale of typical molecular dynamics simulation box sizes. In order to achieve our goals, we comprehensively investigated how the IL relaxed upon weak external perturbations at different wavenumbers. We also studied the steady state flow created by external shear acceleration fields. Short time behavior of instantaneous velocity profiles was compared with the results of linear response theory. The short time response appears to match the prediction from linear response theory while the long time response deviates as the external

field becomes stronger. From this study the range on which a perturbation can be considered "weak" in the linear response sense can be established. The relaxation of initial velocity profiles was also examined and correlated to the decay of transverse current auto correlation function. Even though none of our calculations reached the bulk hydrodynamic limit we are able to make predictions for the bulk viscosity of this system at different temperatures which qualitatively agrees with experimental data[23, 38].

Simulation Details We performed molecular dynamics simulation for the system [HMIM+][CL-]. All of the equilibrium procedures and treatment of long range interaction, are the same as those reported in previous subsection. In order to facilitate equilibration, we initially simulated three different system sizes (343 pairs, 2744 pairs and 8232 pairs) at temperature T=500 K. For each of these, one NVE production simulation was run for about 1ns to calculate transverse current auto correlation functions (TCACs).

For the smallest system (343 ion pairs), non-equlibrium molecular dynamics (NEMD) simulations were run at three different shear rates. For each of the two larger systems (2744 and 8232 ion pairs), NEMD simulations were run at two different shear rates. Each of these NEMD simulations was at least 700 ps in duration in order to guarantee good statistics. In order to study the transient behavior of instantaneous velocity amplitude upon perturbation for each shear rate used in the three systems mentioned before, four independent NEMD simulations were run. The duration of these runs was 20ps for the two smaller systems and 50 ps for the largest.

Finally, in the case of our largest system, we imposed an initial $\cos(kz)$ shape velocity profile and ran 200 independent simulations to observe its decay after the drag is switched off at time zero. Each of these 200 simulations was 10 ps in duration.

All of the above simulations were also performed at T = 400 K but only for the largest system size (8232 pairs corresponding to $263,424$ atoms). Table 5.1 shows the characteristics of each different system.

Table 5.1: System characterization

Pairs of Ions	T (K)	Box Size (nm)	a_0 (nm/ps^2)	η (cp)
8232	500	$l_x = l_y = 10.26$, $l_z = 30.79$	0.005	8.859± 0.103
			0.010	6.423± 0.039
2744	500	$l_x = l_y = l_z = 10.26$	0.03	7.233± 0.108
			0.05	3.602± 0.024
343	500	$l_x = l_y = l_z = 5.125$	0.10	3.981± 0.069
			0.20	1.232± 0.007
			0.30	0.662± 0.003
8232	400	$l_x = l_y = 10.07$, $l_z = 30.20$	0.01	57.14± 1.669
			0.02	6.683± 0.068

Characteristics of our different simulation boxes and corresponding viscosity values from equation (5.12). The error estimates are based on our fit of the corresponding steady state velocity profile, see Fig. 5.7 through Fig. 5.9 and Fig. 5.11.

Theoretical Background Here we use the results previously derived in chapters 2 and 3.

Hydrodynamic Equations We consider only the transverse part of Navier-Stokes equation [8]:

$$\rho\frac{\partial u_x(z,t)}{\partial t} = \rho a_x(z,t) + \eta\frac{\partial^2 u_x(z,t)}{\partial z^2} \tag{5.3}$$

where we define the z direction as the longitudinal direction, $u_x(z,t)$ and $a_x(z,t)$ are the transverse velocity field and external acceleration respectively, ρ is mass density, and η is the coefficient of shear viscosity. This macroscopic equation is only valid at long time scale and large length scale (small wavenumbers). We are going to use this equation as the starting point to discuss three different cases: spontaneous fluctuation(SF), periodic perturbation(PP) and initial pulse perturbation(IPP).

Spontaneous Fluctuation Here we consider an equilibrium case where the external force is zero in equation (5.3) and define the spatial Fourier transform of the dynamical variable $u(\mathbf{r})$ as,

$$u(\mathbf{k},t) = \int_{-\infty}^{+\infty} u(\mathbf{r},t)e^{i\mathbf{k}\cdot\mathbf{r}}\,d\mathbf{r} \tag{5.4}$$

the equilibrium solution to equation (5.3) in k space is,

$$u(\mathbf{k},t) = u(\mathbf{k},0)exp(-\frac{\eta}{\rho}k^2 t) \tag{5.5}$$

Therefore the auto correlation function

$$C(k,t) =< u^*(\mathbf{k},0)u(\mathbf{k},t) > \tag{5.6}$$

evolves exponentially as [8]

$$C(k,t) = C(k,0)exp(-\frac{\eta}{\rho}k^2 t) \tag{5.7}$$

where $C(k,t)$ is only a function of the magnitude of the wavenumber vector $\mathbf{k}$ for isotropic systems. Further define the Fourier transform of the time correlation function $C(t)$ as:

$$C(k,\omega) = \int_0^{+\infty} C(k,t)e^{i\omega t}\,dt \tag{5.8}$$

and directly integrate both sides of equation (5.7), to obtain,

$$\frac{C(k,\omega=0)}{C(k,t=0)} = \int_0^{+\infty} exp(-\frac{\eta}{\rho}k^2 t)\,dt = \frac{\rho}{\eta k^2} \tag{5.9}$$

The left hand side of the above equation is just the area under the normalized time correlation function $C(k,t)/C(k,t=0)$. The coefficient of shear viscosity η can be calculated from this normalized area or the zero frequency value of the spectra (equation (5.8)). This method has been used by Balucani *et.al*[6] for a water system and Urahata and Ribeiro [71] for ionic liquid systems.

Periodic Perturbation In the case of PP, we assume an initial velocity and an acceleration profile as,

$$\begin{cases} u_x(z,t=0) &= 0 \\ a_x(z,t) &= a_0\cos(kz) \end{cases} \tag{5.10}$$

The solution to equation (5.3) becomes,

$$u_x(z,t) = a_0\tau(1-e^{-t/\tau})\cos(kz) = u_0\cos(kz) \tag{5.11}$$

where the relaxation time τ is defined as $\tau = \rho/\eta k^2$. By fitting the steady-state velocity profile at sufficiently long time ($e^{-t/\tau} \to 0$) to a $\cos(kz)$ form and measuring the amplitude u_0, one is able to get the coefficient of shear viscosity as the following:

$$\eta = \frac{a_0\rho}{u_0 k^2} \tag{5.12}$$

This method, called the Periodic Perturbation Method (PP), was first developed by Gosling et. al[25]. Instead of imposing a $\cos(kz)$ shape acceleration, Backer and coworkers have used a step function[5],

$$a_x(z,t) = \begin{cases} a_0 & \text{if } z > 0 \\ -a_0 & \text{if } z < 0 \end{cases} \tag{5.13}$$

Correspondingly, the resulting velocity profile has to be fitted to a parabolic function instead of a $\cos(kz)$ function.

Without any loss of generality, in this work we only focus on $\cos(kz)$ shape accelerations.

Initial Pulse Perturbation In the case of IPP, an initial velocity profile of the form:

$$u_x(z,t) = w_0 \cos(kz) \tag{5.14}$$

is created by a pulse interaction and the external force is zero ($a_0 = 0$), the solution to equation (5.3) gives the decay of the velocity profile as a function of time:

$$u_x(z,t) = w_0 e^{-t/\tau} \cos(kz) = w_0(t) \cos(kz) \tag{5.15}$$

From this solution, we can see that the velocity profile will decay exponentially at large time scale and length scale and the relaxation time $\tau = \rho/\eta k^2$ is inversely proportional to the coefficient of shear viscosity. Thus, shear viscosity can be determined by directly measuring this relaxation time.

Linear Response Theory Although most of the simulation methods to compute viscosity were originally developed from hydrodynamic equations; it is insightful to

understand them based on a microscopic theory. This is because a real simulation usually uses a box size corresponding to finite wavenumbers ($k \neq 0$). We therefore start from linear response theory which is generally valid for weak perturbations at arbitrary wavenumbers.

Periodic Perturbation and Spontaneous Fluctuation As we discussed in section 3.5 of chapter 3, for the case of PP, the dynamical variable B we are interested in can be written as:

$$B(z,t) \equiv \sum_q m_q v_{qx}(t)\delta(z - z_q(t)) \tag{5.16}$$

and the non-equilibrium ensemble average of the dynamical variable $B(z,t)$ becomes (see equation (3.38)),

$$< B(z,t) >= \frac{M}{l_z} a_0 \cos(kz) \int_0^t d\tau \, \frac{C(k,\tau)}{C(k,t=0)} \tag{5.17}$$

where M is the total mass and l_z is the $\mathbf{z}$ direction length of the system. M/l_z gives the length density of the system. The transverse current correlation function (TCAC) is defined as,

$$C(k,t) =< \sum_q m_q v_{qx} e^{-ikz} \sum_p m_p v_{px} e^{ikz} > \tag{5.18}$$

Note that we use momentum here instead of velocity as was used in equation (5.6). Macroscopically these two are only difference by a constant. Equations (5.7) and (5.9) are still valid given the definition of equation (5.18), while it is only exact to use equation (5.18) rather than equation (5.6) for multiple component systems. Obviously, at very long time, the steady state average of $B(z,t)$ goes to,

$$< B(z,t) >= \frac{M}{l_z} a_0 \cos(kz) \int_0^\infty d\tau \, \frac{C(k,\tau)}{C(k,t=0)} = \frac{M}{l_z} a_0 \cos(kz) \frac{C(k,\omega=0)}{C(k,t=0)} \tag{5.19}$$

Noticing that $\frac{<B(z,t)>l_z}{M}$ corresponds to $u_x(z,t)$ in equation (5.11), replacing u_0 with $a_0 C(k,\omega=0)/C(k,t=0)$, we have

$$\eta(k) = \frac{a_0\rho}{u_0 k^2} = \frac{\rho}{k^2}\frac{C(k,t=0)}{C(k,\omega=0)} \tag{5.20}$$

This equation is exactly consistent with equation (5.9). Therefore Equation (5.12) and (5.9) are equivalent even in the case of finite wavenumbers ($k \neq 0$) as long as linear response theory applies. Another interested dynamical variable is the instantaneous velocity amplitude:

$$V(t) = \sum_q 2m_q v_{qx}(t) cos(kz_q(t))/M \tag{5.21}$$

we therefore have (see equation 3.40)

$$\frac{<V(t)>}{a_0} = \int_0^t d\tau \frac{C(k,\tau)}{C(k,t=0)} \tag{5.22}$$

Through a comparison with equation (5.20) it is clear that the long time behavior of $<V(t)>/a_0$ is inversely proportional to the coefficient of shear viscosity. In a recent article Hess[31] actually used this definition of $V(t)$ in order to compute an "instantaneous" viscosity.

Equation (5.22) can be used to test the validity of linear response theory since the left hand side of the equation can be computed from the transient response of an ensemble of non-equilibrium trajectories under an external periodic perturbation force such as in equation (5.10) while the right hand side can be obtained from equilibrium MD simulations. To the best of our knowledge, the use of equations (5.21) and (5.22) to study the response of liquids to external perturbations at short time has never been done on any system. For simplicity in notation, we define the right hand side of

equation (5.22) (i.e. the time integral of the normalized correlation function) as the "spontaneous response curve" (SRC).

Initial Pulse Perturbation and Spontaneous Fluctuation Considering an initial velocity profile as in equation (5.14) and zero external field ($a_0 = 0$), using the same underlying idea as in our linear response derivations but a slightly different approach (see equation 3.48), we have

$$< B(z,t) >= \frac{M}{lz} w_0 \cos(kz) \frac{C(k,t)}{C(k,t=0)} =< B(z,t=0) > \frac{C(k,t)}{C(k,t=0)} \qquad (5.23)$$

Therefore, the time evolution of $< B(z,t) >$ matches the decay of the TCAC and $< B(z,t) >$ preserves its initial $\cos(kz)$ shape. In the case of simple liquids at small wavenumbers ($k = 1.0nm^{-1}$), the TCAC on the right hand side of equation (5.23) is found to be close to an exponential form except for a very short initial decay period[55, 31]. We will show that this is not the case for ionic liquids. The studied IL is still far from this regime even though the TCAC is examined at a much smaller wavenumber($k = 0.2nm^{-1}$) corresponding to a much larger simulation box.

Instead of using the $\cos(kz)$ shape velocity profile in equation (5.14), Maginn and coworkers have imposed an initial Gaussian shape velocity profile $u_x(z, t = 0) = w_0 e^{-b_0 x^2}$[3] and then followed the decay of its amplitude. In contrast to the case of the $\cos(kz)$ profile which is limited in wavenumbers by the simulation box size, the Gaussian shape profile mixes different wavenumbers. This method may provide some advantages over measuring a single relaxation time from the exponential decay in equation (5.15). In our work without any loss of generality for simplicity we only study the case of a $\cos(kz)$ shape velocity decay.

Results and Discussion

Spontaneous Fluctuation We use the following expression to calculate TCACs defined in equation (5.18)[55],

$$u(k,t) = \sum_{q}^{N} m_q \hat{\mathbf{k}}_\perp \cdot \mathbf{v}_q(t) \sin(\mathbf{k} \cdot R_q(t)) \tag{5.24}$$

$$u(k,t) = \sum_{q}^{N} m_q \hat{\mathbf{k}}_\perp \cdot \mathbf{v}_q(t) \cos(\mathbf{k} \cdot R_q(t)) \tag{5.25}$$

where k can be taken as $2\pi/l_x$, $2\pi/l_y$, $2\pi/l_z$ or their linear combinations. $\mathbf{R}_q$ and $\mathbf{v}_q$ are the position and velocity of particle q respectively. $\hat{\mathbf{k}}_\perp$ is a unit vector perpendicular to $\mathbf{k}$. The summation in equation (5.24) and (5.25) can be done over all molecules or all atoms. We found that the molecular definition saves considerable computational time without loss of accuracy. For the smallest k in each of the cubic system in Table 5.1, the longitudinal direction $\mathbf{k}$ is taken to be along the $\mathbf{x}$,$\mathbf{y}$ or $\mathbf{z}$ direction. For each of these three directions, there are two independent vertical directions. For each vertical direction $\hat{\mathbf{k}}_\perp$, both sin and cos(kz) forms of the TCAC in equation (5.24) and (5.25) were calculated. In total, $3 \times 2 \times 2 = 12$ separate contributions are averaged to improve statistics. In the case of the largest system of 8232 pairs, since the box is not cubic, only the $\mathbf{z}$ direction can be counted for the longitudinal direction of the smallest k, therefore $1 \times 2 \times 2 = 4$ separate contributions are averaged. All reported time correlation functions are normalized by their initial values.

Fig. 5.6 (A), (B), (C) and (D) show TCACs for the three different systems at two different temperatures. TCACs for different ILs at much larger wavenumbers ($k \geq 1.4 nm^{-1}$) have been previously reported in other papers[76, 71]. Clearly, we

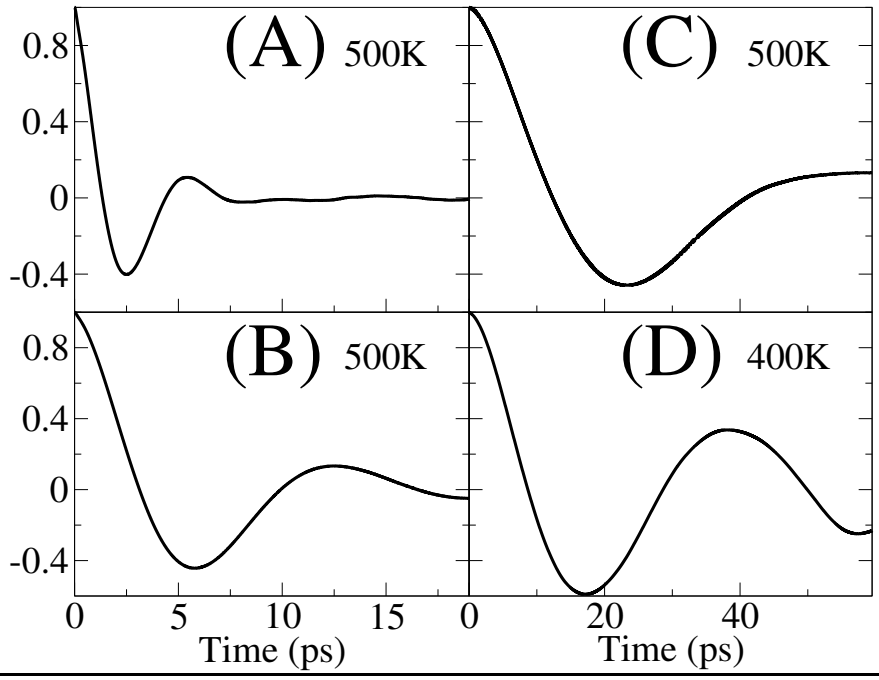

Transverse current time correlation function at different k values and different temperatures. T = 500K (A,B,C) and T = 400 K (D). (A) k = 1.226 nm^{-1} (B) k = 0.612 nm^{-1} (C) k = 0.204 nm^{-1} (D) k= 0.208nm^{-1}.

Figure 5.6: TCACs at different k

observe that negative minima appear at all of the studied frequencies. These short time oscillations indicate non-hydrodynamic behavior[28]. For simpler liquids such as water or supercooled argon, frequencies such as $k = 1.0nm^{-1}$ are quite close to the hydrodynamic limit. For this IL our shortest wavenumber $k = 0.2nm^{-1}$ is still far from the hydrodynamic limit.

Because of the lack of a complete kinetic theory in order to predict the long time behavior of the time correlation functions at finite wavenumbers, the accuracy of long time decay of TCACs is limited by computational power. Therefore, it is hard to obtain a converged $C(k, \omega = 0)$ from the integral over time (0 to $+\infty$) of

TCACs. Noticing that the viscosity is inversely proportional to this zero frequency number($\omega = 0$), a small fluctuation in the magnitude of $C(k, \omega = 0)$ significantly affects the value of viscosity. Direct Fourier transform suffers from the same problem of inaccurate long time decay of the TCACs. We tried the maximum entropy and linear regularization methods to invert the relation in equation (5.8) to obtain the zero frequency value. However, both methods proved unstable. We therefore do not provide viscosities estimated using this method. Nevertheless, the above 3 TCACs at T =500 K and the one computed at T = 400 K together with their corresponding integrals at short time provide the basis for our comparison and interpretation of the dynamics of Ionic liquids under shear perturbations using linear response theory.

Periodic Perturbation We applied several different shear perturbations to the [HMIM+][CL-] system, see Table 5.1. The steady state velocity profiles at T = 500 K corresponding to different frequencies are shown in Fig. 5.7, Fig. 5.8 and Fig. 5.9. The viscosities calculated from equation (5.12) are shown in Table 5.1. The viscosity value from the smallest perturbation and the largest system is supposed to be closest to the viscosity at the hydrodynamical limit ($k = 0$).

Fig. 5.7 (A), Fig. 5.8(A) and Fig. 5.9(A) clearly show that the accelerations (a_0) required to impose flow are larger as the systems become smaller even though they all have similar velocity amplitudes (u_0). Our calculations show that in the range we have studied $\eta(k)$ is a slowly varying function of wavenumber k. Therefore equation (5.20) shows that the acceleration a_0 is approximately proportional to k^2. Hence, the applied shear force needed to generate a given velocity amplitude dramatically increases as

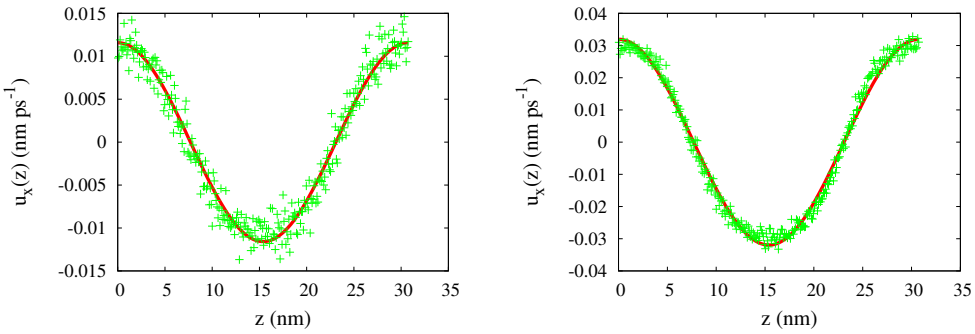

(A) (B)

Steady state velocity profiles at T=500K for the 8232 ion pairs system. Green crosses stand for simulated velocities as a function of z which are fitted to a $cos(kz)$ shape. See equation (5.12) and Table. 5.1. Drag amplitudes are (A) $a_0 = 0.005$ nm/ps^2 (B) $a_0 = 0.01$ nm/ps^2.

Figure 5.7: Velocity profiles for the system of 8232 pairs

the size of system decreases (i.e. the wavenumber k gets larger). This has important consequences in the case of typically small simulation box sizes of a few hundred pairs of ions particularly at lower temperatures. For these system sizes, accelerations required to create a drag may be large enough to significantly perturb liquid structure. For the most part, velocity amplitudes due to the imposed drags in our simulations were much smaller than thermal speed (0.8 nm/ps at 500K and 0.7nm/ps at 400 K). Our largest velocity amplitude is close to 30% of the thermal speed while the rest are less than 5%. As we analyze the pair distribution functions in Fig. 5.10 for the three largest accelerations used in our smallest systems at 500 K we notice that the structure of the liquid appears to be nearly unaffected.

Even though for all our systems at 500 K the shape of the steady state velocity profile appears to have a cos(kz) form, we notice that as we change the acceleration

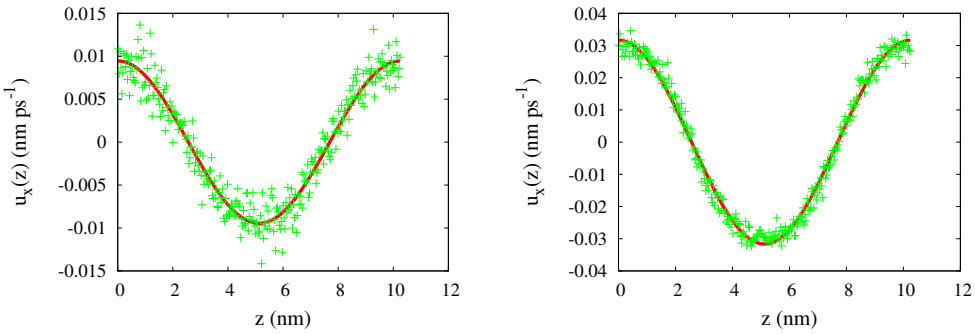

(A) (B)

Same as Fig. 5.7, but for a cubic system with 2744 ion pairs. Drag amplitudes (A) $a_0 = 0.01$ nm/ps^2 (B) $a_0 = 0.02$ nm/ps^2.

Figure 5.8: Velocity profiles for the system of 2744 pairs

(i.e. the amplitude of the drag force) the amplitude of the velocity profile u_0 is not proportional to a_0. This means that Equation (5.19) breaks down and linear response theory fails. As we will show later in this thesis, this failure of linear response theory only happens at long times.

A study of our largest system at 400 K reveals that the response to an acceleration of $a_0 = 0.02 nm/ps^2$ deviates from the predictions of linear response theory both in amplitude and shape of the velocity profile (see Fig. 5.11 (A) and (B)). The flat shape of the velocity profile in Fig. 5.11 (B) could be interpreted as a mixture of different wavenumbers. Therefore, a complete nonlinear response theory that couples different modes is required to deal with this situation.

From a practical perspective, this finding could potentially amount to the Holy Grail for analytical separations since the shape of flow fronts determine to a large extent the efficiency of the process and flat flow fronts are ideal. To the best of

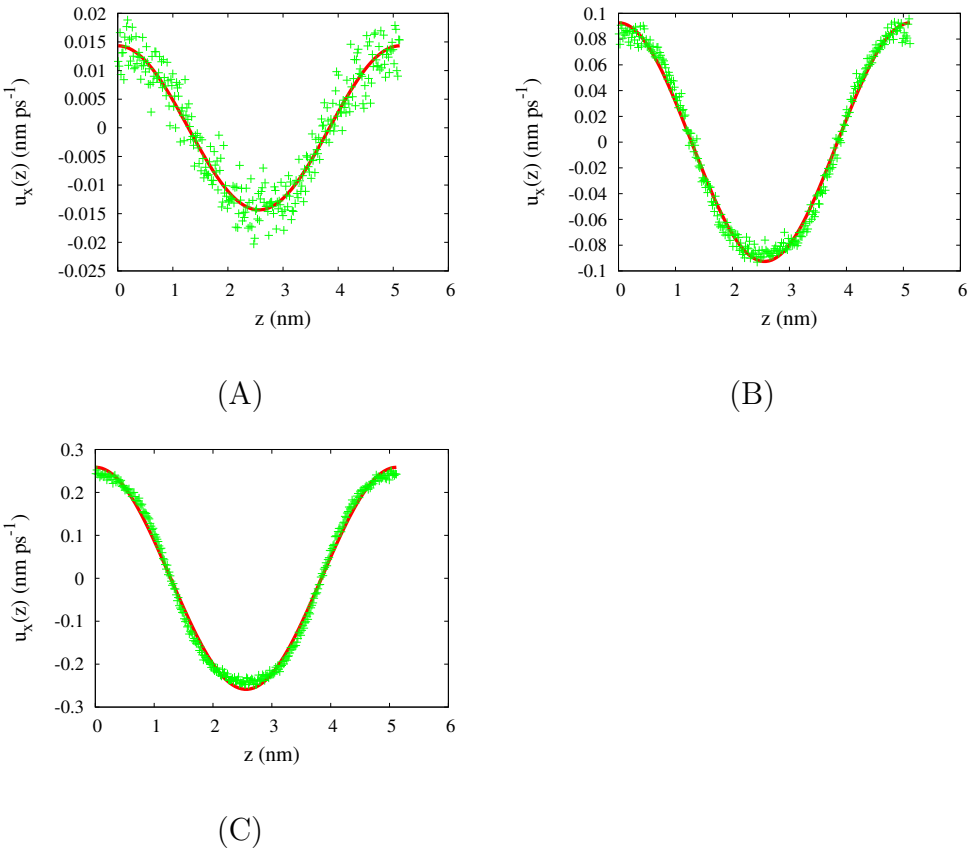

Same as Fig. 5.8, but for 343 ion pairs. Drag amplitudes (A) $a_0 = 0.1$ nm/ps^2 (B) $a_0 = 0.2$ nm/ps^2 (C) $a_0 = 0.3$ nm/ps^2

Figure 5.9: Velocity profiles for the system of 343 pairs

our knowledge the potential to create flat velocity profiles in ionic liquid is something that has not been explored neither computationally nor experimentally.

Even though our largest simulations have not reached the hydrodynamic limit, from the data in Fig. 5.7(A) and Fig. 5.11 (A) we are able obtain best estimates of viscosities at two temperatures $\eta(500\mathbf{K}) = 8.859$cp and $\eta(400\mathbf{K}) = 57.14$cp. (see Table 5.1). There is no direct experimental data of shear viscosity currently available at these two temperatures, however if we fit the existing experimental data from

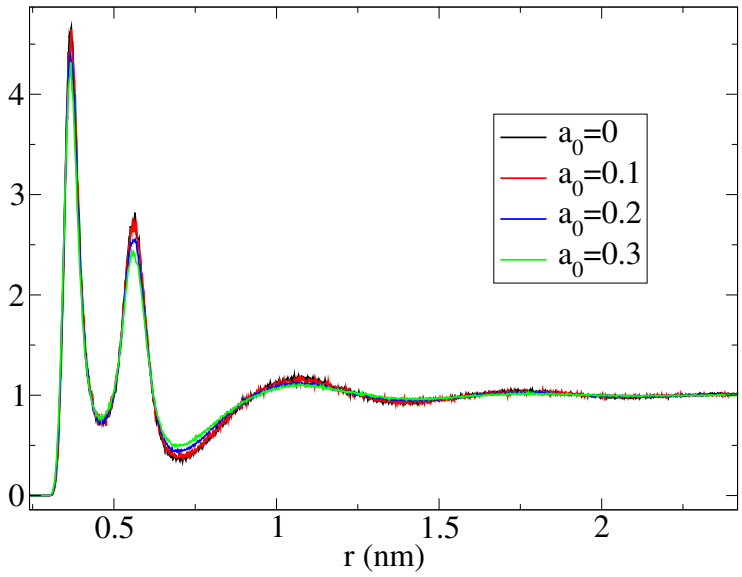

Pair correlation function $g(r)$ of anion CL- and the carbon atom directly connected to the two nitrogen atoms in the ring of [HMIM+]. The cases of the system under three different drag accelerations are compared with the corresponding equilibrium $g(r)$ at T=500K.

Figure 5.10: RDFs of Cl atom and C3 atom

reference [23] to the Vogel-Fulcher-Tammann (VFT) equation $\eta = \eta_0 * exp(B/(T - T_0)$[68, 69, 70], we can estimate what the experimental viscosity should be at $T = 400$ K and $T = 500$K. Fig. 5.12 shows our fit to the experimental data. Parameters are $\eta_0 = 3.5149 * 10^{-5}$ kg/ms, $B = 1362.61$ K, $T_0 = 194.539$. From this fit we obtain values of $\eta(400\mathbf{K}) = 26.68$ cp, and $\eta(500\mathbf{K}) = 3.04$ cp. These numbers are about half the values obtained from our simulations. Given the error in these estimates, and the fact that none of our simulations have actually reached the hydrodynamic limit, the agreement between simulations and experiments appear to be quite satisfactory. Our simulation results can be improved by increasing the size of our already very large systems and once the results are converged to the hydrodynamic limit potential

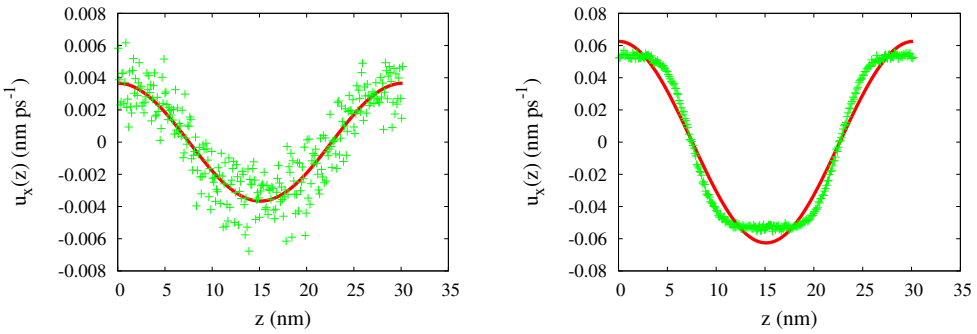

(A) (B)

Same as Fig. 5.7, but for T = 400 K. (A) $a_0 = 0.01$ nm/ps^2 (B) $a_0 = 0.02$ nm/ps^2.

Figure 5.11: Velocity profiles at T=400K

energy parameters could be adjusted or a polarizable force field could be implemented.

Since the instantaneous velocity amplitude $< V(t) >$ shows the response of the ionic liquid under shear perturbation, it is interesting to follow its transient time evolution after the drag is switched on. As explained in previous sections this provides an opportunity for comparison of the short time predictions of linear response theory against actual non-equilibrium results. Fig 5.13 (A),(B),(C) and (D) shows plots of $\frac{<V(t)>}{a_0}$ as a function of time for two different temperatures at different shear rates. The maximum of each of the SRC curves (in black) corresponds to the time at which the TCAC crosses zero. In all cases studied, it appears that non-equilibrium velocity amplitudes match the corresponding SRCs very well before this time. In the case of small accelerations the time evolution of $\frac{<V(t)>}{a_0}$ is still close to that of corresponding SRCs after this time point while for the larger accelerations used in this work $\frac{V(t)}{a_0}$ start

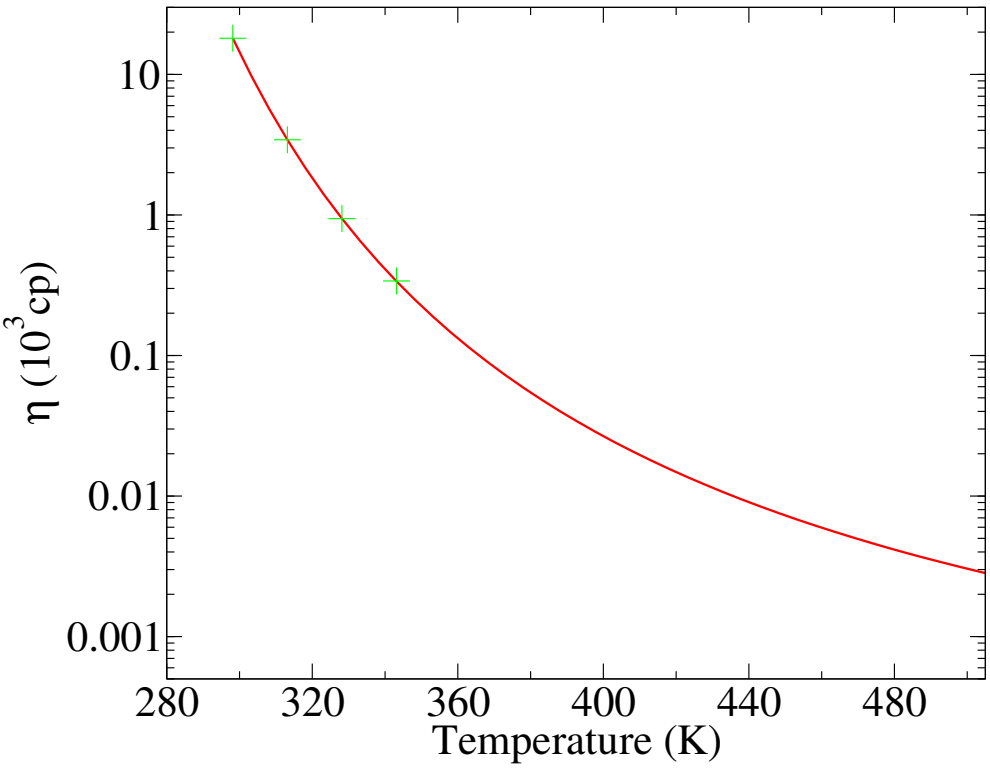

VFT fitting of viscosities as a function of temperature. Experimental data is taken from Table 2 of reference [23] by Gomez et.al. Four green crosses are the experimental data. The solid red line is our fitted VFT curve.

Figure 5.12: VFT fit of viscosities

to deviate. Under linear response $\frac{<V(t)>}{a_0}$ should be independent of the drag amplitude a_0. This is not the case as can be appreciated in Fig 5.13. By looking at the long time value of $\frac{<V(t)>}{a_0}$ in the case of different accelerations it is easy now to explain why viscosities calculated from the steady-state velocity amplitude profiles decrease as the accelerations increase. The viscosity predicted from equilibrium SRCs should correspond to the zero shear rate limit of $V(t)$. However as explained previously since the integral from zero to infinity of the time correlation functions in Fig. 5.6 is required, this task is extremely difficult for the size of systems necessary to reach the

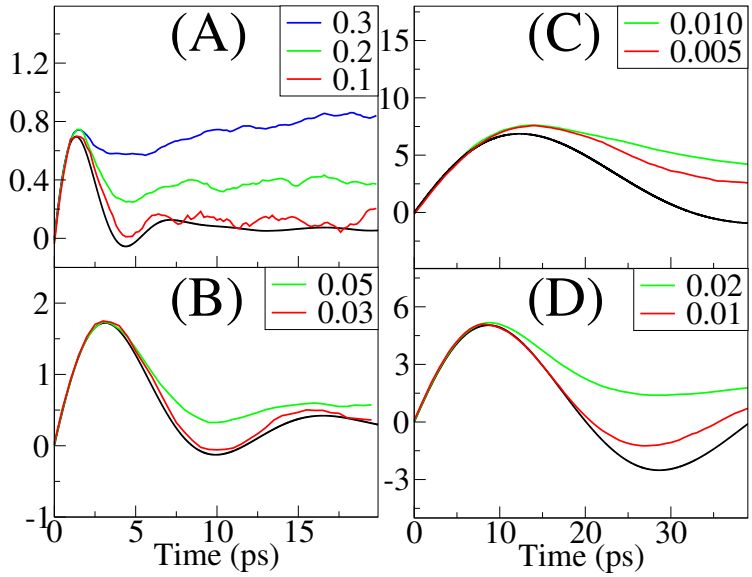

Transient response of the IL under external perturbations at T=500 K(A,B,C) and T = 400(D). The solid black line always corresponds to the equilibrium SRC (integral over time correlation function). All other curves correspond to the normalized instantaneous velocity amplitudes established upon application of different external accelerations a_0. See equation (5.22). (A) k = 1.226 nm^{-1} (B) k = 0.612 nm^{-1} (C) k = 0.204 nm^{-1} (D) k= 0.208nm^{-1}

Figure 5.13: Instantaneous velocity amplitudes

correct hydrodynamic limit.

Initial Pulse Perturbation In order to further test the predictions of linear response, we also studied systems with an initial $\cos(kz)$ shape velocity profile but no applied drag. We did this for our largest system at two different temperatures. The velocity amplitude used was $0.02nm/ps$ close to that created by the larger shear accelerations(see Fig. 5.7 (B) and Fig. 5.11(B)). Fig. 5.14(A) and (B) show the decay of velocity profile and corresponding equilibrium TCACs. Clearly, the first $10ps$ decay through equation (5.23) matches the TCAC very well. This time is consistent with that on which linear response was successful in the case of the periodic perturba-

tion method (see Fig. 5.13 (C) and (D)). To converge these results 200 independent trajectories of 10 ps were run at each temperature. Getting results for longer times involves huge storage and computational times and is beyond our current computational capabilities. Nonetheless, our 10ps results are long enough to conclude that at short time, equation (5.23) is valid. Linear response theory works very well at short times in the case of initial pulse perturbations.

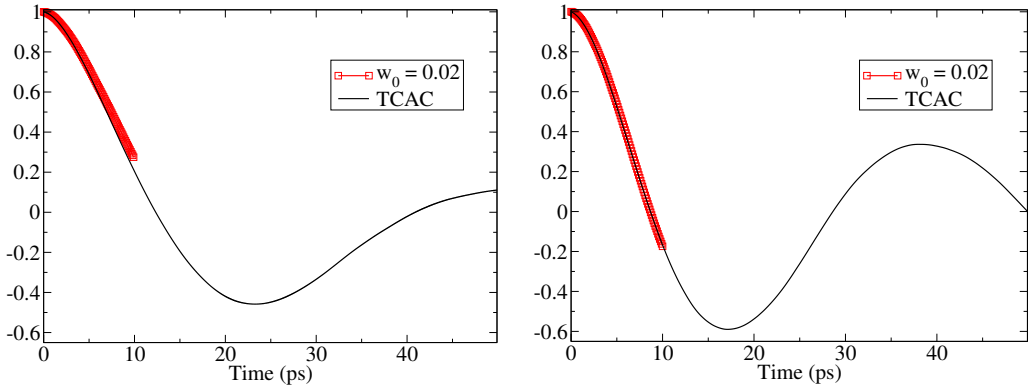

(A) (B)

Calculated $< B(z,t) > / < B(z,0) >$ and TCACs at two different temperatures for our largest 8232 ion pair system. See equation (5.23) and Fig 5.6(C) and (D). (A) T = 500 K (B) T = 400 K

Figure 5.14: Dissipation of IPP

Important to notice is that if the size of our simulations were at the hydrodynamic limit of low k, our TCACs would have been exponentials and this ensemble of short trajectories would have been enough to obtain the time constant corresponding to the relaxation. Since even our largest simulations are not at this limit and a full

microscopic theory predicting the shape of TCACs at finite wavenumbers is missing the non-exponential nature of these curves prevents us from being able to establish the value of the macroscopic viscosity.

CHAPTER 6
EXCITATION WAVELENGTH DEPENDENT EMISSION SPECTRA OF IONIC LIQUIDS

In this chapter we investigate the slow dynamics of 1-butyl-3-methylimidazolium hexafluorophosphate, a very popular room-temperature ionic solvent[35, 37]. Our study predicts the existence of heterogeneity in the liquid and shows that this heterogeneity is the underlying microscopic cause for the recently reported "Red Edge Effect" (REE) observed in the study of fluorescence of the organic probe ANF. This is the first theoretical paper to explain in microscopic terms the relation between REE and dynamic heterogeneity in a room-temperature ionic liquid. The REE is typical of micellar or colloidal systems, which are characterized by microscopic environments that are structurally very different. In contrast in the case of this room-temperature ionic liquid, the REE occurs because of the long period during which molecules are trapped in quasi-static local solvent cages. This trapping time, which is longer than the lifetime of the excited state probe, together with the inability of the surroundings to adiabatically relax, induce a set of site-specific spectroscopic responses. Sub-ensembles of fluorescent molecules associated with particular local environments absorb and emit at different frequencies. We describe in detail the absorption wavelength dependent emission spectra of ANF and show that this dependence on the excitation wavelength λ_{ex} is characteristic of the ionic liquid and, as is to be expected, is absent in the case of a normal solvent such as methanol. Futher, from the analysis of our simulated time resolved REE data we are able to derive an

approximate time scale for reorganization of the solvent around the solute probe[37].

6.1 Steady-state Fluorescence spectra

Methods We performed molecular dynamics simulation for an ANF probe in an ionic liquid system [BMIM+][PF_6-]. Simulations were carried out using the software GROMACS[47, 7]. Potential energy parameters are those previously explained in Chapter 4. Periodic boundary conditions were employed using the particle mesh ewald (PME) method to treat long-range electrostatic interactions[15, 50, 49]. All systems were initially equilibrated for several hundred picoseconds in the NPT ensemble using the Berendsen method until trending in the volume was no longer observed [7]. To compute the absorption and emission spectra of ANF in the IL, we used an ensemble of 12 MD trajectories. Each of these trajectories consisted of an ANF molecule and 125 pairs of [BMIM+][PF_6-] solvent ions. In order to compare the absorption wavelength dependent emission of ANF in the IL with that in a typical organic solvent, we also studied a system consisting of an ANF solute solvated by 179 methanol solvent molecules. All trajectories involving ANF in its ground or excited electronic state were about 1.5 ns in duration.

The ground state charge distribution for ANF was obtained from an *ab initio* calculation at the (HF/6-31G*) theory level using the Gaussian program[20]. The excited state charge distribution was estimated by computing the ground (S_0) and first singlet excited state (S_1) charge difference using the ZINDO Hamiltonian with configuration interaction[61]. These calculations were performed with the software

Hyperchem 7. The charge distribution in the excited state used for our MD calculations was obtained by adding the charge difference obtained from the ZINDO calculation to the ground state charges obtained by the HF method. The calculated ground and excited state dipole moments were 7.73 and 18.73 Debye respectively. This methodology has already been successfully applied in the past by Maroncelli and coworkers to study solvatochromism of betaine-30[54]. Lennard-Jones, stretching, bending and torsional parameters for ANF were taken to be the same in the ground and excited electronic state. This is a reasonable approximation given that ANF is a fairly rigid planar molecule. These parameters and those for methanol were adopted from the OPLS-AA force field [39]. The S_0 to S_1 state energy gap ΔE can be expressed as:

$$\Delta E = \Delta E(g) + \Delta E_{sol} \tag{6.1}$$

where $\Delta E(g)$ denotes gas-phase or intramolecular energy difference which is independent of the solvent and ΔE_{sol} is the solvent-solute interaction energy difference arising from the different charge distributions in the ground and excited electronic state. In our MD calculations $\Delta E(g)$ is taken as an arbitrary fixed constant that simply shifts all points in the spectrum by the same amount. The value of this constant is chosen so that the energy scale of our calculations coincides with experimental values. Considering that different trajectories have different contribution to the whole emission spectrum, we have the following formula to calculate the spectra.

$$I_{ab}(\Delta E_{ex}) = \sum_{l} I_{ab}^{l}(\Delta E_{ex}) \tag{6.2}$$

$$I^l_{em}(\Delta E_{em}) = \int_0^\infty \delta(\Delta E(t) - \Delta E_{em}) \times e^{-\frac{t}{\tau}} dt \tag{6.3}$$

$$I_{em}(\Delta E_{ex}, \Delta E_{em}) = \sum_l I^l_{em}(\Delta E_{em}) I^l_{ab}(\Delta E_{ex}) \tag{6.4}$$

Here $I^l_{ab}(\Delta E_{ex})$ is the probability distribution of absorption energy gaps ΔE_{ex} in trajectory l. $I_{ab}(\Delta E_{ex})$ denotes the total probability distribution at vertical transition excitation energy ΔE_{ex}. $I^l_{em}(\Delta E_{em})$ is the probability distribution of emission energy gaps ΔE_{em} weighted by an exponential decay corresponding to the lifetime of the probe (assumed to be 100 ps as in [BMIM+][BF4-][48]). $I_{em}(\Delta E_{ex}, \Delta E_{em})$ denotes the intensity or joint probability distribution of emission energy ΔE_{em} when excitation energy is ΔE_{ex}. No attempt has been made in these classical simulations to take into account Frank Condon factors or other quantum selection rules. Emission spectra in this chapter are always reported as area normalized.

Results and Discussion Absorption wavelength dependent emission of a probe molecule occurs when solvent relaxation is slower than its fluorescence lifetime[13]. This type of phenomenon is very atypical for a normal liquid and is commonly found in colloidal gels or micelles. Fig. 6.1 describes two possible scenarios. In both cases one photo-excites a molecule into local excited state 1. If solvent relaxation is slow compared to fluorescence, then emission occurs from this local environment. If on the other hand the solvent behaves adiabatically, meaning that it adjusts to the change in dipole moment of the excited state probe on a time scale much faster than the fluorescence lifetime, then the emission is from the solvent relaxed local state 2. It is clear that in a solvent that is locally heterogeneous on the time scale of emission one can selectively photo-excite either local excited state 1 or 2 and therefore guide the out-

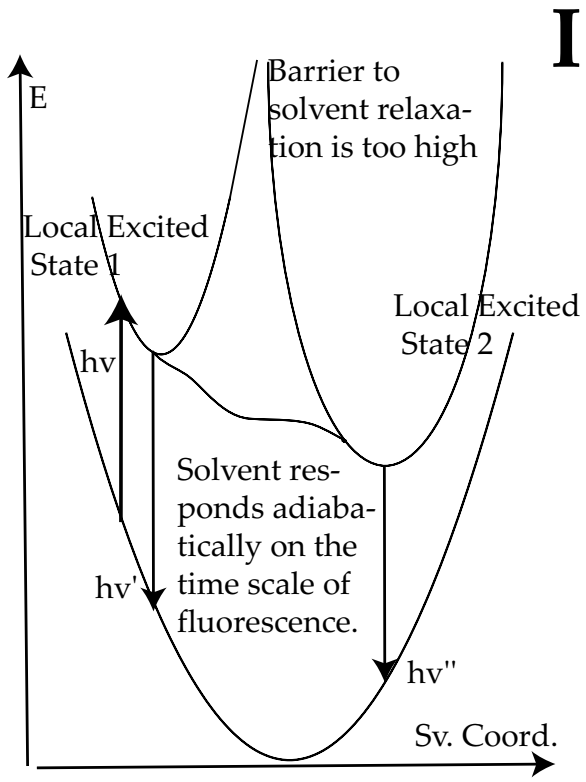

Energy diagram showing two possible scenarios. In one case the response of the solvent is adiabatic and no REE is observed ($h\nu''$). In the other case solvent relaxation is slow and excited state local environments do not interconvert ($h\nu'$). In this case one can observe REE. Sv. coord. stands for solvent coordinate.

Figure 6.1: Two possible scenarios

come of a photo-chemical reaction given that these two do not interchange. In order to study this phenomenon from a molecular perspective we performed molecular dynamics simulations of ANF in methanol and in [BMIM+][PF6-](see above **Methods**). Each trajectory was first equilibrated in the ground electronic state and subsequently its corresponding absorption spectrum was computed by making a histogram of the ground to excited state energy gaps along simulation. After 800ps the charge distribution for ANF was changed to that in the first singlet excited electronic state. In

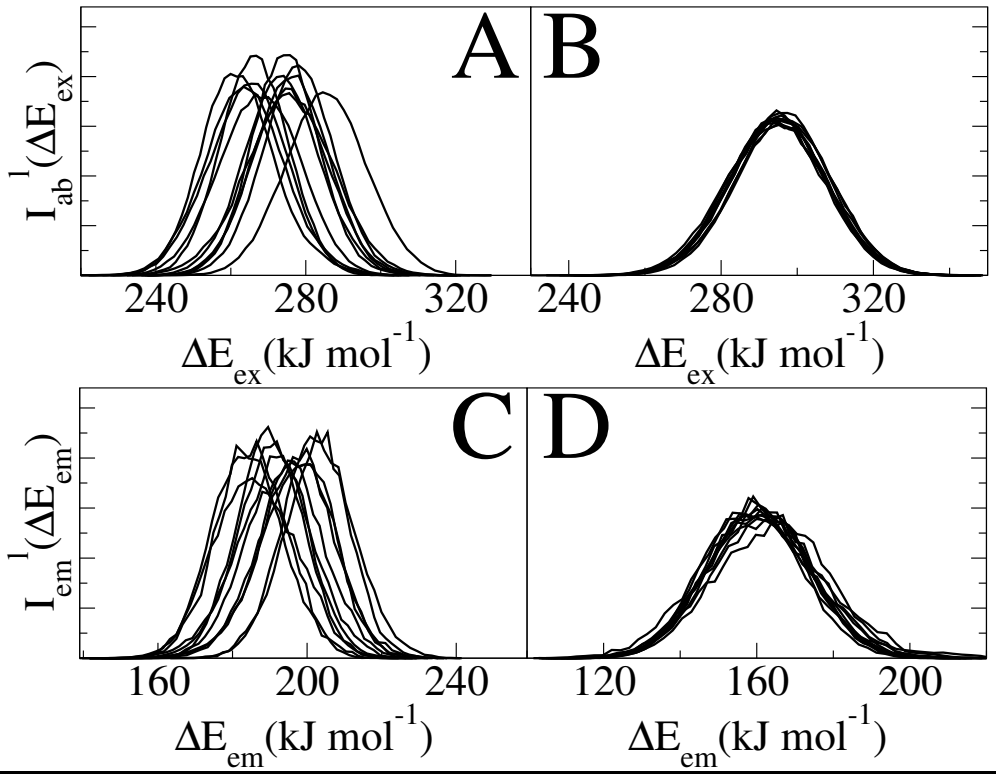

Overlayed are different curves that correspond to the spectrum of ANF in [BMIM+][PF_6-] computed from each of our 12 molecular dynamics trajectories; (absorption (IIA) and emission (IIC)) as well as in methanol(absorption (IIB) and emission (IID)). In the case of the ionic liquid we observe site specific spectra while in methanol all spectra are superimposable. Each of these individual spectra contributes to the total signal. (See equations 6.2 and 6.4).

Figure 6.2: Spectra of ANF in ILs and methanol

order to compute the emission spectrum arising from each individual trajectory we performed the same kind of computation, only in this case the dynamics was driven by the excited state potential. Fig. 6.2 shows absorption and emission spectra of ANF computed in the IL and in methanol. It is clear from these plots that in methanol both in the case of emission and absorption the spectra generated from different trajectories are nearly superimposable. On the other hand in the ionic liquid, the different spectra corresponding to different trajectories are widely different. The behavior of

each of these trajectories gives rise to a site specific response and is the cause for the observed REE. In each of these trajectories ANF is in a different solvent environment

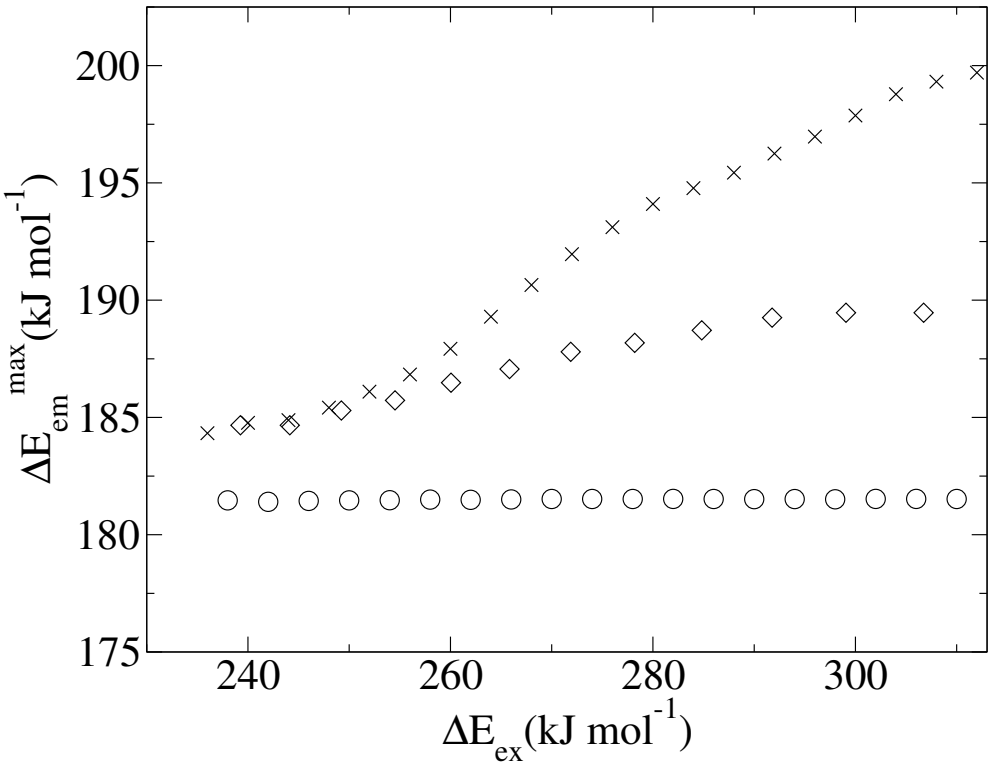

ΔE_{em}^{max} vs ΔE_{ex} both for ANF in [BMIM+][PF_6-] ($\times$), in methanol ($\circ$) and experimental data in [BMIM+][PF_6-]($\diamond$). As explained in the text, in order to display all maxima on the same energy scale as in the experiment, the same constant corresponding to ΔE_{gas} has been added to all points computed in the IL. An arbitrary constant has also been added to all maxima in methanol. We clearly see from this graph that while there is a λ_{ex} dependence in the fluorescence spectra of ANF in the IL, as is to be expected, this effect is absent in methanol.

Figure 6.3: Fluorescence spectra

that does not adiabatically relax after photo-excitation. By applying equation 6.2 we computed corresponding ensemble averaged absorption spectra. Fig. 6.3 shows the λ_{ex} dependent emission maxima of ANF in [BMIM+][PF6-] and methanol. We

compare our results to Samanta's experimental data[48] for the maximum in the different emission spectra as a function of excitation wavelength. The slope of ΔE_{em}^{max} as a function of excitation energy is larger than the one experimentally reported. Nonetheless, these results are in very good agreement with experiments, particularly taking into account that we only included 12 independent trajectories in our ensemble averages. It is clear that solvent dynamics is not adiabatic in the case of the IL. In the experiment, subensembles of ANF molecules characterized by their slowly-relaxing local surrounding are responsible for the different emission spectra obtained by changing λ_{ex}. We also show for comparison results of our simulations of ANF in methanol in which, as expected, no REE is found because solvent relaxation (i.e. averaging) is fast and no locally heterogeneous environments are present. The absence of REE can be appreciated by noticing that the emission frequency is independent from the absorption frequency.

The Relation Between REE and Dynamic Heterogeneity (see section 5.1 of chapter 5) We have demonstrated that ([BMIM+][PF6-]) shows non Gaussian diffusion patterns with subensembles of ions that can be distinguished by their mobility. We have also demonstrated that the experimentally observed REE in the case of ANF can be accounted for by analyzing an ensemble of independent molecular dynamics trajectories. A very important issue yet remains unanswered. What characterizes these local environments that do not relax on the time scale of emission? Are we in the presence of a liquid with polar and apolar local domains? Fig. 6.4 sheds light on this question. For the sake of clarity we may assume that our molecular

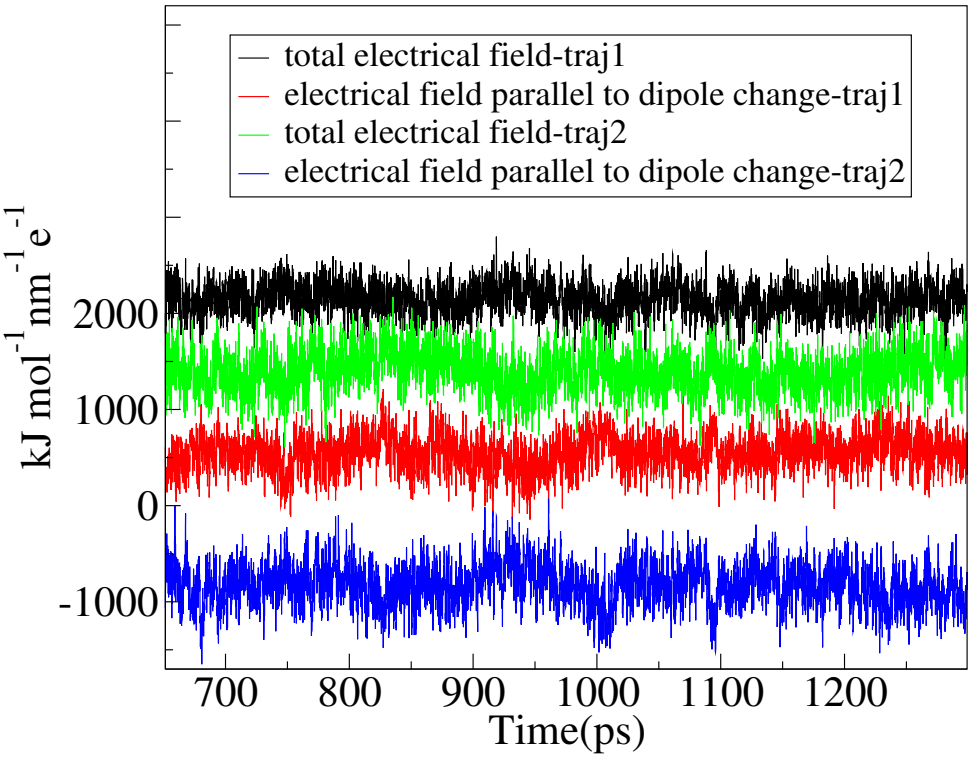

Absolute value of the electric field due to the solvent at the location of one of the carbon atoms close to the center of mass of ANF and the projection of this electric field onto the direction of the ground to excited state dipole moment change $\vec{\Delta\mu}$ as a function of time for two different trajectories. As can be appreciated the projection of the electric field onto $\vec{\Delta\mu}$ is different in each trajectory but nearly constant with respect to time. This phenomenon of constancy with respect to time and variation with respect to space is the cause for the experimentally observed REE.

Figure 6.4: Time evolution of electric field

probe ANF is characterized by a dipole moment $\vec{\mu}_{ground}$ in the ground electronic state and $\vec{\mu}_{excited}$ in the excited electronic state. The dipole moment change in going from ground to excited state is $\vec{\Delta\mu} = \vec{\mu}_{excited} - \vec{\mu}_{ground}$. Fig. 6.4II shows the magnitude and projection of the electric field only due to the solvent onto $\hat{\vec{\Delta\mu}}$. This projection is taken at the location of one of the carbon atoms which is approximately at the center of mass of ANF. It is clear from Fig. 6.4 that neither the absolute value of

the electric field nor its projection along $\vec{\Delta\mu}$ significantly vary throughout each of the two simulations. In fact this is very characteristic of all our MD runs. If we compare different trajectories the absolute value of the electric field significantly varies from one to the other but it remains fairly constant as a function of time in each particular run. The same thing can be said about its projection onto $\vec{\Delta\mu}$. In our simulations the gap between ground and excited state is solely determined by electrostatics. We find the value of the solute-solvent electrostatic energy to be trajectory dependent but nearly time independent, at least on a nanosecond timescale, for each particular run. A similar situation occurs for trajectories driven by the excited state ANF potential. After an initial transient behavior neither the electric field due to the solvent nor $\vec{\Delta\mu}$ appreciably change in magnitude or relative orientation. This phenomenon is clearly a property of the slow dynamics of the solvent and is related to the fact that at room temperature the intermediate cage regime spans a duration on the order of nanoseconds as can be appreciated in Fig.5.1. We conclude that the existence of locally heterogeneous environments responsible for the REE is mainly due to the fact that the typical lifetime for fluorescence in ANF is shorter than the time on which this probe is trapped inside quasi-static solvent cages. Electric field and $\vec{\Delta\mu}$ occur at particular relative orientations that are site specific and that remain relatively constant on this time scale.

6.2 Time Resolved Spectra

In this subsection we further analyze the microscopic origin of the REE and predict the time resolved spectra[37] which directly provides an estimate for the time scale of reorganization in this ionic liquid.

Methods A detailed description of the methodology used to collect data from our molecular dynamics simulations has already been provided in previous section 6.1. Here we only explain specific detail for the calculation of time resolved emission spectra of ANF in [BMIM+][PF6-]. We use equations 6.5 through 6.9 in order to compute time dependent and time independent spectra from an ensemble of molecular dynamics trajectories initially equilibrated in the ground electronic state and photo-excited to the corresponding first singlet excited electronic state:

$$I_{ab}(\Delta E_{ex}) = \sum_{l} I^{l}_{ab}(\Delta E_{ex}) \tag{6.5}$$

$$I^{l}_{em}(\Delta E_{em}) = \int_{0}^{\infty} \delta(\Delta E(t) - \Delta E_{em}) \times e^{-\frac{t}{\tau_f}} dt \tag{6.6}$$

$$I^{l}_{em}(\Delta E_{em}, t) = \int_{t-\Delta t}^{t+\Delta t} \delta(\Delta E(\tau) - \Delta E_{em}) \times e^{-\frac{\tau}{\tau_f}} d\tau \tag{6.7}$$

$$I_{em}(\Delta E_{ex}, \Delta E_{em}) = \sum_{l} I^{l}_{em}(\Delta E_{em}) I^{l}_{ab}(\Delta E_{ex}) \tag{6.8}$$

$$I_{em}(\Delta E_{ex}, \Delta E_{em}, t) = \sum_{l} I^{l}_{em}(\Delta E_{em}, t) I^{l}_{ab}(\Delta E_{ex}) \tag{6.9}$$

Here $I^{l}_{ab}(\Delta E_{ex})$ is the probability distribution of absorption energy gaps ΔE_{ex} in trajectory l. $I_{ab}(\Delta E_{ex})$ denotes the total probability distribution at vertical transition excitation energy ΔE_{ex} computed as a sum over all trajectories. $I^{l}_{em}(\Delta E_{em})$ is the corresponding steady-state probability distribution of emission energy gaps

ΔE_{em} weighted by an exponential decay corresponding to the lifetime (τ_f) of the probe (assumed to be 100 ps as in [BMIM+][BF4-][48]) for trajectory l. $I^l_{em}(\Delta E_{em}, t)$ is the time-dependent intensity of emission computed from trajectory l after initial photo-excitation. $I_{em}(\Delta E_{ex}, \Delta E_{em})$ denotes the intensity or joint probability distribution of emission energy ΔE_{em} when excitation energy is ΔE_{ex}. Correspondingly $I_{em}(\Delta E_{ex}, \Delta E_{em}, t)$ stands for the time-dependent emission spectrum. It should be noted here that these are purely classical simulations. The gap between the ground and excited states has a component that is independent of the solvent $\Delta E(g)$ and a component that is due to the difference in interactions between the solvent with the ground and excited states of the probe molecule. We have made no attempt at taking into account Frank Condon factors or other quantum selection rules. Emission spectra in this section are always reported as area normalized.

Results and Discussions Different consequences arise due to the slow dynamics of the solvent. Figures 6.5(A) and (B) show absorption and steady-state emission spectra of ANF in 3 typical solvent environments. It is clear that each of these 3 trajectories displays very distinct spectrum with maxima at different frequencies. The most interesting feature here is the energy ordering of the absorption and corresponding emission spectra of individual trajectories. Clearly the trajectory with maximum of absorption at a higher frequency also displays an emission spectrum at higher frequency. The opposite is true for the trajectory with absorption spectrum at lower frequency. This ordering phenomenon which is detected in most of our ionic liquid trajectories and is absent in our studies of ANF in methanol[35] is the basic

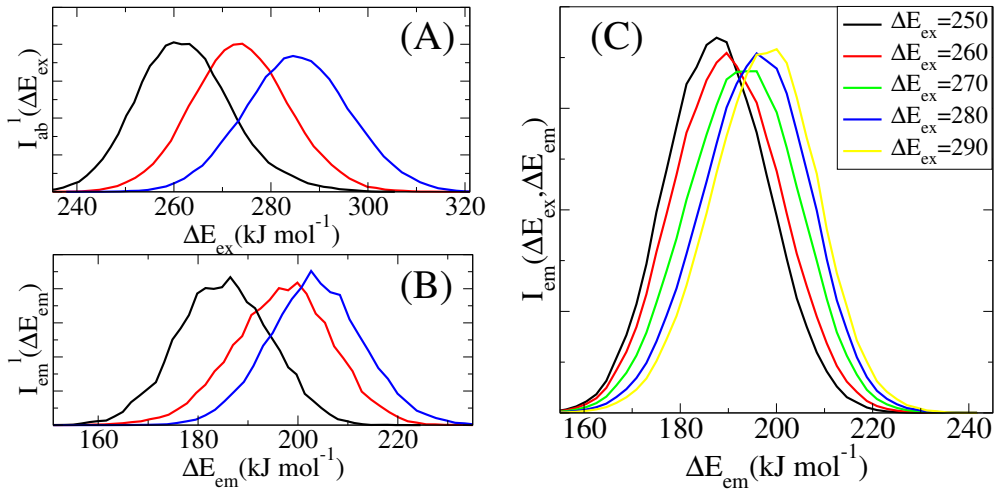

Absorption and steady-state emission fluorescence spectra. (A) Absorption spectra of ANF in [BMIM+][PF_6-] computed from 3 molecular dynamics trajectories. Each line corresponds to the spectrum from a different trajectory. (B) Emission spectra from the same 3 trajectories. (See equations 6.5 and 6.6). (C) Steady-state fluorescence spectra of ANF as a function of excitation energy at room temperature in [BMIM+][PF_6-] (see equation 6.8)

Figure 6.5: Typical local spectra and steady-state fluorescence spectra of ANF

underlying cause for the REE.

The REE can be appreciated more clearly, when the full ensemble of trajectories is used in order to compute the excitation wavelength dependent emission spectra using equation 6.8. The set of ensemble averaged spectra which can be compared with experimental data[48] obtained for the same probe in a slightly different ionic solvent are displayed in Fig. 6.5 (C). In order to analyze the time dependence of the REE, we computed using Equation 6.9 the corresponding emission spectra as a function of λ_{ex} for different emission times. Figure 6.6 shows how the maximum of emission shifts as a function of λ_{ex} and time. This prediction, for which there is still no experimental data reported, is one of the main results of this chapter. It is clear

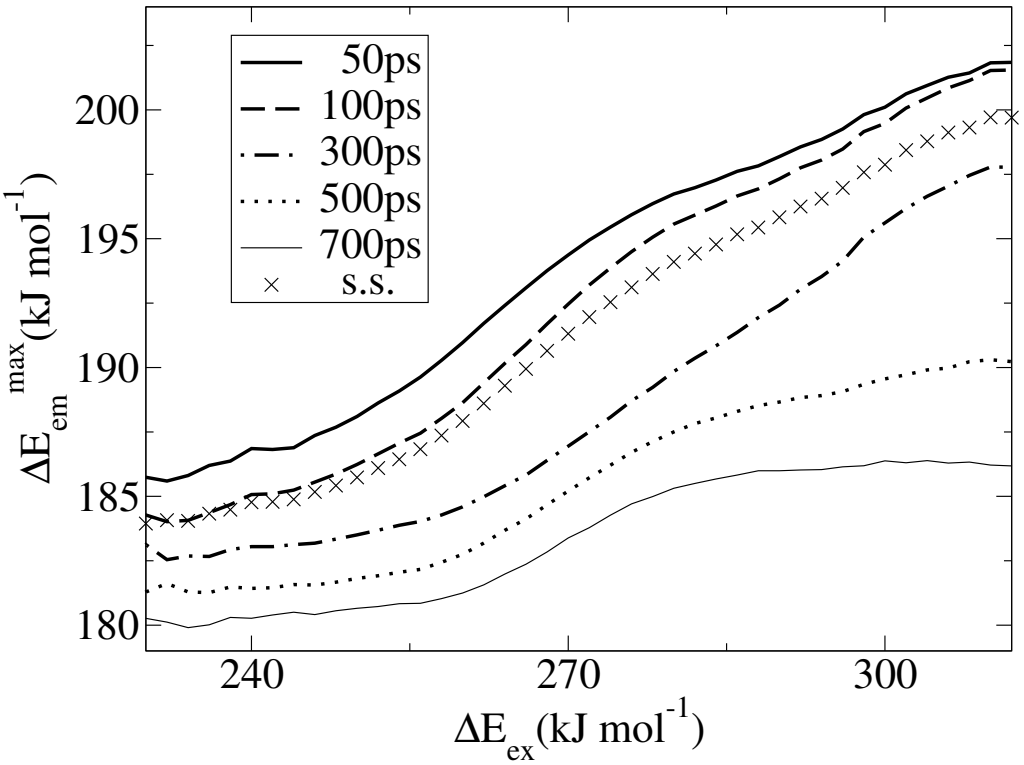

ΔE_{em}^{max} vs ΔE_{ex} for ANF in [BMIM+][PF_6-] at five different times, and computed steady-state (×). In order to display all maxima on the same energy scale as in the experiment, the same constant corresponding to ΔE_{gas} has been added to all points computed in the IL. See equation 6.7 (Here, Δt is taken to be 20ps), see also equation 6.9.

Figure 6.6: Wavelength dependent Stokes shift

from Fig.6.6 that at longer times emission maxima shift to the red. This is simply because to different extent in each trajectory the solvent surrounding the probe relaxes as time evolves. Concurrently, because the dynamics is driven by the excited state potential, the interaction between the ground electronic state of the probe and the solvent becomes more unfavorable. It is also clear from Fig.6.6 that at longer times the dependence of the emission maximum on λ_{ex} becomes weaker. Of course, at infinite time no REE should be observed.

The absorption wavelength dependent emission maxima for the steady state signal computed from our ensemble of trajectories is also plotted in Fig.6.6. Clearly the steady state curve and the time dependent data at 100 ps coincide very closely. This is to be expected given that the lifetime of the probe was assumed to be 100 ps.[48]

From Fig.6.6 we see that the spectrum is still λ_{ex} dependent at 700 ps. It is interesting to compare the timescale required for full loss of correlation between energy of excitation and emission with that of the intermediate cage regime in which the motion of the solvent is neither ballistic nor diffusive. Our previous simulations show that the intermediate cage regime at room temperature spans a duration of nanoseconds. It is likely that solvent and solute motion required to reach full energy relaxation upon photo-excitation must be compatible with the time scale on which the solvent abandons the cage regime and enters into the diffusive regime. Certainly, a large part of the relaxation after photo-excitation occurs on the short sub-picosecond regime. This has been corroborated both experimentally[11, 4] and computationally.[64, 44, 49] Our study predicts that the remaining long time relaxation, which is the cause for the absorption wavelength dependent emission spectrum, takes place on a time scale that is much longer at least on the order of nanoseconds.

CHAPTER 7
OPTICAL KERR EFFECT OF IONIC LIQUIDS

In this chapter, we are going to apply the nonlinear response theory derived in section 3.4 to the case of Optical Kerr Effect in an ionic liquid 1-methoxyethylpyridinium dicyanoamide ([MOEPY+][DCA-] see Fig 4.1) [65].

In the first several sections, we will introduce the basic theory on polarization spectra and explain how to compute the optical kerr effect (OKE) signal in general. Simulation details, results and discussion will be given in the following sections.

7.1 Polarization of Molecules

In general, for incident light $\mathbf{E} = \mathbf{e}_x E_x + \mathbf{e}_y E_y + \mathbf{e}_z E_z$, the induced dipole moment is written as:

$$\begin{aligned}\boldsymbol{\mu} &= (\mathbf{e}_x, \mathbf{e}_y, \mathbf{e}_z) \begin{pmatrix} \mu_x \\ \mu_y \\ \mu_z \end{pmatrix} = (\mathbf{e}_x, \mathbf{e}_y, \mathbf{e}_z) \begin{pmatrix} \alpha_{xx} & \alpha_{xy} & \alpha_{xz} \\ \alpha_{yx} & \alpha_{yy} & \alpha_{yz} \\ \alpha_{zx} & \alpha_{zy} & \alpha_{zz} \end{pmatrix} \begin{pmatrix} E_x \\ E_y \\ E_z \end{pmatrix} \\ &= (\mathbf{e}_x, \mathbf{e}_y, \mathbf{e}_z)\overline{\alpha} \begin{pmatrix} E_x \\ E_y \\ E_z \end{pmatrix}\end{aligned}$$

In general, there exists a matrix $\overline{A}$ which diagonalizes the polarizability tensor $\overline{\alpha}$

$$\overline{A}\overline{\alpha}\overline{A}^{-1} = \begin{pmatrix} \alpha_1 & 0 & 0 \\ 0 & \alpha_2 & 0 \\ 0 & 0 & \alpha_3 \end{pmatrix}$$

therefore,

$$\boldsymbol{\mu} = (\mathbf{e}_x, \mathbf{e}_y, \mathbf{e}_z) \begin{pmatrix} \mu_x \\ \mu_y \\ \mu_z \end{pmatrix} = (\mathbf{e}_x, \mathbf{e}_y, \mathbf{e}_z) \overline{A}^{-1} \begin{pmatrix} \alpha_1 & 0 & 0 \\ 0 & \alpha_2 & 0 \\ 0 & 0 & \alpha_3 \end{pmatrix} \overline{A} \begin{pmatrix} E_x \\ E_y \\ E_z \end{pmatrix} \tag{7.1}$$

Now, we define a rotational operation $\hat{R}(\theta, \phi, \chi)$ which transform the coordinate system $(\mathbf{e}_x, \mathbf{e}_y, \mathbf{e}_z)$ to a new coordinate system $(\mathbf{e}'_x, \mathbf{e}'_y, \mathbf{e}'_z)$:

$$\hat{R}(\theta, \phi, \chi)(\mathbf{e}_x, \mathbf{e}_y, \mathbf{e}_z) = (\mathbf{e}'_x, \mathbf{e}'_y, \mathbf{e}'_z) = (\mathbf{e}_x, \mathbf{e}_y, \mathbf{e}_z)\overline{R}$$

In this new system, $\mathbf{E}$ and $\boldsymbol{\mu}$ are represented by:

$$\mathbf{E} = (\mathbf{e}_x, \mathbf{e}_y, \mathbf{e}_z) \begin{pmatrix} E_x \\ E_y \\ E_z \end{pmatrix} = (\mathbf{e}'_x, \mathbf{e}'_y, \mathbf{e}'_z) \overline{R}^{-1} \begin{pmatrix} E_x \\ E_y \\ E_z \end{pmatrix} = (\mathbf{e}'_x, \mathbf{e}'_y, \mathbf{e}'_z) \begin{pmatrix} E'_x \\ E'_y \\ E'_z \end{pmatrix}$$

$$\boldsymbol{\mu} = (\mathbf{e}'_x, \mathbf{e}'_y, \mathbf{e}'_z) \begin{pmatrix} \mu'_x \\ \mu'_y \\ \mu'_z \end{pmatrix}$$

Therefore, taking $\overline{R} = \overline{A}^{-1}$, we can write the polarization based on the new coordinate system,

$$\begin{aligned}
\boldsymbol{\mu} &= (\mathbf{e}'_x, \mathbf{e}'_y, \mathbf{e}'_z) \begin{pmatrix} \mu'_x \\ \mu'_y \\ \mu'_z \end{pmatrix} = (\mathbf{e}_x, \mathbf{e}_y, \mathbf{e}_z)\overline{A}^{-1} \begin{pmatrix} \alpha_1 & 0 & 0 \\ 0 & \alpha_2 & 0 \\ 0 & 0 & \alpha_3 \end{pmatrix} \overline{A} \begin{pmatrix} E_x \\ E_y \\ E_z \end{pmatrix} \\
&= (\mathbf{e}'_x, \mathbf{e}'_y, \mathbf{e}'_z) \begin{pmatrix} \alpha_1 & 0 & 0 \\ 0 & \alpha_2 & 0 \\ 0 & 0 & \alpha_3 \end{pmatrix} \begin{pmatrix} E'_x \\ E'_y \\ E'_z \end{pmatrix}
\end{aligned}$$

Clearly, the principal axes of polarizability $(\mathbf{e}'_x, \mathbf{e}'_y, \mathbf{e}'_z)$ make,

$$\mu'_x = \alpha_1 E'_x, \qquad \mu'_y = \alpha_2 E'_y, \qquad \mu'_z = \alpha_3 E'_z$$

Inversely, if we obtain the rotational operation matrix $\overline{R}$ which transforms the current coordinate system into the coordinate system of principal axes of polarization, we can write down the polarizability tensor as

$$\overline{\alpha} = \overline{R} \begin{pmatrix} \alpha_1 & 0 & 0 \\ 0 & \alpha_2 & 0 \\ 0 & 0 & \alpha_3 \end{pmatrix} \overline{R}^{-1}$$

In the new coordinate system, the three principal axes of polarizability are

$$\begin{pmatrix} 1 \\ 0 \\ 0 \end{pmatrix}, \begin{pmatrix} 0 \\ 1 \\ 0 \end{pmatrix}, \text{and} \begin{pmatrix} 0 \\ 0 \\ 1 \end{pmatrix}$$

Case study of linear molecule For the case of linear molecules, one of the principal axis of polarizability is the principal axis of the molecule $\hat{\mathbf{u}} = \mathbf{e}_x\hat{u}_1 + \mathbf{e}_y\hat{u}_2 + \mathbf{e}_z\hat{u}_3$, the

other two axes are undetermined but perpendicular to this axis. The principal values of polarizability corresponding to the three principal axes are $\alpha_1, \alpha_2, \alpha_2$ respectively. Obviously, we can take

$$\mathbf{e}'_x = (\mathbf{e}'_x, \mathbf{e}'_y, \mathbf{e}'_z) \begin{pmatrix} 1 \\ 0 \\ 0 \end{pmatrix} = (\mathbf{e}_x, \mathbf{e}_y, \mathbf{e}_z) \begin{pmatrix} \hat{u}_1 \\ \hat{u}_2 \\ \hat{u}_3 \end{pmatrix}$$

The other two axes vertical to $\mathbf{e}'_x$ are

$$\mathbf{e}'_y = (\mathbf{e}'_x, \mathbf{e}'_y, \mathbf{e}'_z) \begin{pmatrix} 0 \\ 1 \\ 0 \end{pmatrix} = (\mathbf{e}_x, \mathbf{e}_y, \mathbf{e}_z) \frac{1}{\sqrt{\hat{u}_1^2 + \hat{u}_2^2}} \begin{pmatrix} -\hat{u}_2 \\ \hat{u}_1 \\ 0 \end{pmatrix}$$

and

$$\mathbf{e}'_z = (\mathbf{e}'_x, \mathbf{e}'_y, \mathbf{e}'_z) \begin{pmatrix} 0 \\ 0 \\ 1 \end{pmatrix} = (\mathbf{e}_x, \mathbf{e}_y, \mathbf{e}_z) \frac{1}{\sqrt{\hat{u}_1^2 + \hat{u}_2^2}} \begin{pmatrix} \hat{u}_1\hat{u}_3 \\ \hat{u}_2\hat{u}_3 \\ -\hat{u}_1^2 - \hat{u}_2^2 \end{pmatrix}$$

Note that we have used the relation

$$\hat{u}_1^2 + \hat{u}_2^2 + \hat{u}_3^2 = 1$$

The internal product of each vector should always be normalized to 1. The transformation matrix $\overline{R}$ is:

$$\overline{R} = \frac{1}{\sqrt{\hat{u}_1^2 + \hat{u}_2^2}} \begin{pmatrix} \hat{u}_1\sqrt{\hat{u}_1^2 + \hat{u}_2^2} & -\hat{u}_2 & \hat{u}_1\hat{u}_3 \\ \hat{u}_2\sqrt{\hat{u}_1^2 + \hat{u}_2^2} & \hat{u}_1 & \hat{u}_2\hat{u}_3 \\ \hat{u}_3\sqrt{\hat{u}_1^2 + \hat{u}_2^2} & 0 & -\hat{u}_1^2 - \hat{u}_2^2 \end{pmatrix}$$

The inverse matrix $\overline{R}^{-1}$ is,

$$\begin{aligned}
\overline{R}^{-1} &= \frac{1}{\hat{u}_1^2+\hat{u}_2^2}\begin{pmatrix} \hat{u}_1-\hat{u}_1\hat{u}_3^2 & \hat{u}_2-\hat{u}_2\hat{u}_3^2 & \hat{u}_3-\hat{u}_3^3 \\ -\hat{u}_2\sqrt{\hat{u}_1^2+\hat{u}_2^2} & \hat{u}_1\sqrt{\hat{u}_1^2+\hat{u}_2^2} & 0 \\ \hat{u}_1\hat{u}_3\sqrt{\hat{u}_1^2+\hat{u}_2^2} & \hat{u}_2\hat{u}_3\sqrt{\hat{u}_1^2+\hat{u}_2^2} & (-\hat{u}_1^2-\hat{u}_2^2)\sqrt{\hat{u}_1^2+\hat{u}_2^2} \end{pmatrix} \\
&= \overline{R}^T
\end{aligned}$$

where $\overline{R}^T$ is just the transpose matrix of $\overline{R}$. Therefore, the polarizability matrix in the original coordinate system $(\mathbf{e}_x, \mathbf{e}_y, \mathbf{e}_z)$ for a linear molecule with principal axis lying in $\hat{\mathbf{u}}$ is given by

$$\begin{aligned}
\overline{\alpha} &= \overline{R}\begin{pmatrix} \alpha_1 & 0 & 0 \\ 0 & \alpha_2 & 0 \\ 0 & 0 & \alpha_2 \end{pmatrix}\overline{R}^{-1} \\
&= \alpha_2\begin{pmatrix} 1 & 0 & 0 \\ 0 & 1 & 0 \\ 0 & 0 & 1 \end{pmatrix} + (\alpha_1-\alpha_2)\begin{pmatrix} \hat{u}_1 \\ \hat{u}_2 \\ \hat{u}_3 \end{pmatrix}(\hat{u}_1 \quad \hat{u}_2 \quad \hat{u}_3)
\end{aligned}$$

Define

$$\alpha = \frac{1}{3}(\alpha_1 + 2\alpha_2)$$

and

$$\gamma = \alpha_1 - \alpha_2$$

The polarizability can be written as

$$\begin{aligned} \overline{\alpha} &= (\alpha - \frac{\gamma}{3})\overline{I} + \gamma \hat{\mathbf{u}}\hat{\mathbf{u}} \\ &= \alpha\overline{I} + \gamma(\hat{\mathbf{u}}\hat{\mathbf{u}} - \frac{1}{3}\overline{I}) \\ &= \alpha\overline{I} + \overline{\beta} \end{aligned} \tag{7.2}$$

where $\overline{I}$ is the 3 by 3 identity matrix. For CO_2 molecule, $\alpha = 2.63\text{Å}^3$ and $\gamma = 2.10\text{Å}^3$[10]. Equation (7.2) separates the total polarizability of a molecule into a spherical part $\alpha\overline{I}$ and a traceless part $\overline{\beta}$. We will see that the auto correlation of the spherical part $< \alpha(0)\alpha(t) >$ and that of the traceless part $< \text{Tr}\overline{\beta}(0)\overline{\beta}(t) >$ correspond to observation observation of a scattering spectrum in two different directions.

7.2 Classical Theory of Light Scattering

Scattering Cross Sections For isotropic systems without preferred orientation in space, only two geometry independent numbers are necessary to describe the dependence of the scattering cross section on the scattering geometry. Define $\left(\frac{d\sigma}{d\Omega}\right)_{\parallel}$ or $\left(\frac{d\sigma}{d\Omega}\right)_{\perp}$ as the scattering cross section if the polarization of the scattered light $\mathbf{e}^s$ is parallel or perpendicular to that of the incident light $\mathbf{e}^i$. For linearly polarized incident light $\mathbf{E} = \mathbf{e}^i E_0(\mathbf{k}, \mathbf{r}, t)$ the total cross section at direction $\mathbf{k}^s$ may be written as

$$\frac{d\sigma}{d\Omega} = \left(\frac{d\sigma}{d\Omega}\right)_{\parallel} \sin^2\phi + \left(\frac{d\sigma}{d\Omega}\right)_{\perp} (1 + \cos^2\phi) \tag{7.3}$$

where ϕ is the angle between the electric polarization vector of the incident radiation, $\mathbf{e}^i$, and the propagation vector of the scattered radiation, $\mathbf{k}^s$. In the case where we observe scattered light in the direction parallel to the incident polarization vector $\mathbf{e}^i$,

the angle ϕ is 0 and the total cross section is

$$\frac{d\sigma}{d\Omega}(\text{obs. } \|) = 2\left(\frac{d\sigma}{d\Omega}\right)_{\perp} \tag{7.4}$$

whereas in case of $\phi = 90$,

$$\frac{d\sigma}{d\Omega}(\text{obs. } \perp) = \left(\frac{d\sigma}{d\Omega}\right)_{\|} + \left(\frac{d\sigma}{d\Omega}\right)_{\perp} \tag{7.5}$$

When the polarization of the scattered light is perpendicular to that of incident light, only the *depolarized* radiation is experimentally observed, which means $\left(\frac{d\sigma}{d\Omega}\right)_{\perp}$ only includes the *depolarized* component. For the case of observation of $\left(\frac{d\sigma}{d\Omega}\right)_{\|}$, both *polarized* and *depolarized* components appear and the polarized component can be written as[24]:

$$\frac{d\sigma_{pol}}{d\Omega} \equiv \left(\frac{d\sigma}{d\Omega}\right)_{\|} - \frac{4}{3}\left(\frac{d\sigma}{d\Omega}\right)_{\perp} \tag{7.6}$$

Classical theory of light scattering Classical theory of electrodynamics indicates that the radiation emitted by an oscillating dipole $\boldsymbol{\mu} = \boldsymbol{\mu}_0 \cos(\omega t)$ is given by[53]

$$\mathbf{B} = k^2(\mathbf{e}_r \times \boldsymbol{\mu})\frac{e^{ikr}}{r}$$

and

$$\mathbf{E} = \mathbf{B} \times \mathbf{e}_r$$

where $\mathbf{e}_r$ is the unit vector along the radial direction $\mathbf{r}$ and $k = \omega/c$. If we write the amplitude of the oscillating dipole as

$$\boldsymbol{\mu}_0 = \mathbf{e}_x\mu_{ox} + \mathbf{e}_y\mu_{oy} + \mathbf{e}_z\mu_{oz}$$

and only look at the radiation in the direction $\mathbf{e}_r = \mathbf{e}_x$:

$$\mathbf{B} = k^2(\mathbf{e}_z\mu_{oy} - \mathbf{e}_y\mu_{oz})\frac{e^{ikr}}{r}\cos(\omega t)$$

$$\mathbf{E} = k^2(\mathbf{e}_y\mu_{oy} + \mathbf{e}_z\mu_{oz})\frac{e^{ikr}}{r}\cos(\omega t)$$

The flux of the radiation is given by the Poynting vector $\mathbf{S}$

$$\mathbf{S} = \frac{c}{4\pi}(\mathbf{E}\times\mathbf{H}^*) = \mathbf{e}_x\frac{ck^4}{4\pi r^2}(\mu_{oy}^2 + \mu_{oz}^2)\cos^2(\omega t)$$

$$\left(\frac{dI}{d\Omega}\right)_x \sin\theta d\theta d\phi = \int \mathbf{S}_x r^2 \sin\theta d\theta d\phi dt = \frac{2\pi^3\nu^4}{c^3}(\mu_{oy}^2 + \mu_{oz}^2)\sin\theta d\theta d\phi$$

where $\nu = \omega/(2\pi)$. The rate of radiation emitted per unit solid angle in the $\mathbf{e}_x$ direction is

$$\left(\frac{dI}{d\Omega}\right)_x = \frac{2\pi^3\nu^4}{c^3}(\mu_{oy}^2 + \mu_{oz}^2)$$

For incident light $\mathbf{E} = \mathbf{e}_x E_0(\mathbf{k},\mathbf{r})\cos(\omega t)$ linearly polarized in the $\mathbf{e}_x$ direction and propagating in the $\mathbf{e}_y$ direction, the induced dipole moment is

$$\begin{aligned}
\boldsymbol{\mu} &= (\mathbf{e}_x,\mathbf{e}_y,\mathbf{e}_z)\begin{pmatrix}\mu_x\\ \mu_y\\ \mu_z\end{pmatrix} = (\mathbf{e}_x,\mathbf{e}_y,\mathbf{e}_z)\begin{pmatrix}\alpha_{xx} & \alpha_{xy} & \alpha_{xz}\\ \alpha_{yx} & \alpha_{yy} & \alpha_{yz}\\ \alpha_{zx} & \alpha_{zy} & \alpha_{zz}\end{pmatrix}\begin{pmatrix}E_0\cos(\omega t)\\ 0\\ 0\end{pmatrix}\\
&= (\mathbf{e}_x,\mathbf{e}_y,\mathbf{e}_z)\begin{pmatrix}\mu_{ox}\cos(\omega t)\\ \mu_{oy}\cos(\omega t)\\ \mu_{oz}\cos(\omega t)\end{pmatrix}
\end{aligned}$$

Therefore, the observed scattering cross section in the $\mathbf{e}_x$ direction which is parallel to the polarization direction of incident light is given by,

$$\left(\frac{d\sigma}{d\Omega}\right)(\text{obs. }\|) = \frac{2\pi^3\nu^4}{c^3}(\mu_{oy}^2 + \mu_{oz}^2) = \frac{2\pi^3\nu^4}{c^3}(\alpha_{yx}^2 + \alpha_{zx}^2)E_0^2$$

If the incident light is still propagating in the $\mathbf{e}_y$ direction but polarized in the $\mathbf{e}_z$ direction $\mathbf{E} = \mathbf{e}_z E_0(\mathbf{k},\mathbf{r})\cos(\omega t)$, then the observed scattered light propagating in the

$\mathbf{e}_x$ direction is given by

$$\left(\frac{d\sigma}{d\Omega}\right)(\text{obs. }\perp) = \frac{2\pi^3\nu^4}{c^3}(\mu_{oy}^2 + \mu_{oz}^2) = \frac{2\pi^3\nu^4}{c^3}(\alpha_{yz}^2 + \alpha_{zz}^2)E_0^2$$

For an isotropic system, the two independent variables $\left(\frac{d\sigma}{d\Omega}\right)_{\parallel}$ and $\left(\frac{d\sigma}{d\Omega}\right)_{\perp}$ are:

$$\left(\frac{d\sigma}{d\Omega}\right)_{\parallel} = \frac{2\pi^3\nu^4E_0^2}{c^3} < \alpha_{xx}^2 > = \frac{2\pi^3\nu^4E_0^2}{c^3} < \alpha_{yy}^2 > = \frac{2\pi^3\nu^4E_0^2}{c^3} < \alpha_{zz}^2 >$$

$$\left(\frac{d\sigma}{d\Omega}\right)_{\perp} = \frac{2\pi^3\nu^4E_0^2}{c^3} < \alpha_{yz}^2 > = \frac{2\pi^3\nu^4E_0^2}{c^3} < \alpha_{yx}^2 > = \frac{2\pi^3\nu^4E_0^2}{c^3} < \alpha_{xz}^2 > = \cdots$$

Taking the average over all possible orientations for molecules in gas phase, we have[53]

$$\begin{aligned} < \alpha_{ij}^2 > &= \tfrac{1}{15}(\textstyle\sum_{p=1}^{3}\alpha_p^2 - \sum_{p=1}^{2}\sum_{q>p}^{3}\alpha_p\alpha_q) \qquad \text{for} \quad i \neq j \\ < \alpha_{ii}^2 > &= \tfrac{1}{15}(\textstyle\sum_{p=1}^{3}3\alpha_p^2 + 2\sum_{p=1}^{2}\sum_{q>p}^{3}\alpha_p\alpha_q) \quad \text{for} \quad i = x, y, z \end{aligned}$$

By introducing the spherical part and anisotropic (traceless) part as in equation (7.2), we can rewrite the above averages as

$$\begin{aligned} < \alpha_{ij}^2 > &\propto \tfrac{1}{5}\mathrm{Tr}[\overline{\beta}\cdot\overline{\beta}] \qquad\qquad \text{for} \quad i \neq j \\ < \alpha_{ii}^2 > &\propto \alpha^2 + \tfrac{4}{15}\mathrm{Tr}[\overline{\beta}\cdot\overline{\beta}] \quad \text{for} \quad i = x, y, z \end{aligned}$$

The polarized and depolarized scattering cross sections are:

$$\frac{d\sigma_{depol}}{d\Omega} \propto \mathrm{Tr}[\overline{\beta}\cdot\overline{\beta}] \tag{7.7}$$

$$\frac{d\sigma_{pol}}{d\Omega} \equiv \left(\frac{d\sigma}{d\Omega}\right)_{\parallel} - \frac{4}{3}\left(\frac{d\sigma}{d\Omega}\right)_{\perp} \propto \alpha^2 \tag{7.8}$$

A real quantum mechanical treatment of the polarization spectra yields the time correlation for the cross section instead of the simple averages in equations (7.7) and (7.8)[53, 24]. The relevant time correlation function for depolarized spectra is

always the time correlation function of $\overline{\beta}$. For depolarized linear Raman scattering spectra, the cross section at frequency ω is written as[24]

$$\frac{d\sigma_{depol}}{d\Omega} \propto \frac{1}{2\pi}\int_{-\infty}^{\infty} dt\, e^{-i\omega t} < \mathrm{Tr}[\overline{\beta}(0)\cdot\overline{\beta}(t)] >= \frac{1}{2\pi}\int_{-\infty}^{\infty} dt\, e^{-i\omega t} C_2(t) \tag{7.9}$$

where we have defined the auto correlation of the anisotropic polarizability as

$$C_2(t) \equiv < \mathrm{Tr}[\overline{\beta}(0)\cdot\overline{\beta}(t)] >$$

Recall that equation (3.25) gives the general relation between 3rd order polarization and external electrical field as

$$\begin{aligned}
< P_i >_t^{(3)} &= < \zeta_{ijkl} > E_j(t)E_k(t)E_l(t) + \\
&\quad \frac{i}{2\hbar}\int_0^t d\tau < [\chi_{ij}(t), \chi_{kl}(\tau)] > E_k(\tau)E_l(\tau)E_j(t) \\
&= \int_0^t dt_1 \int_0^{t_1} dt_2 \int_0^{t_2} dt_3 \; < \zeta_{ijkl} > \\
&\quad \delta(t-t_1)\delta(t_1-t_2)\delta(t_2-t_3)E_j(t_1)E_k(t_2)E_l(t_3) \\
&\quad + \frac{i}{2\hbar}\int_0^t dt_1 \int_0^{t_1} dt_2 \int_0^{t_2} dt_3 \; < [\chi_{ij}(t_1), \chi_{kl}(t_2)] > \\
&\quad \delta(t-t_1)\delta(t_2-t_3)E_j(t_1)E_k(t_2)E_l(t_3) \\
&= \int_0^t dt_1 \int_0^{t_1} dt_2 \int_0^{t_2} dt_3\, R_{ijkl}(t,t_1,t_2,t_3)E_j(t_1)E_k(t_2)E_l(t_3)
\end{aligned}$$

where the general 3rd response function for the system is

$$\begin{aligned}
R_{ijkl}(t,t_1,t_2,t_3) &= < \zeta_{ijkl} > \delta(t-t_1)\delta(t_1-t_2)\delta(t_2-t_3) \\
&\quad + \frac{i}{2\hbar}\delta(t-t_1) < [\chi_{ij}(t_1), \chi_{kl}(t_2)] > \delta(t_2-t_3)
\end{aligned}$$

Considering the time interval $\tau = t_1 - t_2$ and integrating the other time intervals (i.e.

OKE spectra), we have the response function:

$$\begin{aligned} R_{ijkl}(\tau) &= <\zeta_{ijkl}>\delta(\tau) + \frac{i}{2\hbar} <[\chi_{ij}(t_1), \chi_{kl}(t_2)]> \\ &= <\zeta_{ijkl}>\delta(\tau) + \frac{i}{2\hbar} <[\chi_{ij}(\tau), \chi_{kl}(0)]> \end{aligned}$$

Denoting the equilibrium average $<\zeta_{ijkl}>$ as ζ_{ijkl} and considering only the depolarized component of the 3rd nonlinear spectra (anisotropic component of χ is β), the response function at time t for the system becomes

$$\begin{aligned} R_{ijkl}(t) &= \zeta_{ijkl}\delta(t) + \frac{i}{2\hbar} <[\beta_{ij}(t), \beta_{kl}(t=0)]> \\ &= \zeta_{ijkl}\delta(t) - \frac{1}{2\beta} <\beta_{ij}(0)\dot{\beta}_{kl}(t)> \end{aligned}$$

where we have used the Kubo transform to convert the quantum mechanic time correlation function to the corresponding classical version (see section 3.2). For an isotropic system, the $3^4 = 81$ components of $R_{ijkl}(t)$ are not independent and it is sufficient to consider the R_{ijij} component for depolarized spectra[21]

$$R_{ijij}(t) = \zeta_{ijij}\delta(t) - \frac{1}{2\beta} <\beta_{ij}(0)\dot{\beta}_{ij}(t)> \tag{7.10}$$

The second part of $R_{ijij}(t)$ in the above equation is proportional to the first derivative of $C_2(t)$

$$\dot{C}_2(t) = \frac{d}{dt} <\mathrm{Tr}[\overline{\beta}(0)\cdot\overline{\beta}(t)]> \quad \propto \quad <\beta_{ij}(0)\dot{\beta}_{ij}(t)>$$

Thus the time correlation function $C_2(t)$ and its first derivative contain all the dynamical information probed by depolarized linear or nonlinear scattering spectra. For a group of interactive molecules in fluids, the collective polarizability is denoted by $\overline{\Pi}$ with

$$\overline{\Pi} = \Pi_0\overline{I} + \overline{\Pi}_2$$

and the relevant time correlation function of the anisotropic part of the collective polarizability is

$$C_2(t) =< \mathrm{Tr}[\overline{\Pi}_2(0) \cdot \overline{\Pi}_2(t)] >$$

7.3 TCF of the Collective Polarizability

The collective polarizability $\overline{\Pi}$ of a group of molecules is the sum of polarizabilities for all isolated molecules. Each isolated polarizablity is modified by self rotation of the molecule and the interaction with the surrounding molecules. The standard point-dipole/induced-point-dipole (DID) model expresses the isolated polarizability $\overline{\pi}(j)$ for molecule j as a sum of a molecular component (gas phase polarizability) and an interaction-induced component:

$$\overline{\pi}(j) = \overline{\alpha}(j) + \overline{\alpha}(j) \cdot \sum_{k \neq j}^{N} \overline{T}_{jk} \cdot \overline{\pi}(k) \tag{7.11}$$

where the dipole-dipole tensor between molecule j and k is:

$$\overline{T}_{jk} = \frac{1}{r^3} \left(3\hat{r}\hat{r} - \overline{I}\right)\Big|_{\mathbf{r}=\mathbf{r}_{jk}}$$

where $\hat{r} = \mathbf{r}/r$ is the unit vector along the direction $\mathbf{r}$. Equation (7.11) can be solved self-consistently[21] by taking $\overline{\pi}(k) = \overline{\alpha}(k)$ as ansatz. The total collective

polarizability $\overline{\Pi}$ for a system of N particles is

$$\begin{aligned}
\overline{\Pi} &= \Pi_0\overline{I} + \overline{\Pi}_2 = \sum_j^N \overline{\pi}(j) \\
&= \sum_j^N \overline{\alpha}(j) + \sum_j^N \sum_{k\neq j}^N \overline{\alpha}(j)\cdot\overline{T}_{jk}\cdot\overline{\pi}(k) \\
&= \overline{M} + \overline{D} \\
&= \frac{1}{3}\mathrm{Tr}(\overline{M})\overline{I} + \left(\overline{M} - \frac{1}{3}\mathrm{Tr}(\overline{M})\overline{I}\right) + \frac{1}{3}\mathrm{Tr}(\overline{D})\overline{I} + \left(\overline{D} - \frac{1}{3}\mathrm{Tr}(\overline{D})\overline{I}\right) \\
&= \frac{1}{3}\mathrm{Tr}(\overline{M})\overline{I} + \overline{Q} + \frac{1}{3}\mathrm{Tr}(\overline{D})\overline{I} + \overline{K}
\end{aligned}$$

where the anisotropic component of the molecular polarizability $\overline{M}$ and interaction-induced polarizability $\overline{D}$ are

$$\overline{Q} = \left(\overline{M} - \frac{1}{3}\mathrm{Tr}(\overline{M})\overline{I}\right)$$

and

$$\overline{K} = \left(\overline{D} - \frac{1}{3}\mathrm{Tr}(\overline{D})\overline{I}\right)$$

The anisotropic component of the total collective polarizability $\overline{\Pi}$ is the sum of that of the molecular polarizablity and that of the interaction-induced polarizability:

$$\overline{\Pi}_2 = \overline{Q} + \overline{K}$$

Thus, the time correlation function of $\overline{\Pi}$ can be written as

$$\begin{aligned}
C_2(t) &= < \mathrm{Tr}[\overline{\Pi}_2(0)\cdot\overline{\Pi}_2(t)] > \\
&= < \mathrm{Tr}[\overline{Q}(0)\cdot\overline{Q}(t)] > + < \mathrm{Tr}[\overline{K}(0)\cdot\overline{K}(t)] > + \\
&\quad < \mathrm{Tr}[\overline{Q}(0)\cdot\overline{K}(t) + \overline{K}(0)\cdot\overline{Q}(t)] > \\
&= C_2^M(t) + C_2^I(t) + C_2^{MI}(t) \qquad (7.12)
\end{aligned}$$

where

$$C_2^M(t) =< \mathrm{Tr}[\overline{Q}(0) \cdot \overline{Q}(t)] >$$

$$C_2^I(t) =< \mathrm{Tr}[\overline{K}(0) \cdot \overline{K}(t)] >$$

$$C_2^{MI}(t) =< \mathrm{Tr}[\overline{Q}(0) \cdot \overline{K}(t) + \overline{K}(0) \cdot \overline{Q}(t)] >$$

The above equation (7.12) separates the TCF $C_2(t)$ for the anisotropic collective polarizability $\overline{\Pi}_2$ into three components: the molecular component C_2^M, the interaction-induced component $C_2^I(t)$, and the molecular interaction-induced cross correlation component $C_2^{MI}(t)$. This separation enables us to distinguish the pure molecular contribution from the pure interaction-induced contribution. In order to separate out the fraction of the interaction-induced component that tracks the dynamics of molecular reorientation, it is informative to project the interaction-induced anisotropic polarizability $\overline{K}$ onto the molecular anisotropic polarizability $\overline{Q}$[18]. The projected component is

$$\Delta\overline{Q} = \frac{\mathrm{Tr}[\overline{K} \cdot \overline{Q}]}{\mathrm{Tr}[\overline{Q} \cdot \overline{Q}]}\overline{Q}$$

where the coefficient Δ is defined as $\Delta \equiv \frac{\mathrm{Tr}[\overline{K} \cdot \overline{Q}]}{\mathrm{Tr}[\overline{Q} \cdot \overline{Q}]}$. Therefore the anisotropic collective polarizability $\overline{\Pi}_2$ can be separated into a pure reorientational part and a pure collision-induced part (without reorientation):

$$\overline{\Pi}_2 = \overline{Q} + \overline{K} = (1 + \Delta)\overline{Q} + (\overline{K} - \Delta\overline{Q}) = \overline{\Pi}_2^R + \overline{\Pi}_2^{CI}$$

The corresponding time correlation functions are

$$C_2(t) = C_2^R(t) + C_2^{CI}(t) + C_2^{RI}(t) \tag{7.13}$$

$$C_2^R(t) =< \mathrm{Tr}\left[(1+\Delta(0))\overline{Q}(0)\cdot(1+\Delta(t))\overline{Q}(t)\right] >$$

$$C_2^{CI}(t) =< \mathrm{Tr}\left[(\overline{K}(0)-\Delta(0)\overline{Q}(0))\cdot(\overline{K}(t)-\Delta(t)\overline{Q}(t))\right] >$$

$$C_2^{RI}(t) =< \mathrm{Tr}\left[\overline{\Pi}_2^R(0)\cdot\overline{\Pi}_2^{CI}(t)+\overline{\Pi}_2^{CI}(0)\cdot\overline{\Pi}_2^R(t)\right]$$

where $C_2^R(t)$, $C_2^{CI}(t)$ and $C_2^{RI}(t)$ stand for the reorientational contribution, the collisional-induced contribution, and the cross term contribution to $C_2(t)$ respectively.

A test case of compressed CO_2 gas Figure 7.1 shows the time correlation function of anisotropic collective polarizability for compressed CO_2 gas and its components. From Figure 7.1 (A) we see that the sum of the interaction-induced component $C_2^I(t)$ and the cross correlation $C_2^{MI}(t)$ has the opposite sign of the pure molecular component. This is because the anisotropic interaction-induced polarizability $\overline{K}$ has negative contribution to the total anisotropic collective polarizability $\overline{\Pi}_2$. Figure 7.1 (B) shows that the reorientational component $C_2^R(t)$ matches the total TCF very well and the contributions from $C_2^{CI}(t)$ and $C_2^{RI}(t)$ are negligible. This is because CO_2 is a weakly polarizable molecule ($\alpha = 2.63\text{Å}^3$ and $\gamma = 2.10\text{Å}^3$ are both small).

7.4 Optical Kerr Effect of an Ionic Liquid

Optical Kerr Effect (OKE) experiment measures the transient anisotropy in the refractive index $\Delta n(t)$ [51, 21]

$$\Delta n(t) = \int_{-\infty}^{t} d\tau\, I_{pump}(\tau) R(t-\tau)$$

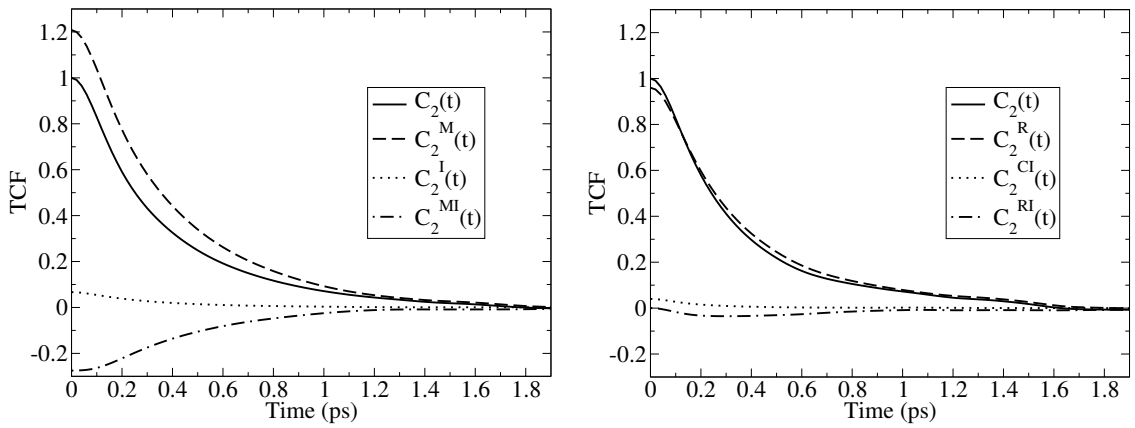

(A) (B)

TCF of anisotropic collective polarizability for compressed CO_2 gas at temperature T=313 K and density ρ=1.105g/cm^3. All of the TCFs are normalized by the initial value $C_2(0)$. The molecular polarizability is calculated using equation (7.2) with $\alpha = 2.63$Å^3 and $\gamma = 2.10$Å^3[10]. C_2^M,C_2^I,C_2^R, and C_2^{CI} stand for the molecular component, interaction-induced component, reorientation component and collision-induced component respectively. C_2^{MI} and C_2^{RI} are the molecular interaction-induced cross term and reorientational collision-induced cross term respectively. (A) Total TCF and their components according to equation (7.12) (B) Total TCF and their components according to equation (7.13).

Figure 7.1: TCF of anisotropic polarizability

where R is the 3rd order nonlinear response function as in equation (7.10). The observed hetero-dyne detected transmission of a Kerr cell is approximately given by

$$\begin{aligned}
I_{OKE}(t) &= \int_{-\infty}^{\infty} d\tau\, I_{probe}(t-\tau)\Delta n(\tau) \\
&= \int_{-\infty}^{\infty} d\tau\, I_{probe}(t-\tau) \int_{-\infty}^{\tau} dt_1\, I_{pump}(t_1) R(\tau - t_1) \\
&= \int_{-\infty}^{\infty} d\tau\, I_{probe}(\tau) \int_{-\infty}^{t-\tau} dt_1\, I_{pump}(t_1) R(t-\tau-t_1) \\
&= \int_{-\infty}^{\infty} d\tau\, I_{probe}(\tau) \int_{0}^{\infty} dt_2\, I_{pump}(t-\tau-t_2) R(t_2) \\
&= \int_{0}^{\infty} dt_2 R(t_2) \int_{-\infty}^{\infty} d\tau\, I_{probe}(\tau) I_{pump}(t-t_2-\tau) \\
&= \int_{0}^{\infty} dt_2 R(t_2) G_0(t-t_2) \\
&= \int_{-\infty}^{t} d\tau\, G_0(\tau) R(t-\tau)
\end{aligned}$$

where $G_0(t)$ is the zero background laser pulse intensity autocorrelation:

$$G_0(t) = \int_{-\infty}^{\infty} d\tau I_{pump}(t) I_{probe}(t-\tau)$$

Recall that the 3rd response function $R(t)$ is a combination of a hyperpolarizability $\zeta\delta(t)$ and a time correlation function $\dot{C}_2(t)$, the instantaneous response of OKE will resemble the blank convolution signal $G_0(t)$ due to the δ function nature of hyperpolarizability. Our simulation only tracks the transient signal from the time correlation function $\dot{C}_2(t)$ which probes the inter- and intra-molecular dynamics of the liquids. We directly write this part of OKE signal as

$$I_{OKE}(t) \propto -\int_{-\infty}^{t} d\tau\, G_0(\tau)\dot{C}_2(t) \tag{7.14}$$

In our calculation, the shape of the probe and pump laser pulses is taken to be a Gaussian function with a $37fs$ full width at half-maximum[66].

Simulation details In order to understand the interaction and dynamics of ionic liquids, we performed molecular dynamics simulation for the 1-methoxy-ethylpyridinium dicyanoamide [MOEPY+][DCA-] system which has been recently experimentally studied [65]. The effective atomic charges distribution obtained from an *ab initio* calculation are provided in Table D.16 and Table D.19 in Appendix D. Our simulation box consists of 64 pairs of ions. Periodic boundary conditions are employed using the particle mesh ewald (PME) method to treat long-range electrostatic interactions[15, 50, 49]. In order to get better energy conservation for this relatively small system, we used a switch function for the LJ interactions instead of a direct cutoff[1]. Five independent trajectories were run at T=400K for 60ns using a time

step of 0.001ps. This long simulation time is necessary because the calculation of collective polarizability is extensively biased by the initial configuration. This is consistent with the fact that ionic liquids display local heterogeneity on a time scale of nanoseconds (see chapters 5 and 6). Data for analysis was recorded every 0.1ps. In order to catch the short time behavior of the OKE signal, we further collect data at every 0.01ps and 0.0001ps from 300 simulations each of which has the initial configuration extracted from the trajectory at every 1ns point of the 5 independent 60ns runs. Each of these 300 runs last for 10ps and 2ps for every 0.01ps and every 0.0001ps data collection respectively.

In order to calculate the collective polarizability, we assigned gas phase point dipole to each atom in the molecule according to the scheme in reference[40]. A list of these parameters is provided in Tables 7.1, and 7.2. The calculated spherical polarizabilities (α) for [MOEPY+] and [DCA-] are 13.36Å^3 and 5.4Å^3 respectively. Those values are much larger than that for CO_2 indicating that [MOEPY+][DCA-] system is highly polarizable.

Table 7.1: Coordinates and polarizabilities of [MOEPY+]

Atom	atom index	x (Å)	y (Å)	z (Å)	α (Å) ^{3}
H1	1	4.24938	0.31338	-0.83530	0.01000
H2	2	3.02142	2.22325	0.23835	0.46636
H3	3	0.67940	1.84972	1.03476	0.65773
H4	4	0.73368	-2.10707	-0.21623	0.65773
H5	5	3.07810	-1.89681	-1.06324	0.46636
N6	6	0.64652	-0.13539	0.42806	2.23174
C7	7	2.58598	-1.04349	-0.61148	0.27040
C8	8	3.23154	0.18742	-0.48113	2.04699
C9	9	2.55437	1.25326	0.11422	0.27040
C10	10	1.25823	1.06596	0.56121	0.28044
C11	11	1.28909	-1.17942	-0.14821	0.28044
C12	12	-0.76629	-0.29325	0.86639	0.45371
C13	13	-1.74655	0.05573	-0.26108	1.14150
C14	14	-4.08012	0.13384	-0.61568	0.57427
H15	15	-0.91010	-1.32578	1.18747	0.30893
H16	16	-0.93099	0.35744	1.72632	0.30893
H17	17	-1.56939	-0.59775	-1.13351	0.38490
H18	18	-1.58655	1.09652	-0.59398	0.38490

Continued on next page

Table 7.1 – continued from previous page

Atom	atom index	x (Å)	y (Å)	z (Å)	α (Å) ^{3}
H19	19	-5.00644	-0.04675	-0.07006	0.38490
H20	20	-4.05773	1.17690	-0.95860	0.38490
H21	21	-4.03547	-0.53295	-1.48721	0.38490
O22	22	-3.01373	-0.13368	0.29386	0.56943

Polarizabilities were fit according to reference [40]. Because a point dipole description is only accurate for larger distances, 1,2- and 1,3-interactions have been omitted in calculating the gas phase polarizabilities.

Table 7.2: Coordinates and polarizabilities of [DCA-]

Atom	atom index	x (Å)	y (Å)	z (Å)	α (Å)^3
C1	1	0.00000	1.15285	0.05355	1.30551
C2	2	0.00000	-1.15285	0.05355	1.30551
N3	3	0.00000	0.00000	0.68568	0.75419
N4	4	0.00000	2.24667	-0.38873	1.00994
N5	5	0.00000	-2.24667	-0.38873	1.00994

Calculation of the Collective Polarizability: Two-body Approximation As we discussed in section 7.3, we can solve equation (7.11) self-consistently to get the collective polarizability for a group of N atoms in the DID model. A more efficient

way is to construct a $3N$ by $3N$ interaction matrix from equation (7.11) and then invert this matrix[2]. We first rewrite equation (7.11) as

$$\overline{\alpha}^{-1}(j) \cdot \overline{\pi}(j) - \sum_{k \neq j}^{N} \overline{T}_{jk} \cdot \overline{\pi}(k) = \overline{I}$$

This equation can be reformatted as follows:

$$\begin{bmatrix} \overline{\alpha}^{-1}(1) & -\overline{T}_{12} & \cdots & -\overline{T}_{1N} \\ -\overline{T}_{21} & \overline{\alpha}^{-1}(2) & \cdots & -\overline{T}_{2N} \\ \cdots & \cdots & \cdots & \cdots \\ -\overline{T}_{N1} & -\overline{T}_{N2} & \cdots & \overline{\alpha}^{-1}(N) \end{bmatrix} \cdot \begin{bmatrix} \overline{\pi}(1) \\ \overline{\pi}(2) \\ \cdots \\ \overline{\pi}(N) \end{bmatrix} = \begin{bmatrix} \overline{I} \\ \overline{I} \\ \cdots \\ \overline{I} \end{bmatrix}$$

where each element of the above $3 \times N$ by $3 \times N$ is a 3 by 3 matrix. The inverse of the $3N$ by $3N$ matrix is:

$$\tilde{B} = \begin{bmatrix} \overline{B}_{11} & \overline{B}_{12} & \cdots & \overline{B}_{1N} \\ \overline{B}_{21} & \overline{B}_{22} & \cdots & \overline{B}_{2N} \\ \cdots & \cdots & \cdots & \cdots \\ \overline{B}_{N1} & \overline{B}_{N2} & \cdots & \overline{B}_{NN} \end{bmatrix}$$

where each component $\overline{B}_{ij}$ of the $3N$ by $3N$ matrix $\tilde{B}$ is a 3 by 3 tensor. The collective polarizability can be written as:

$$\overline{\Pi} = \sum_{i}^{N} \overline{\pi}(j) = \sum_{i}^{N} \sum_{j}^{N} \overline{B}_{ij}$$

The matrix $\tilde{B}$ is symmetrical because the gas phase polarizability α and dipole-dipole tensor $\overline{T}_{ij}$ are both symmetric. Performing the inversion of a symmetrical matrix to get $\overline{\Pi}$ requires more memory but is much more efficient than the self-consistent

approach. In order to facilitate the calculation and reduce the use of memory, we developed a two-body approximation to better implement the inversion method. The number of atoms is $N = 64 \times (22 + 5)$ for our simulation box containing 64 ion pairs. The original inversion method required the inversion of a $3 \times 64 \times (22 + 5) = 5184$ by 5184 atomic interaction matrix. This atomic interaction matrix are made of $64 \times 64 + 64 \times 64 + 2 \times 64 \times 64 = 128 \times 128 = 16384$ blocks among which 64×64 3×22 by 3×22 matrices are cation-cation interactions, 64×64 3×5 by 3×5 matrices are anion-anion interactions, and $2 \times 64 \times 64$ 3×22 by 3×5 matrices are cation-anion interactions. Under the two-body approximation, each of these 16384 blocks is replaced by the corresponding 3 by 3 molecular interaction matrix. The total 5184 by 5184 matrix is resolvent to a 3×128 by 3×128 molecular interaction matrix. The total collective polarizability is obtained by inversion of this molecular interaction matrix.

The original inversion method for the DID model expresses the collective po-

larizability for two interacting molecules a and b as follows:

$$\left[\begin{array}{cccc|cccc}
\overline{T}_{a1a1} & \overline{T}_{a1a2} & \cdots & \overline{T}_{a1aL} & \overline{T}_{a1b1} & \overline{T}_{a1b2} & \cdots & \overline{T}_{a1bM} \\
\overline{T}_{a2a1} & \overline{T}_{a2a2} & \cdots & \overline{T}_{a2aL} & \overline{T}_{a2b1} & \overline{T}_{a2b2} & \cdots & \overline{T}_{a2bM} \\
\cdots & \cdots & \cdots & \cdots & \cdots & \cdots & \cdots & \cdots \\
\overline{T}_{aLa1} & \overline{T}_{aLa2} & \cdots & \overline{T}_{aLaL} & \overline{T}_{aLb1} & \overline{T}_{aLb2} & \cdots & \overline{T}_{aLbM} \\
--- & --- & --- & --- & --- & --- & --- & --- \\
\overline{T}_{b1a1} & \overline{T}_{b1a2} & \cdots & \overline{T}_{b1aL} & \overline{T}_{b1b1} & \overline{T}_{b1b2} & \cdots & \overline{T}_{b1bM} \\
\overline{T}_{b2a1} & \overline{T}_{b2a2} & \cdots & \overline{T}_{b2aL} & \overline{T}_{b2b1} & \overline{T}_{b2b2} & \cdots & \overline{T}_{b2bM} \\
\cdots & \cdots & \cdots & \cdots & \cdots & \cdots & \cdots & \cdots \\
\overline{T}_{bMa1} & \overline{T}_{bMa2} & \cdots & \overline{T}_{bMaL} & \overline{T}_{bMb1} & \overline{T}_{bMb2} & \cdots & \overline{T}_{bMbM}
\end{array}\right]$$

$$\cdot \left[\begin{array}{c} \overline{\pi}(a1) \\ \overline{\pi}(a2) \\ \cdots \\ \overline{\pi}(aL) \\ --- \\ \overline{\pi}(b1) \\ \overline{\pi}(b2) \\ \cdots \\ \overline{\pi}(bM) \end{array}\right] = \left[\begin{array}{c} \overline{I} \\ \overline{I} \\ \cdots \\ \overline{I} \\ -- \\ \overline{I} \\ \overline{I} \\ \cdots \\ \overline{I} \end{array}\right]$$

where L and M are the number of atoms for molecule a and b respectively. For convenience, we have used $\overline{T}_{a1a1} = \overline{\alpha}^{-1}(1)$ as the polarizability inverse of the first atom of molecule a and $\overline{T}_{a1b1} = -\overline{T}_{1(L+1)}$ as the interaction between atom 1 from molecule

a and atom $L+1$ from molecule b. The rest of the symbols in the above matrix have the similar meanings. We first denote the inversion of the above $3 \times (L+M)$ by $3 \times (L+M)$ interaction matrix as $\tilde{H}$:

$$\tilde{H} = \left[\begin{array}{cccc|cccc} \overline{H}_{a1a1} & \overline{H}_{a1a2} & \cdots & \overline{H}_{a1aL} & \overline{H}_{a1b1} & \overline{H}_{a1b2} & \cdots & \overline{H}_{a1bM} \\ \overline{H}_{a2a1} & \overline{H}_{a2a2} & \cdots & \overline{H}_{a2aL} & \overline{H}_{a2b1} & \overline{H}_{a2b2} & \cdots & \overline{H}_{a2bM} \\ \cdots & \cdots & \cdots & \cdots & \cdots & \cdots & \cdots & \cdots \\ \overline{H}_{aLa1} & \overline{H}_{aLa2} & \cdots & \overline{H}_{aLaL} & \overline{H}_{aLb1} & \overline{H}_{aLb2} & \cdots & \overline{H}_{aLbM} \\ - - - & - - - & - - - & - - - & - - - & - - - & - - - & - - - \\ \overline{H}_{b1a1} & \overline{H}_{b1a2} & \cdots & \overline{H}_{b1aL} & \overline{H}_{b1b1} & \overline{H}_{b1b2} & \cdots & \overline{H}_{b1bM} \\ \overline{H}_{b2a1} & \overline{H}_{b2a2} & \cdots & \overline{H}_{b2aL} & \overline{H}_{b2b1} & \overline{H}_{b2b2} & \cdots & \overline{H}_{b2bM} \\ \cdots & \cdots & \cdots & \cdots & \cdots & \cdots & \cdots & \cdots \\ \overline{H}_{bMa1} & \overline{H}_{bMa2} & \cdots & \overline{H}_{bMaL} & \overline{H}_{bMb1} & \overline{H}_{bMb2} & \cdots & \overline{H}_{bMbM} \end{array}\right]$$

The isolated polarizability of molecules a and b are:

$$\overline{\pi}(a) = \sum_{i=a1}^{aL} \sum_{j=a1}^{bM} \overline{H}_{ij}$$

$$\overline{\pi}(b) = \sum_{i=b1}^{bM} \sum_{j=a1}^{bM} \overline{H}_{ij}$$

Also, we divide the above $3 \times (L+M)$ by $3 \times (L+M)$ interaction matrix into four blocks: a $3 \times L$ by $3 \times L$ matrix, a $3 \times L$ by $3 \times M$ matrix, a $3 \times M$ by $3 \times L$ matrix and a $3 \times M$ by $3 \times M$ matrix. Denoting the inverse of the $3 \times L$ by $3 \times L$ matrix

and the $3 \times M$ by $3 \times M$ matrix as $\tilde{F}$ and $\tilde{G}$

$$\tilde{F} = \begin{bmatrix} \overline{F}_{a1a1} & \overline{F}_{a1a2} & \cdots & \overline{F}_{a1aL} \\ \overline{F}_{a2a1} & \overline{F}_{a2a2} & \cdots & \overline{F}_{a2aL} \\ \cdots & \cdots & \cdots & \cdots \\ \overline{F}_{aLa1} & \overline{F}_{aLa2} & \cdots & \overline{F}_{aLaL} \end{bmatrix}$$

$$\tilde{G} = \begin{bmatrix} \overline{G}_{b1b1} & \overline{G}_{b1b2} & \cdots & \overline{G}_{b1bL} \\ \overline{G}_{b2b1} & \overline{G}_{b2b2} & \cdots & \overline{G}_{b2bL} \\ \cdots & \cdots & \cdots & \cdots \\ \overline{G}_{bLb1} & \overline{G}_{bLb2} & \cdots & \overline{G}_{bLbL} \end{bmatrix}$$

we have the gas phase polarizability for molecules a and b:

$$\overline{\alpha}(a) = \sum_{i=a1}^{aL} \sum_{j=a1}^{aL} \overline{F}$$

$$\overline{\alpha}(b) = \sum_{i=b1}^{bM} \sum_{j=b1}^{bL} \overline{G}$$

Thus the $3 \times (L + M)$ by $3 \times (L + M)$ atomic interaction matrix is replaced by the following 3×2 by 3×2 molecular interaction matrix:

$$\tilde{T}_{ab} = \begin{bmatrix} \overline{\alpha}^{-1}(a) & (\overline{I} - \overline{\alpha}^{-1}(a)\overline{\pi}(a)) \cdot \overline{\pi}^{-1}(b) \\ (\overline{I} - \overline{\alpha}^{-1}(b)\overline{\pi}(b)) \cdot \overline{\pi}^{-1}(a) & \overline{\alpha}^{-1}(b) \end{bmatrix}$$

Obviously, the product of the above 3×2 by 3×2 matrix and the isolated 3×2 by 3 polarizability matrix gives a 3×2 by 3 identity matrix:

$$\tilde{T}_{ab} \cdot \begin{bmatrix} \overline{\pi}(a) \\ \overline{\pi}(b) \end{bmatrix} = \begin{bmatrix} \overline{I} \\ \overline{I} \end{bmatrix}$$

In this way, we find the correspond 3×3 matrix for each of the four blocks in the $3 \times (L + M)$ by $3 \times (L + M)$ atomic interaction matrix. This ensures that the assignment of elements in two-body interaction matrix $\tilde{T}_{ab}$ is exact for a 2 body system! Under this two-body approximation, we repeat the above procedure and replace all of blocks (e.g. 3×5 by 3×5 matrix for anion-anion, 3×22 by 3×22 for cation-cation and 3×22 by 3×5 for cation-anion) representing atomic two-body interactions with the corresponding 3 by 3 molecular two-body interaction matrices. The full atomic interaction matrix (e.g. $3 \times 64 \times (22 + 5) = 5184$ by 5184 matrix) will be represented by a molecular interaction matrix (e.g. 3×128 by 3×128). From our test of random configurations in our system, the inverse method based on two-body approximation is about 6 times more efficient. The relative error is around 1e-3 for spherical polarizabilities and 1e-2 for anisotropic polarizabilities.

Results and Discussion Figure 7.2 shows the time correlation function $C_2(t)$ and its different components computed according to equation (7.12) and (7.13). From Figure 7.2 (A) we see that the magnitude of all of the components $C_2^M(t)$, $C_2^I(t)$, and $C_2^{MI}(t)$ are much larger than that of the TCF of anisotropic collective polarizability $C_2(t)$. This indicates that the interaction-induced effect substantially decreases the total collective polarizability which is consistent with the fact that liquid [MOEPY+][DCA-] is a highly polarizable fluid (the spherical polarizability of [MOEPY+] and [DCA-] are 13.36Å^3 and 5.4Å^3 respectively). Figure 7.2 (B) shows that the reorientational component $C_2^R(t)$ resembles the total TCF at times larger than 300ps. The contribution from $C_2^{CI}(t)$ or $C_2^{RI}(t)$ becomes negligible at those

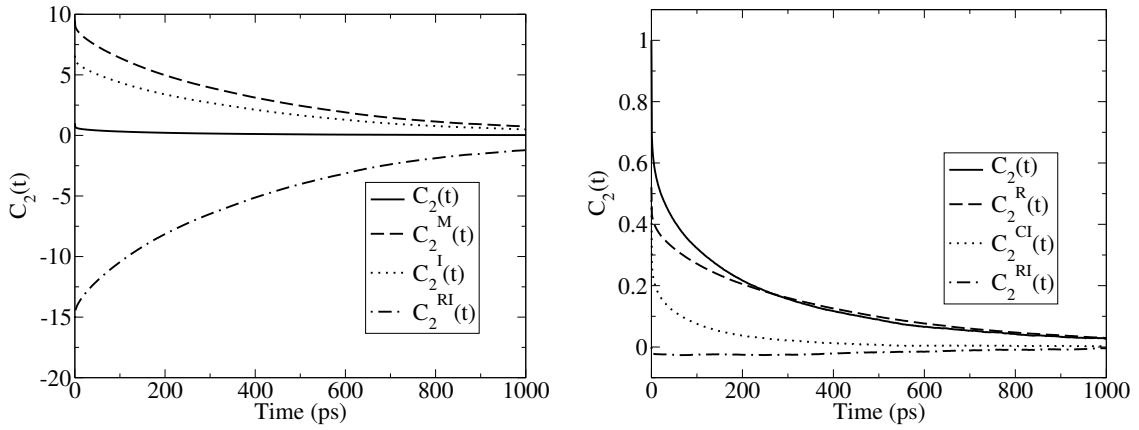

TCF of the anisotropic collective polarizability for [MOEPY+][DCA-] at T=400K and its components. All of the TCFs are normalized by the initial value $C_2(0)$. We use the matrix inversion method to compute the collective polarizability based on two-body approximation. The input atomic polarizability is shown in Table 7.1, and 7.2. Labels are the same as in Figure 7.1. (A) Total TCF and its components according to equation (7.12) (B) Total TCF and its components according to equation (7.13)

Figure 7.2: TCFs of anisotropic polarizability

times. Figure 7.3 (A) and (B) elaborate on the contribution from different components at short times. Clearly, during the first 0.1ps, both reorientational and collision-induced components are important. The contribution of the collision-induced part starts to significantly decrease after 10ps. Because $C_2(t)$ is proportional to the response function of Raman scattering spectra, we can directly conclude that at an initial short time both reorientational and collision-induced effects are important to the total time decay of the signal while at a longer time ($t > 300ps$), only the reorientional effect contributes.

In order to compute the total OKE spectra and its components, we fit the

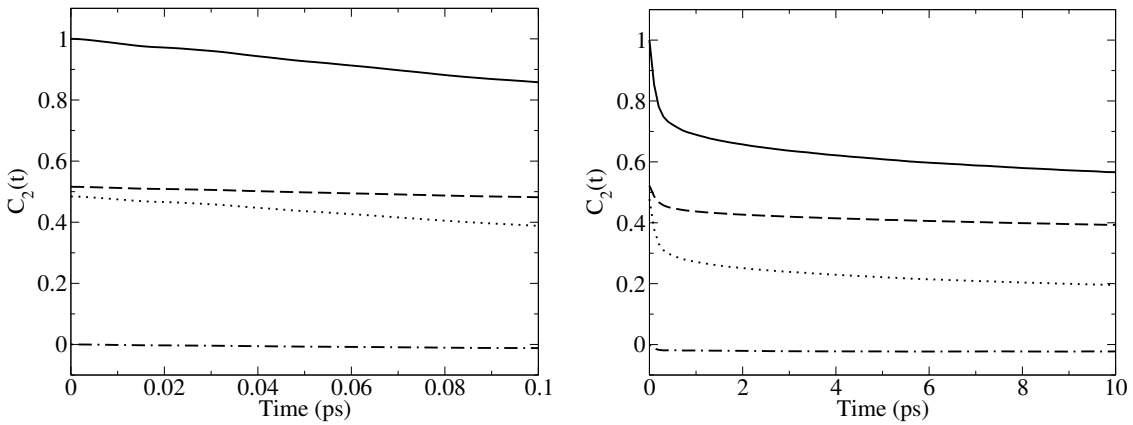

TCF of anisotropic collective polarizability for [MOEPY+][DCA-] at short times. Labels are the same as in Figure 7.2 (B).

Figure 7.3: TCF of anisotropic polarizability at short times

long time decay of $C_2(t)$, $C_2^R(t)$, and $C_2^{CI}(t)$ to exponential forms. The result of fitting is shown in Figure 7.4. We can see that the asymptotic behavior of those functions are all close to that of exponential decay. The calculated $-\dot{C}_2(t)$ and its components as well as the corresponding OKE spectra are shown in Figure 7.5. It is interesting to see that the collision-induced component contributes about 70% of the total signal while the reorientational and cross terms only play a minor role at short times in the OKE response. This is in contrast to that of linear Raman spectra where both reorientational and collision-induced contributions are important to the short decay of the signal (see Figure 7.3). The asymptotic behavior of the OKE signal and its component are shown in Figure 7.6. Even though the collision-induced term dominates the short time signal, the long time signal still resembles its reorientational

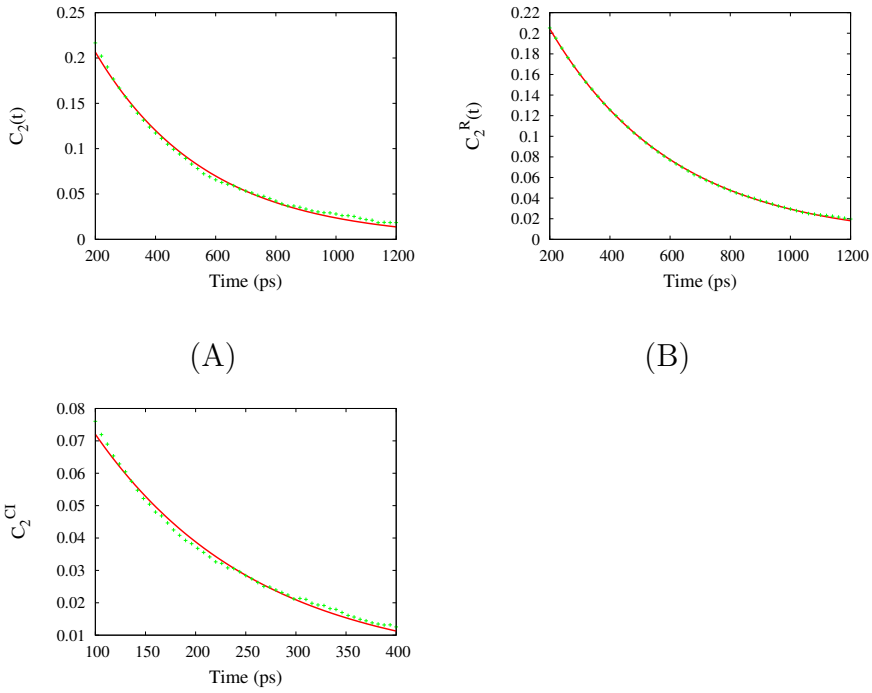

Time correlation function of anisotropic collective polarizability (A) and its reorientational (B) and collisional induced component (C) at long times. Red lines stand for the fitting to the exponential form $a \times e^{-t/b}$. Fitting parameters are a = 0.355 ± 0.001, b=$368.8 \pm 0.9(ps)$ for $C_2(t)$ and $a = 0.3319 \pm 0.0002$, $b = 412.1 \pm 0.2(ps)$ for $C_2^R(t)$ and $a = 0.1337 \pm 0.0007$, $b = 161.7 \pm 0.8$ for $C_2^{CI}(t)$.

Figure 7.4: Exponential fit of TCFs

component.

The experimentally reported OKE signal at a lower temperature T=300K for [MOEPY+][DCA-] is replotted in Figure 7.7[66]. Due to the slow dynamical nature of ionic liquids, our simulation was run at a higher temperature T=400K in order to get better convergence using relatively short runs. A high temperature enhances the motion of reorientation and therefore the computed long time decay of OKE signal in Figure 7.6 is faster than that of experimentally reported spectra at the lower

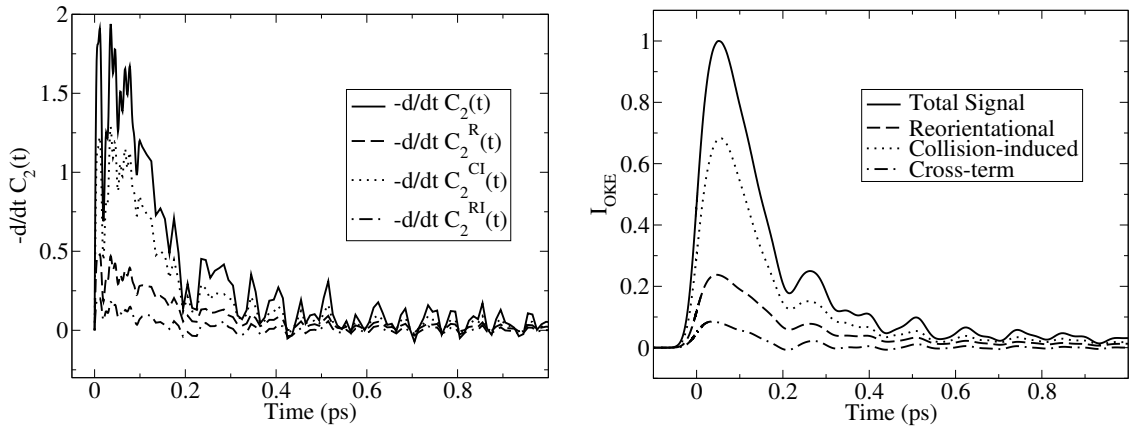

(A) (B)

(A)$-\dot{C}_2(t)$ and its components at short times. (B) the corresponding OKE signal computed from equation (7.14). Note that the instantaneous hyperpolarizability component has been excluded.

Figure 7.5: First derivative of the TCFs at short times

temperature. Nevertheless, our simulation explained the short time collision-induced nature of OKE signal and confirmed that the long time decay is still caused by the reorientational process.

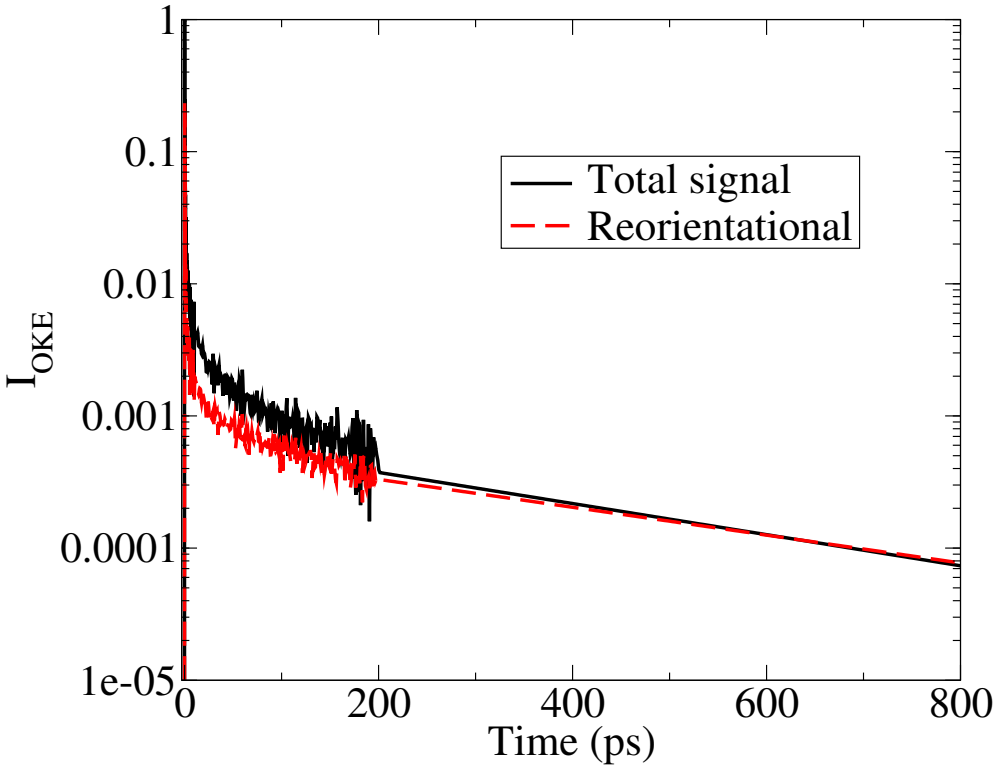

The OKE signal at long times were computed using a combination of short time functions and the long time fitted functions shown in Figure 7.4. We also computed the spectra without fitting the long time part TCFs to the exponential form. The resulting total spectrum has more oscillations at long times but still resembles the decay of reorientational component.

Figure 7.6: OKE signal at a long time and its reorientational component

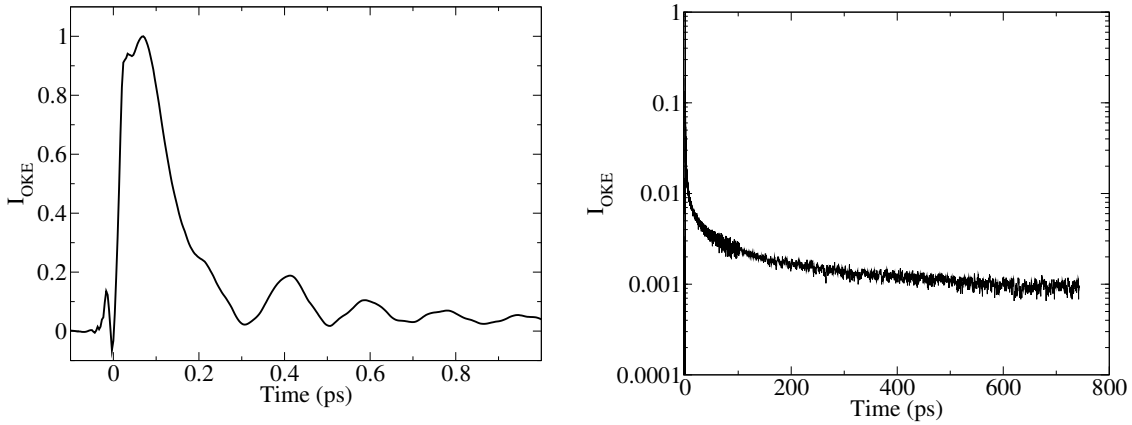

(A) (B)

(A) short time window (-0.1 to 1ps). (B) long time window (-3 to 740ps). This figure is replotted from Shirota and Castner's experimental data[65].

Figure 7.7: Experimental OKE signal at T=300K

CHAPTER 8
SUMMARY

In this thesis we have demonstrated that the diffusive dynamics of some imidazolium based ionic liquids is in many ways analogous to that of other glassy or supercooled liquids. For example, at 500K [BMIM+][PF6-] behaves like a normal Gaussian fluid, while at 300K there is a large deviation from Fickian behavior. As has been observed in other glassy systems, mobile and immobile subsets of ions are clustered in space. Mobile and immobile subgroups appear to be far apart and within the mobile subensemble of cations, van Hove correlation functions show secondary peaks indicating diffusion through hopping mechanisms. Rotationally and translationally mobile subensembles are highly correlated in the case of the cations but totally decoupled in the case of the anions. This is due to the higher symmetry of the [PF6-] anion. Rotational hopping processes are present both in the case of the cations and the anions.

We have studied the shear viscosity and the response to an applied external perturbation for a typical room-temperature ionic liquid such as [HMIM+][CL-]. We have demonstrated that the hydrodynamic limit in which the flow is Newtonian can not be reached on systems that are on the tens of nanometers scale. This is in contrast to other systems such as supercooled argon or room temperature water in which the hydrodynamical limit can be easily observed using nanometer size computer simulations. We tested the validity of linear response theory and the fluctuation dissipation theorem on this system. Even though the applied perturbation strength was rela-

tively weak (as compared to other systems studied in which such perturbations are in the linear regime) the system satisfied the linear response predictions on a several picoseconds time scale after which large deviations were observed. As a consequence of this non-linearity we have observed a flat velocity profile reminiscent of polymer flow. This finding is quite interesting because of its potential applicability in the field of analytical separations. Since the size of some of our systems is quite large and pores of these dimensions are commercially available, experimental confirmation of these results should be at hand.

Experiments and our simulations have shown that electronic photoexcitation of a typical chromophore such as ANF dissolved in [BMIM+][PF6-] results in an absorption wavelength dependent emission spectrum. The emission maxima as a function of excitation wavelength has a positive slope. If excitation is on the blue (red) end of the absorption spectrum, emission also appears shifted to the blue (red). Our computer simulations show that this observation can be rationalized in terms of local solvent environment around individual subensemble probe members. As opposed to our calculations in a typical organic solvent such as methanol, in the case of the ionic liquid, the single-molecule absorption spectrum is different for ANF probes in different local solvent surroundings. As complete solvent relaxation is slow compared to the lifetime of the probe, only partial relaxation occurs, and memory of the initial energy gap between ground and excited states remains at the time of fluorescence. By analyzing our time-dependent data we conclude that even though the excitation wavelength dependence λ_{ex} is much more dramatic at short times such as 100ps

than at long times such as 500ps, the maxima of emission still depends on excitation wavelength λ_{ex} on the time scale of nanoseconds.

We hope that our understanding of these phenomena will be useful to the ionic liquids community in the development of tools to harness their potential, particularly in order to control the outcome of chemical and photo-chemical reactions.

APPENDIX A
GENERALIZED LANGEVIN EQUATION

This appendix provides an alternative way to derive GLE for a dynamical variable $A(t)$ and its time correlation function $< A^*(0)A(t) >$. We first define TCFs and their Laplace transformations as the following:

$$\Psi(t) =< A^*(0)A(t) > / < |A(0)|^2 > \qquad \tilde{\Psi}(s) = \int_0^\infty dt\, e^{-st}\Psi(t) \tag{A.1}$$

$$\varphi(t) = \dot{\Psi}(t) =< A^*(0)\dot{A}(t) > / < |A(0)|^2 > \qquad \tilde{\varphi}(s) = s\tilde{\Psi}(s) - 1$$

$$\Phi(t) = -\dot{\varphi}(t) =< \dot{A}^*(0)\dot{A}(t) > / < |A(0)|^2 > \qquad \tilde{\Phi}(s) = -s\tilde{\varphi}(s) + \varphi(0)$$

we have,

$$\frac{d^2\Psi(t)}{dt^2} = -\Phi(t)$$

and its Laplace transform:

$$s^2\tilde{\Psi}(s) - s\Psi(0) - \varphi(0) = -\tilde{\Phi}(s) \tag{A.2}$$

Further,

$$\tilde{\Psi}(s) = \frac{s\Psi(0) + \varphi(0) - \tilde{\Phi}(s)}{s^2}$$

$$s^2\tilde{\Psi}(s) - s\Psi(0) = \varphi(0) - \tilde{\Phi}(s)$$

$$[s^2\tilde{\Psi}(s) - s\Psi(0)]\frac{s\Psi(0) + \varphi(0) - \tilde{\Phi}(s)}{s^2} = [\varphi(0) - \tilde{\Psi}(s)]\tilde{\Psi}(s)$$

$$[s\tilde{\Psi}(s) - \Psi(0)]\frac{s\Psi(0) + \varphi(0) - \tilde{\Phi}(s)}{s} = [\varphi(0) - \tilde{\Psi}(s)]\tilde{\Psi}(s)$$

$$
\begin{aligned}
s\tilde{\Psi}(s) - \Psi(0) &= \left[\frac{s\Psi(0) + \varphi(0) - \tilde{\Phi}(s)}{s}\right]^{-1} [\varphi(0) - \tilde{\Psi}(s)]\tilde{\Psi}(s) \\
&= -\left[\frac{s\Psi(0) + \varphi(0) - \tilde{\Phi}(s)}{s}\right]^{-1} [\tilde{\Psi}(s) - \varphi(0)]\tilde{\Psi}(s) \\
&= -\frac{\tilde{\Phi}(s) - \varphi(0)}{1 - s^{-1}\tilde{\Phi}(s) + s^{-1}\varphi(0)}\tilde{\Psi}(s) \\
&= -\tilde{K}(s)\tilde{\Psi}(s) + \varphi(0)\tilde{\Psi}(s) \qquad \text{(A.3)}
\end{aligned}
$$

where,

$$\tilde{K}(s) = \frac{s\tilde{\Phi}(s) - \varphi(0)\tilde{\Phi}(s) + \varphi^2(0)}{s - \Phi(s) + \varphi(0)}$$

In order to write down explicitly the inverse transform of $\tilde{K}(s)$, we reconsider equation (2.5) in Laplace space [27]:

$$\tilde{A}(s) = (s - i\hat{L})^{-1}A(0) = \tilde{R}(s)A(0) \qquad \text{(A.4)}$$

where $\tilde{R}(s)$ is called the resolvent operator. Recall the definition of projection operation, we have the following equalities:

$$\hat{P}\dot{B}(t) = A(0) < A^*(0)\dot{B}(t) > / < |A(0)| >^2 \qquad \text{(A.5)}$$

$$
\begin{aligned}
\frac{d}{dt}\hat{P}B(t) &= \frac{d}{dt}\left[A(0) < A^*(0)B(t) > / < |A(0)|^2 >\right] \\
&= A(0) < A^*(0)\dot{B}(t) > / < |A(0)|^2 > \qquad \text{(A.6)}
\end{aligned}
$$

therefore, $\hat{P}$ and d/dt commutes, Note in the above case,

$$i\hat{L}(\hat{P}B(t)) = \dot{A}(0) < A^*(0)B(t) > / < |A(0)|^2 > \neq \frac{d}{dt}(\hat{P}B(t)) \qquad \text{(A.7)}$$

Because the variable $\hat{P}B(t)$ is not implicitly dependent of time t (or we can say $\hat{P}B(t)$ is not a dynamical variable any more). Consider a specific case $B = A$, from

equation (A.5) and (A.6), we have

$$\frac{d(\hat{P}A(t))}{dt} = A(0)\dot{\Psi}(t) = \hat{P}\dot{A}(t) = \hat{P}i\hat{L}A(t) = \hat{P}i\hat{L}\hat{P}A(t) + \hat{P}i\hat{L}\hat{Q}A(t) \tag{A.8}$$

also,

$$\begin{aligned} \hat{P}i\hat{L}\hat{P}A(t) &= \hat{P}i\hat{L}A(0)\Psi(t) = \hat{P}\dot{A}(0)\Psi(t) \\ &= A(0)\Psi(t) < A^*(0)\dot{A}(0) > / < |A|^2 >= A(0)\Psi(t)\varphi(0) \end{aligned} \tag{A.9}$$

$$\hat{P}i\hat{L}\hat{Q}A(t) = A(0) < A^*(0)i\hat{L}\hat{Q}A(t) > / < |A|^2 > \tag{A.10}$$

Combining equations (A.8) to (A.10), we have

$$\dot{\Psi}(t) = \Psi(t)\varphi(0) + < A^*(0)i\hat{L}\hat{Q}A(t) > / < |A|^2 > \tag{A.11}$$

Manipulating $\hat{Q}A(t)$ in the same way as we did for $\hat{P}B(t)$ in equation (A.5) and (A.6), we have

$$\begin{aligned} \frac{d(\hat{Q}A(t))}{dt} &= \hat{Q}\dot{A}(t) = \hat{Q}[i\hat{L}\hat{P}A(t) + i\hat{L}\hat{Q}A(t)] \\ &= (1-\hat{P})i\hat{L}\hat{P}A(t) + \hat{Q}i\hat{L}\hat{Q}A(t) \\ &= \dot{A}(0)\Psi(t) - A(0)\varphi(0)\Psi(t) + \hat{Q}i\hat{L}\hat{Q}A(t) \end{aligned} \tag{A.12}$$

Take the Laplace transform of equation (A.11) and (A.12), we have

$$s\tilde{\Psi}(s) - 1 = \tilde{\Psi}(s)\varphi(0) + < A^*(0)i\hat{L}\hat{Q}\tilde{A}(s) > / < |A|^2 > \tag{A.13}$$

and

$$s\hat{Q}\tilde{A}(s) - \hat{Q}A(0) = \dot{A}(0)\tilde{\Psi}(s) - A(0)\varphi(0)\tilde{\Psi}(s) + i\hat{Q}\hat{L}\hat{Q}\tilde{A}(s) \tag{A.14}$$

where $\hat{Q}A(0) = 0$ according to the definition of projection operator, and

$$\hat{Q}\tilde{A}(s) = \int_0^\infty dt\, \hat{Q}A(t)e^{-st}$$

is the Laplace transform of $\hat{Q}A(t)$. Solving equation (A.14) and (A.13) gives,

$$\hat{Q}\tilde{A}(s) = \tilde{\Psi}(s)[s - i\hat{Q}\hat{L}]^{-1}[\dot{A}(0) - A(0)\varphi(0)] \tag{A.15}$$

and

$$\begin{aligned}
s\tilde{\Psi}(s) - 1 &= \tilde{\Psi}(s)\varphi(0) + \frac{\tilde{\Psi}(s)}{<|A|^2>} < A^*(0)i\hat{L}[s - i\hat{Q}\hat{L}]^{-1}\dot{A}(0) > \\
&\quad -\tilde{\Psi}(s)/<|A|^2>< A^*(0)i\hat{L}[s - i\hat{Q}L]^{-1}A(0)\varphi(0) > \\
&= -\tilde{\Psi}(s)\left[-\frac{< A^*(0)i\hat{L}[s - i\hat{Q}\hat{L}]^{-1}\dot{A}(0) >}{<|A|^2>}\right] \\
&\quad +\tilde{\Psi}(s)\left[\varphi(0)\left(1 - \frac{A^*(0)i\hat{L}[s - i\hat{Q}\hat{L}]^{-1}A(0)}{<|A|^2>}\right)\right] \\
&= -\tilde{\Psi}(s)\left[\frac{< \dot{A}^*(0)[s - i\hat{Q}\hat{L}]^{-1}\dot{A}(0) >}{<|A|^2>}\right] \\
&\quad +\tilde{\Psi}(s)\left[\varphi(0)\left(1 + \frac{\dot{A}^*(0)[s - i\hat{Q}\hat{L}]^{-1}A(0)}{<|A|^2>}\right)\right] \\
&= -\tilde{\Psi}(s)\left[\frac{< \dot{A}^*(0)[s - i\hat{Q}\hat{L}]^{-1}\dot{A}(0) >}{<|A|^2>}\right] \\
&\quad +\tilde{\Psi}(s)\left[\varphi(0)\left(1 + \frac{< \dot{A}^*(0)[s - i\hat{Q}\hat{L}]^{-1}\hat{P}\dot{A}(0) >}{<|A|^2>\varphi(0)}\right)\right] \\
&= -\tilde{\Psi}(s)\left[\frac{< \dot{A}^*(0)[s - i\hat{Q}\hat{L}]^{-1}\hat{Q}\dot{A}(0) >}{<|A|^2>} - \varphi(0)\right] \\
&= -\tilde{K}(s)\tilde{\Psi}(s) + \varphi(0)\tilde{\Psi}(s)
\end{aligned} \tag{A.16}$$

where

$$\tilde{K}(s) = \frac{< \dot{A}^*(0)[s - i\hat{Q}\hat{L}]^{-1}\hat{Q}\dot{A}(0) >}{<|A|^2>}$$

which gives the direct expression for $\tilde{K}(s)$ in equation (A.3). the inverse Laplace transform gives:

$$\frac{d\Psi(t)}{dt} = i\Omega\Psi(t) - \int_0^t d\tau\, \Psi(\tau)K(t-\tau) \tag{A.17}$$

where,

$$i\Omega = \varphi(0)$$

and $K(\tau)$ is the inverse Laplace transform of $\tilde{K}(s)$:

$$K(\tau) = < \dot{A}^*(0)e^{i\tau\hat{Q}\hat{L}}\hat{Q}\dot{A}(0) > / < |A|^2 >$$

Equation (A.17) is the GLE for the time correlation function $\Psi(t)$. It is easy to obtain the GLE for the dynamical variable $A(t)$ based on the this equation. We first write down the following relation from equation (A.15) and (A.16)

$$\tilde{\Psi}(s) = [s - i\Omega + \tilde{K}(s)]^{-1}$$

$$\hat{Q}\tilde{A}(s) = \tilde{\Psi}(s)[s - i\hat{Q}\hat{L}]^{-1}\hat{Q}i\hat{L}A(0)$$

Rewriting $A(t)$:

$$A(t) = \hat{P}A(t) + \hat{Q}A(t) = \frac{< A(0)A(t) >}{< |A|^2 >}A(0) + \hat{Q}A(t) = \Psi(t)A(0) + \hat{Q}A(t)$$

and its Laplace transform:

$$\begin{aligned} \tilde{A}(s) &= \tilde{\Psi}(s)A(0) + \hat{Q}\tilde{A}(s) \\ &= \frac{A(0)}{s - i\Omega + \tilde{K}(s)} + \frac{1}{s - i\Omega + \tilde{K}(s)}[s - i\hat{Q}\hat{L}]^{-1}\hat{Q}i\hat{L}A(0) \end{aligned}$$

Reformating the above expression, we have the equation in Laplace space:

$$s\tilde{A}(s) - i\Omega\tilde{A}(s) + \tilde{K}(s) = A(0) + [s - i\hat{Q}\hat{L}]^{-1}\hat{Q}i\hat{L}A(0)$$

$$s\tilde{A}(s) - A(0) = i\Omega\tilde{A}(s) - \tilde{A}(s)\tilde{K}(s) + \tilde{f}(s)$$

and the corresponding equation in time domain:

$$\frac{dA(t)}{dt} = i\Omega A(t) - \int_0^t d\tau\, A(\tau)K(t-\tau) + f(t)$$

with

$$f(t) = e^{it(1-\hat{P})\hat{L}}(1-\hat{P})i\hat{L}A(0)$$

$$K(t) =< f^*(0)f(t) > \qquad i\Omega = \frac{< A^*(0)i\hat{L}A(0) >}{|A|^2}$$

Thus we obtained the GLE (2.11) for the dynamical variable $A(t)$ using the projection operator and Laplace transformation.

APPENDIX B
DYSON DECOMPOSITION

This appendix is designed to prove Dyson decomposition (3.42):

$$e^{i\hat{L}t} - e^{i\hat{L}_0 t} = \int_0^t ds e^{i\hat{L}(t-s)} i(\hat{L} - \hat{L}_0) e^{i\hat{L}_0 s}$$

which is

$$\begin{aligned}
e^{i\hat{L}t} - e^{i\hat{L}_0 t} &= e^{i\hat{L}t} \int_0^t ds\, e^{-i\hat{L}s} i\hat{L} e^{i\hat{L}_0 s} - e^{i\hat{L}t} \int_0^t ds\, e^{-i\hat{L}s} i\hat{L}_0 e^{i\hat{L}_0 s} \\
e^{i\hat{L}t} - e^{i\hat{L}t} i\hat{L} \int_0^t ds\, e^{-i\hat{L}s} e^{i\hat{L}_0 s} &= e^{i\hat{L}_0 t} - e^{i\hat{L}t} \int_0^t ds\, e^{-i\hat{L}s} e^{i\hat{L}_0 s} i\hat{L}_0 \\
1 - i\hat{L} \int_0^t ds\, e^{-i\hat{L}s} e^{i\hat{L}_0 s} &= e^{-i\hat{L}t} e^{i\hat{L}_0 t} - \int_0^t ds\, e^{-i\hat{L}s} e^{i\hat{L}_0 s} i\hat{L}_0 \\
1 - e^{-i\hat{L}t} e^{i\hat{L}_0 t} &= i\hat{L} \int_0^t ds e^{-i\hat{L}s} e^{i\hat{L}_0 s} - \int_0^t ds\, e^{-i\hat{L}s} e^{i\hat{L}_0 s} i\hat{L}_0
\end{aligned} \tag{B.1}$$

The left hand side of above equation is

$$\begin{aligned}
lhs &= 1 - \sum_{j=0}^{\infty} \frac{1}{j!} (-i\hat{L}t)^j \sum_{n=0}^{\infty} \frac{1}{n!} (i\hat{L}_0 t)^n \\
&= 1 - \left[1 + \sum_{n=1}^{\infty} \frac{(-i\hat{L})^n t^n}{n!} \right] \sum_{m=0}^{\infty} \frac{(i\hat{L}_0)^m}{m!} t^m \\
&= 1 - \sum_{m=0}^{\infty} \frac{(i\hat{L}_0)^m}{m!} t^m - \sum_{n=1}^{\infty} \sum_{m=0}^{\infty} \frac{(-i\hat{L})^n}{n!} \frac{(i\hat{L}_0)^m}{m!} t^{n+m} \\
&= -\sum_{m=1}^{\infty} \frac{(i\hat{L}_0)^m}{m!} t^m - \sum_{n=1}^{\infty} \frac{(-i\hat{L})^n}{n!} t^n - \sum_{n=1}^{\infty} \sum_{m=1}^{\infty} \frac{(-i\hat{L})^n}{n!} \frac{(i\hat{L}_0)^m}{m!} t^{n+m}
\end{aligned}$$

Part of the right hand side of equation (B.1) is

$$\begin{aligned}
\Delta &= \int_0^t ds e^{-i\hat{L}s} e^{i\hat{L}_0 s} \\
&= \int_0^t ds \sum_{n=0}^{\infty} \frac{1}{n!}(-i\hat{L}s)^n \sum_{m=0}^{\infty} \frac{1}{m!}(i\hat{L}_0 s)^m \\
&= \sum_{n=0}^{\infty}\sum_{m=0}^{\infty} \frac{(-i\hat{L})^n}{n!}\frac{(i\hat{L}_0)^m}{m!} \int_0^t ds\, s^n s^m \\
&= \sum_{n=0}^{\infty}\sum_{m=0}^{\infty} \frac{(-i\hat{L})^n}{n!}\frac{(i\hat{L}_0)^m}{m!}\frac{1}{n+m+1} t^{n+m+1}
\end{aligned}$$

Therefore, the right hand side of equation (B.1) is

$$\begin{aligned}
rhs &= i\hat{L}\Delta - \Delta i\hat{L}_0 \\
&= -\sum_{n=0}^{\infty}\sum_{m=0}^{\infty} \frac{(-i\hat{L})^{n+1}}{n!}\frac{(i\hat{L}_0)^m}{m!}\frac{1}{n+m+1} t^{n+1}t^m \\
&\quad -\sum_{n=0}^{\infty}\sum_{m=0}^{\infty} \frac{(-i\hat{L})^n}{n!}\frac{(i\hat{L}_0)^{m+1}}{m!}\frac{1}{n+m+1} t^n t^{m+1} \\
&= -\sum_{p=1}^{\infty}\sum_{m=0}^{\infty} \frac{(-i\hat{L})^p}{(p-1)!}\frac{(i\hat{L}_0)^m}{m!}\frac{1}{p+m} t^p t^m \\
&\quad -\sum_{n=0}^{\infty}\sum_{q=1}^{\infty} \frac{(-i\hat{L})^n}{n!}\frac{(i\hat{L}_0)^q}{(q-1)!}\frac{1}{q+n} t^n t^q \\
&= -\sum_{p=1}^{\infty} \frac{(-i\hat{L})^p}{p!} t^p - \sum_{p=1}^{\infty}\sum_{m=1}^{\infty} \frac{(-i\hat{L})^p}{(p-1)!}\frac{(i\hat{L}_0)^m}{m!}\frac{1}{p+m} t^p t^m \\
&\quad -\sum_{q=1}^{\infty} \frac{(i\hat{L}_0)^q}{q!} t^q - \sum_{n=1}^{\infty}\sum_{q=1}^{\infty} \frac{(-i\hat{L})^n}{n!}\frac{(i\hat{L}_0)^q}{(q-1)!}\frac{1}{q+n} t^n t^q \\
&= -\sum_{m=1}^{\infty} \frac{(i\hat{L}_0)^m}{m!} t^m - \sum_{n=1}^{\infty} \frac{(-i\hat{L})^n}{n!} t^n \\
&\quad -\sum_{q=1}^{\infty}\sum_{n=1}^{\infty} \frac{(-i\hat{L})^n}{n!}\frac{(i\hat{L}_0)^q}{(q-1)!}\frac{1}{q+n} t^n t^q - \sum_{p=1}^{\infty}\sum_{m=1}^{\infty} \frac{(-i\hat{L})^p}{(p-1)!}\frac{(i\hat{L}_0)^m}{m!}\frac{1}{p+m} t^p t^m \\
&= -\sum_{m=1}^{\infty} \frac{(i\hat{L}_0)^m}{m!} t^m - \sum_{n=1}^{\infty} \frac{(-i\hat{L})^n}{n!} t^n - \Pi
\end{aligned}$$

where the first two terms are the same with the that of lhs and the third term

$$
\begin{aligned}
\Pi &= \sum_{q=1}^{\infty}\sum_{n=1}^{\infty}\frac{(-i\hat{L})^n}{n!}\frac{(i\hat{L}_0)^q}{(q-1)!}\frac{1}{q+n}t^n t^q + \sum_{p=1}^{\infty}\sum_{m=1}^{\infty}\frac{(-i\hat{L})^p}{(p-1)!}\frac{(i\hat{L}_0)^m}{m!}\frac{1}{p+m}t^p t^m \\
&= \sum_{n=1}^{\infty}\sum_{m=1}^{\infty}\frac{(-i\hat{L})^n}{n!}\frac{(i\hat{L}_0)^m}{(m-1)!}\frac{1}{n+m}t^{n+m} + \sum_{n=1}^{\infty}\sum_{m=1}^{\infty}\frac{(-i\hat{L})^n}{(n-1)!}\frac{(i\hat{L}_0)^m}{m!}\frac{1}{n+m}t^{n+m} \\
&= \sum_{n=1}^{\infty}\sum_{m=1}^{\infty}\frac{(-i\hat{L})^n(-i\hat{L}_0)^m}{n+m}\frac{1}{(n-1)!}\frac{1}{(m-1)!}(\frac{1}{n}+\frac{1}{m})t^{n+m} \\
&= \sum_{n=1}^{\infty}\sum_{m=1}^{\infty}\frac{(-i\hat{L})^n(i\hat{L}_0)^m}{n+m}\frac{1}{(n-1)!(m-1)!}\frac{m+n}{mn}t^{n+m} \\
&= \sum_{n=1}^{\infty}\sum_{m=1}^{\infty}\frac{(-i\hat{L})^n(i\hat{L}_0)^m}{m!n!}t^{n+m} \\
&= \sum_{n=1}^{\infty}\sum_{m=1}^{\infty}\frac{(-i\hat{L})^n}{n!}\frac{(i\hat{L}_0)^m}{m!}t^{n+m}
\end{aligned}
$$

which is the third term of the left hand side of equation (B.1). Thus, we proved the equality of equation (B.1).

APPENDIX C
MODIFICATION TO GROMACS SOURCE CODE

In order to save the data from the simulation of a very large system, Gromacs souce code should be modified to save intermediate variables $\sum_q m_q v_{qx} \cos(kz_q)$ and $\sum_q m_q v_{qx} \sin(kz_q)$ instead of coordinates z_q and v_{qx}. Gromacs new version of 3.3 has the option to apply a cos form acceleration in its *.mdp* file. To apply differet forms of acceleration, the source code also has to be modified.

To save intermediate variables, source code md.c and mdrun.c should be modified. Several subroutines added in source code /src/kernel/md.c are

```
static void pz_write_traj(FILE *log,t_commrec *cr,
                t_nsborder *nsb,
                rvec *xx,rvec *vv)
{


  if (MASTER(cr))  {
#ifdef DEBUG
   // fprintf(log,"Going to open trajectory file: %s\n",traj);
#endif
  }


#define MX(xvf) moveit(log,cr->left,cr->right,#xvf,xvf,nsb)
```

```
  if (cr->nnodes > 1) {
    MX(xx);
    MX(vv);
  }
}

void pzmdrunner(int *na, int *nb, char *fnout1, char *fnout2,
         t_commrec *cr,t_commrec *mcr,int nfile,t_filenm fnm[],
         bool bVerbose,bool bCompact,
         int nDlb,int nstepout,
         t_edsamyn *edyn,int repl_ex_nst,int repl_ex_seed,
         unsigned long Flags)
{
  double     nodetime=0,realtime;
  t_inputrec *inputrec;
  t_state    *state;
  rvec       *buf,*f,*vold,*vt;
  real       tmpr1,tmpr2;
  real       *ener;
  t_nrnb     *nrnb;
  t_nsborder *nsb;
  t_topology *top;
  t_groups   *grps;
```

```
t_graph    *graph;
t_mdatoms  *mdatoms;
t_forcerec *fr;
t_fcdata   *fcd;
time_t     start_t=0;
bool       bVsites,bParVsites;
t_comm_vsites vsitecomm;
int        i,m;
char       *gro;
FILE       *fxvg1;
FILE       *fxvg2;


int  nk,nj,ntotal, nmax, n1,n2,n3,knumber,dim;
real rbox1,rbox2,rbox3,vnorm;
rvec *kvect, *vkvect, *nkvect;
rvec temp1, temp2, vtest1,vtest2;


/* Initiate everything (snew sets to zero!) */
snew(ener,F_NRE);
snew(fcd,1);
snew(nsb,1);
snew(top,1);
```

```
snew(grps,1);

snew(inputrec,1);

snew(state,1);

snew(nrnb,cr->nnodes);


if (bVerbose && MASTER(cr))

  fprintf(stderr,"Getting Loaded...\n");


if (PAR(cr)) {

  /* The master thread on the master node reads from disk,

   then passes  everything

   around the ring, and finally frees the stuff

   */

  if (MASTER(cr))

    distribute_parts(cr->left,cr->right,cr->nodeid,

                     cr->nnodes,inputrec,

                     ftp2fn(efTPX,nfile,fnm),nDlb);


  /* Every node (including the master)

       reads the data from the ring */

  init_parts(stdlog,cr,

        inputrec,top,state,&mdatoms,nsb,
```

```
        MASTER(cr) ? LIST_SCALARS | LIST_INPUTREC : 0,
        &bParVsites,&vsitecomm);
} else {
  /* Read it up... */
  init_single(stdlog,inputrec,ftp2fn(efTPX,nfile,fnm),
         top,state,&mdatoms,nsb);
  bParVsites=FALSE;
}
if (inputrec->eI == eiSD) {
  /* Is not read from TPR yet, so we allocate space here */
  snew(state->sd_X,nsb->natoms);
}
snew(buf,nsb->natoms);
snew(f,nsb->natoms);
snew(vt,nsb->natoms);
snew(vold,nsb->natoms);

if (bVerbose && MASTER(cr))
  fprintf(stderr,"Loaded with Money\n\n");

/* Index numbers for parallellism... */
nsb->nodeid      = cr->nodeid;
```

```
top->idef.nodeid = cr->nodeid;


/* Group stuff (energies etc) */

init_groups(stdlog,mdatoms,&(inputrec->opts),grps);

/* Copy the cos acceleration to the groups struct */

grps->cosacc.cos_accel = inputrec->cos_accel;


/* Periodicity stuff */

if (inputrec->ePBC == epbcXYZ) {

  graph=mk_graph(&(top->idef),top->atoms.nr,FALSE,FALSE);

  if (debug)

    p_graph(debug,"Initial graph",graph);

}

else

  graph = NULL;


/* Distance Restraints */

init_disres(stdlog,top->idef.il[F_DISRES].nr,

            top->idef.il[F_DISRES].iatoms,

            top->idef.iparams,inputrec,mcr,fcd);


/* Orientation restraints */
```

```
init_orires(stdlog,top->idef.il[F_ORIRES].nr,
            top->idef.il[F_ORIRES].iatoms,
            top->idef.iparams,state->x,mdatoms,inputrec,mcr,
            &(fcd->orires));


/* Dihedral Restraints */
init_dihres(stdlog,top->idef.il[F_DIHRES].nr,
            top->idef.il[F_DIHRES].iatoms,
            top->idef.iparams,inputrec,fcd);


/* check if there are vsites */
bVsites=FALSE;
for(i=0; (i<F_NRE) && !bVsites; i++)
  bVsites = ((interaction_function[i].flags & IF_VSITE) &&
              (top->idef.il[i].nr > 0));


/* Initiate forcerecord */
fr = mk_forcerec();
init_forcerec(stdlog,fr,inputrec,top,cr,mdatoms,nsb,
              state->box,FALSE,
              opt2fn("-table",nfile,fnm),
              opt2fn("-tablep",nfile,fnm),FALSE);
```

```
fr->bSepDVDL = ((Flags & MD_SEPDVDL) == MD_SEPDVDL);


/* Initialize QM-MM */
if(fr->bQMMM){
  init_QMMMrec(cr,mdatoms,state->box,top,inputrec,fr);
}


/* Initiate PPPM if necessary */
if (fr->eeltype == eelPPPM)
  init_pppm(stdlog,cr,nsb,FALSE,TRUE,state->box,
                    getenv("GMXGHAT"),inputrec);
if ((fr->eeltype == eelPME) || (fr->eeltype == eelPMEUSER))
  (void) init_pme(stdlog,cr,inputrec->nkx,
                  inputrec->nky,inputrec->nkz,
                  inputrec->pme_order,
                  /*HOMENR(nsb),*/nsb->natoms,
                  mdatoms->bChargePerturbed,
                  inputrec->bOptFFT,inputrec->ewald_geometry);


/* Make molecules whole at start of run */
if (fr->ePBC != epbcNONE)  {
  do_pbc_first(stdlog,state->box,fr,graph,state->x);
```

```
}


/* Now do whatever the user wants us to do (how flexible...)*/

switch (inputrec->eI) {

case eiMD:

case eiSD:

case eiBD:

  //

  // Define a extra variable *fxvg1  and *fxvg2 to

  //    open the file *fnout1

  // and *fnout2

  //

  fxvg1 = fopen(fnout1,"w");

  fxvg2 = fopen(fnout2,"w");

  //

  // Variables to determine the value of k vector

  //

  nk = *na ;

  nj = *nb ;

  nmax = ((nk*2+1)*(nk*2+1)*(nk*2+1) - 1)/2;

  ntotal = nmax;

  snew(kvect, nmax);
```

```
snew(nkvect,nmax);

snew(vkvect,2*nmax);


temp1[0] = 1.0;

temp1[1] = 0.0;

temp1[2] = 0.0;

temp2[0] = 0.0;

temp2[1] = 1.0;

temp2[2] = 0.0;

rbox1 = state->box[0][0];

rbox2 = state->box[1][1];

rbox3 = state->box[2][2];

knumber = 0;

//

// Determining the value of vectors: kvect , vkvect

//

//for (n1=-nk; n1 < nk + 1; n1++) {

  //for (n2=-nk; n2 < nk + 1; n2++) {

    //for (n3=-nk; n3< nk + 1; n3++) {

      //if ( (n1*n1+n2*n2+n3*n3) != 0 ) {

for (n1=nk; n1 > -1; n1--) {

  for (n2=nk; n2 > -nk - 1; n2--) {
```

```
            for (n3=nk; n3 > -nk - 1; n3--) {
              if ( (n1>0) || ((n1==0)&&(n2>0)) ||
                    ((n1==0)&&(n2==0)&&(n3>0))) {
                kvect[knumber][0] = 2.0 * 3.1416 / rbox1 * (float)n1;
                kvect[knumber][1] = 2.0 * 3.1416 / rbox2 * (float)n2;
                kvect[knumber][2] = 2.0 * 3.1416 / rbox3 * (float)n3;
                nkvect[knumber][0] = (float)n1;
                nkvect[knumber][1] = (float)n2;
                nkvect[knumber][2] = (float)n3;
                pznorm(nkvect[knumber],&vnorm);
                //
                // Actually if we use nkvect instead of kvect,
                // we may not use norm again
                // This is waiting to be updated
                //
                (void) cross(kvect[knumber], temp1 , vtest1);
                if ( pznorm(vtest1, &vnorm)) {
                  for (dim =0; dim<3; dim++)
                    vkvect[knumber][dim] = vtest1[dim];
                  (void)
cross(kvect[knumber],vkvect[knumber],vkvect[knumber+nmax]);
                  pznorm(vkvect[knumber+nmax],&vnorm);
```

```
            }
            else {
              (void) cross(kvect[knumber],temp2,vtest2);
              if ( pznorm(vtest2,&vnorm)) {
                for (dim =0; dim<3; dim++)
                  vkvect[knumber][dim] =vtest2[dim];
                (void)
cross(kvect[knumber],vkvect[knumber],vkvect[knumber+nmax]);
                pznorm(vkvect[knumber+nmax],&vnorm);
              }
              else {
       fprintf(stderr,"\n error in getting the vectors\n");
       gmx_fatal(FARGS,"can not get correct vectical vectors
              ...\n" );
              }
            }
            fprintf(fxvg1,"k%1d,%3d%3d%3d ",knumber,n1,n2,n3);
            fprintf(fxvg2,"k%1d,%3d%3d%3d ",knumber,n1,n2,n3);
            knumber++;
          }
        }
      }
```

```
}
fprintf(fxvg1,"\n");
fprintf(fxvg2,"\n");
if ( knumber > nmax ) {
  fprintf(stderr,"\nWARNING:
  Number of ntotal are wrong %d .gt. %d \n",
    knumber,nmax);
  gmx_fatal(FARGS,"Wrong number of the vectors
     ...%d .gt. %d\n",knumber,nmax );
  ///stop;
}
else{
  ntotal = knumber;
}
start_t=pzdo_md(&nj, fxvg1, fxvg2, kvect, vkvect,
      nkvect, ntotal, (&(top->atoms))->nres,
      stdlog,cr,mcr,nfile,fnm,
      bVerbose,bCompact,bVsites,
      bParVsites ? &vsitecomm : NULL,
      nstepout,inputrec,grps,top,ener,fcd,state,vold,vt,
      f,buf, mdatoms,nsb,nrnb,graph,edyn,fr,
      repl_ex_nst,repl_ex_seed,
```

```
        Flags);
  fclose(fxvg1);
  fclose(fxvg2);
  sfree(kvect);
  sfree(vkvect);
  sfree(nkvect);
  break;
case eiCG:
  start_t=do_cg(stdlog,nfile,fnm,inputrec,top,grps,nsb,
                state,f,buf,mdatoms,ener,fcd,
                nrnb,bVerbose,bVsites,
                bParVsites ? &vsitecomm : NULL,
                cr,mcr,graph,fr);
  break;
case eiLBFGS:
  start_t=do_lbfgs(stdlog,nfile,fnm,inputrec,top,grps,nsb,
                   state,f,buf,mdatoms,ener,fcd,
                   nrnb,bVerbose,bVsites,
                   bParVsites ? &vsitecomm : NULL,
                   cr,mcr,graph,fr);
  break;
case eiSteep:
```

```
  start_t=do_steep(stdlog,nfile,fnm,inputrec,top,grps,nsb,
                   state,f,buf,mdatoms,ener,fcd,
                   nrnb,bVerbose,bVsites,
                   bParVsites ? &vsitecomm : NULL,
                   cr,mcr,graph,fr);
  break;
case eiNM:
  start_t=do_nm(stdlog,cr,nfile,fnm,
                bVerbose,bCompact,nstepout,inputrec,grps,
                top,ener,fcd,state,vold,vt,f,buf,
                mdatoms,nsb,nrnb,graph,edyn,fr);
  break;
case eiTPI:
  start_t=do_tpi(stdlog,nfile,fnm,inputrec,top,grps,nsb,
                 state,f,buf,mdatoms,ener,fcd,
                 nrnb,bVerbose,
                 cr,mcr,graph,fr);
  break;
default:
  gmx_fatal(FARGS,"Invalid integrator (%d)...\n",inputrec->eI);
}
```

```
  /* Some timing stats */
if (MASTER(cr)) {
  realtime=difftime(time(NULL),start_t);
  if ((nodetime=node_time()) == 0)
    nodetime=realtime;
}
else
  realtime=0;

/* Convert back the atoms */
md2atoms(mdatoms,&(top->atoms),TRUE);

/* Finish up, write some stuff
 * if rerunMD, don't write last frame again
 */
finish_run(stdlog,cr,ftp2fn(efSTO,nfile,fnm),
           nsb,top,inputrec,nrnb,nodetime,realtime,
           inputrec->nsteps,
           EI_DYNAMICS(inputrec->eI));

/* Does what it says */
print_date_and_time(stdlog,cr->nodeid,"Finished mdrun");
```

```
}

static int pznorm(rvec x, real *xnorm)
{

  /* RETURNS INPUT VECTOR X NORMALIZED TO UNIT LENGTH.
     XNORM IS THE ORIGINAL LENGTH OF X.   */
  real TEMP, TEMP1, TEMP2;

  TEMP = x[0];
  TEMP1 = x[1];
  TEMP2 = x[2];
  *xnorm = TEMP * TEMP + TEMP1 * TEMP1 + TEMP2 * TEMP2;
  if (*xnorm <= 1e-5)
    return 0;
  *xnorm = sqrt(*xnorm);
  x[0] /=*xnorm;
  x[1] /=*xnorm;
  x[2] /=*xnorm;
  return 1;
}  /* Norm */

static void moveit(FILE *log,
```

```
    int left,int right,char *s,rvec xx[],t_nsborder *nsb)
{
  if (!xx)
    return;

  move_rvecs(log,FALSE,FALSE,left,right,xx,
     NULL,nsb->nnodes-1,nsb,NULL);
}
```

The original routine do_md should be modified to make the corresponding pzdo_md routine.

```
time_t pzdo_md(int *na, FILE *fp1, FILE *fp2, rvec
kv[], rvec vkv[], rvec nkv[], int ncount, int
nres,
             FILE *log,t_commrec *cr,t_commrec
*mcr,int nfile,t_filenm fnm[],
             bool bVerbose,bool bCompact,
             bool bVsites, t_comm_vsites
*vsitecomm,
             int stepout,t_inputrec
*inputrec,t_groups *grps,t_topology *top,
             real ener[],t_fcdata *fcd,
             t_state *state,rvec vold[],rvec
```

```
vt[],rvec f[],
             rvec buf[],t_mdatoms
*mdatoms,t_nsborder *nsb,t_nrnb nrnb[],
             t_graph *graph,t_edsamyn
*edyn,t_forcerec *fr,
             int repl_ex_nst,int repl_ex_seed,
             unsigned long Flags)
```

To calculate the current, the following variables are defined:

```
  //
  /* define the following variables to calculate
 * current */
  //
  char *fshort = "%11.4e";
  int  nj;
  int  mi,mj,mp;
  rvec *cmx, *cmv;
  real  molmass, sqrtn;
  real jlcos, jlsin, jtcos1, jtsin1, jtcos2,
jtsin2, vdotpk, rdotpk, vdotpk1,vdotpk2;


  nj = *na;
  sqrtn =sqrt((float)nres) ;
```

After the lines

```
    xx = (do_per_step(step,inputrec->nstxout) ||
bLastStep) ? state->x : NULL;
    vv = (do_per_step(step,inputrec->nstvout) ||
bLastStep) ? state->v : NULL;
    ff = (do_per_step(step,inputrec->nstfout)) ? f
: NULL;
```

add

```
    fp_trn =
write_traj(log,cr,traj,nsb,step,t,state->lambda,
                        nrnb,nsb->natoms,xx,vv,ff,state->box);
    //
    // output the current to fp1, fp2
    //
    //nj = *na;  see above
    if ( do_per_step(step,nj)) {
      xx = state->x;
      vv = state->v;
      pz_write_traj(NULL,cr,nsb,xx,vv);
      snew(cmx,nres);
      snew(cmv,nres);
```

```
      mp = 0;
      for (mi=0; mi<nres; mi++) {
        for (mj =0; mj<DIM; mj++) {
          cmx[mi][mj] = 0.0;
          cmv[mi][mj] = 0.0;
        }
        molmass = 0.0;
        while ( (mp < nsb->natoms) &&
(mdatoms->resnr[mp] ==  mi) ) {
          for ( mj=0; mj<DIM; mj++) {
            cmx[mi][mj] +=
mdatoms->massT[mp]*xx[mp][mj];
            cmv[mi][mj] +=
mdatoms->massT[mp]*vv[mp][mj];
          }
          molmass += mdatoms->massT[mp];
          mp ++ ;
        }
        for (mj=0; mj<DIM; mj++)
          cmx[mi][mj] /= molmass;
      }
      for (mp=0; mp < ncount; mp++) {
```

```
          jlcos = 0.0;

          jlsin = 0.0;

          jtcos1 = 0.0;

          jtsin1 = 0.0;

          jtcos2 = 0.0;

          jtsin2 = 0.0;

          for (mi=0; mi< nres; mi++) {

            rdotpk = 0.0;

            vdotpk = 0.0;

            vdotpk1 = 0.0;

            vdotpk2 = 0.0;

            for (mj=0; mj<DIM; mj++) {

              rdotpk = rdotpk + kv[mp][mj] *
cmx[mi][mj];

              vdotpk = vdotpk + nkv[mp][mj] *
cmv[mi][mj];

              vdotpk1 = vdotpk1 + vkv[mp][mj] *
cmv[mi][mj];

              vdotpk2 = vdotpk2 + vkv[mp+ncount][mj]
* cmv[mi][mj];

            }

            jlcos += vdotpk * cos(rdotpk);
```

```
    jlsin += vdotpk * sin(rdotpk);

    jtcos1 += vdotpk1 * cos( rdotpk);

    jtsin1 += vdotpk1 * sin( rdotpk);

    jtcos2 += vdotpk2 * cos( rdotpk);

    jtsin2 += vdotpk2 * sin( rdotpk);
  }
  jlcos = jlcos / sqrtn;

  jlsin = jlsin / sqrtn;

  jtcos1 = jtcos1 / sqrtn;

  jtsin1 = jtsin1 / sqrtn;

  jtcos2 = jtcos2 / sqrtn;

  jtsin2 = jtsin2 / sqrtn;


  //jlcos /=  mdatoms->tmass;

  //jlsin /=  mdatoms->tmass;

  //jtcos1 /= mdatoms->tmass;

  //jtsin1 /= mdatoms->tmass;

  //jtcos2 /= mdatoms->tmass;

  //jtsin2 /= mdatoms->tmass;


  if (mp != 0) {

    (void) fprintf(fp1,"\n");
```

```
        (void) fprintf(fp2,"\n");
      }


      fprintf(fp1,fshort,jlcos);
      fprintf(fp1," ");
      fprintf(fp1,fshort,jlsin);


      fprintf(fp2,fshort,jtcos1);
      fprintf(fp2," ");
      fprintf(fp2,fshort,jtsin1);
      fprintf(fp2," ");
      fprintf(fp2,fshort,jtcos2);
      fprintf(fp2," ");
      fprintf(fp2,fshort,jtsin2);
    }
    (void) fprintf(fp1,"\n");
    (void) fprintf(fp2,"\n");
    sfree(cmx);
    sfree(cmv);
  }
```

To call the above routines, the following lines should be added to the file mdrun.c:

At line 184 of the file mdrun.c after

```
 static int  nthreads=1;
```

add

```
  static int  nj = 1000;
  static int  intk = 2;
```

At line 215 of the file mdrun.c after

```
{ "-stepout", FALSE, etINT, {&nstepout},
      "HIDDENFrequency of writing the remaining runtime" },
```

add

```
    { "-nj",
 FALSE, etINT, {&nj}, "frequency to output the current" },
    { "-k",
   FALSE, etINT, {&intk}, "maximum number of vectors"}
```

At line 265 of the file mdrun.c after this line

```
Flags = Flags | (bGlas     ? MD_GLAS     : 0);
```

add

```
  pzmdrunner(&intk,&nj,opt2fn_null("-olc",NFILE,fnm),
             opt2fn_null("-otc",NFILE,fnm),
            cr,mcr,NFILE,fnm,bVerbose,bCompact,nDLB,nstepout,
            edyn,repl_ex_nst,repl_ex_seed,Flags);
```

We also modified the routine to apply different acceleration forms. Basically, follow the applied option cos_acceleration in the mdp file and see which routines call this option and then modify the corresponding acceleration form and boundary conditions.

APPENDIX D
GEOMETRY AND EFFECTIVE POTENTIAL OF MOLECULES

1-butyl-3-methylimidazolium Cation ([BMIM+])

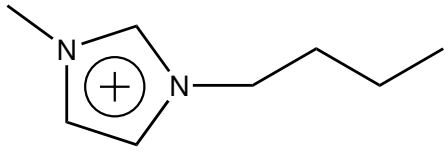

Figure D.1: [BMIM+] cation

Table D.1: Coordinates of [BMIM+]

Atom	atom index	x (nm)	y (nm)	z (nm)
N1	1	4.4860	3.2432	2.7775
N2	2	4.6471	3.1220	2.8967
C3	3	4.5972	3.1594	2.7735
C4	4	4.4661	3.2636	2.9116
C5	5	4.4173	3.3012	2.6629
C6	6	4.5484	3.1814	2.9860
C7	7	4.7940	3.0161	3.0680
C8	8	4.7686	3.0417	2.9177
H9	9	4.6497	3.1451	2.6787

Continued on next page

Table D.1 – continued from previous page

Atom	atom index	x (nm)	y (nm)	z (nm)
H10	10	4.3786	3.3089	2.9588
H11	11	4.4379	3.4118	2.6772
H12	12	4.3187	3.2744	2.6494
H13	13	4.4851	3.2671	2.5820
H14	14	4.5439	3.1444	3.0896
H15	15	4.7154	2.9574	3.1058
H16	16	4.7975	3.1087	3.1188
H17	17	4.7546	2.9338	2.8819
H18	18	4.8541	3.0695	2.8611
C19	19	4.9256	2.9305	3.0927
H20	20	4.9250	2.8338	3.0360
H21	21	4.9902	3.0302	3.0725
C22	22	4.9538	2.8927	3.2448
H23	23	5.0490	2.8386	3.2518
H24	24	4.9774	2.9832	3.3136
H25	25	4.8686	2.8452	3.2830

Table D.2: Nonbonding parameters of [BMIM+]

Atom	atom type	charge (e)	σ (nm)	ϵ (kJ/mol)
N1	opls_557	0.24016	3.25000e-01	7.11280e-01
N2	opls_559	0.06881	3.25000e-01	7.11280e-01
C3	opls_558	-0.05841	3.55000e-01	2.92880e-01
C4	opls_561	-0.27761	3.55000e-01	2.92880e-01
C5	opls_905	-0.33178	3.50000e-01	2.76144e-01
C6	opls_560	-0.12324	3.55000e-01	2.92880e-01
C7	opls_136	0.0	3.50000e-01	2.76144e-01
C8	opls_908	-0.16652	3.50000e-01	2.76144e-01
H9	opls_563	0.2376	2.42000e-01	1.25520e-01
H10	opls_565	0.25557	2.42000e-01	1.25520e-01
H11	opls_911	0.16774	2.50000e-01	6.27600e-02
H12	opls_911	0.16774	2.50000e-01	6.27600e-02
H13	opls_911	0.16774	2.50000e-01	6.27600e-02
H14	opls_564	0.24141	2.42000e-01	1.25520e-01
H15	opls_140	0.0	2.50000e-01	1.25520e-01
H16	opls_140	0.0	2.50000e-01	1.25520e-01
H17	opls_911	0.14241	2.50000e-01	6.27600e-02
H18	opls_911	0.14241	2.50000e-01	6.27600e-02
C19	opls_136	0.0	3.50000e-01	2.76144e-01

Continued on next page

Table D.2 – continued from previous page

Atom	atom type	charge (e)	σ (nm)	ϵ (kJ/mol)
H20	opls_140	0.0	2.50000e-01	1.25520e-01
H21	opls_140	0.0	2.50000e-01	1.25520e-01
C22	opls_135	0.00087	3.50000e-01	2.76144e-01
H23	opls_140	0.0417	2.50000e-01	1.25520e-01
H24	opls_140	0.0417	2.50000e-01	1.25520e-01
H25	opls_140	0.0417	2.50000e-01	1.25520e-01

Table D.3: Dihedral parameters of [BMIM+]

AI	AJ	AK	AL	C_0	C_1	C_2	C_3
1	4	6	2	45.00810	0.00000	-45.00810	0.00000
1	4	6	14	45.00810	0.00000	-45.00810	0.00000
3	1	4	6	11.72304	0.00000	-11.72304	0.00000
3	1	4	10	13.39776	0.00000	-13.39776	0.00000
3	1	5	11	1.17230	3.51691	0.00000	-4.68922
3	1	5	12	1.17230	3.51691	0.00000	-4.68922
3	1	5	13	1.17230	3.51691	0.00000	-4.68922
3	2	6	4	20.09664	0.00000	-20.09664	0.00000
3	2	6	14	20.09664	0.00000	-20.09664	0.00000

Continued on next page

Table D.3 – continued from previous page

AI	AJ	AK	AL	C_0	C_1	C_2	C_3
3	2	8	7	-3.55878	2.09340	1.46538	0.00000
3	2	8	17	0.37053	1.11160	0.00000	-1.48213
3	2	8	18	0.37053	1.11160	0.00000	-1.48213
4	1	3	2	19.46862	0.00000	-19.46862	0.00000
4	1	3	9	19.46862	0.00000	-19.46862	0.00000
4	1	5	11	1.17230	3.51691	0.00000	-4.68922
4	1	5	12	1.17230	3.51691	0.00000	-4.68922
4	1	5	13	1.17230	3.51691	0.00000	-4.68922
5	1	3	2	30.35430	0.00000	-30.35430	0.00000
5	1	3	9	30.35430	0.00000	-30.35430	0.00000
5	1	4	6	30.35430	0.00000	-30.35430	0.00000
5	1	4	10	30.35430	0.00000	-30.35430	0.00000
6	2	3	1	41.86800	0.00000	-41.86800	0.00000
6	2	3	9	41.86800	0.00000	-41.86800	0.00000
6	2	8	7	-3.55878	2.09340	1.46538	0.00000
6	2	8	17	0.37053	1.11160	0.00000	-1.48213
6	2	8	18	0.37053	1.11160	0.00000	-1.48213
7	19	22	23	0.62802	1.88406	0.00000	-2.51208
7	19	22	24	0.62802	1.88406	0.00000	-2.51208

Continued on next page

Table D.3 – continued from previous page

AI	AJ	AK	AL	C_0	C_1	C_2	C_3
7	19	22	25	0.62802	1.88406	0.00000	-2.51208
8	2	3	1	30.35430	0.00000	-30.35430	0.00000
8	2	3	9	30.35430	0.00000	-30.35430	0.00000
8	2	6	4	30.35430	0.00000	-30.35430	0.00000
8	2	6	14	30.35430	0.00000	-30.35430	0.00000
8	7	19	20	0.62802	1.88406	0.00000	-2.51208
8	7	19	21	0.62802	1.88406	0.00000	-2.51208
8	7	19	22	2.93076	-1.46538	0.20934	-1.67472
10	4	6	2	45.00810	0.00000	-45.00810	0.00000
10	4	6	14	30.35430	0.00000	-30.35430	0.00000
15	7	8	2	-4.09888	5.09115	2.96844	-3.96071
15	7	8	17	0.62802	1.88406	0.00000	-2.51208
15	7	8	18	0.62802	1.88406	0.00000	-2.51208
15	7	19	20	0.62802	1.88406	0.00000	-2.51208
15	7	19	21	0.62802	1.88406	0.00000	-2.51208
15	7	19	22	0.62802	1.88406	0.00000	-2.51208
16	7	8	2	-4.09888	5.09115	2.96844	-3.96071
16	7	8	17	0.62802	1.88406	0.00000	-2.51208
16	7	8	18	0.62802	1.88406	0.00000	-2.51208

Continued on next page

Table D.3 – continued from previous page

AI	AJ	AK	AL	C_0	C_1	C_2	C_3
16	7	19	20	0.62802	1.88406	0.00000	-2.51208
16	7	19	21	0.62802	1.88406	0.00000	-2.51208
16	7	19	22	0.62802	1.88406	0.00000	-2.51208
19	7	8	2	5.77569	-2.67327	0.95878	-4.06120
19	7	8	17	0.62802	1.88406	0.00000	-2.51208
19	7	8	18	0.62802	1.88406	0.00000	-2.51208
20	19	22	23	0.62802	1.88406	0.00000	-2.51208
20	19	22	24	0.62802	1.88406	0.00000	-2.51208
20	19	22	25	0.62802	1.88406	0.00000	-2.51208
21	19	22	23	0.62802	1.88406	0.00000	-2.51208
21	19	22	24	0.62802	1.88406	0.00000	-2.51208
21	19	22	25	0.62802	1.88406	0.00000	-2.51208
2	4	6	14	9.21096	0.00000	-9.21096	0.00000
1	6	4	10	9.21096	0.00000	-9.21096	0.00000
3	4	1	5	8.37360	0.00000	-8.37360	0.00000
1	2	3	9	9.21096	0.00000	-9.21096	0.00000
3	6	2	8	8.37360	0.00000	-8.37360	0.00000

Note: AI,AJ,AK,AL are atom index. The unit of C_0, C_1, C_2, and C_3 is kJ/mol.

The parameters for strech and bend terms taken from OPLSS force field are also avaiable on line[39, 50].

1-hexyl-3-methylimidazolium Cation ([HMIM+])

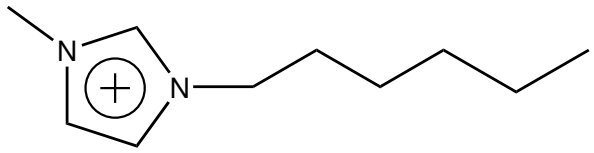

Figure D.2: [HMIM+] cation

Table D.4: Coordinates of [HMIM+]

Atom	atom index	x (nm)	y (nm)	z (nm)
N1	1	1.7095	-3.7944	-1.2304
N2	2	1.6545	-3.5714	-1.2514
C3	3	1.7405	-3.6734	-1.2774
C4	4	1.5735	-3.7814	-1.1984
C5	5	1.7935	-3.9174	-1.2404
C6	6	1.5405	-3.6474	-1.2034
C7	7	1.6165	-3.3844	-1.4134
C8	8	1.6635	-3.4284	-1.2724
H9	9	1.8295	-3.6454	-1.3324
H10	10	1.5035	-3.8634	-1.1674
H11	11	1.7895	-3.9634	-1.1374
H12	12	1.8955	-3.8754	-1.2554

Continued on next page

Table D.4 – continued from previous page

Atom	atom index	x (nm)	y (nm)	z (nm)
H13	13	1.7825	-3.9844	-1.3214
H14	14	1.4515	-3.5974	-1.1844
H15	15	1.5155	-3.4164	-1.4254
H16	16	1.6535	-3.4564	-1.4884
H17	17	1.6215	-3.3704	-1.1954
H18	18	1.7695	-3.3964	-1.2564
C19	19	1.6385	-3.2464	-1.4474
H20	20	1.5685	-3.1944	-1.4074
H21	21	1.7285	-3.2074	-1.4004
C22	22	1.6315	-3.2064	-1.5924
H23	23	1.5405	-3.2584	-1.6264
H24	24	1.7285	-3.2454	-1.6374
C25	25	1.6175	-3.0604	-1.6234
H26	26	1.5425	-3.0274	-1.5634
H27	27	1.7055	-3.0074	-1.6074
C28	28	1.6015	-3.0344	-1.7724
H29	29	1.5255	-3.1094	-1.8054
H30	30	1.5685	-2.9294	-1.7784
H31	31	1.6905	-3.0384	-1.8324

The parameter of [HMIM+] for atom 1-21 are the same with that of cation [BMIM+], we only provide parameters for the rest atoms in Table D.5.

Table D.5: Nonbonding parameters of [HMIM+]

Atom	atom type	charge (e)	σ (nm)	ϵ (kJ/mol)
C22	opls_136	0.0	3.50000e-01	2.76144e-01
H23	opls_140	0.0	2.50000e-01	1.25520e-01
H24	opls_140	0.0	2.50000e-01	1.25520e-01
C25	opls_136	0.0	3.50000e-01	2.76144e-01
H26	opls_140	0.0	2.50000e-01	1.25520e-01
H27	opls_140	0.0	2.50000e-01	1.25520e-01
C28	opls_135	0.00087	3.50000e-01	2.76144e-01
H29	opls_140	0.0417	2.50000e-01	1.25520e-01
H30	opls_140	0.0417	2.50000e-01	1.25520e-01
H31	opls_140	0.0417	2.50000e-01	1.25520e-01

Note: The nonbonding parameters for atoms 1 to 22 can be found in the previous Table D.2

Table D.6: Dihedral parameters of [HMIM+]

AI	AJ	AK	AL	C_0	C_1	C_2	C_3
8	7	19	22	2.93076	-1.46538	0.20934	-1.67472
15	7	19	22	0.62802	1.88406	0	-2.51208
16	7	19	22	0.62802	1.88406	0	-2.51208
7	19	22	23	0.62802	1.88406	0	-2.51208
7	19	22	24	0.62802	1.88406	0	-2.51208
7	19	22	25	2.93076	-1.46538	0.20934	-1.67472
20	19	22	23	0.62802	1.88406	0	-2.51208
20	19	22	24	0.62802	1.88406	0	-2.51208
20	19	22	25	0.62802	1.88406	0	-2.51208
21	19	22	23	0.62802	1.88406	0	-2.51208
21	19	22	24	0.62802	1.88406	0	-2.51208
21	19	22	25	0.62802	1.88406	0	-2.51208
19	22	25	26	0.62802	1.88406	0	-2.51208
19	22	25	27	0.62802	1.88406	0	-2.51208
19	22	25	28	2.93076	-1.46538	0.20934	-1.67472
23	22	25	26	0.62802	1.88406	0	-2.51208
23	22	25	27	0.62802	1.88406	0	-2.51208
23	22	25	28	0.62802	1.88406	0	-2.51208
24	22	25	26	0.62802	1.88406	0	-2.51208

Continued on next page

Table D.6 – continued from previous page

AI	AJ	AK	AL	C_0	C_1	C_2	C_3
24	22	25	27	0.62802	1.88406	0	-2.51208
24	22	25	28	0.62802	1.88406	0	-2.51208
22	25	28	29	0.62802	1.88406	0	-2.51208
22	25	28	30	0.62802	1.88406	0	-2.51208
22	25	28	31	0.62802	1.88406	0	-2.51208
26	25	28	29	0.62802	1.88406	0	-2.51208
26	25	28	30	0.62802	1.88406	0	-2.51208
26	25	28	31	0.62802	1.88406	0	-2.51208
27	25	28	29	0.62802	1.88406	0	-2.51208
27	25	28	30	0.62802	1.88406	0	-2.51208
27	25	28	31	0.62802	1.88406	0	-2.51208

Note: AI,AJ,AK,AL are all atom indices. The parameters for all indices less than 22 can be found in the previous Table D.3

hexafluophosphate Anion ([PF_6-])

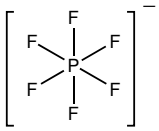

Figure D.3: [PF_6-] cation

Table D.7: Coordinates of [PF_6-]

Atom	atom index	x (nm)	y (nm)	z (nm)
P1	1	2.0167	0.7809	2.8044
F2	2	1.9029	0.8738	2.8550
F3	3	2.0545	0.7370	2.9494
F4	4	1.9818	0.8246	2.6580
F5	5	2.1247	0.6820	2.7457
F6	6	2.1174	0.9017	2.8140
F7	7	1.9110	0.6646	2.7907

Table D.8: Stretching parameters of [PF_6-]

Atom index	Atom index	r_{eq} (nm)	K_r (kJ/(mol·nm^2)
1	2	0.156935	4184000.0
1	3	0.156935	4184000.0
1	4	0.156935	4184000.0
1	5	0.156935	4184000.0
1	6	0.156935	4184000.0
1	7	0.156935	4184000.0

Table D.9: Bending parameters of [PF_6-]

Atom index	Atom index	Atom index	θ_{eq} (degree)	K_θ (kJ/(mol·rad^2)
2	1	3	90.0	836.800
2	1	4	90.0	836.800
2	1	5	180.0	836.800
2	1	6	90.0	836.800
2	1	7	90.0	836.800
3	1	4	180.0	836.800
3	1	5	90.0	836.800
3	1	6	90.0	836.800
3	1	7	90.0	836.800
4	1	5	90.0	836.800
4	1	6	90.0	836.800
4	1	7	90.0	836.800
5	1	6	90.0	836.800
5	1	7	90.0	836.800
6	1	7	180.0	836.800

2-amino-7-nitrofluorene Probe (ANF)

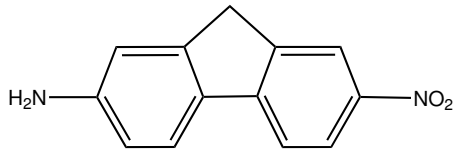

Figure D.4: Fluorescent probe ANF

Table D.10: Coordinates of ANF

Atom	atom index	x (nm)	y (nm)	z (nm)
C1	1	1.7025	1.7275	2.8325
C2	2	1.6911	1.7827	2.7048
C3	3	1.6796	1.6943	2.5971
C4	4	1.7122	1.5829	2.8498
C5	5	1.6927	1.4948	2.7415
C6	6	1.6760	1.5531	2.6134
N7	7	1.6731	1.3659	2.7578
H8	8	1.6978	1.7842	2.9191
H9	9	1.7009	1.5420	2.9505
H10	10	1.6409	1.4824	2.5351
C11	11	1.6780	2.0387	2.7181
C12	12	1.7017	2.1545	2.6493

Continued on next page

Table D.10 – continued from previous page

Atom	atom index	x (nm)	y (nm)	z (nm)
C13	13	1.7302	2.1484	2.5171
C14	14	1.6896	1.9159	2.6527
C15	15	1.6911	1.9048	2.5126
C16	16	1.7299	2.0235	2.4446
H17	17	1.6610	2.0361	2.8289
H18	18	1.6867	2.2412	2.7143
H19	19	1.7564	2.0271	2.3363
C20	20	1.6754	1.7690	2.4679
N21	21	1.7486	2.2707	2.4433
O22	22	1.7696	2.3654	2.5164
O23	23	1.7433	2.2660	2.3135
H24	24	1.6688	1.3465	2.8570
H25	25	1.5813	1.3366	2.7156
H26	26	1.7487	1.7332	2.3946
H27	27	1.5755	1.7547	2.4263

The excited state charges are calculated based on a INDO Hamiltoain of CI using Hyperchem and *ab initio* calculation using Gaussian 03 (see section 4.2 in chapter 4).

Table D.11: Nonbonding parameters of ANF

Atom	atom type	q_g(e)	q_e(e)	σ (nm)	ϵ (kJ/mol)
C1	CA	-0.098073	-0.077499	0.355	0.293076
C2	CA	-0.133973	-0.085986	0.355	0.293076
C3	CA	0.186973	0.223324	0.355	0.293076
C4	CA	-0.400764	-0.381327	0.355	0.293076
C5	CA	0.542449	0.609969	0.355	0.293076
C6	CA	-0.482755	-0.481454	0.355	0.293076
N7	NT	-0.934832	-0.890169	0.33	0.711756
H8	HA	0.161595	0.170777	0.242	0.125604
H9	HA	0.200105	0.208665	0.242	0.125604
H10	HA	0.212443	0.220198	0.242	0.125604
C11	CA	-0.206424	-0.188210	0.355	0.293076
C12	CA	-0.213081	-0.216435	0.355	0.293076
C13	CA	0.055530	0.164585	0.355	0.293076
C14	CA	0.116735	0.073611	0.355	0.293076
C15	CA	0.135815	0.149327	0.355	0.293076
C16	CA	-0.322881	-0.363726	0.355	0.293076
H17	HA	0.163062	0.160752	0.242	0.125604
H18	HA	0.194180	0.199418	0.242	0.125604
H19	HA	0.211855	0.214657	0.242	0.125604

Continued on next page

Table D.11 – continued from previous page

Atom	atom type	q_g(e)	q_e(e)	σ (nm)	ϵ (kJ/mol)
C20	CT	-0.206611	-0.203482	0.35	0.2763288
N21	NO	0.801428	0.644742	0.325	0.502416
O22	ON	-0.481254	-0.579920	0.296	0.711756
O23	ON	-0.478396	-0.574883	0.296	0.711756
H24	H	0.384169	0.393701	0.0	0.0
H25	H	0.380493	0.389395	0.0	0.0
H26	HC	0.113780	0.117661	0.25	0.125604
H27	HC	0.098432	0.102309	0.25	0.125604

q_g and q_e stand for the ground and first excited electronic state respectively.

Table D.12: Stretching parameters of ANF

Atom index	Atom index	r_{eq} (nm)	K_r (kJ/(mol·nm^2)
1	2	0.14000	392721.8
1	4	0.14000	392721.8
1	8	0.10800	307311.1
2	3	0.14000	392721.8
2	14	0.14000	392721.8
3	6	0.14000	392721.8
3	20	0.15100	265443.1
4	5	0.14000	392721.8
4	9	0.10800	307311.1
5	6	0.14000	392721.8
5	7	0.13400	402770.2
6	10	0.10800	307311.1
7	24	0.10100	363414.2
7	25	0.10100	363414.2
11	12	0.14000	392721.8
11	14	0.14000	392721.8
11	17	0.10800	307311.1
12	13	0.14000	392721.8
12	18	0.10800	307311.1

Continued on next page

Table D.12 – continued from previous page

Atom index	Atom index	r_{eq} (nm)	K_r (kJ/(mol·nm^2)
13	16	0.14000	392721.8
13	21	0.14600	334944.0
14	15	0.14000	392721.8
15	16	0.14000	392721.8
15	20	0.15100	265443.1
16	19	0.10800	307311.1
20	26	0.10900	284702.4
20	27	0.10900	284702.4
21	22	0.12250	460548.0
21	23	0.12250	460548.0

Table D.13: Bending parameters of ANF

Atom index	Atom index	Atom index	θ_{eq} (degree)	K_θ (kJ/(mol·rad^2)
1	2	3	120.000	527.537
1	2	14	120.000	527.537
1	4	5	120.000	527.537
1	4	9	120.000	293.076
2	3	6	120.000	527.537

Continued on next page

Table D.13 – continued from previous page

Atom index	Atom index	Atom index	θ_{eq} (degree)	K_θ (kJ/(mol·rad^2)
2	3	20	120.000	586.152
2	14	11	120.000	527.537
2	14	15	120.000	527.537
3	6	5	120.000	527.537
3	6	10	120.000	293.076
3	20	15	109.500	334.944
3	20	26	109.500	293.076
3	20	27	109.500	293.076
4	1	2	120.000	527.537
4	5	6	120.000	527.537
4	5	7	120.100	586.152
5	6	10	120.000	293.076
5	7	24	111.000	293.076
5	7	25	111.000	293.076
7	5	6	120.100	586.152
8	1	2	120.000	293.076
8	1	4	120.000	293.076
9	4	5	120.000	293.076
11	12	13	120.000	527.537

Continued on next page

Table D.13 – continued from previous page

Atom index	Atom index	Atom index	θ_{eq} (degree)	K_θ (kJ/(mol·rad^2)
11	12	18	120.000	293.076
11	14	15	120.000	527.537
12	13	16	120.000	527.537
12	13	21	120.000	711.756
13	16	15	120.000	527.537
13	16	19	120.000	293.076
13	21	22	117.500	669.888
13	21	23	117.500	669.888
14	2	3	120.000	527.537
14	11	12	120.000	527.537
14	15	16	120.000	527.537
14	15	20	120.000	586.152
15	16	19	120.000	293.076
15	20	26	109.500	293.076
15	20	27	109.500	293.076
17	11	12	120.000	293.076
17	11	14	120.000	293.076
18	12	13	120.000	293.076
20	3	6	120.000	586.152

Continued on next page

Table D.13 – continued from previous page

Atom index	Atom index	Atom index	θ_{eq} (degree)	K_θ (kJ/(mol·rad^2)
20	15	16	120.000	586.152
21	13	16	120.000	711.756
23	21	22	125.300	669.888
25	7	24	106.400	365.089
27	20	26	107.800	276.329

Table D.14: Dihedral parameters of ANF

AI	AJ	AK	AL	C_0	C_1	C_2	C_3
1	2	3	6	30.35430	0.00000	-30.35430	0.00000
1	2	3	20	30.35430	0.00000	-30.35430	0.00000
1	2	14	11	30.35430	0.00000	-30.35430	0.00000
1	2	14	15	30.35430	0.00000	-30.35430	0.00000
1	4	5	6	30.35430	0.00000	-30.35430	0.00000
1	4	5	7	30.35430	0.00000	-30.35430	0.00000
2	1	4	5	30.35430	0.00000	-30.35430	0.00000
2	1	4	9	30.35430	0.00000	-30.35430	0.00000
2	3	6	5	30.35430	0.00000	-30.35430	0.00000
2	3	6	10	30.35430	0.00000	-30.35430	0.00000

Continued on next page

Table D.14 – continued from previous page

AI	AJ	AK	AL	C_0	C_1	C_2	C_3
2	3	20	15	0.00000	0.00000	0.00000	0.00000
2	3	20	26	0.00000	0.00000	0.00000	0.00000
2	3	20	27	0.00000	0.00000	0.00000	0.00000
2	14	15	16	30.35430	0.00000	-30.35430	0.00000
2	14	15	20	30.35430	0.00000	-30.35430	0.00000
3	2	14	11	30.35430	0.00000	-30.35430	0.00000
3	2	14	15	30.35430	0.00000	-30.35430	0.00000
4	1	2	3	30.35430	0.00000	-30.35430	0.00000
4	1	2	14	30.35430	0.00000	-30.35430	0.00000
4	5	6	3	30.35430	0.00000	-30.35430	0.00000
4	5	6	10	30.35430	0.00000	-30.35430	0.00000
4	5	7	24	8.49920	0.00000	-8.49920	0.00000
4	5	7	25	8.49920	0.00000	-8.49920	0.00000
6	3	20	15	0.00000	0.00000	0.00000	0.00000
6	3	20	26	0.00000	0.00000	0.00000	0.00000
6	3	20	27	0.00000	0.00000	0.00000	0.00000
6	5	7	24	8.49920	0.00000	-8.49920	0.00000
6	5	7	25	8.49920	0.00000	-8.49920	0.00000
7	5	6	3	30.35430	0.00000	-30.35430	0.00000

Continued on next page

Table D.14 – continued from previous page

AI	AJ	AK	AL	C_0	C_1	C_2	C_3
7	5	6	10	30.35430	0.00000	-30.35430	0.00000
8	1	2	3	30.35430	0.00000	-30.35430	0.00000
8	1	2	14	30.35430	0.00000	-30.35430	0.00000
8	1	4	5	30.35430	0.00000	-30.35430	0.00000
8	1	4	9	30.35430	0.00000	-30.35430	0.00000
9	4	5	6	30.35430	0.00000	-30.35430	0.00000
9	4	5	7	30.35430	0.00000	-30.35430	0.00000
11	12	13	16	30.35430	0.00000	-30.35430	0.00000
11	12	13	21	30.35430	0.00000	-30.35430	0.00000
11	14	15	16	30.35430	0.00000	-30.35430	0.00000
11	14	15	20	30.35430	0.00000	-30.35430	0.00000
12	11	14	2	30.35430	0.00000	-30.35430	0.00000
12	11	14	15	30.35430	0.00000	-30.35430	0.00000
12	13	16	15	30.35430	0.00000	-30.35430	0.00000
12	13	16	19	30.35430	0.00000	-30.35430	0.00000
12	13	21	22	4.81482	0.00000	-4.81482	0.00000
12	13	21	23	4.81482	0.00000	-4.81482	0.00000
14	2	3	6	30.35430	0.00000	-30.35430	0.00000
14	2	3	20	30.35430	0.00000	-30.35430	0.00000

Continued on next page

Table D.14 – continued from previous page

AI	AJ	AK	AL	C_0	C_1	C_2	C_3
14	11	12	13	30.35430	0.00000	-30.35430	0.00000
14	11	12	18	30.35430	0.00000	-30.35430	0.00000
14	15	16	13	30.35430	0.00000	-30.35430	0.00000
14	15	16	19	30.35430	0.00000	-30.35430	0.00000
14	15	20	3	0.00000	0.00000	0.00000	0.00000
14	15	20	26	0.00000	0.00000	0.00000	0.00000
14	15	20	27	0.00000	0.00000	0.00000	0.00000
16	13	21	22	4.81482	0.00000	-4.81482	0.00000
16	13	21	23	4.81482	0.00000	-4.81482	0.00000
16	15	20	3	0.00000	0.00000	0.00000	0.00000
16	15	20	26	0.00000	0.00000	0.00000	0.00000
16	15	20	27	0.00000	0.00000	0.00000	0.00000
17	11	12	13	30.35430	0.00000	-30.35430	0.00000
17	11	12	18	30.35430	0.00000	-30.35430	0.00000
17	11	14	2	30.35430	0.00000	-30.35430	0.00000
17	11	14	15	30.35430	0.00000	-30.35430	0.00000
18	12	13	16	30.35430	0.00000	-30.35430	0.00000
18	12	13	21	30.35430	0.00000	-30.35430	0.00000
20	3	6	5	30.35430	0.00000	-30.35430	0.00000

Continued on next page

Table D.14 – continued from previous page

AI	AJ	AK	AL	C_0	C_1	C_2	C_3
20	3	6	10	30.35430	0.00000	-30.35430	0.00000
20	15	16	13	30.35430	0.00000	-30.35430	0.00000
20	15	16	19	30.35430	0.00000	-30.35430	0.00000
21	13	16	15	30.35430	0.00000	-30.35430	0.00000
21	13	16	19	30.35430	0.00000	-30.35430	0.00000
24	5	7	25	8.37360	0.00000	-8.37360	0.00000
22	23	21	13	87.92280	0.00000	-87.92280	0.00000
3	5	6	10	9.21096	0.00000	-9.21096	0.00000
2	4	1	8	9.21096	0.00000	-9.21096	0.00000
1	5	4	9	9.21096	0.00000	-9.21096	0.00000
4	6	5	7	8.37360	0.00000	-8.37360	0.00000
13	15	16	19	9.21096	0.00000	-9.21096	0.00000
12	14	11	17	9.21096	0.00000	-9.21096	0.00000
11	13	12	18	9.21096	0.00000	-9.21096	0.00000
12	16	13	21	8.37360	0.00000	-8.37360	0.00000

Note: AI,AJ,AK,AL are atom index. The unit of C_0,C_1,C_2,and, C_3 is kJ/mol.

1-methoxy-ethylpyridinium ([MOEPY+])

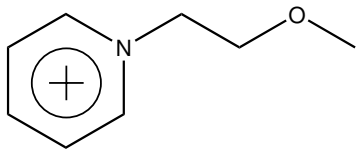

Figure D.5: [MOEPY+] cation

Table D.15: Coordinates of [MOEPY+]

Atom	atom index	x (nm)	y (nm)	z (nm)
H1	1	-2.0677	1.5989	1.7908
H2	2	-2.1551	1.7735	1.9726
H3	3	-2.0435	1.9651	2.0097
H4	4	-1.7682	1.8809	1.7047
H5	5	-1.8861	1.6849	1.6459
N6	6	-1.9009	1.9546	1.8514
C7	7	-1.9200	1.7419	1.7298
C8	8	-2.0162	1.6950	1.8118
C9	9	-2.0644	1.7838	1.9105
C10	10	-2.0007	1.9060	1.9324
C11	11	-1.8584	1.8693	1.7587
C12	12	-1.8306	2.0832	1.8717

Continued on next page

Table D.15 – continued from previous page

Atom	atom index	x (nm)	y (nm)	z (nm)
C13	13	-1.8595	2.1807	1.7607
C14	14	-1.7602	2.3910	1.6776
H15	15	-1.8611	2.1261	1.9669
H16	16	-1.7199	2.0725	1.8679
H17	17	-1.9637	2.2059	1.7353
H18	18	-1.8218	2.1358	1.6677
H19	19	-1.7013	2.4788	1.7131
H20	20	-1.7215	2.3492	1.5901
H21	21	-1.8560	2.4293	1.6520
O22	22	-1.7797	2.2963	1.7853

Table D.16: Nonbonding parameters of [MOEPY+]

Atom	atom index	charge(e)	σ(nm)	ϵ (kJ/mol)
H1	opls_526	0.09287854	0.242	0.12552
H2	opls_525	0.19239150	0.242	0.12552
H3	opls_524	0.27792361	0.242	0.12552
H4	opls_524	0.27792361	0.242	0.12552
H5	opls_525	0.19239150	0.242	0.12552

Continued on next page

Table D.16 – continued from previous page

Atom	atom index	charge(e)	σ(nm)	ϵ (kJ/mol)
N6	opls_520	0.61503816	0.325	0.71128
C7	opls_522	-0.09464031	0.355	0.29288
C8	opls_523	0.15873689	0.355	0.29288
C9	opls_522	-0.09464031	0.355	0.29288
C10	opls_521	-0.36933925	0.355	0.29288
C11	opls_521	-0.36933925	0.355	0.29288
C12	opls_908	-0.13478131	0.35	0.276144
C13	opls_182	0.00167019	0.35	0.276144
C14	opls_181	-0.29082167	0.35	0.276144
H15	opls_911	0.07905346	0.25	0.06276
H16	opls_911	0.07905346	0.25	0.06276
H17	opls_185	0.05363432	0.25	0.12552
H18	opls_185	0.05363432	0.25	0.12552
H19	opls_185	0.14694203	0.25	0.12552
H20	opls_185	0.14694203	0.25	0.12552
H21	opls_185	0.14694203	0.25	0.12552
O22	opls_180	-0.16159354	0.29	0.58576

Table D.17: Dihedral parameters of [MOEPY+]

AI	AJ	AK	AL	C_0	C_1	C_2	C_3
1	8	9	2	30.33400	0.00000	-30.33400	0.00000
1	8	9	10	30.33400	0.00000	-30.33400	0.00000
2	9	10	3	30.33400	0.00000	-30.33400	0.00000
2	9	10	6	30.33400	0.00000	-30.33400	0.00000
5	7	8	1	30.33400	0.00000	-30.33400	0.00000
5	7	8	9	30.33400	0.00000	-30.33400	0.00000
5	7	11	4	30.33400	0.00000	-30.33400	0.00000
5	7	11	6	30.33400	0.00000	-30.33400	0.00000
6	12	13	17	-4.09614	5.08774	2.96646	-3.95806
6	12	13	18	-4.09614	5.08774	2.96646	-3.95806
6	12	13	22	9.89307	-4.71746	3.67774	-8.85334
7	8	9	2	30.33400	0.00000	-30.33400	0.00000
7	8	9	10	30.33400	0.00000	-30.33400	0.00000
8	7	11	4	30.33400	0.00000	-30.33400	0.00000
8	7	11	6	30.33400	0.00000	-30.33400	0.00000
8	9	10	3	30.33400	0.00000	-30.33400	0.00000
8	9	10	6	30.33400	0.00000	-30.33400	0.00000
10	6	11	4	30.33400	0.00000	-30.33400	0.00000
10	6	11	7	30.33400	0.00000	-30.33400	0.00000

Continued on next page

Table D.17 – continued from previous page

AI	AJ	AK	AL	C_0	C_1	C_2	C_3
10	6	12	13	3.80116	-6.95172	-1.01671	4.16726
10	6	12	15	0.37028	1.11085	0.00000	-1.48114
10	6	12	16	0.37028	1.11085	0.00000	-1.48114
11	6	10	3	30.33400	0.00000	-30.33400	0.00000
11	6	10	9	30.33400	0.00000	-30.33400	0.00000
11	6	12	13	3.80116	-6.95172	-1.01671	4.16726
11	6	12	15	0.37028	1.11085	0.00000	-1.48114
11	6	12	16	0.37028	1.11085	0.00000	-1.48114
11	7	8	1	30.33400	0.00000	-30.33400	0.00000
11	7	8	9	30.33400	0.00000	-30.33400	0.00000
12	6	10	3	30.33400	0.00000	-30.33400	0.00000
12	6	10	9	30.33400	0.00000	-30.33400	0.00000
12	6	11	4	30.33400	0.00000	-30.33400	0.00000
12	6	11	7	30.33400	0.00000	-30.33400	0.00000
12	13	22	14	1.71544	2.84512	1.04600	-5.60656
15	12	13	17	0.62760	1.88280	0.00000	-2.51040
15	12	13	18	0.62760	1.88280	0.00000	-2.51040
15	12	13	22	0.97906	2.93717	0.00000	-3.91622
16	12	13	17	0.62760	1.88280	0.00000	-2.51040

Continued on next page

Table D.17 – continued from previous page

AI	AJ	AK	AL	C_0	C_1	C_2	C_3
16	12	13	18	0.62760	1.88280	0.00000	-2.51040
16	12	13	22	0.97906	2.93717	0.00000	-3.91622
17	13	22	14	1.58992	4.76976	0.00000	-6.35968
18	13	22	14	1.58992	4.76976	0.00000	-6.35968
19	14	22	13	1.58992	4.76976	0.00000	-6.35968
20	14	22	13	1.58992	4.76976	0.00000	-6.35968
21	14	22	13	1.58992	4.76976	0.00000	-6.35968
6	7	11	4	9.20480	0.00000	-9.20480	0.00000
8	11	7	5	9.20480	0.00000	-9.20480	0.00000
7	9	8	1	9.20480	0.00000	-9.20480	0.00000
8	10	9	2	9.20480	0.00000	-9.20480	0.00000
6	9	10	3	9.20480	0.00000	-9.20480	0.00000
10	11	6	12	8.36800	0.00000	-8.36800	0.00000

Note: AI,AJ,AK,AL are atom index. The unit of C_0, C_1, C_2, and C_3 is kJ/mol.

dicyanoamide ([DCA-])

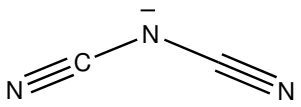

Figure D.6: [DCA-] anion

Table D.18: Coordinates of [DCA-]

Atom	atom index	x (nm)	y (nm)	z (nm)
C1	1	1.3158	-0.1196	0.1265
C2	2	1.5025	-0.2869	0.0737
N3	3	1.4132	-0.1768	0.0248
N4	4	1.2407	-0.0879	0.2110
N5	5	1.5770	-0.3720	0.0946

Table D.19: Nonbonding parameters of [DCA-]

Atom	atom index	charge(e)	σ(nm)	ϵ (kJ/mol)
C1	opls_261	0.50873113	0.365	0.62760
C2	opls_261	0.50873113	0.365	0.62760
N3	opls_303	-0.60193173	0.325	0.71128
N4	opls_753	-0.70776526	0.320	0.71128
N5	opls_753	-0.70776526	0.320	0.71128

Table D.20: Stretching parameters of [DCA-]

Atom index	Atom index	r_{eq} (nm)	K_r (kJ/(mol·nm^2)
1	3	0.14630	282001.6
1	4	0.11570	543920.0
2	3	0.14630	282001.6
2	5	0.11570	543920.0

Table D.21: Bending parameters of [DCA-]

Atom index	Atom index	Atom index	θ_{eq} (degree)	K_θ (kJ/(mol·rad^2)
1	3	2	123.200	418.400
4	1	3	180.000	585.760
5	2	3	180.000	585.760

REFERENCES

[1] M. P. Allen and D. J. Tildesley. *Computer Simulation of Liquids*. Oxford University Press Inc. New York, 1st edition, 1987.

[2] J. Applequist, J. R. Carl, and K. Fung. An atom dipole interaction model for molecular polarizability. application to polyatomic molecules and determination of atom polarizabilities. *J. Am. Chem. Soc.*, 94(9):2952–2960, 1972.

[3] G. Arya, E. Maginn, and H. Chang. Efficient viscosity estimation from molecular dynamics simulation via momentum impulse relaxation. *J. Chem. Phys.*, 113(6):2079–2087, 2000.

[4] S. Arzhantsev, H. Jin, N. Ito, and M. Maroncelli. Observing the complete solvation response of dcs in imidazolium ionic liquids, fromthe femtosecond to nanosecond regimes. *Chem. Phys. Lett.*, 417:524–529, 2006.

[5] J. A. Backer, C. P. Lowe, H. C. J. Hoefsloot, and P. D. Ledema. Poiseuille flow to measure the viscosity of particle model fluids. *J. Chem. Phys.*, 122:154503, 2005.

[6] U. Balucani, J. P. Brodholt, P. Jedlovszky, and R. Vallauri. Viscosity of liquid water from computer simulations with a polarizable potential model. *Phys. Rev. E*, 62(2):2971–2973, Aug 2000.

[7] H. J. C. Berendsen, D. van der Spoel, and R. van Drunen. Gromacs: A message-passing parallel molecular dynamics implementation. *Comp. Phys. Comm.*, 91:43–56, 1995.

[8] J. P. Boon and S. Yip. *Molecular Hydrodynamics*, chapter 2. McGraw-Hill Inc. New York, 1980.

[9] R. W Boyd. *Nonlinear Optics*, chapter 1. Academic Press, Inc. San Diego, USA, 2 edition, 2003.

[10] N. J. Bridge and A. D. Buckingham. The polarization of laser light scattered by gases. *Proc. Roy. Soc. A*, 295:334–349, 1966.

[11] P. K. Chowdhury, M. Halder, L. Sanders, T. Calhoun, J. L. Anderson, D. W. Armstrong, X. Song, and J. W. Petrich. Dynamic solvation in room-temperature ionic liquids. *J. Phys. Chem. B*, 108(29):10245–10255, 2004.

[12] M. G. Del Popolo and G. A. Voth. On the structure and dynamics of ionic liquids. *J. Phys. Chem. B*, 108(5):1744–1752, 2004.

[13] A. Demchenko. The red-edge effects: 30 years of exploration. *Luminescence*, 17:19–42, 2002.

[14] C. Donati, J. Douglas, W. Kob, S. Plimpton, P. Poole, and S. Glotzer. Stringlike cooperative motion in a supercooled liquid. *Phys. Rev. Lett.*, 80(11):2338–2341, 1998.

[15] U. Essmann, L. Perera, M. L. Berkowitz, T. Darden, H. Lee, and L. G. Pedersen. A smooth particle mesh ewald method. *J. Chem. Phys.*, 103(19):8577–8593, 1995.

[16] D. J. Evans and G. P. Morriss. *Statistical Mechanics of Nonequilibrium Liquids*, chapter 5. Academic Press, Inc. Amsterdam, The Netherlands, 1990.

[17] S. A. Forsyth, J. M. Pringle, and D. R. MacFarlane. Ionic liquids - an overview. *Aust. J. Chem.*, 57(2):113–119, 2004.

[18] D. Frenkel and J. P. McTague. Molecular dynamics studies of orientational and collision-induced light scattering in molecular fluids. *J. Chem. Phys.*, 71(4):2801–2818, 1980.

[19] D. Frenkel and B. Smit. *Understanding Molecular Simulation: From Algorithms to Applications*. Academic Press, Inc. Orlando, FL. USA, 2nd edition, 2001.

[20] M. Frisch, G. Trucks, H. Schlegel, G. Scuseria, M. Robb, J. Cheeseman, J. Montgomery, T. Vreven, K. Kudin, J. Burant, J. Millam, S. Iyengar, J. Tomasi, V. Barone, B. Mennucci, M. Cossi, G. Scalmani, N. Rega, G. Petersson, H. Nakatsuji, M. Hada, M. Ehara, K. Toyota, R. Fukuda, J. Hasegawa, M. Ishida, T. Nakajima, Y. Honda, O. Kitao, H. Nakai, M. Klene, X. Li, J. Knox, H. Hratchian, J. Cross, C. Adamo, J. Jaramillo, R. Gomperts, R. Stratmann, O. Yazyev, A. Austin, R. Cammi, C. Pomelli, J. Ochterski, P. Ayala, K. Morokuma, G. Voth, P. Salvador, J. Dannenberg, V. Zakrzewski, S. Dapprich, A. Daniels, M. Strain, O. Farkas, D. Malick, A. Rabuck, K. Raghavachari, J. Foresman, J. Ortiz, Q. Cui, A. Baboul, S. Clifford, J. Cioslowski, B. Stefanov, G. Liu, A. Liashenko, P. Piskorz, I. Komaromi, R. Martin, D. Fox, T. Keith, M. Al-Laham, C. Peng, A. Nanayakkara, M. Challacombe, P. Gill, B. Johnson, W. Chen, M. Wong, C. Gonzalez, and J. Pople. Gaussian 03, revision a.1. *Gaussian, Inc., Pittsburgh PA*, 2003.

[21] L. C. Geiger and B. M. Ladanyi. Molecular dynamics simulation study of nonlinear optical response of fluids. *Chem. Phys. Lett.*, 159:413–420, 1989.

[22] N. Giovambattista, M. Mazza, S. Buldyrev, F. Starr, and H. Stanley. Dynamic heterogeneities in supercooled water. *J. Phys. Chem. B*, 108(21):6655–6661, 2004.

[23] E. Gomez, B. Gonzalez, A. Dominguez, E. Tojo, and J. Tojo. Dynamic viscosities of a series of 1-alkyl-3-methylimidazolium chloride ionic liquids and their binary mixtures with water at several temperatures. *J. Chem. Eng. Data*, 51(2):696–701, 2006.

[24] R. G. Gordon. Correlation functions for molecular motion. In *Advances in Magnetic resonance*, volume 3, pages 1–33. Academic press New York, 1968.

[25] E. M. Gosling, I. R. McDonald, and K. Singer. On the calculation by molecular dynamics of the shear viscosity of a simple fluid. *Mol. Phys.*, 26(6):1475–1484, 1973.

[26] W. Gotze and L. Sjogren. Relaxation processes in supercooled liquids. *Rep. Prog. Phys.*, 55:241–376, 1992.

[27] J. P. Hansen and I. R. McDonald. *Theory of simple liquids*, chapter 8, page 266. Academic Press, Inc. Amsterdam, The Netherlands, 2nd edition, 1990.

[28] J. P. Hansen and I. R. McDonald. *Theory of simple liquids*. Academic Press, Inc. Amsterdam, The Netherlands, 2nd edition, 1990.

[29] J. P. Hansen and I. R. McDonald. *Theory of simple liquids*, chapter 7, 8, 9. Academic Press, Inc. Amsterdam, The Netherlands, 3rd edition, 2006.

[30] R. W. Hellwarth. Third-order optical susceptibilities of liquids and solids. *Prog. Quantum Electron.*, 5:1–68, 1977.

[31] B. Hess. Determining the shear viscosity of model liquids from molecular dynamics simulations. *J. Chem. Phys.*, 116:209–217, 2002.

[32] R. W. Hockney. The potential calculation and some applications. *Methods Comput. Phys.*, 9:136–211, 1970.

[33] J. D. Holbrey, W. M. Reichert, M. Nieuwenhuyzen, S. Johnston, K. R. Seddon, and R. D. Rogers. Crystal polymorphism in 1-butyl-3-methylimidazolium halides: supporting ionic liquid formation by inhibition of crystallization. *Chem. Comm.*, (14):1636–1637, 2003.

[34] J. D. Holbrey and K. R. Seddon. Ionic liquids. *Clean Technol. and Environ. Policy*, 1(4):223–236, 1999.

[35] Z. Hu and C. J. Margulis. Heterogeneity in a room-temperature ionic liquid: Persistent local environments andthe red-edge effect. *Proc. Natl. Acad. Sci. USA*, 103(4):831–836, 2006.

[36] Z. Hu and C. J. Margulis. Room-temperature ionic liquids: Viscosity, slow dynamics and the red edge effect. *Acc. Chem. Res.*, in press, 2007.

[37] Z. Hu and C.J. Margulis. A study of the time-resolved fluorescence spectrum and red edge effect of anf in a room-temperature ionic liquid. *J. Phys. Chem. B*, 110(23):11025–11028, 2006.

[38] Z. Hu and C.J. Margulis. On the response of an ionic liquids to external perturbations and the calculation of shear viscosity. *J. Phys. Chem. B*, 111(18):4705–4714, 2007.

[39] W. L. Jorgensen, D. S. Maxwell, and J. Tirado-Rives. Development and testing of the opls all-atom force field on conformational energetics and properties of organic liquids. *J. Am. Chem. Soc.*, 118(45):11225–11236, 1996.

[40] G. A. Kaminski, H. A. Stern, B. J. Berne, R. A. Friesner, Y. X. Cao, R. B. Murphy, R. Zhou, and T. A. Halgren. Development of a polarizable force field for proteins via ab initio quantum chemistry: First generation model and gas phase tests. *J. Comput. Chem.*, 23:1515–1531, 2002.

[41] W. Kob and H. Andersen. Testing mode-coupling theory for a supercooled binary lennard-jones mixtures: The van hove correlation function. *Phys. Rev. E*, 51(5):4626–4641, 1995.

[42] W. Kob and H. C. Andersen. Scaling behavior in the β-relaxation regime of a supercooled lennard-jones mixture. *Phys. Rev. Lett.*, 73(10):1376–1379, Sep 1994.

[43] W. Kob, C. Donati, S. Plimpton, P. Poole, and S. Glotzer. Dynamical heterogeneities in a supercooled lennard-jones liquid. *Phys. Rev. Lett.*, 79(15):2827–2830, 1997.

[44] M. N. Kobrak and V. Znamenskiy. Solvation dynamics of room-temperature ionic liquids: evidence for collective solvent motion on sub-picosecond timescales. *Chem. Phys. Lett.*, 395(1-3):127–132, 2004.

[45] R. Kubo. Statistical-mechanical theory of irreversible processes. i. general theory and simple applications to magnetic and conduction problems. *J. Phys. Soc. Japan*, 12(6):570–586, 1957.

[46] A. S. Larsen, J. D. Holbrey, F. S. Tham, and C. A. Reed. Designing ionic liquids: Imidazolium melts with inert carborane anions. *J. Am. Chem. Soc.*, 122(30):7264–7272, 2000.

[47] E. Lindahl, B. Hess, and D. van der Spoel. Gromacs 3.0: A package for molecular simulation and trajectory analysis. *J. Mol. Mod.*, 7:306–317, 2001.

[48] P. Mandal, M Sarkar, and A. Samanta. Excitation-wavelength-dependent fluorescence behavior of some dipolar molecules in room-temperature ionic liquids. *J. Phys. Chem. A*, 108(42):9048–9053, 2004.

[49] C. J. Margulis. Computational study of imidazolium based ionic solvents with alkyl substituents of different lengths. *Mol. Phys.*, 102(9-10):829–838, 2004.

[50] C. J. Margulis, H. A. Stern, and B. J. Berne. Computer simulation of a "green chemistry" room-temperature ionic solvent. *J. Phys. Chem. B*, 106(46):12017–12021, 2002.

[51] D. McMorrow, W. T. Lotshaw, and G. A. Kenney-Wallace. Femotosecond optical kerr studies on the origin of the nonlinear responses in simple liquids. *IEEE J. Quantum Electron.*, 24(2):443–454, 1989.

[52] D. A. McQuarrie. *Statistical Mechanics*, chapter 16. University Science Books, Sausalito, California, 1976.

[53] D. A. McQuarrie. *Statistical Mechanics*, chapter 21. University Science Books, Sausalito, California, 1976.

[54] S. R. Mente and M. Maroncelli. Computer simulations of the solvatochromism of betaine-30. *J. Phys. Chem. B*, 103(36):7704–7719, 1999.

[55] B. J. Palmer. Transverse-current autocorrelation-function calculations of the shear viscosity for molecular liquids. *Phys. Rev. E*, 49(1):359–366, Jan 1994.

[56] D. Potter. *Computational Physics*. Wiley, Inc. New York, 1973.

[57] A. Rahman. Correlations in the motion of atoms in liquid argon. *Phys. Rev.*, 136(2A):A405–A411, 1964.

[58] J. J. M. Ramos, C. A. M. Afonso, and L. C. Branco. Glass transition relaxation and fragility in two room temperature ionic liquids. *J. Therm. Anal. Calorim.*, 71(2):659–666, 2003.

[59] D. R. Reichmann and P. Charbonneau. Mode-coupling theory. *J. Stat. Mech.: Theory and Experiment*, page P05013, 2005.

[60] M. Ribeiro. Translational and reorientational heterogeneity in the glass-forming liquid ca2k3(no3)7. *Phys. Chem. Chem. Phys.*, 6:771–774, 2004.

[61] J. Ridley and M. Zerner. An intermediate neglect of differential overlap technique for spectroscopy: Pyrrole and the azines. *Theor. Chim. Acta*, 32:111–134, 1973.

[62] J. J. Sakuari. *Modern Quantum Mechanics*. Addison-Wesley Publishing Company, Inc. New York, 2nd edition, 1994.

[63] P. Schofield. Wavelength-dependent fluctuations in classical fluids i. the long wavelength limit. *Proc. Phys. Soc.*, 88:149–170, 1966.

[64] Y. Shim, J. S. Duan, M. Y. Choi, and H. J. Kim. Solvation in molecular ionic liquids. *J. Chem. Phys.*, 119(13):6411–6414, 2003.

[65] H. Shirota and E.W. Castner. Physical properties and intermolecular dynamics of an ionic liquid compared with its isoelectronic neutral binary solution. *J. Phys. Chem. A*, 109(42):9388–9392, 2005.

[66] H. Shirota and E.W. Castner. Why are viscosities lower for ionic liquids with -$ch_2si(ch_3)_3$ vs -$ch_2c(ch_3)_3$) substitutions on the imidazolium cations? *J. Phys. Chem. B*, 109(46):21576–21585, 2005.

[67] U. C. Singh and P. A. Kollman. An approach to computing electrostatic charges for molecules. *J. Comput. Chem.*, 5:129–145, 1984.

[68] H. Tokuda, K. Hayamizu, K. Ishii, M. A. B. H. Susan, and M. Watanabe. Physicochemical properties and structures of room temperature ionic liquids. 1. variation of anionic species. *J. Phys. Chem. B*, 108(42):16593–16600, 2004.

[69] H. Tokuda, K. Hayamizu, K. Ishii, M. A. B. H. Susan, and M. Watanabe. Physicochemical properties and structures of room temperature ionic liquids. 2. variation of alkyl chain length in imidazolium cation. *J. Phys. Chem. B*, 109(13):6103–6110, 2005.

[70] H. Tokuda, K. Ishii, M.A.B.H. Susan, S. Tsuzuki, K. Hayamizu, and M. Watanabe. Physicochemical properties and structures of room-temperature ionic liquids. 3. variation of cationic structures. *J. Phys. Chem. B*, 110(6):2833–2839, 2006.

[71] S. Urahata and M. Ribeiro. Collective excitations in an ionic liquid. *J. Chem. Phys.*, 124:074513, 2006.

[72] D. van der Spoel, E. Lindahl, B. Hess, A. van Buuren, E. Apol, P. Meulenhoff, D. Tieleman, A. Sijbers, K. Feenstra, van Drunen R., and Berendsen H. *Gromacs User Manual version 3.2*. www.gromacs.org, 2004.

[73] L. van Hove. Correlations in space and time and born approximation scattering in systems of interacting particles. *Phys. Rev.*, 95(1):249–262, 1954.

[74] L. Verlet. Computer experiments on classical fluids. i. thermodynamical properties of lennard-jones molecules. *Phys. Rev.*, 159:98–103, 1967.

[75] J. K. Wilkes. Properties of ionic liquid solvents for catalysis. *J. Mol. Catal. A: Chem.*, 214:11–17, 2004.

[76] T. Y. Yan, C. J. Burnham, M. G. Del Popolo, and G. A. Voth. Molecular dynamics simulation of ionic liquids: The effect of electronic polarizability. *J. Phys. Chem. B*, 108(32):11877–11881, 2004.

[77] R. Zwanzig. Time-correlation functions and transport coefficients in statistical mechanics. *Annu. Rev. Phys. Chem.*, 16:67–102, 1965.